Density Matrix Equations in Astrophysics and Cosmology

Hendrik Vogel

München 2016

Density Matrix Equations in Astrophysics and Cosmology

Hendrik Vogel

Dissertation
an der Fakultät für Physik
der Ludwig–Maximilians–Universität
München

vorgelegt von
Hendrik Vogel
aus Braunschweig

München, den 26. Juli 2016

Erstgutachter: Dr. habil. Georg G. Raffelt
Zweitgutachter: Prof. Dr. Gerhard Buchalla
Tag der mündlichen Prüfung: 25. Juli 2016

Zusammenfassung

Die Boltzmanngleichung beschreibt den Transport von Teilchen und Energie. Der Boltzmannformalismus erreicht jedoch dann seine Grenzen, wenn Teilchen mischen, d.h. falls Teilchen mit unterschiedlichen Quantenzahlen wie Spin und Flavor Korrelationen entwickeln. Zur expliziten Berücksichtigung dieser Korrelationen verwenden wir den Dichtematrixformalismus, welcher Phasenraumdichten zu Matrizen erweitert. Diese Matrizen enthalten auf den Nebendiagonalen Informationen über die relativen Phasen von verschiedenen Zuständen. Die vorliegende Doktorarbeit wendet diesen Dichtematrixformalismus auf drei astrophysikalische und kosmologische Systeme an.

Zunächst studieren wir die Mischung von Photonen und axion-ähnlichen Teilchen in extragalaktischen Magnetfeldern. Dieses System enthält zwei Längenskalen: Die Kohärenzlänge der Magnetfelder und die Oszillationslänge. Für GeV–TeV Photonenenergien, welche in Blazaren erzeugt werden, wurde die Oszillationslänge bisher größer als die Kohärenzlänge eingeschätzt. Diese Annahme wurde benutzt, um Längenskalen, die bei der Photonpropagation auftreten, zu trennen. Wir werden jedoch zeigen, dass ein weiterer Beitrag zur Photondispersion, der vor Kurzem hergeleitet wurde, eine klare Skalentrennung verhindert. Die Oszillationslänge verringert sich durch diesen neuen Effekt proportional zur Photonenenergie und kann für TeV-Energien die gleiche Größenordnung wie die Kohärenzlänge der Magnetfelder annehmen. Wir zeigen, dass in diesem Regime der traditionelle Ansatz seine Gültigkeit verliert. Man benötigt weitere Informationen über die Magnetfeldstruktur, um die Transferfunktion des Photons genau berechnen zu können. Diese Beobachtung ist vor allem für das künftige Cherenkov Telescope Array wichtig, da dieses TeV-Photonen mit großer Sensitivität messen wird.

Anschließend beschäftigen wir uns mit Neutrinooszillationen in kompakten astrophysikalischen Objekten. Es wurde kürzlich nachgewiesen, dass neben Flavoroszillationen eine Mischung von verschieden Helizitäten auf dem refraktiven Niveau stattfindet. Außerdem wurde gezeigt, dass Korrelationen zwischen Teilchen und Antiteilchen (Paarkorrelationen) entstehen. Wir leiten die Dichtematrixgleichungen, die diese beiden Phänomene beschreiben, her. Dabei bestätigen und erweitern wir vorangegangene Ergebnisse. Außerdem diskutieren wir phänomenologische Implikationen dieser Korrelationen. In typischen kompakten astrophysikalischen Objekten sind beide Effekte klein. Wir zeigen, dass Paarkorrelationen zu konzeptionellen Problemen führen, da Teilchenzahl keine lorentzinvariante Größe mehr darstellt. Wir unterbreiten Vorschläge, wie dieses Problem gelöst werden könnte.

Schließlich wird die Dichtematrixgleichung häufig in der resonanten Leptogenese angewendet. Sie kann aus dem Schwinger-Keldysh-Formalismus im Heisenbergbild für quasi-entartete Teilchen hergeleitet werden. Es wurde vor Kurzem im Interaktionsbildansatz und im starken Verwaschungsregime gezeigt, dass die Leptonenasymmetrie im Dichtematrixformalismus unterschätzt wird. Eine direkte Gegenüberstellung war jedoch nicht möglich, da unterschiedliche

Annahmen in die Ergebnisse einflossen. Wir werden in dieser Arbeit einen Vergleich zwischen dem Heisenberg- und Interaktionsbild zeigen, der in einem Spielzeugmodell und im schwachen Verwaschungsregime vollzogen wird. Wir finden identische Ergebnisse und identifizieren drei Quellen, die zur Asymmetrie beitragen: konventionelles Mischen, Oszillationen und eine destruktive Interferenz zwischen diesen beiden. Diese Interferenz wurde in vorhergehenden Arbeiten nicht berücksichtigt. Sie kann aber unterschiedliche Ergebnisse in der Literatur erklären, falls die Interferenz auch im starken Verwaschungsregime bestehen bleibt.

Abstract

The Boltzmann equation is a convenient tool to describe transport of particles and energy, but it is not without limitations. It cannot be applied directly if particles mix, i.e., if particles with different quantum numbers like flavor or spin develop correlations. To capture this effect explicitly, we promote phase space densities to matrices in spin and flavor space with the phase information stored on the off-diagonals. This thesis explores this density matrix formalism and applies it to three different astrophysical and cosmological systems.

First, we study mixing between photons and axion-like particles in extragalactic magnetic fields. This system contains two length scales, the coherence length of the magnetic fields and the oscillation length. The oscillation length was believed to be much larger than the coherence length for GeV–TeV energy photons that are emitted from blazars. This hierarchy was used to justify the separation of different length scales that enter photon propagation. However, we show how a new contribution to the photon dispersion, which was recently derived, prevents a clear separation of scales. The oscillation length shrinks with increasing energy and can be of the same order as the coherence length of the magnetic field for TeV energies. We demonstrate that in this regime the traditional approach breaks down and one requires more detailed information about the magnetic field structure to compute the photon transfer function. This observation is important for the upcoming Cherenkov Telescope Array that will probe TeV-energy photons with unprecedented sensitivity.

We then turn to neutrino oscillations in compact astrophysical objects. Besides flavor oscillations, it was recently shown that different helicity eigenstates mix on the refractive level and that correlations between particles and antiparticles (pair correlations) can build up. We derive the density matrix equations associated with these two phenomena confirming and extending earlier results, and we discuss phenomenological implications. Both effects are small in typical compact astrophysical objects. We find that pair correlations lead to the conceptual problem that particle numbers appear to be non-invariant under Lorentz transformations, and we provide some ideas on how this issue may be resolved.

Finally, the density matrix equation is often applied to resonant leptogenesis. Here, this equation may be obtained from the Heisenberg-picture Schwinger-Keldysh formalism for quasi-degenerate particles. Recently, it was shown in an interaction-picture approach and for strong washout that in the density matrix formalism the lepton asymmetry was underestimated. A direct comparison was, however, not possible because of different types of approximations. We present a consistent comparison between the Heisenberg and interaction-picture approaches in a toy model of resonant leptogenesis and for weak washout. We find identical results and identify three sources to the asymmetry: mixing, oscillations, and a destructive interference term between them. This interference term has been missed in previous works. It may reconcile the conflicting results of previous studies if the interference contribution persists in the strong-washout regime.

List of publications

During my doctoral research I have worked on a number of different topics of which three feature in this thesis. These works are

[1] A. Kartavtsev, G. Raffelt, and H. Vogel, Separation of scales in ALP-photon oscillations, *in preparation*.

[2] A. Kartavtsev, G. Raffelt, and H. Vogel, Neutrino propagation in media: flavor, helicity, and pair correlations, *Phys. Rev. D* **91** (2015) 125020, arXiv:1504.03230.

[3] A. Kartavtsev, P. Millington, and H. Vogel, Lepton asymmetry from mixing and oscillations, *accepted by JHEP* (2016), arXiv:1601.03086.

The following publications are not directly related to density matrix equations and are not part of this thesis

[4] H. Vogel and J. Redondo, Dark Radiation constraints on minicharged particles in models with a hidden photon, *JCAP* **1402** (2014) 029, arXiv:1311:2600.

[5] N. Vinyoles and H. Vogel, Minicharged particles from the Sun: a cutting-edge bound, *JCAP* **1603** (2016) 002, arXiv:1511:01122.

Contents

Chapter 1

Introduction

Transport phenomena in astrophysics and cosmology

The evolution of a macroscopic object is determined by the small-scale interactions of its constituents. Kinetic transport equations establish the connection between the two by determining for all times the distribution in coordinate and momentum space of the particles in the object. This distribution may be aggregated to obtain macroscopic observables. A good understanding of the transport equations allows us to check the consistency of our model of particle physics with astrophysical and cosmological observations. A possible mismatch hints towards either an incomplete particle theory or an insufficient description of transport phenomena. It is therefore of paramount importance to identify for a given particle content all relevant contributions to kinetic transport.

The rich phenomenology of stars, black holes and the cosmos results from an interplay of disruptive and balancing forces that rearrange the phase space distributions of particles in coordinate and momentum space. Examples can be found on all astrophysical and cosmological scales. Galaxies and galaxy clusters are formed by gravitational collapse in the potential wells of dark matter over-densities [6]. Dark matter is often thought to decouple from the primordial plasma in the early universe, thereby obtaining a relic density that is set by its cross section to Standard Model (SM) particles [7, 8]. In a similar way, the observed baryon asymmetry of the universe [9, 10] must be created by out-of-equilibrium processes [11, 12]. When the plasma cooled down to keV temperatures, big-bang nucleosynthesis started fusing protons and neutrons to helium [13, 14]. More massive nuclei are still created today in stars and supernovae.

Stellar objects contain a plethora of different transport channels [15, 16] with varying importance. Photons are emitted from ionized gas and lead to a net energy flow from hotter to cooler regions (radiative transport). This is the most important channel for the interior of the Sun where macroscopic matter movement, i.e., energy transport through convective currents is small. Stars also produce neutrinos in nuclear reactions. For the Sun, the emitted neutrinos are an energy sink because their weak interactions allow them to leave unimpeded. In supernovae or neutron star mergers, the densities are so large that the mean free path of neutrinos becomes of the same order as the typical dimensions of these compact objects. This coincidence of scales renders the neutrinos the most relevant particles for energy and lepton number transport. Radiative transport is suppressed due to the tiny mean free path of photons. Graviton emission may be treated as a small energy sink.

We derive information about distant objects by detecting the radiation they emit, which has to be transported through the intergalactic medium [17, 18]. Photon spectra allow us to extract the

temperature and chemical composition of the surface of these objects, but the signal is altered by scattering on background media and birefringence due to magnetic fields (Faraday rotation). The signal may also be lost due to pair creation on background light. The propagation of charged particles like cosmic rays is even more complex because they are deflected by magnetic fields that pervade the universe. The propagation in these backgrounds have to be taken into account if we want to infer properties of astrophysical objects from data. Gravitational waves, on the other hand, are almost unaware of these backgrounds and propagate freely. This is also true for neutrinos, although here one has to take into account flavor and spin oscillations.

A convenient tool to study transport phenomena is the Boltzmann equation [19]. Its original formulation applies to non-relativistic classical gases. It tracks the evolution of phase space densities $f(t, \mathbf{x}, \mathbf{p})$ for the different gas components, which are modeled as hard spheres with corresponding collisions. Correlations between these spheres that are caused by collisions are assumed to be forgotten between encounters (molecular chaos assumption [20]). The Boltzmann equation takes the form

$$\dot{f} = \left(\dot{f}\right)_{\text{force}} + \left(\dot{f}\right)_{\text{diff}} + \left(\dot{f}\right)_{\text{coll}} , \tag{1.1}$$

which means that the evolution of the phase-space densities is determined by external forces, diffusion, and collisions between gas constituents.

This formalism can be extended from classical gases to quantum states: while the uncertainty principle prohibits phase space densities with simultaneously defined coordinates and momenta, $f(t, \mathbf{x}, \mathbf{p})$ may be replaced by Wigner functions [21], which are smeared over a few $\hbar$ in phase space [20]. The evolution equation for the Wigner functions (Moyal's equation [22]) reduces to the classical Boltzmann equation in the limit $\hbar \to 0$, and we may often treat coordinates and momenta as continuous classical variables if the system varies on scales large compared with the de Broglie wavelength of the field quanta.

The Boltzmann equation is useful to describe the transport of elementary particles when generalized to relativistic propagation [23, 24]. Quantum statistics and particle collisions may be accounted for in a semi-classical fashion. The resulting equation is suitable for many of the systems mentioned above but it fails to account for particle oscillations during propagation. The Boltzmann equation does not capture Faraday rotation nor neutrino flavor oscillations because it discards correlations between discrete quantum numbers of particles. While neglecting correlations between momenta and/or coordinates of particles is often justified for astrophysical and cosmological systems, correlations that involve discrete quantum numbers like spin or flavor are crucial to understand particle transport of, e.g., neutrinos, and should not be discarded.

This thesis will be devoted to some phenomenological and theoretical aspects of a generalization of the Boltzmann equation that takes into account the mixing of particles with different discrete quantum numbers: the density matrix equation (see Refs. [25, 26] and references therein).

The density matrix equation

When we talk about particles like electrons or photons we have in mind a field with properties that are determined by discrete quantum numbers. These are, e.g., the spins and the charges they carry with respect to gauge groups. It is convenient to further assign baryon and lepton

numbers to each field in order to describe apparent conservation laws of the SM Lagrangian. We may subdivide these classes further by distinguishing three lepton flavors (e, μ, τ) and six quark flavors (u, d, s, c, b, t) that are conserved under the strong and electromagnetic interactions. A consequence is that pair production from a photon always creates a particle-antiparticle pair of the same type (e.g. e^+e^-) and that the quarks that enter a gluon vertex are required to have identical flavor.

This flavor conservation is broken by the misalignment of the weak interaction and the Yukawa bases: W-bosons that scatter with quarks do not produce an eigenstate of the strong interaction but a coherent combination thereof. For the leptonic sector, production of, e.g., an electron neutrino may be described by a coherent superposition of different neutrino mass eigenstates. In other words, a state that is prepared with an electron neutrino has non-trivial correlations when written in the mass basis. These correlations are the reason for neutrino oscillations and have to be taken into account in a kinetic description of neutrino transport [26].

Particle number densities are proportional to an expectation value of the form $\langle a_i^\dagger a_i \rangle$, where a_i is an annihilation operator and $a_i^\dagger$ a creation operator for a particle of type i. The brackets $\langle \ldots \rangle$ denote the ensemble expectation value, which is defined as the trace over the quantum-statistical density operator that contains the information about the initial preparation of a system. Similarly, we define off-diagonal number densities by taking the expectation value of creation/annihilation operators of different types, i.e., $\langle a_j^\dagger a_i \rangle$ with $i \neq j$. These terms contain phase information. Together, we may define the matrix of densities ρ_{ij} via [26]

$$\begin{aligned} (2\pi)^3 \delta^{(3)}(\mathbf{p}-\mathbf{k}) \rho_{ij}(t,\mathbf{p}) &= \langle a_j^\dagger(t,\mathbf{p}) a_i(t,\mathbf{k}) \rangle \,, \\ (2\pi)^3 \delta^{(3)}(\mathbf{p}-\mathbf{k}) \bar{\rho}_{ij}(t,\mathbf{p}) &= \langle b_i^\dagger(t,-\mathbf{p}) b_j(t,-\mathbf{k}) \rangle \,, \end{aligned} \tag{1.2}$$

for particles (ρ) and antiparticles ($\bar{\rho}$).

These matrices of densities follow an evolution equation that is commonly called the "density matrix equation". Note that some confusion might arise because the quantum statistical density operator is sometimes referred to as a "density matrix" as well. This operator has to be distinguished from the matrix of densities ρ_{ij} and the density matrix equation.

The density matrix equation can be obtained by considering the expectation values of the Heisenberg equation for the particle number operators. The right-hand side will contain a commutator term $\langle [\hat{H}, a_j^\dagger a_i] \rangle$. For two-particle interactions this commutator does not reduce to a matrix of densities but contains higher order correlations [27], i.e., expectation values of four creation/annihilation operators. This four-operator expectation value will be a dynamical quantity which in turn depends on higher order correlations. This is the famous Bogolyubov-Born-Green-Kirkwood-Yvon (BBGKY) hierarchy of correlation functions [28–31]: in a multi-body system one-particle distributions implicitly depend on all multi-particle correlations.

We need additional approximations to close the resulting system of evolution equations. We will be mainly interested in propagation in media where refraction is more important than collisions. In this case, it is suitable to apply the mean-field limit [32]: the Hamiltonian operator reduces to a one-particle operator by replacing pairs of creation/annihilation operators by their expectation value. Stated differently: quantum fluctuations are ignored and expectation values reduce to classical mean-fields. This approach discards collisions, which are encoded in higher

order correlations.

The mean-field approach is similar to the molecular chaos assumption in the way that it decomposes multi-particle expectation values into one-particle expectation values. But while the mean-field approximation a priori discards collisions, molecular chaos is imposed at a later stage to simplify collision terms.

In general, the density matrix equation may be expressed as:

$$\dot{\rho} = (\dot{\rho})_{\text{refr}} + (\dot{\rho})_{\text{force}} + (\dot{\rho})_{\text{diff}} + (\dot{\rho})_{\text{coll}} \ , \tag{1.3}$$

where the refractive contribution is a commutator $-i[\mathsf{H}, \rho]$ between the matrix of densities and a matrix of oscillation frequencies H (Hamiltonian matrix). The Hamiltonian matrix has to be determined from the Hamiltonian operator. In general, the commutator $[\mathsf{H}, \rho]$ does not vanish and the correlations on the off-diagonals of ρ contribute to the evolution of the number densities. This confluence of correlations and number densities is the crucial difference when compared to the Boltzmann formalism.

Note that flavor oscillations are not confined to the Faraday effect, conventional neutrinos or heavy meson systems. Misalignment between interaction and propagation eigenstates appears regularly in theories beyond the SM as well. Extended Higgs sectors which can be found in two-Higgs doublet models [33] or in supersymmetric theories [34], often contain explicit mixing of, e.g., CP-even and CP-odd states. Sterile neutrinos [35, 36], which are a good dark matter candidate, may obtain significant number densities via mixing with the active neutrino flavors. Similarly, if an additional $U(1)$ gauge symmetry is added to the SM, the conventional photon mixes kinetically with the new gauge boson [37]. In this thesis, we will present three systems for which the misalignment between interaction and propagation eigenstates generates interesting phenomena: mixing between photons and axion-like particles (chapter 3), helicity oscillations and pair correlations of neutrinos in supernovae (chapter 4), and resonant leptogenesis (chapter 5).

Mixing between photons and axion-like particles

First, we study the propagation of axion-like particles (ALPs) in extragalactic magnetic fields. The QCD axion [38–41] is a pseudoscalar whose defining property is that it solves the strong CP-problem, i.e., the fine-tuning problem associated with the non-detection of the neutron's electric dipole moment [42, 43]. A coupling of the axion to the chiral anomaly dynamically drives the CP-violation in the SM to zero (see e.g. Ref. [44]). The axion mixes with the π^0, which induces an axion mass and an axion coupling to two photons. The mixing also relates the mass and coupling strength of the axion. Axion-like particles generalize the concept of the QCD axion. An effective coupling to two photons is assumed similar to the one of the axion but the mass scale is set independently.

Explicitly, the ALP a couples to two photons via the term

$$\mathcal{L}_{a\gamma\gamma} = -\frac{g_{a\gamma\gamma}}{4} a F^{\mu\nu} \tilde{F}_{\mu\nu} = g_{a\gamma\gamma} a \mathbf{E} \cdot \mathbf{B} \, , \tag{1.4}$$

where $g_{a\gamma\gamma}$ is the coupling constant, $F^{\mu\nu}$ the photon field strength tensor and $\tilde{F}^{\mu\nu}$ its dual. This term can be rewritten as a scalar product of an electric and a magnetic field. This means that

an ALP in a magnetic field background may be converted into an oscillating electric field that is aligned with the magnetic field, i.e., ALPs mix with linearly polarized photons.

This mixing is used by experiments [45] like ADMX [46], ALPS [47, 48], CAST [49], IAXO [50], and MADMAX [51] to discover axions and axion-like particles. They use strong magnetic fields in which ALPs and photons may interconvert. The conversion probability depends on the magnetic field strength and the exposure time to a coherent magnetic field. Laboratory experiments therefore usually require strong magnetic fields. On the other hand, weak magnetic fields that are coherent over distances of several megaparsecs may be found in extragalactic space [52, 53]. Here, ALP-photon oscillations may be observed in the energy spectra of blazars. The propagation of photons and ALPs will be the topic of chapter 3.

The mixing may be treated within the density matrix formalism. Assuming that Faraday rotation may be neglected and that the magnetic field direction is constant, the density matrix is a 2×2 Hermitean matrix

$$\rho = \begin{pmatrix} \rho_{\parallel} & \rho_{\parallel a} \\ \rho_{a\parallel} & \rho_a \end{pmatrix} , \tag{1.5}$$

with the photon number density $\rho_{\parallel}$, ALP number density ρ_a and coherences $\rho_{\parallel a} = \rho^{\dagger}_{a\parallel}$. For a magnetic field that is transversal to the direction of motion, the Hamiltonian matrix reads

$$\mathsf{H} = \begin{pmatrix} \Delta_\gamma - i\frac{\Gamma_\gamma}{2} & g_{a\gamma}|\mathbf{B}| \\ g_{a\gamma}|\mathbf{B}| & \Delta_a \end{pmatrix} . \tag{1.6}$$

The off-diagonals contain the mixing due to the magnetic field. The ALP dispersion Δ_a is determined by its mass m_a, the photon dispersion Δ_γ is due to forward scattering on background media. Most importantly, photons are absorbed by pair creation with the extragalactic background light (EBL), which is indicated by the absorption rate Γ_γ. To leading order the ALP is not absorbed by background media because its coupling strength $g_{a\gamma}$ is tiny [54].

This asymmetry in the absorption signifies the relevance of ALP-photon mixing — photons that oscillate into ALPs are shielded from absorption [55]. The ALPs freely propagate and photons may regenerate in the magnetic field of our galaxy for us to be detected. The number of photons with GeV–TeV energies may be enhanced by orders of magnitude through this mechanism because these energetic photons are usually absorbed very efficiently.

In general, oscillations between mixing states are suppressed if their dispersive phase velocities are very different. For ALPs, dispersion is controlled by a mass term and for photons, background media induce non-zero indices of refraction. Previous works [56–58] assumed that the only contributions to the photon refraction were from background electrons and background magnetic fields. For gamma rays in the GeV–TeV range, the photon refraction from these two contributions is orders of magnitude smaller than the mixing induced by typical magnetic fields. This means that for small ALP masses the Hamiltonian matrix is dominated by its off-diagonals such that the mixing angle is maximal and ALP-photon conversion is very efficient. Moreover, the length scale that is associated with the conversions (oscillation length) was found to be large compared to typical coherence lengths of magnetic fields of a few megaparsec [52, 53]. Thus, the ALP-photon system was not able to probe the exact structure of the magnetic field, and the mag-

netic field was often approximated by a domain-like grid with constant lattice spacing and constant absolute value of the magnetic field strength [56–58]. The orientation of the magnetic field was taken to vary instantly at the boundaries of each domain assuming a new random direction.

In chapter 3, we show that these simplifications for the structure of the magnetic field cannot be justified once we include a recently derived [59] contribution to the refraction from the cosmic microwave background (CMB). Photons undergo forward scattering on the CMB through the effective four-photon vertex that is generated by a box diagram with charged fermions in the loop [60]. The refraction is dominated by those background particles with the highest energy density; a quantity that is very large for CMB photons.

This new refractive term dominates the components of the Hamiltonian matrix for TeV energies. This has a number of consequences as we will demonstrate. The mixing angle becomes suppressed and the oscillation length $l_{\rm osc} \sim 78.5\,{\rm Mpc}\,(E\,[{\rm TeV}])^{-1}$ becomes comparable to $l_{\rm c}$. The ALP-photon system is now able to resolve the structure of the magnetic field. It becomes sensitive to the underlying probability distributions of the magnetic field strength and of the coherence length. If $l_{\rm osc}$ is smaller than $l_{\rm c}$ the propagation of the photons becomes quasi-adiabatic: the photon survival probability becomes only sensitive to the initial and final magnetic field configurations and to the mean absorption length of ALPs, which is induced by back-conversions into photons.

Pair correlations

Chapter 4 takes a closer look at the evolution equations of neutrinos in core-collapse supernovae. Neutrinos dominate the transport of energy and lepton number. In our current understanding of core-collapse supernovae, this transport is crucial to enable stellar explosions (see e.g. Ref. [61]). A shock wave is formed when matter bounces off the stiff core of a gravitationally collapsing star. It propagates outwards but loses most of its energy dissociating iron. The initial energy of the shock wave is not enough to shed the outer layers of the star. Neutrinos that are emitted from the supernova core sustain the shock wave with their energy deposition. This picture is confirmed by numerical simulations, which are however very sensitive to the approximations in the neutrino transport (see e.g. Ref. [62]).

Note that flavor oscillations may be crucial for neutrino energy transport. The flavor content of the neutrino stream determines the efficiency of the energy transport since electron neutrinos can be absorbed thereby providing all their energy to the shock wave. The other neutrino flavors only lose energies through scattering, which is not as efficient. Moreover, the heavy lepton neutrinos typically possess larger energies because they decouple from hotter areas of the supernova core [63]. If these neutrinos oscillate into electron neutrinos, their larger energy is combined with the more efficient absorption.

To date, neutrino flavor oscillations are neglected in supernova simulations and neutrino transport is described by Boltzmann equations [61]. The reason is that very dense matter suppresses oscillations because interaction and propagation eigenstates are almost aligned [64, 65]. While this argument applies to, e.g., the core of the Sun, it is not so clear-cut for supernovae: the neutrinos themselves are an irreducible background and lead to non-linear density matrix equations already on the refractive level. It is an open research question, whether these non-linearities lead

to significant flavor conversions [66–84].

Because of these non-linearities, one may wonder about other seemingly small contributions to the neutrino propagation that might become important in dense objects. Recently, the conventional picture of flavor oscillations has been extended to include helicity oscillations and pair correlations [85–90]. Helicity oscillations describe transitions between different neutrino helicities. Neutrino transport is sensitive to the neutrino helicity for the following reasons. For Dirac neutrinos the "wrong-helicity states" correspond to sterile components that leave a supernova without energy deposition. For Majorana neutrinos a helicity flip changes a neutrino to an antineutrino with altered cross section and lepton number. In collisions, these helicity flips are usually suppressed by $[m/(2E)]^2$ with neutrino mass m and energy E. The novelty in the approaches of Vlasenko, Cirigliano and Fuller [85–87] was that helicity transitions are obtained already at linear order in the mass insertion $m/(2E)$, if the background medium induces helicity off-diagonal refractive indices. Such refractive indices may be generated by background currents and electromagnetic fields that provide the angular momentum needed for helicity flips. While helicity transitions remain small even at the refractive level, resonant enhancement of helicity transitions may be obtained [87], albeit a significant amount of tuning is necessary.

While helicity oscillations may not be important for supernova dynamics, their conceptual meaning is well-understood. The physical interpretation of pair correlations however is more elusive and they are best understood if we take a look at the corresponding correlators in the density matrix equation. This equation has been generalized [88–90] to include helicity oscillations and pair correlations on the refractive level and in the mean-field approximation by Volpe and collaborators. Helicity oscillations are described with correlators of the form $\langle a^\dagger_{j,h} a_{i,s}\rangle$ with helicity indices $s, h, \in \{+, -\}$. Pair correlations on the other hand are introduced by terms of the type $\langle a^\dagger b^\dagger\rangle$, i.e., expectation values of a neutrino and an antineutrino operator. Pair correlations have been discarded previously [26] on the grounds that they should oscillate fast with a frequency $2E$ and therefore average out to zero. Volpe and collaborators argued [88–90] that such correlations are an important concept in nuclear physics and should be included in the most general treatment of neutrino transport. Even if they oscillated quickly their average may not vanish.

Large parts of chapter 4 will be devoted to the puzzling pair correlations. We will re-derive the most general density matrix equations in the mean-field approximations, explicitly showing the terms of the Hamiltonian matrix up to first order in the mass insertion $m/(2E)$. For Dirac neutrinos we confirm previous results. For Majorana neutrinos we demonstrate that some lepton-number violating correlators have been missed in previous works [90]. Moreover, we interpret pair correlations physically finding that these correspond to spontaneous pair creation of back-to-back neutrino/antineutrino pairs with zero total momentum. Their contribution to the kinetic equations is usually small and of the same order as helicity oscillations. In contrast to helicity oscillations, pair correlations cannot be resonantly enhanced in supernovae since such a resonance requires number densities orders of magnitude above those of astrophysical objects.

We also discuss a conceptual issue that pertains to the constraint that the neutrino/antineutrino pair is created back-to-back and with zero total momentum. This condition holds in every reference frame, which leads to the issue that particle number ceases to be a Lorentz covariant quantity once pair correlations are included. This problem remains open but we discuss some ideas how to restore physical particle numbers.

Sources of leptogenesis

To actually use the density matrix equation (1.3) for practical purposes, a few approximations have to be introduced. These include, e.g., using a perturbative approximation scheme [26] or the mean-field approximation [88–90]. In systems far from equilibrium, the density matrix equation simplified this way may not capture all relevant effects. An alternative way of describing out-of-equilibrium phenomena is the closed-time-path (CTP) formalism (Schwinger-Keldysh formalism [91, 92]). Ensemble expectation values may be written as a path integral with a closed time contour that first leads forward and then backwards in time. Out of equilibrium, the two time directions are not equivalent and the information stored in the different evolutions of these two time directions is used to derive the so-called Kadanoff-Baym equations [93, 94]. These equations may be decomposed into a kinetic equation, which gives the time-evolution of field excitations, and a constraint equation, which stores the information about what the dynamical excitations actually are. Especially far from equilibrium, these excitations may not be associated with quasi-free particles. This distinction will be of relevance in chapter 5, where we study the generation of lepton-number asymmetry in a toy model of baryogenesis via leptogenesis.

Baryogenesis refers to the process of creating the apparent asymmetry between baryons and antibaryons. This baryon asymmetry cannot be realized for the particle content of the SM and a standard cosmology because the combined amount of CP violation, baryon number violation and departure from equilibrium (the Sakharov conditions [11]) is too small [12, 95, 96]. An attractive scenario beyond the SM is baryogenesis via leptogenesis introduced by Fukugita and Yanagida [97]. This class of models introduces heavy Majorana neutrinos which may generate a lepton asymmetry through lepton-number violating out-of-equilibrium decays. The decays proceed through CP-violating complex Yukawa couplings, and therefore all three Sakharov conditions are fulfilled. The excess lepton number is converted to baryon number via B+L-violating sphaleron processes [98]. This scenario is attractive because heavy Majorana neutrinos may mix with the three conventional neutrinos, thereby generating small neutrino masses via the seesaw mechanism [99–102].

A hierarchical mass spectrum of the heavy Majorana neutrinos is problematic because these models require in general large masses of the order 10^7–$10^8\,\mathrm{GeV}$ [103], which are out of reach of collider experiments and this mechanism is ruled out if the reheating temperature is too low to generate a sufficient amount of these massive neutrinos [96, 104]. An alternative scenario [105–107] relies on quasi-degenerate masses of two heavy neutrinos, which resonantly enhances CP-violation. This resonant leptogenesis allows the masses to be in the TeV-range; potentially in reach of current and future colliders.

The lepton asymmetry from resonant leptogenesis is dominantly generated by two different sources. The first contribution is conventionally called the *mixing* source. It describes the CP-violation that arises through the interference of the tree level decay and the absorptive part of one-loop corrections. The second contribution is called the *oscillation* source. It describes the build-up of correlations during propagation and the subsequent flavor-violating oscillations.

Recently, resonant leptogenesis has been approached by two different methods. In a series of works, Dev, Millington, Pilaftsis, and Teresi [108–111] derived the generated lepton asymmetry in the interaction picture representation of non-equilibrium field theory and in the strong-washout

regime. They identified the oscillation source and incorporated mixing with effective Yukawa couplings, finding that both sources contribute additively to the asymmetry. They also comment that a density matrix approximation discards the contribution from mixing [110]. The reason is that the density matrix formalism assumes the mixing particles to have approximately equal energies, i.e., they are approximated to lie on the same energy shell where shell is to be understood as the pole of a delta function. Such an approach would underestimate the generated asymmetry. This ansatz is used by Garbrecht and collaborations [112, 113] who compute the asymmetry in the Heisenberg representation of non-equilibrium field theory. The resulting kinetic equation is akin to the neutrino transport equations in the density matrix approach.

A comparison between these two different approaches is difficult to obtain because of the different approximation schemes that are applied. While the Heisenberg picture and interaction picture are equivalent in quantum mechanics, in non-equilibrium field theory it was believed that the interaction picture approach fails due to ill-defined products of Dirac delta functions (pinch singularities [114–117]). In a recent publication by Millington and Pilaftsis [118], it was shown that this pathology can be cured if finite-time effects are consistently taken into account. A direct comparison between results obtained in the interaction picture and the conventional Heisenberg picture approach has never been performed.

In chapter 5, we provide such a comparison in a scalar toy model of leptogenesis in the weak-washout regime. We derive the asymmetry in both approaches demonstrating their equivalence. In this computation, we find the dynamical field excitations analytically without resorting to a quasi-particle ansatz. We show that the lepton asymmetry contains three delta functions with different energies, i.e., three different energy shells. Two of these shells correspond to the quasi-particle poles of the two heavy neutrinos and the asymmetry that is generated on these shells is the conventional mixing contribution. The third shell has an energy that is given by the average thermal energy of the two heavy neutrinos. This shell contains two contributions to the asymmetry: one term is the oscillation source, and the second term may be interpreted as destructive interference between mixing and oscillations. This interference has been missed in previous studies but may also help to reconcile the discrepant results of different groups. We show that the interference may approximately cancel the mixing contribution in the quasi-degenerate regime such that oscillations alone can be a good approximation. On the other hand, for larger mass differences both mixing and oscillations contribute additively and must be included for a correct result as argued in Ref. [110].

Outline

In chapter 2, we will familiarize the reader with different approaches to kinetic theory. Starting with the Boltzmann equation, we introduce the density matrix formalism. We show the derivation in the interaction picture approach following Ref. [26] with a special emphasis on the approximations that are needed in the derivation. As a preparation for later chapters, we also introduce the closed-time path formalism that leads to the Kadanoff-Baym equations. We demonstrate how the Boltzmann and density matrix equations may be obtained as limiting expressions. The density matrix equation is applied in chapter 3 in a phenomenological way to ALP-photon mixing. This is followed in chapter 4 by a study of pair correlations in compact astrophysical objects. The first

part of this chapter contains a technical derivation of the extended density matrix equations. In the second part we estimate the typical magnitude of pair correlations and their contribution to supernova dynamics. We also discuss conceptual problems of pair correlations. In chapter 5, we use the closed-time path formalism to derive the asymmetry in the Heisenberg and interaction pictures. We find that the asymmetry obtained in both approach is identical. We also compare with previously obtained results. The overall conclusion of this thesis will be drawn in chapter 6.

Chapter 2

Kinetic equations

Kinetic equations track the microscopic dynamics of non-equilibrium systems. Depending on the properties of the constituents and the system, different types of equations yield the most convenient approach. The original Boltzmann equation (see Ref. [19] and Sec. 2.2) was derived to describe classical gases by considering the evolution of one-particle distribution functions $f(t, \mathbf{x}, \mathbf{p})$ (phase space densities). This formalism can be extended to include (general) relativistic corrections. Quantum statistics and particle interactions may be incorporated semi-classically.

On the other hand, to allow for coherence of spins and flavors requires promoting the single-valued phase space densities to matrices of densities in spin and flavor space. These matrices are defined as the ensemble expectation values of field operators, and their diagonal entries are the usual phase space densities, i.e., they are measurable quantities.

The dynamics of these densities are described by the equations of motions. Typically, these equations are complicated to solve and need to be simplified. In this thesis, we will use two different formalisms to arrive at the equations of motion. The first approach, which is applied extensively, is the density matrix formalism described in Sec. 2.4, which uses the expectation value of the Liouville equation. We will show two ways to simplify the equations: the mean-field approximation and the perturbative expansion.

The second approach to extract kinetic equations relies on the closed-time-path (CTP) formalism. This method allows us to obtain relations between Green's functions for which we can solve with a consistent truncation in terms of self-energies. Unfortunately, the resulting equations are hard to solve. A short introduction to this approach will be given in Sec. 2.5, where we will also show that the CTP formalism contains the Boltzmann and density matrix equations as limiting cases.

2.1 Expectation values

Before we start with the kinetic equations, let us define what we mean by expectation values. In the study of transport phenomena, we are interested in the expectation values of operators at a given time, which take the form

$$\langle \bullet \rangle (t) \equiv \mathcal{Z}^{-1} \mathrm{tr} \hat{\rho}(t) \bullet \,, \tag{2.1}$$

where the bullet point is to be replaced by some operator, $\hat{\rho}(t)$ is the quantum-statistical density operator, which contains the information about how the system is prepared, and $\mathcal{Z} = \mathrm{tr}\, \hat{\rho}$ is the

partition function. To describe classical systems, $\hat{\rho}$ in Eq. (2.1) has to be replaced by a classical distribution function $\tilde{\rho}$, the bullet becomes a function and the trace yields an integration over phase-space.

Note that Eq. (2.1) is in stark contrast to scattering-matrix theory, where we are instead interested in the overlap of states evaluated at different times: specifically, in and out asymptotic states. On the other hand, ensemble expectation values contain the overlap of states evaluated at the same time, i.e., two in-states. In this thesis, we will be mostly concerned with this in-in formalism.

2.2 The Boltzmann equation

In this thesis, we are predominantly concerned with coherence that cannot be treated with single-valued phase-space densities. Nevertheless, it is useful to take a look at the derivation of the classical Boltzmann equation and the approximations required to obtain a closed kinetic equation. The interested reader may find an excellent introduction to the Boltzmann equations in Ref. [20].

Consider a gas of N identical particles with a distribution function $\tilde{\rho}[t, (\mathbf{x}_1, \mathbf{p}_1), \cdots, (\mathbf{x}_N, \mathbf{p}_N)]$, which is the classical analogue to the density operator $\hat{\rho}$ in Eq. (2.1). The classical distribution function $\tilde{\rho}$ tracks the positions $\mathbf{x}_i$ and momenta $\mathbf{p}_i$ at a time t of all N particles. If the dynamics of the system is governed by a classical Hamiltonian function H_{cl}, the time evolution of $\tilde{\rho}$ is given by the Liouville equation

$$\frac{\partial \tilde{\rho}}{\partial t} = -\{H_{\mathrm{cl}}, \tilde{\rho}\}_{\mathrm{Poisson}}\,, \tag{2.2}$$

and the right-hand side contains the Poisson-bracket, which is defined as

$$\{f, g\}_{\mathrm{Poisson}} \equiv \sum_{i=1}^{N} \left(\frac{\partial f}{\partial \mathbf{p}_i} \frac{\partial g}{\partial \mathbf{x}_i} - \frac{\partial g}{\partial \mathbf{p}_i} \frac{\partial f}{\partial \mathbf{x}_i} \right) . \tag{2.3}$$

Given $\tilde{\rho}$, we may ask for the one-particle distribution function $f_1(\mathbf{y}_1, \mathbf{k}_1)$ at a phase-space point $(\mathbf{y}_1, \mathbf{k}_1)$. This function is determined by the expectation value of Dirac delta functions

$$\begin{aligned} f_1(t, \mathbf{y}_1, \mathbf{k}_1) &= \sum_{i=1}^{N} \langle \delta^{(3)}(\mathbf{x}_i - \mathbf{y}_1) \delta^{(3)}(\mathbf{p}_i - \mathbf{k}_1) \rangle \\ &= \sum_{i=1}^{N} \int \prod_{j=1}^{N} \mathrm{d}^3\mathbf{x}_j \, \mathrm{d}^3\mathbf{p}_j \, \tilde{\rho}[t, (\mathbf{x}_1, \mathbf{p}_1), \ldots, (\mathbf{x}_N, \mathbf{p}_N)] \, \delta^{(3)}(\mathbf{x}_i - \mathbf{y}_1) \delta^{(3)}(\mathbf{p}_i - \mathbf{k}_1)\,, \end{aligned} \tag{2.4}$$

which for identical particles evaluates to

$$f_1(t, \mathbf{y}_1, \mathbf{k}_1) = N \int \prod_{j=2}^{N} \mathrm{d}^3\mathbf{x}_j \, \mathrm{d}^3\mathbf{p}_j \, \tilde{\rho}[t, (\mathbf{y}_1, \mathbf{k}_1), (\mathbf{x}_2, \mathbf{p}_2), \ldots, (\mathbf{x}_N, \mathbf{p}_N)]\,. \tag{2.5}$$

Similarly, we can define a two-particle distribution function by taking the expectation values of products of Dirac delta functions, thereby describing the correlations between two different particles

$$f_2[t,(\mathbf{y}_1,\mathbf{k}_1),(\mathbf{y}_2,\mathbf{k}_2)] = \frac{N!}{(N-2)!}\int\prod_{j=3}^{N}\mathrm{d}^3\mathbf{x}_j\,\mathrm{d}^3\mathbf{p}_j\,\tilde{\rho}[t,(\mathbf{y}_1,\mathbf{k}_1),(\mathbf{y}_2,\mathbf{k}_2),\ldots,(\mathbf{x}_N,\mathbf{p}_N)]\,. \tag{2.6}$$

The dynamics of these distribution functions are given by the expectation value of the Liouville equation (2.2) (see e.g. Ref. [20])

$$\frac{\partial}{\partial t}f_1(t,\mathbf{y},\mathbf{k}) = -\frac{\mathbf{k}}{m}\frac{\partial f_1}{\partial\mathbf{y}} + \frac{\partial}{\partial\mathbf{k}}\int\mathrm{d}^3\mathbf{x}_2\,\mathrm{d}^3\mathbf{p}_2\frac{\partial}{\partial\mathbf{y}}\left[V(|\mathbf{y}-\mathbf{x}_2|)\right]\,f_2[t,(\mathbf{y},\mathbf{k}),(\mathbf{x}_2,\mathbf{p}_2)]\,, \tag{2.7}$$

where we assumed a classical Hamiltonian $H_{\mathrm{cl}} = \sum_i k_i^2/(2m) + \sum_{i<j}V(|\mathbf{x}_j-\mathbf{x}_i|)$ with a symmetric two-body potential V.

The first term on the right-hand side describes spatial fluxes into the phase-space volume of f_1. The second term is due to interactions in the gas and describes scattering between the gas constituents. It is called the collision term and often abbreviated with $C[f]$. Equation (2.7) is not closed and we see that the dynamics of the one-particle distribution function depends on the two-particle distribution function. Similarly, the dynamics of f_2 depends on a suitably generalized three-particle distribution function f_3, which in turn derives its dynamics from higher-order distribution functions. This system of N equations is the famous Bogolyubov-Born-Green-Kirkwood-Yvon (BBGKY) hierarchy [28–31].

In typical many-body systems, the number of coupled equations corresponds to the number of particles, which is of the order of Avogadro's number. This number is so huge that solving the BBGKY hierarchy exactly for general potentials becomes impossible. We are forced to impose simplifications. One possibility is to truncate the BBGKY hierarchy, i.e., neglect higher order correlations. This truncation can be justified by noting that f_1 depends on f_i via $i-1$ products of the potential V, which will be small for perturbative coupling strengths. In other words, higher order correlations can be safely neglected when the probability for 3-body interactions are much smaller than those for 2-body scatterings. Retaining only the first order in V, we are left with two coupled equations of motion, one for f_1 and one for f_2.

The resulting expression can be further simplified by imposing the so-called *molecular chaos hypothesis*, which states that before each collision two particles are uncorrelated, i.e., correlations are forgotten and the two-particle distribution function decomposes into a product of statistically independent one-particle distribution functions

$$f_2[t,(\mathbf{x}_1,\mathbf{p}_1),(\mathbf{x}_2,\mathbf{p}_2)] \approx f_1(t,\mathbf{x}_1,\mathbf{p}_1)f_1(t,\mathbf{x}_2,\mathbf{p}_2)\,. \tag{2.8}$$

After a collision these particles are correlated. However, the decomposition into one-particle distributions can still be applied: the phase space densities are conserved (Liouville's theorem) and so they may be expressed in terms of initially independent states.

Using these approximations and the equation of motion for f_2 (see Ref. [20] for the detailed

calculation), one arrives at the usual form of the classical Boltzmann equation for a dilute gas

$$\frac{\partial}{\partial t} f_1(\mathbf{k}) + \frac{\mathbf{k}}{m} \frac{\partial}{\partial \mathbf{y}} f_1(\mathbf{k}) = \int \mathrm{d}^3\mathbf{p}_2 \, \mathrm{d}^3\mathbf{p}_3 \, \mathrm{d}^3\mathbf{p}_4 \, T(\mathbf{k}, \mathbf{p}_2, \mathbf{p}_3, \mathbf{p}_4) [f_1(\mathbf{p}_3) f_1(\mathbf{p}_4) - f_1(\mathbf{k}) f_1(\mathbf{p}_2)] \,, \tag{2.9}$$

where the right-hand side shows the usual gain and loss terms, and T is the transfer matrix that contains the details of the interaction, i.e., it picks the combinations of the momenta $\mathbf{p}_2, \mathbf{p}_3$ and $\mathbf{p}_4$ that lead to scattering into and out of the mode $\mathbf{k}$. All distribution functions implicitly depend on the same coordinates $(t, \mathbf{y})$; an approximation that is justified if the range of the potential is much smaller than the typical scale of inhomogeneities (see Ref. [119] page 207).

The classical Boltzmann equation (2.9) can be generalized in a number of ways. We may include quantum-statistics by expanding the gain and loss terms with Pauli blocking or Bose stimulation functions. For quantum fields, the collision term may be further generalized by interpreting the transfer matrix T as the usual squared matrix element. The extension to relativistic systems may be performed by applying Liouville's theorem to relativistic phase space including non-Minkowski metrics [23, 24]. The derivative of a distribution function along an affine connection is given by [7]

$$\hat{L}[f] = \left(p^\mu \frac{\partial}{\partial x^\mu} - \Gamma^\mu_{\alpha\beta} p^\alpha p^\beta \frac{\partial}{\partial x^\mu} \right) f = C[f] \,, \tag{2.10}$$

where $\hat{L}$ is the Liouville operator, the information about the metric is contained in the Christoffel symbols $\Gamma^\mu_{\alpha\beta}$, and the details of the collisions are hidden in $C[f]$. In a Friedmann-Lemaître-Robertson-Walker background, the distribution function is homogeneous and isotropic, and the relativistic Boltzmann equation (2.10) simplifies to [7]

$$p^0 \frac{\partial}{\partial t} f - \frac{\dot{a}}{a} \mathbf{p}^2 \frac{\partial}{\partial p^0} f = C[f] \,, \tag{2.11}$$

where a is the cosmological scale factor.

Let us comment on some applications of the Boltzmann equation in astrophysics and cosmology. The most prominent variation of the Boltzmann equation is arguably the Lee-Weinberg equation [8]. By integrating the Boltzmann equation in an expanding background over relativistic phase space, we obtain a rate equation for the total number density. For example one may study how dark matter particles reach and fall out of equilibrium, and compute their relic abundance. We have used a similar method to compute the energy density in a hidden sector [4] (see Ref. [120] for a summary). The system of equations studied there has been obtained by weighing the distribution functions by energy before integrating over phase space. Besides thermalization, another important application is the generation of nuclei in the early universe. This fusion process is described with a set of coupled Boltzmann equations (see Ref. [121] for a popular code).

2.3 Intermission: Schrödinger, Heisenberg, and interaction pictures

Before we continue with the derivation of generalized kinetic equations, we would like to remind the reader of basic properties of the Schrödinger, Heisenberg and interaction picture. In the following chapters, we will often switch between these different descriptions of quantum mechanics.

Let us assume that we wanted to calculate the expectation value of an operator $\langle \hat{A} \rangle$; an object which might be time-dependent. If the operator is assumed to be time-independent whereas the states that enter the expectation value, or equivalently the density matrix of the system $\hat{\rho}_{\mathrm{S}}(t)$, track the evolution, we are in the so-called Schrödinger picture. States are usually written in the bra-ket formalism, in which the density matrix reads

$$\hat{\rho}_{\mathrm{S}}(t) = \sum_n p_n |n(t)\rangle\langle n(t)| \,, \tag{2.12}$$

where $|n\rangle$ is a normalized pure state in the Schrödinger picture. The p_n are probabilities, which represent how the system is prepared initially. They have to fulfill a normalization condition $\sum p_n = 1$. We call $\hat{\rho}$ a pure state if also $\sum_n p_n^2 = 1$. Mixed states are characterized by $\sum_n p_n^2 < 1$. The density matrix in Eq. (2.12) appears to be diagonal. This statement is basis dependent. Since the superposition of pure states yields again a pure state, off-diagonal entries in the density matrix can be obtained after a change of basis. For example, if a photon is in a pure, circular polarized state, Eq. (2.12) will be diagonal in the basis of circular polarizations. We may however describe circular polarization as a properly normalized superposition of linear polarizations. In this basis, Eq. (2.12) will not be diagonal anymore.

The evolution of the state $|n(t)\rangle$ in Eq. (2.12) is given by the Schrödinger equation

$$i\frac{\partial}{\partial t}|n(t)\rangle = \hat{H}|n(t)\rangle \,, \tag{2.13}$$

with the Hamiltonian operator $\hat{H}$. The Schrödinger equation may be solved by

$$|n(t)\rangle = U(t, t_i)|n(t_i)\rangle \,, \tag{2.14}$$

where the unitary time-evolution operator $U(t, t_i)$ with initial time t_i takes the form

$$U(t, t_i) = \mathcal{T}\left[\exp\left(-i\int_{t_i}^{t} \mathrm{d}t'\, \hat{H}(t')\right)\right] \,, \tag{2.15}$$

with the time ordering operator $\mathcal{T}$. This general solution can be simplified to give $U(t, t_i) = \exp\left[-i\hat{H}\,(t - t_i)\right]$ if the Hamiltonian is time-independent, as we will assume in the following if not otherwise stated. Note that the solution (2.15) will still be useful for our treatment of the interaction picture where the Hamiltonian is in general time-dependent.

For a static Hamiltonian, we can immediately derive the von-Neumann equation, which is the quantum-mechanical analogue of the Liouville equation (2.2):

$$i\frac{\partial}{\partial t}\hat{\rho}_{\mathrm{S}} = [\hat{H}, \hat{\rho}_{\mathrm{S}}]\,. \tag{2.16}$$

When the Hamiltonian can be written as a square matrix, e.g., when the Hamiltonian effectively reduces to a sum of field bilinears, we can solve the Schrödinger equation (2.13) directly. We will find that refraction is of this form in Chapter 3. If the interactions in the Hamiltonian become more complicated and go beyond simple two-particle vertices, it becomes difficult to find a simple matrix representation, and we will resort to different approaches.

The Heisenberg picture is an alternative to the Schrödinger picture approach. Here, we consider the density matrix $\hat{\rho}_{\mathrm{H}}$ to be time-independent while the operator evolves with time $\hat{A}_{\mathrm{H}}(t)$. We can switch from one picture to the other by applying the time-evolution operator. For example, a Heisenberg field operator evolves according to

$$\phi_{\mathrm{H}}(t, \mathbf{x}; t_i) = e^{i\hat{H}\,(t-t_i)}\phi_{\mathrm{H}}(t_i, \mathbf{x}; t_i)e^{-i\hat{H}\,(t-t_i)}\,, \tag{2.17}$$

where again t_i denotes the initial time at which the time evolution operator equals zero. We have separated this initial time surface from the other variables with a semicolon in anticipation of our treatment of the interaction picture in Sec. 5.5 (see also Ref. [118]). Taking the time-derivative of Eq. (2.17), we obtain the Heisenberg equation of motion

$$i\frac{\partial}{\partial t}\phi_{\mathrm{H}} = -[\hat{H}, \phi_{\mathrm{H}}]\,. \tag{2.18}$$

Although the Schrödinger and Heisenberg pictures are conceptually simple, it is not so easy to actually calculate expectation values of field operators, like two-point functions, for arbitrary times. If we know how to diagonalize the Hamiltonian in Eq. (2.17), the exponentials can be computed straight-forwardly and we are able to obtain an explicit representation of the field ϕ in terms of creation and annihilation operators. These are eigenmodes of the Hamiltonian (see e.g. Ref. [122]),

$$\phi_{\mathrm{H}}(t, \mathbf{x}; t_i) = \int \mathrm{d}\Pi_{\mathbf{p}} \left[a_{\mathrm{H},\mathbf{p}}(t_i; t_i)e^{-ip\cdot x} + a^{\dagger}_{\mathrm{H},\mathbf{p}}(t_i; t_i)e^{ip\cdot x}\right]\,, \tag{2.19}$$

where for simplicity we have assumed a real scalar field. We have also written $x^0 = t - t_i$ and have introduced the abbreviation $\mathrm{d}\Pi_{\mathbf{p}} = \mathrm{d}^3\mathbf{p}/[(2\pi)^3 2E_p]$ for the relativistic momentum integration. The operators a_{H} and $a^{\dagger}_{\mathrm{H}}$ are the familiar annihilation and creation operators. The excitations that are created by $a^{\dagger}_{\mathrm{H}}$ are eigenstates of the Hamiltonian, and thus have well-defined energies. They can be interpreted as particles, as usual. Their number in a given state can be determined by taking the expectation value $\langle a^{\dagger}a\rangle$, and it is the evolution of these operators that we aim to describe.

If the Hamiltonian incorporates interactions which cannot be diagonalized, the representation of the field ϕ in Eq. (2.19) in terms of eigenstates of the Hamiltonian breaks down. However, we can split the Hamiltonian into a diagonalizable part $\hat{H}_0$ and an interaction piece $\hat{H}_{\mathrm{int}}$ that contains

the non-diagonalizable parts. If the product $\hat{H}_{\rm int}\,(t-t_i) \ll 1$, we can expand the non-diagonal part of Eq. (2.17). This approach leads to the interaction picture in which we define the fields

$$\phi_{\rm I}(t,\mathbf{x};t_i) = e^{i\hat{H}_0\,(t-t_i)}\phi_{\rm H}(t_i,\mathbf{x};t_i)e^{-i\hat{H}_0\,(t-t_i)}\,. \tag{2.20}$$

The important difference to Eq. (2.17) is that the time evolution of the interaction picture field is only due to the diagonalizable part of the Hamiltonian. Heisenberg and interaction picture fields at equal time can be connected through

$$\phi_{\rm H}(t,\mathbf{x};t_i) = U^\dagger_{\rm I,int}(t,t_i)\phi_{\rm I}(t,\mathbf{x};t_i)U_{\rm I,int}(t,t_i)\,, \tag{2.21}$$

where $U_{\rm I,int}$ is analogous to Eq. (2.15) but with the Hamiltonian replaced by its interaction part written in the interaction picture. Given this evolution relation, the interaction picture density matrix also fulfills [118]

$$\hat{\rho}_{\rm I}(t;t_i) = U_{\rm I,int}(t;t_i)\hat{\rho}_{\rm I}(t_i;t_i)U^\dagger_{\rm I,int}(t;t_i)\,. \tag{2.22}$$

The density matrices of all three pictures are prepared identically at the initial time t_i:

$$\hat{\rho}_{\rm H}(;t_i) = \hat{\rho}_{\rm I}(t_i;t_i) = \hat{\rho}_{\rm S}(t_i;t_i)\,, \tag{2.23}$$

where the Heisenberg picture density matrix is time-independent. In the interaction picture, both the field and density operators are time-dependent.

2.4 Density matrix equations

The different pictures provide us with a toolbox to compute the time evolution of expectation values. In the Heisenberg and interaction pictures, we will now derive a quantum generalization of the Boltzmann equation for Dirac neutrinos that has the power to account for quantum statistics, collisions, and coherences between spins and flavors consistently. Our object of interest will be the expectation value of bilinears of creation/annihilation operators. In this formalism, the evolution of each momentum mode will be described by a square matrix, whose dimensions are determined by the number of discrete degrees of freedom. Conventional number densities will be given by the diagonal entries and coherences naturally appear as the off-diagonal entries. The kinetic equation that pertains to this matrix is usually referred to as the density matrix equation; a convention we will pursue in the following as well. Note however that the described object is actually a matrix of number densities that is fundamentally different from the density matrices in Sec. 2.3. Despite our naming scheme, the distinction between the two will always be made clear by calling the object of Sec. 2.3 the "density matrix operator".

The derivation of the density matrix equation for neutrinos has been performed before in Ref. [26], which we will follow in this section. Additionally, we will keep track of helicity as has been done before in Refs. [85, 90, 123]. We follow through in some detail in order to familiarize the reader with intermediate steps and to facilitate the understanding of the more involved calculations in Chapter 4. We will omit the subscript H for the Heisenberg picture and unless otherwise stated, all quantities are to be understood in this picture.

The plane-wave decomposition of the Dirac neutrino field ψ can be written as

$$\psi_i(x) = \int \frac{\mathrm{d}^3\mathbf{p}}{(2\pi)^3} \sum_s \left[a_{i,s}(t,\mathbf{p}) u_{i,s}(\mathbf{p}) e^{i\mathbf{p}\cdot\mathbf{x}} + b^\dagger_{i,s}(t,\mathbf{p}) v_{i,s}(\mathbf{p}) e^{-i\mathbf{p}\cdot\mathbf{x}} \right] . \tag{2.24}$$

Here, $a_{i,s}(t,\mathbf{p})$ is again an annihilation operator: it removes a neutrino of flavor i with helicity s and momentum $\mathbf{p}$ from a given state. In the same way, $b^\dagger_{i,s}(t,\mathbf{p})$ is an antineutrino creation operator. It produces an excitation of flavor i with momentum $\mathbf{p}$ and the opposite helicity $-s$. The bispinors u, v carry the properties of the field under Lorentz boosts.

The field defined in Eq. (2.24) has various important properties. For a free field Lagrangian, ψ fulfills the free Klein-Gordon equation and, being a fermion, the Dirac equation

$$\begin{aligned} (\Box + m_i^2)\psi_i &= 0 \,, \\ (i\partial\!\!\!/ - m_i)\psi_i &= 0 \,, \end{aligned} \tag{2.25}$$

where $\Box = \partial^\mu \partial_\mu$, m_i is a neutrino mass eigenvalue with $i \in 1, 2, 3$ and $\partial\!\!\!/ = \gamma^\mu \partial_\mu$ is the contraction of the four-derivative with the Dirac matrices (see Appendix A.3). From these equations it follows that also u_i fulfills

$$(p\!\!\!/ - m_i) u_i(\mathbf{p}) = 0 \,. \tag{2.26}$$

We will choose a chiral representation for the bispinors (see Appendix A.3). In the presence of interactions a source term might be added on the right-hand side of Eq. (2.25).

Finally, we need the equal-time anticommutation relations for the creation/annihilation operators:

$$\{a_{i,s}(t,\mathbf{p}), a^\dagger_{j,h}(t,\mathbf{k})\} = \{b_{i,s}(t,\mathbf{p}), b^\dagger_{j,h}(t,\mathbf{k})\} = (2\pi)^3 \delta_{ij} \delta_{sh} \delta^{(3)}(\mathbf{p}-\mathbf{k}) \,. \tag{2.27}$$

All other anticommutators vanish.

We are now able to define the main object of this section, the density matrices ρ for neutrinos and $\bar{\rho}$ for antineutrinos

$$\langle a^\dagger_{j,h}(t,\mathbf{k}) a_{i,s}(t,\mathbf{p}) \rangle \equiv (2\pi)^3 \delta^{(3)}(\mathbf{p}-\mathbf{k}) \rho_{ij,sh}(t,\mathbf{p}) \,, \tag{2.28}$$

$$\langle b^\dagger_{i,s}(t,-\mathbf{k}) b_{j,h}(t,-\mathbf{p}) \rangle \equiv (2\pi)^3 \delta^{(3)}(\mathbf{p}-\mathbf{k}) \bar{\rho}_{ij,sh}(t,\mathbf{p}) \,. \tag{2.29}$$

The density matrices can be very large. Indeed, for the three usual neutrino flavors and two possible helicity states, these matrices have 36 complex-valued entries. Hermiticity of ρ reduces the number of parameters: the diagonals are real-valued and the off-diagonals are related through complex conjugation. The diagonals can therefore safely be interpreted as occupation numbers akin to the Boltzmann distribution functions. The crucial difference to the latter formalism are the off-diagonals, which now carry non-trivial phase information. They express coherence between different neutrino flavors and helicities. Although we refer to the indices i, j as "flavor", the above definition is actually basis covariant. The chosen sequence of indices in Eqs. (2.28) makes the matrices for neutrinos and antineutrinos transform in the same way under flavor rotations [26]. Finally, note that the Dirac delta functions in Eqs. (2.28) are a consequence of an

infinite quantization volume [26]. Physically, they correspond to the simple statement that a finite number density in an infinite space leads to an infinite amount of particles. This volume will always drop out of our calculations, and we will omit it in the following.

The bilinears chosen in Eqs. (2.28) are not the only possible combinations; in Chapter 4, we will study more exotic bilinears. For now, let us note that the off-diagonals of the density matrices violate energy conservation slightly because neutrinos have different masses. This energy non-conservation will have to be compensated by the background medium.

To find the time evolution of the density matrices, we define

$$\begin{aligned} \mathcal{D}_{ij}(t,\mathbf{p}) &= a_j^\dagger(t,\mathbf{p})a_i(t,\mathbf{p})\,, \\ \overline{\mathcal{D}}_{ij}(t,\mathbf{p}) &= b_i^\dagger(t,\mathbf{p})b_j(t,\mathbf{p})\,, \end{aligned} \tag{2.30}$$

where for simplicity we omitted the helicity index. These operators follow the Heisenberg equation of motion (2.18). Splitting the Hamiltonian into free $\hat{H}_0$ and interaction $\hat{H}_{\rm int}$ parts, we obtain

$$\dot{\mathcal{D}}_{ij}(t,\mathbf{p}) = i[\hat{H}_0(t),\mathcal{D}(t,\mathbf{p})]_{ij} + i[\hat{H}_{\rm int}(t),\mathcal{D}(t,\mathbf{p})]_{ij}\,. \tag{2.31}$$

Taking the expectation value on both sides, we can pull the time derivative out of the expectation value

$$\dot{\rho}_{ij}(t,\mathbf{p}) = i\langle[\hat{H}_0(t),\mathcal{D}(t,\mathbf{p})]\rangle_{ij} + i\langle[\hat{H}_{\rm int}(t),\mathcal{D}(t,\mathbf{p})]\rangle_{ij}\,. \tag{2.32}$$

This differential equation contains on the left-hand side the required time derivative of the matrix of densities. On the right-hand side we encounter a number of commutators, which involve $\mathcal{D}$ instead of ρ. Let us inspect the free part of the Hamiltonian first. In the mass basis, we expect $\hat{H}_0$ to be diagonal and to yield $\omega_{i,\mathbf{p}} = (\mathbf{p}^2 + m_i^2)^{1/2}$ when acting on a single-particle free state. In an arbitrary basis, the Hamiltonian will cease to be diagonal and read

$$\hat{H}_0(t) = \sum_{i,j}\int \frac{\mathrm{d}^3\mathbf{p}}{(2\pi)^3}\left[a_i^\dagger(t,\mathbf{p})\Omega_{ij}(\mathbf{p})a_j(t,\mathbf{p}) + b_i^\dagger(t,\mathbf{p})\Omega_{ij}(\mathbf{p})b_j(t,\mathbf{p})\right]\,, \tag{2.33}$$

where Ω denotes vacuum energy matrices with eigenvalues ω_i. By using the bilinear form of Eq. (2.33), the first commutator in Eq.(2.32) is evaluated straight-forwardly by rewriting the commutator as a sum of two anticommutators

$$[ab,cd] = a[b,cd] + [a,cd]b\,, \tag{2.34}$$

$$[ab,c] = a\{b,c\} - \{a,c\}\,, \tag{2.35}$$

which can be evaluated easily with the usual anticommutation relations (2.27).

Hence, we see from the anticommutation relations (2.27) that each time we evaluate the commutator, a pair of creation/annihilation operators vanishes. Evaluating the free part, we obtain

$$i\dot{\rho}_{ij}(t,\mathbf{p}) = [\Omega,\rho(t,\mathbf{p})]_{ij} - \langle[\hat{H}_{\rm int}(t),\mathcal{D}(t,\mathbf{p})]\rangle_{ij}\,, \tag{2.36}$$

where a minus sign appears during the reordering of the operators.

If the second term in Eq. (2.36) was in a bilinear form, we could proceed in the same way for both the interaction term as for the free Hamiltonian. However, in general the interaction term is more complicated, and we need to apply some approximation scheme for its evaluation. There are two ways to proceed. In Chapter 4, we will use the mean-field approximation to rewrite the interaction in a bilinear form. The mean-field approximation assumes that particles propagate in a mean classical background that can be pulled out of expectation values. This treatment is similar to the molecular chaos hypothesis we used in the Boltzmann approach; higher order correlations are split up into two-field correlators.

A more general approach that goes beyond the mean-field approximation was used in Ref. [26] and makes use of a perturbation series of the Heisenberg fields. For weak interactions, we can truncate the perturbation series of the operator ξ after the first order so that

$$\xi(t) = \xi_{\mathrm{I}}(t) + i\int_{t_i}^{t} \mathrm{d}t' [\hat{H}_{\mathrm{I,int}}(t-t'), \xi_{\mathrm{I}}(t)]\,, \tag{2.37}$$

where $\hat{H}_{\mathrm{I,int}}$ is the interaction picture representation of the interaction Hamiltonian. With this expression, Eq. (2.36) may be written as

$$\begin{aligned}\dot{\rho}_{ij}(t,\mathbf{p}) = &-i[\Omega, \rho(t,\mathbf{p})]_{ij} + i\langle[\hat{H}_{\mathrm{I,int}}(t), \mathcal{D}_{\mathrm{I}}(t,\mathbf{p})]\rangle_{ij} \\ &- \int_{t_i}^{t} \mathrm{d}t' \,\langle[\hat{H}_{\mathrm{I,int}}(t-t'), [\hat{H}_{\mathrm{I,int}}(t), \mathcal{D}_{\mathrm{I}}(t,\mathbf{p})]]\rangle_{ij}\,.\end{aligned} \tag{2.38}$$

We may see that neglecting higher order terms in Eq. (2.37) and conversely in the evolution equation of ρ is similar to the truncation of the BBGKY-hierarchy in the derivation of the Boltzmann equation. Higher order correlations that would appear in the next orders of perturbation theory are set to zero. Equation (2.38) still contains two insertions of the Hamiltonian in the second line. This corresponds to six creation/annihilation operators after the commutators have been evaluated. Assuming molecular chaos, these six-point correlators decompose into expectation values of bilinears.

Equation (2.38) still mixes Heisenberg picture and interaction picture operators, and we have to impose further approximations to close it. We approximate the last term, which gives the collisions, by separating different time scales. First of all, we assume that the time scale of a single interaction, or equivalently the inverse energy scale of a collision, is short compared to the overall evolution of the system and of ρ. This allows us to extend the time integration to infinity since the interaction will have stopped after a short time so the error we introduce is small. Moreover, for small coupling constants, $\mathcal{D}$ will not evolve drastically during a single interaction, and we set $\mathcal{D}_{\mathrm{I}} \approx \mathcal{D}$. If the system is Markovian, i.e., it does not have any memory of past interactions, we can use this approximation for every interaction, so that $\mathcal{D}_{\mathrm{I}} \approx \mathcal{D}$ holds for all times. Moreover, we set the interaction picture Hamiltonian equal to their Heisenberg picture counterparts to leading order.

With these approximations, the density matrix equation simplifies to

$$\begin{aligned}i\dot{\rho}_{ij}(t,\mathbf{p}) =&[\Omega, \rho(t,\mathbf{p})]_{ij} - \langle[\hat{H}_{\mathrm{int}}(t), \mathcal{D}(t,\mathbf{p})]\rangle_{ij} \\ &-i\frac{1}{2}\langle\int \mathrm{d}t' \,[\hat{H}_{\mathrm{int}}(t-t'), [\hat{H}_{\mathrm{int}}(t), \mathcal{D}(t,\mathbf{p})]]\rangle_{ij}\,,\end{aligned} \tag{2.39}$$

where we restored energy conservations by extending the time integral to minus infinity using the identity for the Heaviside step-function:

$$\theta(x) = \frac{1}{2}\int \mathrm{d}s\, e^{2\pi s}\left(\delta(s) - \frac{i}{\pi}\mathcal{P}\frac{1}{s}\right) . \tag{2.40}$$

The principal value term $\mathcal{P}(1/s)$ gives a correction to the dispersion relation and is usually neglected [26].

With Eq. (2.39) we now have a kinetic equation that consistently treats refraction and collisions. A great advantage of this equation over the Boltzmann equation is that we may consistently derive the quantum mechanical collision term from the interaction Hamiltonian.

2.5 Closed-time-path formalism and Kadanoff-Baym equations

The derivation of the density matrix equation in Eq. (2.39) required a substantial number of approximations. Especially, we identified the fields in the Heisenberg and interaction pictures to close the density matrix equation, i.e., we assumed very weak interactions so that our degrees of freedom are almost free-streaming particles. If the environment is very dense or if the interactions are strong, we do not know what the physical degrees of freedom are and this approximation will fail; we have to adopt a different approach. A rigorous treatment of non-equilibrium systems may be performed with the closed-time-path (Schwinger-Keldysh [91, 92]) formalism, which relies on the first principles of quantum field theory and statistical physics. We will show that the Boltzmann and the density matrix formalism can be obtained in limiting cases. This section will be helpful to understand Chapter 5, where we will compare the lepton asymmetry obtained within the Boltzmann, density matrix and Schwinger-Keldysh formalism.

The idea behind the following approach is that number densities are two-point functions, which contain two field operators. Alternatively, these two-point functions may be viewed as propagators or Green's functions. In scattering theory we have a powerful machinery to calculate such Green's functions in the form of the path integral formalism: Green's functions are given by derivatives of the partition function with respect to an external source. While in scattering theory the expectation values are with an *in*-state, i.e., infinitely in the past, from the right-hand side and an *out*-state from the left, the expectation values we are interested in are taken at equal time. Following the ansatz by Schwinger [91] (see also [92, 118, 124–128]), we can still write such an expectation value as a path integral. To show this we will restrict ourselves to the simpler scalar fields in the following.

Starting from

$$\mathcal{Z} = \langle \mathrm{in}|\mathrm{in}\rangle \,, \tag{2.41}$$

we may insert unity in the form of a complete eigenbasis at time t_f of the Heisenberg field $\Phi_{\mathrm{H}}(x)$

$$\mathbb{1} = \int \mathcal{D}\Phi\, |\Phi(\mathbf{x}), t_f; t_i\rangle\langle\Phi(\mathbf{x}), t_f; t_i| \,. \tag{2.42}$$

The product $\langle\Phi(\mathbf{x}), t_f; t_i|\mathrm{in}\rangle$ is just a path integral with $\Phi(x)$ as the boundary condition at time t_f. The other expectation value reads $\langle\mathrm{in}|\Phi(\mathbf{x}), t_f; t_i\rangle$, which propagates back in time. If we assume for now that this propagation is driven by an external source $J(x)$, which is different for the forward and backward time directions, the partition function becomes

$$\mathcal{Z}[J_a] = \int \mathcal{D}\Phi_a \exp\left[i\int_{t_i}^{t_f} \mathrm{d}t' \int \mathrm{d}^3\mathbf{x}\, \mathcal{L}[\Phi_a] + i\int_{t_i}^{t_f} \mathrm{d}t' \int \mathrm{d}^3\mathbf{x}\, J_a(x)\Phi^a(x)\right] , \tag{2.43}$$

where the index $a = \{1, 2\}$ tracks the different time directions via the metric $g_{ab} = \mathrm{diag}(1, -1)$. Note that paths forward and backward in time are connected through the boundary condition at t_f. However, the exact condition is integrated over. Due to this time path, this method is often referred to as the closed-time-path (CTP) technique.

In order to describe two-point functions, we introduce another bilocal source $K^{ab}(x, z)$, which adds a term $(1/2)\int \mathrm{d}^4x\mathrm{d}^4z\, K_{ab}(x, z)\Phi^a(x)\Phi^b(z)$ to the exponent of Eq. (2.43) [128]. If we wanted to describe higher order correlations, we would need a higher number of sources. In this thesis, we will however restrict ourselves to two-point functions. Neglecting higher order correlations can be justified by Gaussian initial conditions [118] or by a truncation scheme reminiscent of the BBGKY procedure. This truncation would then lead to dissipation [125].

Having introduced the source $K^{ab}(x, z)$, the connected two-point function G_{ab} may be defined via the following relations [128]

$$\frac{\delta\mathcal{W}[J, K]}{\delta J_a(x)} = \langle\Phi_a(x)\rangle \equiv \varphi_a, \quad \frac{\delta\mathcal{W}[J, K]}{\delta K_{ab}(x, z)} = \frac{1}{2}\left[\langle\Phi_a(x)\rangle\langle\Phi_b(z)\rangle + G_{ab}(x, z)\right] , \tag{2.44}$$

where $\mathcal{W} = -i\ln(\mathcal{Z})$ is the generating functional of connected Green's functions. Here, we defined the full propagator as a fluctuation around the classical field, which will later be set to zero, $\varphi \to 0$. We obtain the desired effective action Γ by performing a Legendre transformation with new variables φ and G

$$\Gamma[\varphi, G] = \mathcal{W}[J, K] - \int \mathrm{d}^4x\, \frac{\delta\mathcal{W}[J, K]}{\delta J_a(x)} J_a(x) - \int \mathrm{d}^4x\mathrm{d}^4y\, \frac{\delta\mathcal{W}[J, K]}{\delta K_{ab}(x, z)} K_{ab}(x, z) , \tag{2.45}$$

Additionally, Γ fulfills the stationarity conditions

$$\frac{\delta\Gamma[\varphi, G]}{\delta\varphi_a(x)} = -J_a(x) - \int \mathrm{d}^4z\, K_{ab}(x, z)\varphi^b(z) , \tag{2.46a}$$

$$\frac{\delta\Gamma[\varphi, G]}{\delta G_{ab}(x, z)} = -\frac{1}{2}K_{ab}(x, z) . \tag{2.46b}$$

The physical limit corresponds to vanishing sources, and we see that Eq. (2.46) provides equations of motion for the classical field φ and the connected Green's function G. If we find an explicit expression for the effective action, we may use these equations of motion to compute the propagator.

The two-particle irreducible (2PI) effective action has been computed by Cornwall, Jackiw and Tomboulis in Ref. [129]. It reads

$$\Gamma[\varphi, G] = S[\varphi] + \frac{i}{2}\mathrm{Tr}\ln G^{-1} + \frac{i}{2}\mathrm{Tr}\left(G_0^{-1}[\varphi]G\right) + \Gamma_2[\varphi, G] + \mathrm{const} . \tag{2.47}$$

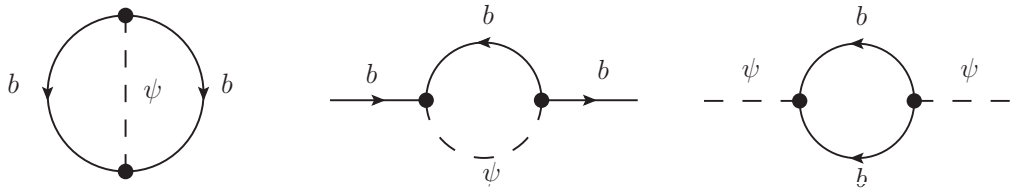

Figure 2.1: 2PI-diagram and the corresponding self-energies for the toy model of leptogenesis of Chapter 5. There the coupling between the real scalar ψ_i and the complex scalar b are of the form $h_i\psi^i bb + h_i^*\psi^i b^* b^*$.

Here, $S[\varphi]$ is the tree-level action, $iG_0^{-1} = \delta^2 S[\varphi]/(\delta\varphi_a\delta\varphi_b)$ is the inverse of the tree-level propagator, and $\Gamma_2[\varphi, G]$ is the contribution from all two-particle irreducible (2PI) diagrams, i.e., all diagrams that cannot be separated by cutting two-lines. Note that the propagators in the loops are the full propagators G [128], which will be important to obtain self-consistent equations of motion.

The equations of motion can now be obtained by plugging the explicit expression (2.47) into Eq. (2.46). We obtain the Schwinger-Dyson equation

$$G_{ab}^{-1}(x,z) = G_{0,ab}^{-1}(x,z) - \Pi_{ab}(x,z)\,, \tag{2.48}$$

where the self-energy $\Pi_{ab}(x,z)$ is given by [128]

$$\Pi_{ab}(x,z) \equiv 2i\frac{\delta\Gamma_2[\varphi,G]}{\delta G_{ab}(x,z)}\,. \tag{2.49}$$

Diagrammatically, this prescription corresponds to cutting one propagator in the 2PI-diagrams. Usually it is sufficient to approximate these diagrams as one-loop self-energies. Note that the self-energy in Eq. (2.48) is sometimes defined with a relative minus sign [130]. For the toy model of leptogenesis we use in Chapter 5, the two-loop diagrams and the corresponding one-loop self-energies are shown in Fig. 2.1.

We invert Eq. (2.48) by multiplying with $G(z,y)$ from the right and integrating over intermediate momenta. We will also need the tree-level propagator

$$G_{0,ab}^{-1}(x,y) = i\left(\Box_x + m^2\right)\delta^{(4)}(x-y)g_{ab}\,, \tag{2.50}$$

which is diagonal, i.e., it does not mix fields propagating forward and backward in time. With this expression, the inverted Schwinger-Dyson equation reads

$$i\left(\Box_x + m^2\right)G_{ab}(x,y) = \delta^{(4)}(x-y)\delta_{ab} + \int \mathrm{d}^4 z\,\Pi_{ac}(x,z)G^c{}_b(z,y)\,. \tag{2.51}$$

We have come a long way from rewriting the partition function into a closed time path to find a relation for the fully dressed propagators. Our original goal was to find kinetic equations for physical quantities like number densities. How does the CTP propagator relate to observables?

First note, that as soon as $\varphi \to 0$ the Green's functions are just the second functional derivative with respect to the external source J_a, which corresponds to the usual definition of the propagator.

Hence, $G^{11} = \langle \mathcal{T}\phi(x)\phi(y)\rangle \equiv G_{\rm FM}$ is just the time-ordered or Feynman propagator. $G^{22} = \langle \tilde{\mathcal{T}}\phi(x)\phi(y)\rangle \equiv G_{\rm D}$ on the other hand is the expectation value of two field operators with anti-time ordering $\tilde{\mathcal{T}}$. This propagator is sometimes referred to as the Dyson propagator [20]. We are led to write

$$G(x,y) = \begin{pmatrix} G_{\rm FM}(x,y) & G_<(x,y) \\ G_>(x,y) & G_{\rm D}(x,y) \end{pmatrix} , \tag{2.52}$$

with the positive ($G_>$) and negative ($G_<$) frequency Wightman propagators

$$\begin{aligned} G_>(x,y) &= \langle \phi(x)\phi(y)\rangle \, , \\ G_<(x,y) &= \langle \phi(y)\phi(x)\rangle \, . \end{aligned} \tag{2.53}$$

The Wightman propagators will be crucial for our further computations. We will also see that they carry kinetic information. For now, let us note that the expressions in the matrix of Eq. (2.52) are related: only two are independent, so we only need to track two of these propagators to obtain all the information:

$$G_{\rm FM}(x,y) = \theta(x^0-y^0)G_>(x,y) + \theta(y^0-x^0)G_<(x,y) \, , \tag{2.54a}$$
$$G_{\rm D}(x,y) = \theta(x^0-y^0)G_<(x,y) + \theta(y^0-x^0)G_>(x,y) \, . \tag{2.54b}$$

Moreover, it is useful to define the statistical (Hadamard) propagator $G_{\rm F}$ (not be confused with the Feynman propagator $G_{\rm FM}$), and the spectral function (or Jordan propagator) G_ρ:

$$G_{\rm F}(x,y) = \frac{1}{2}\left[G_>(x,y) + G_<(x,y)\right] = \frac{1}{2}\langle\{\phi(x),\phi(y)\}\rangle \, , \tag{2.55a}$$
$$G_\rho(x,y) = i\left[G_>(x,y) - G_<(x,y)\right] = i\langle[\phi(x),\phi(y)]\rangle \, . \tag{2.55b}$$

The naming scheme for these two propagators is in line with their physical meaning. We will see that the spectral function will tell us what the relevant excitations of the system are, while the statistical propagator contains the statistical or kinetic information. In equilibrium, these two functions are degenerate and we only have one degree of freedom. In non-equilibrium systems, both functions contain complimentary information. The CTP formalism naturally introduces these two degrees of freedom because each field might either live on the time path running forward or the time path backward in time. These two paths give different information because in non-equilibrium situations time translation invariance is broken.

Finally, we define the retarded and advanced propagators

$$G_{\rm R}(x,y) = \theta(x^0-y^0)G_\rho(x,y) \, , \tag{2.56a}$$
$$G_{\rm A}(x,y) = -\theta(y^0-x^0)G_\rho(x,y) \, , \tag{2.56b}$$

which, however, do not carry all the information of the system in contrast to the sets $G_{\rm F}, G_\rho$ or $G_<, G_>$.

The evolution equations for the Wightman propagators are the off-diagonals of Eq (2.51). These equations are called the Kadanoff-Baym equations and they read

$$i\left(\Box_x + m^2\right)G_{\gtrless} + i\int {\rm d}^4z\,\Pi_{\rm h}G_{\gtrless} + i\int {\rm d}^4z\,\Pi_{\gtrless}G_{\rm h} = \frac{1}{2}\int {\rm d}^4z\left[\Pi_{\gtrless}G_{\lessgtr} - \Pi_{\lessgtr}G_{\gtrless}\right] , \tag{2.57}$$

where we omitted the arguments, and defined the Hermitean parts of the self-energies and propagators as

$$G_{\rm h}(x,y) \equiv \frac{1}{2}\left(G_{\rm R}+G_{\rm A}\right) = \frac{1}{2}{\rm sign}(x^0-y^0)G_\rho(x,y)\,, \tag{2.58}$$

$$\Pi_{\rm h}(x,y) \equiv \frac{1}{2}\left(\Pi_{\rm R}+\Pi_{\rm A}\right) = \frac{1}{2}{\rm sign}(x^0-y^0)\Pi_\rho(x,y)\,. \tag{2.59}$$

The signum function arises from Eq. (2.56).

The terms in Eq. (2.57) can be understood in the following way: the right-hand side contains all the collisional information. The $\Pi_h G_{\gtrless}$ terms are corrections to the mass; they play a role when refraction is considered. Finally, the $\Pi_{\gtrless} G_{\rm h}$ introduces off-shell effects to the dispersion relation of the particle. We have seen similar terms in the density matrix formalism where we discarded a principal value term.

The Kadanoff-Baym equations (2.57) may be restated in terms of the statistical propagators and the spectral function [128]

$$\left(\Box_x + m^2\right) G_{\rm F}(x,y) = \int_{-\infty}^{y^0} {\rm d}^4 z\, \Pi_{\rm F}(x,z) G_\rho(z,y) - \int_{-\infty}^{x^0} {\rm d}^4 z\, \Pi_\rho(x,z) G_{\rm F}(z,y)\,, \tag{2.60}$$

$$\left(\Box_x + m^2\right) G_\rho(x,y) = -\int_{y^0}^{x^0} {\rm d}^4 z\, \Pi_\rho(x,z) G_\rho(z,y)\,, \tag{2.61}$$

where we would like to emphasize the arguments of the time integration.

2.5.1 Time scale separation and the Wigner transform

For typical out-of-equilibrium systems, we can introduce further approximations. As we have assumed in the derivation for the density matrix equations, microscopic time scales of individual interactions are much faster than the macroscopic evolution of the full system so that we may separate the physics related to these scales. It is useful to express the propagator in terms of center (X) and relative (r) coordinates

$$X^\mu = \frac{x^\mu + y^\mu}{2}\,, \quad r^\mu = x^\mu - y^\mu\,, \tag{2.62}$$

and the corresponding center (Q) and relative (q) momenta

$$Q^\mu = \frac{p^\mu + k^\mu}{2}\,, \quad q^\mu = p^\mu - k^\mu\,. \tag{2.63}$$

In equilibrium, all propagators are only functions of the relative coordinates r^μ due to time-translation invariance and homogeneity. Close to equilibrium any dependence on the center coordinates will be slow. We may make this manifest by taking the Fourier transform with respect to the relative coordinates, which extracts the fast dynamics. This transform is called a Wigner transform $G(X,Q)$ and is defined as

$$G(X,Q) \equiv \int_{-\infty}^{\infty} {\rm d}^4 r\, e^{iQ\cdot r} G(X,r)\,. \tag{2.64}$$

We would like to obtain the Kadanoff-Baym equations (2.57) in terms of the Wigner transform. A useful identity is

$$\int \mathrm{d}^4 r\, e^{iQ\cdot r} \int \mathrm{d}^4 z\, A(x,z)B(z,y) = e^{-i\diamond}\left[A(X,Q)\cdot B(X,Q)\right] , \tag{2.65}$$

with the diamond operator defined as

$$\diamond\,(A\cdot B) = \frac{1}{2}\left(\frac{\partial A}{\partial X^\mu}\frac{\partial B}{\partial Q_\mu} - \frac{\partial A}{\partial Q_\mu}\frac{\partial B}{\partial X^\mu}\right) . \tag{2.66}$$

Note that this definition is reminiscent of the Poisson bracket (2.3). The Kadanoff-Baym equations now become

$$i\left(\frac{1}{4}\partial_X^2 - Q^2 - iQ^\mu\partial_{X^\mu} + m^2\right) G_\gtrless = e^{-i\diamond}\left(-i\Pi_\mathrm{h} G_\gtrless - i\Pi_\gtrless G_\mathrm{h} + \frac{1}{2}\Pi_\gtrless G_\lessgtr - \frac{1}{2}\Pi_\lessgtr G_\gtrless\right) . \tag{2.67}$$

A complementary equation can be derived by inverting the Schwinger-Dyson equation (2.48) not from the right-hand side as done before but multiplying with the propagator from the left-hand side. Adding and subtracting these equations, we obtain the constraint and kinetic equations

$$\left(2Q^2 - \frac{1}{2}\partial_X^2\right) G_\gtrless = \left\{m^2, G_\gtrless\right\} + e^{-i\diamond}\left(\{\Pi_h, G_\gtrless\} + \{\Pi_\gtrless, G_\mathrm{h}\} + \frac{i}{2}[\Pi_>, G_<] + \frac{i}{2}[\Pi_<, G_>]\right) , \tag{2.68a}$$

$$2Q^\mu\partial_{X^\mu} G_\gtrless = -i\left[m^2, G_\gtrless\right] + e^{-i\diamond}\left(-i[\Pi_h, G_\gtrless] - i[\Pi_\gtrless, G_\mathrm{h}] + \frac{1}{2}\{\Pi_>, G_<\} - \frac{1}{2}\{\Pi_<, G_>\}\right) . \tag{2.68b}$$

Especially the kinetic equation (2.68b) will be used in the following to derive the Boltzmann equation and the density matrix equation. However, both equations have to be fulfilled for a physical solution of the kinetic equation. Note that although we have performed a Wigner transformation, the only further approximation we have introduced is that the mass m is constant in space and time. We have also kept the commutators of the self-energy and the mass with the Wightman propagators in expressions (2.68). The reason is that later on we will consider Π, m and G to be matrices in flavor space. For the propagators and self-energies, this notation is unambiguous and the equations generalize straight-forwardly. For matrix-valued masses, we will use sans-serif symbols M in the following. Single-valued physical masses are denoted by the expressions m and M.

2.5.2 Boltzmann limit

To obtain the Boltzmann limit, let us start by examining equilibrium solutions of the Kadanoff-Baym equations. This study will also shed light on the physical information contained in the propagators. The intuition obtained in this way may then be used to derive the Boltzmann equation. We will see that this equation is applicable close to equilibrium.

First note that the Wigner transform of the spectral function obeys the spectral sum rule [130]

$$\int \frac{\mathrm{d}Q_0}{2\pi}\, Q_0 G_\rho(X,Q) = i\,, \tag{2.69}$$

which can be derived from the canonical commutation relations of the field ϕ. Moreover, the Kubo-Martin-Schwinger (KMS) relation provides us with the equilibrium solution [94]

$$G_{>,\mathrm{eq}}(X,Q) = e^{\frac{Q_0}{T}} G_{<,\mathrm{eq}}(X,Q)\,, \tag{2.70}$$

where T is the temperature of the system.

Equilibrium is characterized by time-independence and homogeneity. Any derivative must vanish and the kinetic equations (2.68b) therefore reads

$$2Q^\mu \partial_{X^\mu} G_{\mathrm{eq},\gtrless} = 0\,. \tag{2.71}$$

For the constraint equations (2.68a), we approximate to lowest order in self-energies

$$\left(Q^2 - m^2\right) G_{\mathrm{eq},\gtrless} = 0\,, \tag{2.72}$$

which is just the on-shell dispersion relation in Fourier space for a Klein-Gordon field. To this order, the constraint equation, tells us that our degrees of freedom are just free fields. To the next order the dispersion relation is altered to give a Breit-Wigner shaped function [130].

In equilibrium, the conditions (2.69–2.72) are simultaneously solved by the following ansatz

$$G_{<,\mathrm{eq}} = 2\pi\,\mathrm{sign}(Q_0)\delta(Q^2 - m^2) n_{\mathrm{eq}}(Q_0)\,, \tag{2.73a}$$
$$G_{>,\mathrm{eq}} = 2\pi\,\mathrm{sign}(Q_0)\delta(Q^2 - m^2)[1 + n_{\mathrm{eq}}(Q_0)]\,, \tag{2.73b}$$

where $n_{\mathrm{eq}} = 1/[\exp(Q_0/T) - 1]$ is the Bose-Einstein distribution. This definition is consistent with the intuition that the spectral functions provide us with information about the particle content of the theory; it reads $G_\rho = i2\pi\,\mathrm{sign}(Q_0)\delta(Q^2 - m^2)$. We see that $G_{\gtrless}$ are proportional to G_ρ in this case. Imposing such a proportionality is called a Kadanoff-Baym ansatz.

If we now imagine an out-of-equilibrium system, we should expect that our solution close to equilibrium resembles the solutions of Eqs. (2.73). We will therefore make a Kadanoff-Baym ansatz, in which we replace n_{eq} by the out-of equilibrium distribution function $f(X_0, Q_0)$. For non-trivial dynamics, we have to find suitable approximations for the right-hand side of the kinetic equations (2.68b). First, we will apply the so called gradient expansion to lowest order, i.e. we expand $\exp(-i\diamond)$ in derivatives and neglect higher order derivatives. We will only retain the lowest order $\exp(-i\diamond) = 1$. This approximation is justified when the time scale associated with changes in the macroscopic system, which is given by ∂_X^{-1}, is large compared to the time scale of interactions ∂_Q. The diamond operator may be seen as the ratio of the two time-scales and will therefore be small [131]. From a different perspective, one could interpret an expansion of the diamond operator as an expansion with respect to couplings. The evolution of the macroscopic system is driven by interactions between fields in and out of equilibrium. Hence, any non-zero

derivative ∂_X corresponds to an additional dependence on coupling constants. Since the right-hand side of Eq. (2.68b) is already proportional to the self-energies, higher orders of the diamond operator correspond to greater powers of the coupling constant.

For the Boltzmann equation, we assume a one-flavor system. Then all commutators vanish and our kinetic equation reads

$$2Q^\mu \partial_{X^\mu} G_{\gtrless} = \Pi_> G_< - \Pi_< G_> \,. \tag{2.74}$$

Inserting our ansatz for the Wightman propagators and assuming a homogeneous system, we obtain for the time derivative of $f(X_0, Q_0)$

$$\partial_{X_0} f(X_0, Q_0) = \frac{\Pi_>}{2Q_0} f(X_0, Q_0) - \frac{\Pi_<}{2Q_0}[1 + f(X_0, Q_0)] \,. \tag{2.75}$$

This equation already starts to look like the Boltzmann equation with a gain and a loss term on the right-hand side. To proceed further, we have to specify the model to compute the self-energies. In Chapter 5, we will consider a model where a real scalar may decay into two complex scalars. In a *C*-symmetric medium and with one flavor of the real scalar, the self-energies read

$$\Pi_>(Q) = -|h|^2 \int \mathrm{d}\Pi_p \mathrm{d}\Pi_k \, (2\pi)^4 \delta^{(4)}(Q - p - k)[1 + n_{\mathrm{eq}}(p)][1 + n_{\mathrm{eq}}(k)] \,, \tag{2.76}$$

$$\Pi_<(Q) = -|h|^2 \int \mathrm{d}\Pi_p \mathrm{d}\Pi_k \, (2\pi)^4 \delta^{(4)}(Q - p - k) n_{\mathrm{eq}}(p) n_{\mathrm{eq}}(k) \,, \tag{2.77}$$

where h is the coupling constant, and the Bose-Einstein distributions arise from the equilibrium Wightman propagators of the complex scalars that form the background medium. We see that these self-energies together with Eq. (2.75) yield the expected Boltzmann equation.

2.5.3 Density matrix limit

We may equally derive the density matrix equation from the Kadanoff-Baym formalism. In order to obtain coherence, we need a system of at least two flavors, and in anticipation of Chapter 5 we will show here the derivation for two real scalars.

All the propagators and self-energies we have shown further above are now matrices, and the products of self-energies and propagators are generalized to matrix multiplications in a straightforward way. For matrix-valued Wightman propagators, the commutators in Eq. (2.68) do not vanish identically, and they will give us the oscillations between the two scalar flavors. For a solution of the constraint equations, we will neglect again any terms proportional to the self-energies. Moreover, we will assume that both scalars are almost mass-degenerate. If we approximate $m_1^2 + m_2^2 = 2m_1^2 = 2m_2^2 = 2\bar{m}^2$, the constraint equation (2.68a) reads

$$\left(Q^2 - \bar{m}^2\right) G^{ij}_{\gtrless} = 0 \,, \tag{2.78}$$

which states that all components of the Wightman propagators lie on the same shell $\delta(Q^2 - \bar{m}^2)$. Writing all equations for a single shell like this is referred to as the middle-shell[or single-shell approximation. We will compare results from the full Kadanoff-Baym equations to this approximations in Chapter 5.

Close to equilibrium, we may again make the ansatz (see Eqs. (2.73) and Ref. [132])

$$G^{ij}_{<} = 2\pi \,\mathrm{sign}(Q_0)\delta(Q^2 - \bar{m}^2)\rho^{ij}(Q_0)\,, \tag{2.79a}$$

$$G^{ij}_{>} = 2\pi \,\mathrm{sign}(Q_0)\delta(Q^2 - \bar{m}^2)\left[\delta^{ij} + \rho^{ij}(Q_0)\right]\,. \tag{2.79b}$$

Inserting these expressions into the kinetic equations, integrating over the mass shells and performing the gradient expansion to leading order, we obtain

$$i\dot{\rho} = \frac{1}{2Q_0}\left[\mathsf{M}^2 + \Pi_\mathrm{h}, \rho\right] + i\left(\frac{1}{4Q_0}\left\{\Pi_>, \rho\right\} - \frac{1}{4Q_0}\left\{\Pi_<, \mathbb{1} + \rho\right\}\right)\,. \tag{2.80}$$

Here, we have neglected the commutator $[\Pi_\gtrless, G_\mathrm{h}]$ since the self-energies are already proportional to the coupling, and a tree-level G_h is diagonal [132]; this commutator is consequently suppressed by another factor of Δm^2.

For a comparison with Eq. (2.36), note that the first term in Eq. (2.80) can be brought to leading order into the standard form by writing $\Delta m^2/(2Q_0) \approx \Delta\omega$, which is true for a quasi-degenerate spectrum. The Π_h can be viewed as medium corrections to the particle masses and hence modifies the oscillation term. The anticommutator terms on the right-hand side are the usual collision terms, which exhibit the anticipated form of gain and loss terms. The exact form of these terms will again depend on the model in question.

Chapter 3

Separation of scales in ALP-photon oscillations

Photons that propagate through extragalactic space are attenuated by pair creation on the extragalactic background light. We study oscillations between photons and axion-like particles (ALPs) that may occur in the extragalactic magnetic fields and shield the photons from this absorption. The ALP-photon system may be readily described within the density matrix formalism, which takes into account the different contributions to the dispersion, mixing, and absorption. In contrast to previous works we concentrate on the non-maximal mixing regime, which is inevitably obtained for GeV–TeV photon energies due to a recently discovered contribution to the photon dispersion from forward-scattering on CMB photons. The refraction on the CMB suppresses the oscillation length of the ALP-photon system to typically assumed coherence lengths of the magnetic field. Previously, extragalactic magnetic fields were modeled to have a grid-like domain structure and discontinuous magnetic fields at the domain borders. We show that these assumptions have to be discarded when the oscillation length and coherence length become similar. For very high energies the propagation of the photon-ALP system becomes quasi-adiabatic and resolves the inhomogeneities of the magnetic field. We present numerical and analytical results.[1]

3.1 Introduction: transparency problem of the universe

When black holes accrete matter from surrounding gas clouds, large amounts of energy are emitted. These active galactic nuclei (AGNs) generate photons with GeV–TeV energies in jets, and the object is called a blazar if the jet points towards Earth. Photons that are emitted from AGNs propagate enormous distances through space which is filled with infrared dust emission and starlight; the extragalactic background light (EBL). The gamma rays from blazars undergo pair creation on this background light and therefore some signal is lost. Cherenkov telescopes have to correct their measured energy spectra for this absorption if they want to infer the spectrum of sources. A precise knowledge of the absorption rate is required.

The energy density of the EBL that determines this absorption rate is however only poorly known: direct measurements are difficult to obtain because of foreground pollution from surrounding stars and dust, lower bounds have been obtained by counting known galaxies [133], and upper limits can be obtained from constraining the maximal absorption on well-understood

[1] This chapter is based on the manuscript "Separation of scales in ALP-photon oscillations," [1] which is currently prepared for publication by A. Kartavtsev, G. Raffelt and myself.

sources. These upper limits have come suspiciously close [134–141] to the strict lower limit from galaxy counts even conflicting direct EBL measurements like those from Ref. [142]. This low power in the EBL is called the transparency problem of the universe. It has led to several findings of hard blazar spectra which are difficult to explain within astrophysical models [143–147]; although not without controversy [148, 149]. Especially in a publication by Meyer and Horns [150], it was claimed that there is a pair production anomaly that calls for non-standard mechanisms.

Such a mechanism might be present if axion-like particles (ALPs) exist (see e.g. Ref. [56] and Refs. [151–154] for alternatives). Axion-like particles derive their name from the QCD axion [38–41] as they possess the same type of interactions with two photons: they couple to the product of electric and magnetic field $\mathbf{E} \cdot \mathbf{B}$ with a coupling strength $g_{a\gamma}$. This means that in a magnetic field, ALPs mix with photons, i.e., magnetic fields instigate conversions from photon into ALPs and vice versa. In contrast to axions, the mass m_a and coupling constant $g_{a\gamma}$ of ALPs are unrelated so that for a given mass the coupling $g_{a\gamma}$ for ALPs may be larger than for axions permitting more efficient conversions.

The ALP-photon coupling allows for the following mechanism. Photons convert to ALPs in the magnetic fields of our galaxy [155], in the source itself [156–162], in clusters [163–165] and/or in extragalactic space [57, 162]. The power transferred to ALPs is protected from absorption because ALPs typically interact much more weakly than photons [54]. The ALPs freely propagate. Naïvely this would lead to a dimming of TeV sources. However, photons may be regenerated from back conversions in the magnetic field of our galaxy or in the magnetic field close to it, thereby enhancing the signal of TeV sources and leading to an apparently more transparent universe. This mechanism has been successfully applied to individual sources [56, 166], but it has also been used to constrain some of the parameters space [167, 168]. The upcoming Cherenkov Telescope Array (CTA) will enable us to test this mechanism [169].

In this chapter, we are concerned with ALP-photon conversion in extragalactic magnetic fields, which typically contain very weak magnetic fields $B \lesssim 10^{-9}\,\mathrm{G}$ [53]. The propagation of the photon-ALP system may be described within the density matrix formalism with photon and ALP number densities on the diagonals of the matrix of densities and their coherence on the off-diagonals [170].

A maximal mixing angle is crucial to obtain a sufficiently transparent universe [56, 57]. The mixing angle depends on the ratio of the off-diagonal entries of the Hamiltonian matrix to the diagonal entries. For a simplified mixing of ALPs with one photon polarization with energy ω the 2×2 mixing matrix reads

$$\mathsf{H} = \begin{pmatrix} \Delta_\gamma & \frac{g_{a\gamma} B_\mathrm{T}}{2} \\ \frac{g_{a\gamma} B_\mathrm{T}}{2} & -\frac{m_a^2}{2\omega} \end{pmatrix} , \tag{3.1}$$

where B_T is the magnetic field transversal to the direction of motion. The photon dispersion Δ_γ was thought to obtain contributions from background magnetic fields and forward scattering on free electrons; both of which are small compared to $g_{a\gamma} B_\mathrm{T}/2$ for GeV–TeV energies leading to a large mixing angle.

However, a crucial contribution to the dispersion has been missed in previous works: photons undergo forward scattering on CMB photons [59]. Since the energy density of the CMB photons

is huge, this dispersion is sizable. It grows linearly with energy and dominates the entries of the Hamiltonian matrix for $\omega \gtrsim 1\,\mathrm{TeV}$ and maximal extragalactic magnetic fields $B \lesssim 10^{-9}\,\mathrm{G}$ [53]. Previously, for every mass m_a, there was an energy for which the off-diagonals dominated H and the mixing became maximal. This statement does not hold anymore due to the CMB refraction: the mixing angle is suppressed for TeV energies. As we will show in this chapter, this suppression leads to quantitatively and qualitatively modified results for ALP-photon propagation in extragalactic magnetic fields.

If we knew the exact magnetic field structure on the line of sight from Earth to the source, we could compute the number of photons and ALPs that are expected at Earth by inserting the functional structure of the magnetic field into the density matrix equation. However, this structure is not known and we only have some rough ideas about the typical scales of galactic and extragalactic magnetic fields. From Faraday rotation measurements, it was inferred that typical magnetic fields in galaxies are of the order of $10\,\mu\mathrm{G}$ with coherence length of several tens of kpc [171]. Coherent magnetic fields in clusters spread over distances up to a Mpc with field strength below $1\,\mu\mathrm{G}$. Magnetic fields with the largest coherence lengths can be found in extragalactic space, but so far only lower limits $B > 10^{-18}\,\mathrm{G}$ from time delays of cascade radiation [172] and upper limits on, e.g., primordial magnetic fields $B < 10^{-9}\,\mathrm{G}$ [173] have been found (see Ref. [53] and references therein). Their coherence scale is bounded only by the current Hubble horizon [53]. Realistic models with magnetic fields generated by quasar outflows may be found in Ref. [52], which predicts $B \sim 10^{-9}\,\mathrm{G}$ and coherence lengths of several Mpc. For numerically simulated magnetic field distributions see Refs. [174, 175].

Although exact computations for individual sources are not possible, we may obtain predictions for an ensemble of blazar spectra, if we assume statistical properties for the extragalactic magnetic field. From this statistical distribution we may draw a large number of different magnetic field configurations and compute the exact evolution for each of these magnetic fields. Statistical information about the photon and ALP transfer functions could then be extracted. This Monte-Carlo method [176, 177] has been readily applied in the literature. It will be called "simulations" in the following.

Simulations are computationally demanding. A different approach was adopted by Mirizzi and Montanino [178]. They demonstrated that the mean and variances of the transfer functions could be computed with a set of coupled differential equations that are much easier to apply than simulations. These equations were derived for a maximal mixing angle and special assumptions about the magnetic field structure: the magnetic field was assumed to be grid-like with constant domain size, constant absolute value of the magnetic field strength, but sudden changes of the magnetic field direction at the borders of the domains. These assumptions for the magnetic field are identical to those that are usually assumed in simulations and agree well with the result obtained with the Monte-Carlo method [178].

Due to the refraction on the CMB, these assumptions have to be reexamined. In extragalactic space, maximal mixing is only a good approximations for photon energies up to $100\,\mathrm{GeV}$. For larger energies, the mixing angle is suppressed and the differential equation approach by Mirizzi and Montanino [178] cannot be applied naïvely anymore. We will show however that their formalism can be extended straight-forwardly to non-maximal mixing as well.

A more serious concern pertains to the magnetic field structure with constant domain size

and discontinuous magnetic fields at the boundaries ("hard edges"). The CMB refraction suppresses the oscillation length of the ALP-photon system, which now decreases with energy: $l_{\rm osc} \approx 78.5(\mathrm{TeV}/\omega)\,\mathrm{Mpc}$. If we assume a domain size of the magnetic field of the order of $l_{\rm c} = 10\,\mathrm{Mpc}$, which has been applied in Ref. [58], we see that $l_{\rm osc} \approx l_{\rm c}$ for photon energies of the order of $\omega \approx 10\,\mathrm{TeV}$. At this energy scale the ALP-photon system is able to probe the magnetic field structure in more detail.

Domains with hard edges lead to unphysical resonances when the two lengths scales becomes of similar size. The reason is that in one domain the ALP-photon system oscillates by approximately 2π, i.e., the conversion probability is close to zero. Since the domain size is assumed to be identical for every domain, this statement holds true in every domain, and oscillations into ALPs are strongly suppressed. This resonant behavior can be mended by introducing fluctuations in the domain sizes. We will show that the ALP-photon system becomes sensitive to the exact probability distribution of the domain sizes already before $l_{\rm osc} \approx l_{\rm c}$, i.e., a constant domain size has to be discarded once $l_{\rm osc}$ approaches $l_{\rm c}$.

When $l_{\rm osc} \gtrsim l_{\rm c}$, the ALP-photon evolution becomes not only quantitatively but also qualitatively different. The oscillations in the ALP-photon system are so fast that changes in the magnetic field structure are probed, i.e., the boundary between two domains cannot be assumed to be discontinuous anymore but more physical continuous transitions have to be modeled. We show analytically and numerically that in this regime the photon evolution becomes quasi-adiabatic: the transfer function is sensitive to the initial and final configurations of the magnetic field and to the absorption of ALPs due to back-reactions into photons.

The importance of the structure of the magnetic field has been mentioned in a recent paper by Wang and Lai [179]. They find that the photon transfer function depends on the structure of the magnetic field. We believe, however, that their approach is misleading because they do not compare magnetic field structures that are equivalent in the maximal mixing regime. Here, the oscillation length is much larger than the typical scale of variation and the ALP-photon system should not be able to see the magnetic field structure. We will comment on their findings in the main part of this chapter.

Although we neglect redshift in the following and although the parameters for the magnetic fields and the EBL are only semi-realistic, our arguments are of principle nature: for a given distribution of magnetic field strengths and coherence lengths, non-maximal mixing and quasi-adiabaticity will be qualitatively and quantitatively important for large energies or large ALP masses.

Note that the refraction on the CMB is only important for propagation in extragalactic space. In laboratory experiments [46, 49, 51, 180, 181], typical magnetic fields are much larger than in extragalactic space. With magnetic fields of several Tesla that are homogeneous over several meters, the mixing angle is maximal and the conversion probability is still proportional to $B^2 l^2$ where l is the spatial extent of the magnetic field.

This chapter has the following structure: in the next section 3.2 we take a look at the Hamiltonian matrix that describes ALP-photon oscillations. We present the entries of this matrix, their numerical values and parametrical dependencies. These values will be used to discuss the physical implications of CMB refraction, i.e., non-maximal mixing and a suppressed oscillation length in Sec. 3.3. We will see that maximal mixing cannot be obtained for large energies

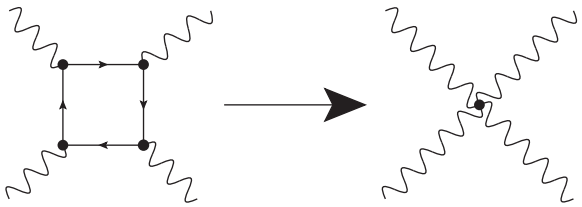

Figure 3.1: Origin of the Euler-Heisenberg term in the Lagrangian (3.2)*. The electron loop is integrated out to an effective four-photon vertex.*

which motivates us to adopt the formalism of Mirizzi and Montanino to non-maximal mixing in Sec. 3.4. This is followed by numerical results in Sec. 3.5 that show the unnatural resonance between oscillation length and coherence length of the magnetic field when hard edges are assumed. Noticing that the magnetic field structure is resolved by the ALP-photon system, we study analytically and numerically the mean photon and ALP transfer functions for continuous magnetic field distributions (Sec. 3.6). We conclude in Sec. 3.7.

3.2 The Hamiltonian matrix of ALP-photon conversion

Let us consider the propagation of photons and ALPs with energy ω in a background of a magnetic field. The effective Lagrange density of these two particles reads

$$\begin{aligned}\mathcal{L}_{\mathrm{ALP}} =& \frac{1}{2}\left(\partial_\mu a \partial^\mu a - m_a^2 a^2\right) - \frac{1}{4}F^{\mu\nu}F_{\mu\nu} - \frac{g_{a\gamma}}{4}aF^{\mu\nu}\tilde{F}_{\mu\nu} \\ &+ \frac{\alpha^2}{90 m_e^4}\left[\left(F_{\mu\nu}F^{\mu\nu}\right)^2 + \frac{7}{4}\left(F_{\mu\nu}\tilde{F}^{\mu\nu}\right)^2\right],\end{aligned} \tag{3.2}$$

with the ALP field a, its mass m_a, the photon field strength tensor $F^{\mu\nu}$ and its dual $\tilde{F}^{\mu\nu}$, and the ALP-photon coupling constant $g_{a\gamma}$. The term $-\frac{g_{a\gamma}}{4}aF^{\mu\nu}\tilde{F}_{\mu\nu} = g_{a\gamma}a\mathbf{E}\cdot\mathbf{B}$ induces the mixing between ALPs and photons with a polarization parallel to a background magnetic field. The last term in Eq. (3.2) is the Euler-Heisenberg coupling [60] of four photons via an electron loop, which contains the fine structure constant α and the electron mass m_e (see Fig. 3.1).

From this Lagrangian we may derive the equations of motion. For propagation in z-direction we obtain

$$\left(\partial_t^2 - \partial_z^2\right)\mathbf{A} + \mathsf{M}_{\mathrm{eff}}^2\mathbf{A} = 0\,, \tag{3.3}$$

where $\mathbf{A}$ is the three-component wave function

$$\mathbf{A} \equiv \begin{pmatrix} A_x \\ A_y \\ a \end{pmatrix}, \tag{3.4}$$

with the linear photon polarizations A_x and A_y in the x and y-direction respectively. The ALP is contained in the third component, again denoted by a. $\mathsf{M}_{\mathrm{eff}}^2$ is the effective mass matrix that

takes into account refraction on the background medium. In vacuum this matrix reads $\mathsf{M}^2_{\rm vac} = \mathrm{diag}\left(0, 0, m_a^2\right)$. In the extragalactic medium the effective mass matrix squared depends on the choice of the reference frame for the photon polarizations because refraction and mixing depend on the relative alignment with the background magnetic field.

If we choose $A_x = A_\perp$ and $A_y = A_\parallel$ relative to the magnetic field, $\mathsf{M}^2_{\rm eff}$ takes the form

$$\mathsf{M}^2_{\rm eff} = \begin{pmatrix} Q_\perp & Q_{\rm R} & 0 \\ Q_{\rm R} & Q_\parallel & Q_{a\gamma} \\ 0 & Q_{a\gamma} & m_a^2 \end{pmatrix} , \tag{3.5}$$

with complex mass parameters to account for absorption on the background. Here, $Q_{\perp,\parallel} = 2\omega^2(n^{\perp,\parallel}_{\rm refr} - 1)$ are related to the index of refraction, $Q_{\rm R}$ is the contribution from Faraday rotation and $Q_{a\gamma}$ is the mixing between photons and ALPs.

Before we give explicit expressions for the masses and mixings let us reduce the second order differential equation (3.3) to first order, using the small wavelength approximation [170]. In momentum space, the derivatives may be rewritten as $(\omega - k_z)(\omega + k_z)$. If the effective masses are small compared to the energy, the momentum k_z and ω will be approximately equal: $(\omega - k_z)(\omega + k_z) \approx 2\omega(\omega - k_z)$. The crucial dynamics is contained in the difference between the energy and the momentum of both photons and ALPs.

Dividing by 2ω, we may take the partial Fourier transform of the z-direction to obtain the evolution equation [170, 182]

$$i\partial_z \mathbf{A} = \left(\mathsf{H}_{\rm dis} - i\mathsf{H}_{\rm abs}\right)\mathbf{A} , \tag{3.6}$$

where $\mathsf{H}_{\rm dis}$ is a Hermitian matrix that contains the dispersion, and $\mathsf{H}_{\rm abs}$ is Hermitian and contains the absorption. Both of these matrices are derived from the Hamiltonian of the system and will be called Hamiltonian matrices in the following. In Eq. (3.6) we discarded a term proportional to ω because it describes phase oscillations that are identical for all photon polarizations and the ALP: it cancels out in the calculation of actual particle numbers.

If we assume that the EBL is isotropic, the absorptive Hamiltonian matrix reads

$$\mathsf{H}_{\rm abs} = \begin{pmatrix} \Gamma_\gamma/2 & 0 & 0 \\ 0 & \Gamma_\gamma/2 & 0 \\ 0 & 0 & 0 \end{pmatrix} . \tag{3.7}$$

Note that we have neglected a direct absorption of ALPs which is proportional to the square of the small coupling $g_{a\gamma}$. Nevertheless, absorption will be translated to the ALP sector once we take into account the mixing and the corresponding misalignment between interaction and propagation eigenstates.

For high-energy photons, the main source of absorption is due to the pair creation process $\gamma\gamma_{\rm bkg} \to e^+e^-$. The absorption rate is given by [178]

$$\Gamma_\gamma(\omega) = \int_{m_e^2/\omega}^{\infty} \mathrm{d}\epsilon \frac{\mathrm{d}n_{\gamma,\rm bkg}}{\mathrm{d}\epsilon} \int_{-1}^{1-\frac{2m_e^2}{\omega\epsilon}} \mathrm{d}\xi \, \frac{1-\xi}{2} \sigma_{\gamma\gamma}(\beta) , \tag{3.8a}$$

$$\sigma_{\gamma\gamma}(\beta) = \sigma_0 \cdot (1-\beta^2)\left[2\beta(\beta^2-2) + (3-\beta^4)\log\frac{1+\beta}{1-\beta}\right] , \tag{3.8b}$$

where [183] $\sigma_0 = 3\sigma_T/16 \approx 1.25 \times 10^{-25}\,\mathrm{cm}^2$ with the Thomson cross section σ_T, ϵ is the background photon energy, ξ is the cosine of the angle between the incident and the background photon, and $\beta = [1 - 4m_e^2/s]^{\frac{1}{2}}$ with $s = 2\omega\epsilon(1-\xi)$ is the electron velocity in the center of mass frame. To obtain the optical depth, the absorption rate has to be integrated over the distance or, equivalently, redshift. To date, blazars are observed at redshifts of maximally $z \approx 0.944$ [184] for which the redshift dependence of energies, densities and magnetic fields have to be taken into account. Nevertheless, we will neglect redshift in the following since our goal is a conceptual one that is merely clouded by this additional layer of complication. For our purposes, the optical depth is just the average absorption rate times the distance to the source.

For definiteness[2], we approximate the number density at $z = 0$ through [187]

$$\frac{\mathrm{d}n_{\gamma,\mathrm{bkg}}(\epsilon)}{\mathrm{d}\epsilon} \approx 10^{-3}\left(\frac{\epsilon}{1\,\mathrm{eV}}\right)^{-2.55}\,\mathrm{cm}^{-3}\,\mathrm{eV}^{-1}\,, \tag{3.9}$$

which leads to an absorption coefficient [178]

$$\Gamma_\gamma(\omega) \approx 1.1 \times 10^{-3}\left(\frac{\omega}{\mathrm{TeV}}\right)^{1.55}\,\mathrm{Mpc}^{-1}\,. \tag{3.10}$$

The dispersive part of the Hamiltonian matrix contains the refraction of photons, the mass of the ALPs and the mixing between ALPs and photons. If we again choose the reference frame such that $A_x = A_\perp$ and $A_y = A_\parallel$, the dispersive Hamiltonian reads

$$\mathsf{H}_{\mathrm{dis}} = \begin{pmatrix} \Delta_\perp & \Delta_\mathrm{R} & 0 \\ \Delta_\mathrm{R} & \Delta_\parallel & \Delta_{a\gamma} \\ 0 & \Delta_{a\gamma} & \Delta_a \end{pmatrix}\,, \tag{3.11}$$

where $\Delta_a = -m_a^2/(2\omega)$ is the dispersion caused by the ALP mass (see Tab. 3.1 for numerical values). Photon-ALP mixing is induced by the magnetic field $\mathbf{B}$ through

$$\Delta_{a\gamma} = \frac{g_{a\gamma}}{2} B \sin\theta \approx 1.5 \times 10^{-2}\sin\theta\left(\frac{g_{a\gamma}}{10^{-11}\,\mathrm{GeV}^{-1}}\right)\left(\frac{B}{\mathrm{nG}}\right)\,\mathrm{Mpc}^{-1}\,, \tag{3.12}$$

where $B = |\mathbf{B}|$, and θ is the angle between the magnetic field and the z-direction. This shows that magnetic fields that are parallel to the direction of motion do not contribute. Only the projection of the magnetic field that is perpendicular to the direction of motion mixes photons and ALPs.

We will assume that the ALP-photon coupling constant is $g_{a\gamma} = 10^{-11}\,\mathrm{GeV}^{-1}$ in the following; a value still close to the upper bound $< 8.8 \times 10^{-11}\,\mathrm{GeV}^{-1}$ from CAST [49]. For ultralight ALPs $m_a < 4.4 \times 10^{-10}\,\mathrm{eV}$, this coupling strength is excluded by gamma-ray limits from SN1987a, $g_{a\gamma} < 5.3 \times 10^{-12}\,\mathrm{GeV}^{-1}$ [188].

[2]Note that this model for the absorption rate, which is also approximately found in Ref. [185], is observationally disfavored [136] and a useful alternative is given, e.g., in Ref. [183]. We thank Marco Roncadelli for pointing this out. Despite this, we will still use the formulas of Mirizzi and Montanino [178] to obtain the qualitative features. Thereby, we underestimate the strength of absorption compared to Ref. [183] where the spectral index is probably closer to -1.85 [186].

Contributions to H	Numerical value [Mpc^{-1}]
$\Delta_{\rm CMB}$	$8\times10^{-2}\left(\frac{\omega}{\rm TeV}\right)$
$\Gamma_\gamma/2$	$5.5\times10^{-4}\left(\frac{\omega}{\rm TeV}\right)^{1.55}$
Δ_a	$-7.8\times10^{-2}\left(\frac{m_a}{10^{-9}\,\rm eV}\right)^2\left(\frac{\rm TeV}{\omega}\right)$
$\Delta_{a\gamma}$	$1.5\times10^{-2}\sin\theta\left(\frac{g_{a\gamma}}{10^{-11}\,\rm GeV^{-1}}\right)\left(\frac{B}{\rm nG}\right)$
$\Delta_{\rm B}$	$4.1\times10^{-9}\sin^2\theta\left(\frac{\omega}{\rm TeV}\right)\left(\frac{B}{\rm nG}\right)^2$
$\Delta_{\rm pl}$	$-1.1\times10^{-11}\left(\frac{\rm TeV}{\omega}\right)\left(\frac{n_e}{10^{-7}\,\rm cm^{-3}}\right)$
$\Delta_{\rm R}$	$-2.2\times10^{-34}\cos\theta\left(\frac{\rm TeV}{\omega}\right)^2\left(\frac{B}{\rm nG}\right)\left(\frac{n_e}{10^{-7}\,\rm cm^{-3}}\right)$

Table 3.1: Numerical values for the various contributions to the Hamiltonian matrix H*: refraction on the CMB ($\Delta_{\rm CMB}$), inverse absorption length $\Gamma_\gamma/2$, the axion mass dispersion (Δ_a), ALP-photon mixing ($\Delta_{a\gamma}$), birefringence through a magnetic field ($\Delta_{\rm B}$), coherent scattering on the electron plasma ($\Delta_{\rm pl}$), and Faraday rotation ($\Delta_{\rm R}$).*

The other off-diagonals come from Faraday rotation. They read [17]

$$\Delta_{\rm R}=-\frac{\omega_{\rm pl}^2\omega_{\rm g}}{\omega^2}\cos\theta\approx2.2\times10^{-34}\cos\theta\left(\frac{\rm TeV}{\omega}\right)^2\left(\frac{B}{\rm nG}\right)\left(\frac{n_e}{10^{-7}\,\rm cm^{-3}}\right)\,\rm Mpc^{-1}\,, \tag{3.13}$$

with the plasma frequency squared $\omega_{\rm pl}^2=4\pi\alpha n_e/m_e$ and the gyrofrequency $\omega_g=eB/(\gamma m_e)$ with the usual Lorentz transformation parameter $\gamma=E/m_e\approx1$ for non-relativistic electrons. We see that Faraday rotation is completely negligible and we will discard any contribution from the Faraday effect in the following.

The photon dispersions $\Delta_\perp$ and $\Delta_\parallel$ can be decomposed into three physically different contributions

$$\Delta_\perp=2\Delta_{\rm B}+\Delta_{\rm pl}+\Delta_{\rm CMB}\,, \tag{3.14a}$$
$$\Delta_\parallel=\tfrac{7}{2}\Delta_{\rm B}+\Delta_{\rm pl}+\Delta_{\rm CMB}\,, \tag{3.14b}$$

where, see e.g. Ref. [178],

$$\Delta_{\rm B}=\frac{\alpha\omega}{45\pi}\left(\frac{e|\mathbf{B}|\sin\theta}{m_e^2}\right)^2\approx4.1\times10^{-9}\sin^2\theta\left(\frac{\omega}{\rm TeV}\right)\left(\frac{B}{\rm nG}\right)^2\,\rm Mpc^{-1}\,, \tag{3.15}$$

$$\Delta_{\rm pl}=-\frac{2\pi\alpha n_e}{\omega m_e}\approx-1.1\times10^{-11}\left(\frac{\omega}{\rm TeV}\right)^{-1}\left(\frac{n_e}{10^{-7}\,\rm cm^{-3}}\right)\,\rm Mpc^{-1}\,, \tag{3.16}$$

are the birefringence induced by a background magnetic field ($\Delta_{\rm B}$) and the dispersion induced by coherent scattering on the background electrons ($\Delta_{\rm pl}$) with density n_e. This density is bounded

by the baryon number density of the universe to be $n_e < 2.7 \times 10^{-7}\,\mathrm{cm}^{-3}$, if one takes the cosmological parameters of PLANCK [189] and conservatively assumes that all baryons are free protons.

Another contribution that was found recently [59] comes from coherent scattering on the cosmic microwave background. The index of refraction induced by an electromagnetic background field $\delta n_{\mathrm{refr}} = \mathrm{Re}(n_{\mathrm{refr}} - 1)$ is proportional to the energy density ϱ_{EM} of that field [190–194]

$$\delta n_{\mathrm{refr}} = \frac{44\alpha^2}{135}\frac{\varrho_{\mathrm{EM}}}{m_e^4}\,. \tag{3.17}$$

In the extragalactic medium, the strongest contribution comes from the CMB with $\varrho_{\mathrm{CMB}} \approx 2\times10^{-15}\,\mathrm{eV}^4$, which induces a shift $\delta n_{\mathrm{refr}}^{\mathrm{CMB}} \approx 5.1\times10^{-43}$. This shift is reflected in the dispersive Hamiltonian matrix via

$$\Delta_{\mathrm{CMB}} = \omega\,\delta n_{\mathrm{refr}}^{\mathrm{CMB}} \approx 8\times10^{-2}\left(\frac{\omega}{\mathrm{TeV}}\right)\mathrm{Mpc}^{-1}\,, \tag{3.18}$$

which is larger than all the other contributions to the dispersion of both photon polarizations for realistic magnetic fields and energies $\omega \gtrsim 10\,\mathrm{MeV}$. We are interested in gamma rays with energies in the GeV–TeV range where Δ_{B} and Δ_{pl} may be neglected and $\Delta_\perp = \Delta_\parallel$ to a good approximation. The dominance of the CMB refraction is the most important result of this section and will lead to all the modifications presented further below.

The direction of the magnetic field is not constant along a line of sight. It is therefore convenient to express the dispersive Hamiltonian matrix in a fixed coordinate system with an arbitrary azimuth angle ϕ which gives the orientation of the magnetic field in the x-y-plane. In this frame, the dispersive Hamiltonian matrix reads

$$\mathsf{H}_{\mathrm{dis}} = \begin{pmatrix} \Delta_{11} & \Delta_{12} & s_\phi\,\Delta_{a\gamma} \\ \Delta_{21} & \Delta_{22} & c_\phi\,\Delta_{a\gamma} \\ s_\phi\,\Delta_{a\gamma} & c_\phi\,\Delta_{a\gamma} & \Delta_a \end{pmatrix}, \tag{3.19}$$

which can be obtained from Eq. (3.11) by a rotation with angle ϕ. Here, we defined $s_\phi \equiv \sin\phi$ and $c_\phi \equiv \cos\phi$. The diagonal photonic components of the dispersive Hamiltonian are $\Delta_{11} = \Delta_\perp\,c_\phi^2 + \Delta_\parallel\,s_\phi^2$ and $\Delta_{22} = \Delta_\parallel\,c_\phi^2 + \Delta_\perp\,s_\phi^2$. The off-diagonal components $\Delta_{12} = \Delta_{21} = (\Delta_\parallel - \Delta_\perp)\,c_\phi s_\phi \approx 0$, where the approximation follows because we only consider CMB refraction.

3.3 Physical impact of large dispersion

Mixing between different particle species is inefficient if the dispersion-induced phase velocity difference of the two species is large. This suppression may be compensated by large off-diagonal entries of the Hamiltonian matrix. The ALP dispersion is controlled by the ALP mass. It becomes large for very massive ALPs and small photon energies. On the other hand, the photon dispersion on the CMB grows linearly with energy. For a given energy range, the ALP contribution can always artificially be argued away by considering small ALP masses. The CMB

dispersion Δ_{CMB}, on the other hand, inevitably dominates the photon dispersions $\Delta_\perp$ and $\Delta_\parallel$ for ω around $100\,\mathrm{GeV}$, and the realistic magnetic field strengths and coupling constants presented in Tab. 3.1.

Note that also absorption may lead to a suppression of mixing if the absorption rate dominates the Hamiltonian matrix. With the parametrization of the absorption in Eq. (3.10), the absorption rate grows more than linear but will not be larger than the CMB dispersion for energies up to $20\,\mathrm{TeV}$ that are considered here. We will now take a look how the different terms of the dispersive Hamiltonian affect the mixing angle and the oscillation lengths.

3.3.1 Impact on the mixing angle

The strength of the photon-ALP mixing depends on the magnitude of $\Delta_{a\gamma}$ relative to the diagonal components of the Hamiltonian matrix. Let us choose a coordinate system in which $\phi = 0$ such that the Hamiltonian simplifies to

$$\mathsf{H} = \begin{pmatrix} \Delta_\perp - i\frac{\Gamma}{2} & 0 & 0 \\ 0 & \Delta_\parallel - i\frac{\Gamma}{2} & \Delta_{a\gamma} \\ 0 & \Delta_{a\gamma} & \Delta_a \end{pmatrix} . \tag{3.20}$$

In general, this matrix may be diagonalized with a unitary transformation. We would like to comment on the limiting case: if the absolute value of the absorption can be neglected compared to the dispersive terms, the unitary matrix becomes effectively an orthogonal matrix with one mixing angle φ. This angle reads

$$\varphi = \frac{1}{2}\arctan\frac{2\Delta_{a\gamma}}{\Delta_\parallel - \Delta_a} . \tag{3.21}$$

Note that because $\Delta_a < 0$ and $\Delta_\parallel > 0$ the contributions of the ALP mass and that of the CMB always add up. They cannot cancel each other and must be separately small to achieve large mixing. If this is the case and $\Delta_{a\gamma} \gg \Delta_\parallel - \Delta_a$ then the photon-ALP mixing is close to maximal, $\varphi \to \pi/4$. In previous works, e.g., Refs [56–58] where the CMB refraction was absent and dispersion on the background magnetic field was neglected, the expression (3.21) lead to a critical energy [178]

$$\omega_{\mathrm{c}} = \omega\frac{|\Delta_a - \Delta_{\mathrm{pl}}|}{2\Delta_{a\gamma}} \approx 2.5\times10^{-2}\frac{|m_a^2 - \omega_{\mathrm{pl}}^2|}{(10^{-10}\,\mathrm{eV})^2}\left(\frac{\mathrm{nG}}{B_{\mathrm{T}}}\right)\left(\frac{10^{-11}\,\mathrm{GeV}}{g_{a\gamma}}\right)\,\mathrm{TeV} . \tag{3.22}$$

For higher energies than ω_{c} the mixing was assumed to be maximal and dispersion is neglected altogether. This is the regime studied by Mirizzi and Montanino [178]. Note however, that this approximation is only valid if the mixing angle that is induced by absorption can be neglected simultaneously. This is not the case for $\omega > 10\,\mathrm{TeV}$ if CMB dispersion is absent.

On the other hand, if $\Delta_{a\gamma} \ll \Delta_\parallel - \Delta_a$ the photon-ALP mixing is close to zero. For sizable ALP masses, this condition is fulfilled at low photon energies because the Δ_a term becomes large. For energies in the GeV–TeV range, the mixing becomes small because the CMB refraction in $\Delta_\parallel$ dominates over $\Delta_{a\gamma}$, see Eqs. (3.14b) and (3.18).

3.3.2 Impact on the oscillation length

Large dispersion also modifies the oscillation length. To quantify this statement, let us compute the probability of creating an ALP from an initially pure photon state with polarization along the magnetic field direction $\mathbf{A}_\parallel = (0,1,0)$. Assuming $\mathsf{H} = \text{const.}$ and $\mathsf{H}_{\rm abs} = 0$, we can integrate Eq. (3.6) to obtain $\mathbf{A}(z) = \mathsf{U}_{\rm dis}(z)\mathbf{A}_\parallel$. The evolution operator $\mathsf{U}_{\rm dis}$ is Hermitian and it can be evaluated by diagonalizing the Hamiltonian matrix:

$$\begin{aligned}\mathsf{U}_{\rm dis}(z) =& \exp\left(-i\mathsf{H}_{\rm dis}z\right)\\ =& e^{-i\frac{(\Delta_a+\Delta_\parallel)z}{2}}\begin{pmatrix} e^{-i(\delta-\Delta_{a\gamma}/2)z} & 0 & 0\\ 0 & c_\varphi^2 e^{-i\Delta_{\rm osc}z/2} + s_\varphi^2 e^{i\Delta_{\rm osc}z/2} & is_{2\varphi}\sin\frac{\Delta_{\rm osc}z}{2}\\ 0 & is_{2\varphi}\sin\frac{\Delta_{\rm osc}z}{2} & c_\varphi^2 e^{i\Delta_{\rm osc}z/2} + s_\varphi^2 e^{-i\Delta_{\rm osc}z/2}\end{pmatrix},\end{aligned} \tag{3.23}$$

where we use $s_\varphi \equiv \sin\varphi$ and $c_\varphi \equiv \cos\varphi$, and define for later convenience δ and $\Delta_{\rm osc}$,

$$\Delta_{\rm osc} = \left[(\Delta_\parallel - \Delta_a)^2 + 4\Delta_{a\gamma}^2\right]^{\frac{1}{2}}, \tag{3.24}$$

$$\delta = \Delta_\perp - \tfrac{1}{2}(\Delta_\parallel + \Delta_a) + \tfrac{1}{2}\Delta_{a\gamma}. \tag{3.25}$$

Here, the oscillations frequency $\Delta_{\rm osc}$ is the energy difference between the propagation eigenstates of the ALP and $A_\parallel$. This frequency is associated with the rapidness of mixing between ALPs and photons.

Projecting $\mathbf{A}(z)$ on the ALP state $\mathbf{A}_a = (0,0,1)$, we find the standard transition probability

$$P_{a\gamma} = |\mathbf{A}_a^\dagger \mathsf{U}(z)\mathbf{A}_\parallel|^2 = \sin^2(2\varphi)\sin^2\left(\frac{\Delta_{\rm osc}z}{2}\right). \tag{3.26}$$

From this expression we see that we may define the oscillation length in terms of the oscillation frequency as:

$$l_{\rm osc} = \frac{2\pi}{\Delta_{\rm osc}} = \frac{2\pi}{\left[(\Delta_\parallel - \Delta_a)^2 + 4\Delta_{a\gamma}^2\right]^{\frac{1}{2}}}. \tag{3.27}$$

In the regime where the photon dispersion on the CMB dominates, $\Delta_\parallel - \Delta_a$ grows with the photon energy, and the oscillation length decreases as the photon energy increases. At GeV–TeV energies it becomes inversely proportional to the energy, $l_{\rm osc} \approx 2\pi/(\omega\delta n_{\rm refr}^{\rm CMB})$. For $\omega = 1\,\text{TeV}$, the oscillation length is $l_{\rm osc} \approx 78.5\,\text{Mpc}$ and reduces to $l_{\rm osc} \approx 7.85\,\text{Mpc}$ for $\omega = 10\,\text{TeV}$. We see that the oscillation length becomes comparable to the coherence lengths of extragalactic magnetic fields that can be obtained from, e.g., quasar outflow [52]. If the oscillation length becomes smaller than the coherence length of the magnetic field, the ALP-photon system starts probing the detailed structure of the magnetic field. Incorrect results will be obtained if the assumptions about the structure of the magnetic field are too simplistic as we will demonstrate in the following.

3.4 Generalization: non-maximal mixing

An ALP mass and refraction on the cosmic microwave background suppress the mixing angle and the oscillation length. Although related, these two effects are different phenomena. Here, we will take a look at non-maximal mixing and how the differential equation approach of Mirizzi and Montanino [178] generalizes to arbitrary mixing angles. This analysis will be useful for the generalization of the assumption that the coherence length is always smaller than the oscillation length (see Sec. 3.5). For now we will adopt a simple model for the magnetic field: it consists of domains with length l_c and magnetic field strength B. The magnetic field changes discontinuously on the border of each domain ("hard edges").

3.4.1 Evolution equation

The magnetic field structure has to be inserted into the evolution equation. Instead of using Eq. (3.6) directly, it is more convenient to work in the formalism of density matrices because we directly get rid of irrelevant phases. Here, the density matrix is given by

$$\rho = \mathbf{A} \otimes \mathbf{A}^\dagger = \begin{pmatrix} \rho_{11} & \rho_{12} & \rho_{1a} \\ \rho_{21} & \rho_{22} & \rho_{2a} \\ \rho_{a1} & \rho_{a2} & \rho_{aa} \end{pmatrix} . \tag{3.28}$$

Using Eq. (3.6) one can show that it satisfies the equation

$$i\partial_z \rho = \mathsf{H}\,\rho - \rho\,\mathsf{H}^\dagger , \tag{3.29}$$

where we have to distinguish between the Hamiltonian and its conjugate because of the photon absorption.

For high energy photons we do not measure the polarization but just count photon numbers. The total transfer function for the photons is obtained from Eq. (3.29) by adding the two polarizations $T_\gamma \equiv \rho_{11} + \rho_{22}$. The ALP transfer function is just $T_a \equiv \rho_{aa}$.

3.4.2 Differential equation description for hard edges

The original result by Mirizzi and Montanino [178] for the evolution of the transfer functions $T_{a,\gamma}$ reads

$$l_\mathrm{c} \frac{\mathrm{d}}{\mathrm{d}z} T_\gamma = -\langle \tilde{P}_{a\gamma} \rangle_\theta \left(\tfrac{1}{2} T_\gamma - T_a \right) - \Gamma_\gamma l_\mathrm{c}\, T_\gamma , \tag{3.30a}$$

$$l_\mathrm{c} \frac{\mathrm{d}}{\mathrm{d}z} T_a = +\langle \tilde{P}_{a\gamma} \rangle_\theta \left(\tfrac{1}{2} T_\gamma - T_a \right) , \tag{3.30b}$$

where $\langle \tilde{P}_{a\gamma} \rangle_\theta$ is the conversion probability for maximal mixing $\tilde{P}_{a\gamma} = \Delta_{a\gamma}^2 l_\mathrm{c}^2$ averaged over the polar angle of the magnetic field θ. We see that $\langle \tilde{P}_{a\gamma} \rangle_\theta$ determines the mixing between ALPs and photons, and only photons suffer absorption, which is described through the term $\Gamma_\gamma l_\mathrm{c}$. Equation (3.30) can be solved analytically with a solution given in Ref. [178].

The set of differential equations (3.30) has been obtained via a perturbative expansion in the absorption $\Gamma_\gamma l_\mathrm{c} \ll 1$ and mixing $\Delta_\mathrm{osc} l_\mathrm{c} \ll 1$ while neglecting any terms on the diagonals of the dispersive Hamiltonian. Once we take into account dispersion from CMB refraction, $\Delta_\mathrm{osc} l_\mathrm{c} \ll 1$ is not a valid approximation anymore and Eq. (3.30) cannot be applied.

If the absorption rate is small compared to the domain size, $\Gamma_\gamma l_\mathrm{c} \ll 1$, we may still perform a perturbative expansion in this parameter and resum purely dispersive terms taking into account non-maximal mixing. As we will demonstrate now, a differential equation similar to Eq. (3.30) can be obtained.

In each domain n of length l_c, the Hamiltonian is constant so that the solution of the Schrödinger equation, $\mathbf{A}(l_\mathrm{c}) = \mathsf{U}(l_\mathrm{c})\mathbf{A}(0)$, can be used to relate density matrices in two neighboring domains,

$$\rho_{n+1} = \mathsf{U}_n(l_\mathrm{c})\rho_n\mathsf{U}_n^\dagger(l_\mathrm{c})\,. \tag{3.31}$$

The evolution operator U for a constant Hamiltonian is defined as

$$\mathsf{U}(l_\mathrm{c}) = \exp\left[-i(\mathsf{H}_\mathrm{dis} - i\mathsf{H}_\mathrm{abs})l_\mathrm{c}\right]\,. \tag{3.32}$$

An expansion of Eq. (3.32) would contain three different contributions: a purely dispersive term, a term only containing absorption and an interference between dispersion and absorption. The purely dispersive term has been resummed in Eq. (3.23). Assuming $\Gamma_\gamma l_\mathrm{c} \ll 1$, we can perform a perturbative expansion in the absorption while retaining the exact dispersion, which we know how to diagonalize. The evolution operator can be rewritten as

$$\mathsf{U}(l_\mathrm{c}) = \exp\left[-i\mathsf{H}_\mathrm{dis}l_\mathrm{c}\right]\exp\left[i\mathsf{H}_\mathrm{dis}l_\mathrm{c}\right]\exp\left[-i\left(\mathsf{H}_\mathrm{dis} - i\mathsf{H}_\mathrm{abs}\right)l_\mathrm{c}\right] = \exp\left[-i\mathsf{H}_\mathrm{dis}l_\mathrm{c}\right]\tilde{\mathsf{U}}(l_\mathrm{c})\,, \tag{3.33}$$

where for $\tilde{\mathsf{U}}(l_\mathrm{c})$ we have a perturbative expansion (see page 84 of Ref. [122])

$$\tilde{\mathsf{U}}(l_\mathrm{c}) = \mathbb{1} + (-i)\int_0^{l_\mathrm{c}} \mathrm{d}l'\,\mathsf{H}_\mathrm{I}(l') + \mathcal{O}\left[\mathsf{H}_\mathrm{I}^2(l')\right]\,, \tag{3.34}$$

with the interaction picture Hamiltonian matrix

$$\mathsf{H}_\mathrm{I}(l') \equiv \exp\left[i\mathsf{H}_\mathrm{dis}l'\right](-i\mathsf{H}_\mathrm{abs})\exp\left[-i\mathsf{H}_\mathrm{dis}l'\right]\,. \tag{3.35}$$

For small absorption per domain $\Gamma_\gamma l_\mathrm{c}$, Eq. (3.34) is meaningful. Note that the expansion has been performed solely in the absorption, whereas purely dispersive terms are fully taken into account. This is the main difference compared to the previous derivation of Ref. [178].

With this expansion, the evolution operator reads to first order

$$\mathsf{U}(l_\mathrm{c}) \approx \exp\left[-i\mathsf{H}_\mathrm{dis}l_\mathrm{c}\right] - i\exp\left[-i\mathsf{H}_\mathrm{dis}l\right]\int_0^{l_\mathrm{c}} \mathrm{d}l'\,\mathsf{H}_\mathrm{I}(l')\,, \tag{3.36}$$

and all the exponential functions can be straight-forwardly calculated by diagonalizing the Hermitian matrix H_dis. In the coordinate frame where $\phi = 0$, the expression has been shown in Eq. (3.23). For a general magnetic field, Eq. (3.23) has to be rotated with an orthogonal matrix

$$\mathsf{O} = \begin{pmatrix} c_\phi & -s_\phi & 0 \\ s_\phi & c_\phi & 0 \\ 0 & 0 & 1 \end{pmatrix}\,. \tag{3.37}$$

Following this approach, we obtain an analytical expression for the time evolution of the ALP-photon system in one domain and an arbitrary rotated coordinate system.

As shown by Ref. [178], a differential equation can be obtained by taking the limit

$$\rho_{n+1} - \rho_n \approx l_\mathrm{c} \partial_z \rho_n \,, \tag{3.38}$$

which is well motivated if the rate of change is small and becomes exact if ρ varies in a linear fashion. Equation (3.31) can now be cast into

$$l_\mathrm{c} \partial_z \rho_n \approx \mathsf{U}_n(l_\mathrm{c}) \rho_n \mathsf{U}_n^\dagger(l_\mathrm{c}) - \rho_n \,. \tag{3.39}$$

In order to predict the photon transfer functions after propagation through many domains, we have to fix a magnetic field distribution. The exact realization of the magnetic field along the line of sight to a single source is unknown such that model predictions are hard to obtain (see however Refs. [195, 196]). If we observe multiple sources we may compare the observed mean photon transfer function and its variance with theoretical predictions from the statistical properties of the extragalactic magnetic field. Previous works [56–58, 178] relied on the hard-edges approximation with constant domain size. If the oscillation length is much larger than the coherence length, hard edges are a justified approximation because the ALP-photon system is not able to adapt to the sudden changes of the magnetic field. The propagation is non-adiabatic.

To obtain the mean transfer functions we take the expectation value of Eq. (3.39) with respect to the properties of the magnetic field distribution. Previously [56–58, 178], it was assumed that along the line of sight, the angle ϕ is randomly distributed in $[0, 2\pi)$ and $\cos\theta$ is randomly distributed in $[-1, 1]$, while the absolute value of the magnetic field strength B and the domain length l_c was held constant.

We may generalize these assumptions by including the expectation values with respect to the magnetic field $\mathbf{B}$ and the domain size l_c, i.e., $\mathbf{B}$ and l_c now fluctuate from domain to domain. If we finally assume that the photon crosses sufficiently many domains such that the average over these variables is justified, the differential equation for an ensemble-averaged density matrix $\bar{\rho}$ reads

$$\langle l_\mathrm{c} \rangle_{l_\mathrm{c}} \partial_z \bar{\rho} \approx \langle \mathsf{U}\, \bar{\rho}\, \mathsf{U}^\dagger \rangle_{l_\mathrm{c},\mathbf{B}} - \bar{\rho} \,, \tag{3.40}$$

where $\langle \bullet \rangle_{l_\mathrm{c},\mathbf{B}} = \int \mathrm{d}^3\mathbf{B}\, P(\mathbf{B}) \int_0^\infty \mathrm{d}l_\mathrm{c}\, P(l_\mathrm{c})\, \bullet$, with appropriately normalized probability densities P, and where $\bar{\rho}$ denotes the density matrix for the mean.

The calculation of the expectation value in Eq. (3.40) is lengthy but straightforward if we assume that the probability distribution for the magnetic field is isotropic in the plane perpendicular to the direction of propagation, i.e., $\langle \bullet \rangle_\mathbf{B} = \int \mathrm{d}^2\mathbf{B}\, P'(\mathbf{B}) \int_0^{2\pi} \mathrm{d}\phi/(2\pi)\, \bullet$, with a new probability distribution P'. With this assumption the coherences on the off-diagonals of $\bar{\rho}$ decouple from the diagonal number densities. Introducing the mean transfer functions $T_\gamma \equiv \bar{\rho}_{11} + \bar{\rho}_{22}$ and $T_a \equiv \bar{\rho}_{aa}$ the system of 9 equations (3.40) reduces to two coupled equations:

$$\langle l_\mathrm{c} \rangle_{l_\mathrm{c}} \frac{\mathrm{d}}{\mathrm{d}z} T_\gamma = -\langle P_{a\gamma} \rangle_{l_\mathrm{c},\mathbf{B}} \left(\tfrac{1}{2} T_\gamma - T_a \right) - \Gamma_\gamma \langle l_\mathrm{c} \rangle_{l_\mathrm{c}} T_\gamma \,, \tag{3.41a}$$

$$\langle l_\mathrm{c} \rangle_{l_\mathrm{c}} \frac{\mathrm{d}}{\mathrm{d}z} T_a = +\langle P_{a\gamma} \rangle_{l_\mathrm{c},\mathbf{B}} \left(\tfrac{1}{2} T_\gamma - T_a \right) , \tag{3.41b}$$

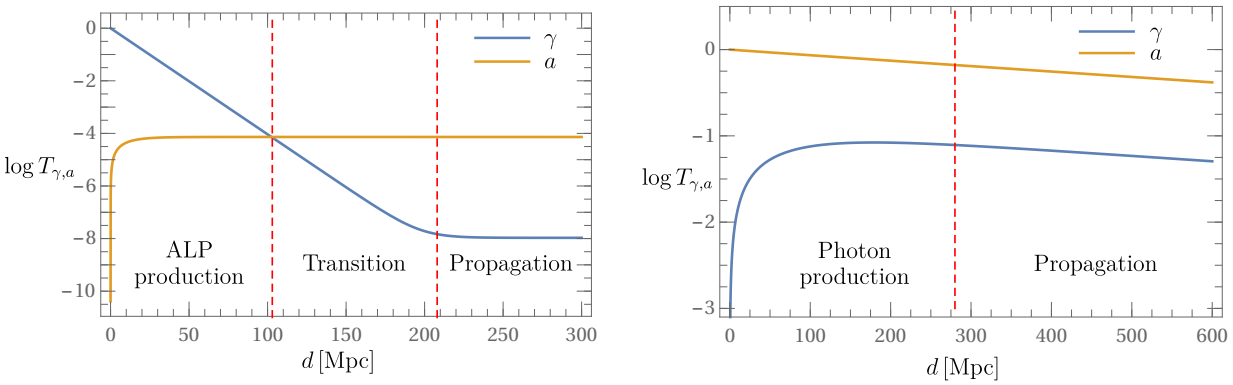

Figure 3.2: Typical photon and ALP transfer functions as a function of the distance from the source for a pure photon initial condition (left) and a pure ALP initial condition (right). The photon transfer function is shown in blue and the ALP transfer function in orange. Qualitatively different behavior is separated with red dashed lines.

where $\langle P_{a\gamma}\rangle_{l_c,\mathbf{B}}$ is the photon-ALP oscillation probability shown in Eq. (3.26), which has been further averaged over l_c and $\mathbf{B}$. For an example of one term in the derivation see Appendix D.

The absorptive term has been derived similarly to the dispersive terms using Eq. (3.36). For zero mixing angle $\varphi \to 0$, this gives exactly $\Gamma_\gamma l_c$. By taking this limit, we neglect some terms that describe the interference between absorption and dispersion and that are proportional to the mixing angle φ.

The similarity between the differential equation (3.41) derived here and the differential equation (3.30) by Mirizzi and Montanino is striking. Indeed, we see that Eq. (3.30) may be obtained from Eq. (3.41) in the limit of constant domain sizes and maximal mixing $P_{a\gamma} \to \tilde{P}_{a\gamma}$. Furthermore, the analytical solution shown in Ref. [178] also applies to our Eq. (3.41).

Typical results for $T_{a,\gamma}$ as a function of the distance are shown in Fig. 3.2 for an initial photon state (left) and an initial ALP state (right). If we start with photons, these are absorbed efficiently while producing a population of ALPs. At some distance the number of photons will be less than the number of ALPs and the system starts to be ALP dominated, i.e., the hierarchy between photons and ALPs is inverted. Finally, the decline of the number of photons is halted because of back-reactions from ALPs to photons. The system then propagates in this quasi-static state with a small power loss from ALPs converting into photons with subsequent absorption.

In the right plot of Fig. 3.2, the initial population consists of ALPs only. After a number of photons are produced, we enter the propagation phase again: the ALP and photon transfer functions run parallel to each other and slowly decrease because of power loss in the photonic sector.

3.5 Generalization: varying domain lengths

In the last section, we have seen that the assumption of maximal mixing may be relaxed straightforwardly. The mixing between the photon and ALP system is controlled by $P_{a\gamma}$ which should be

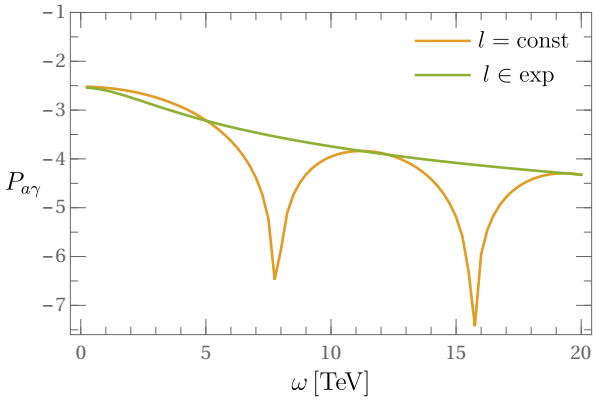

Figure 3.3: Average conversion probabilities $\langle P_{a\gamma} \rangle$ per domain for a constant domain size $l = 10\,\mathrm{Mpc}$ (orange) and for a domain size drawn from an exponential distribution (green).

appropriately averaged. With $P_{a\gamma}$ given in Eq. (3.26), and using the definition of the oscillation length (3.27), we see that the conversion probability in one domain is

$$P_{a\gamma} = \sin^2(2\varphi) \sin^2\left(\pi \frac{l_\mathrm{c}}{l_\mathrm{osc}}\right), \tag{3.42}$$

which becomes formally zero for $l_\mathrm{c} = l_\mathrm{osc}$. The reason is that the coherence length permits one full cycle of photon-ALP-photon conversion inside its domain, i.e., we obtain a resonant suppression of photon-ALP oscillations. Since l_c is assumed to be constant, a vanishing $P_{a\gamma}$ holds in every domain. This will inevitably happen for a certain energy given the numerical values in Tab. 3.1. Averaging over the magnetic field does not change this picture very much because l_osc is dominated by Δ_CMB and almost independent of the magnetic field.

In reality, such resonances are not expected to occur because not every domain should have the same size, and domains will not always be crossed to their full extent. This variation may be taken into account by giving the domain lengths a probability distribution. In the maximal mixing regime, the ALP-photon system will only be sensitive to the first two moments of the magnetic field structure (see the differential equation in Ref. [178]). This will help us to normalize different magnetic field distributions such that the photon transfer functions are equal for low energies. For large energies this approach is expected to lead to different transfer functions because the conversion probability (3.26) is sensitive to higher moments of the probability distribution.

We choose two extreme probability distributions for the magnetic field coherence length. Besides the constant length scale discussed above, we study an exponential distribution with probability density function $p(l_\mathrm{c}) = (1/\bar{l})\exp[-l_\mathrm{c}/\bar{l}]$, with expectation value $\bar{l}$ and variance $(\bar{l})^2$. This distribution for the length scale corresponds to a Poisson distribution for the number of domains.

The average conversion probabilities for constant domain length $l_\mathrm{c} = 10\,\mathrm{Mpc}$ and a domain size drawn from an exponential distribution with $\langle l_\mathrm{c} \rangle = 5\,\mathrm{Mpc}$ is shown in Fig. 3.3. We see that $\langle P_{a\gamma} \rangle$ becomes tiny at energies $\omega \approx 8$ and $16\,\mathrm{TeV}$ for $l_\mathrm{c} = \mathrm{const}$. The reason is that at $\omega \approx 8\,\mathrm{TeV}$ the oscillation length $l_\mathrm{osc} \approx 10\,\mathrm{Mpc} = l_\mathrm{c}$ for the first time. As argued above, the sine function in

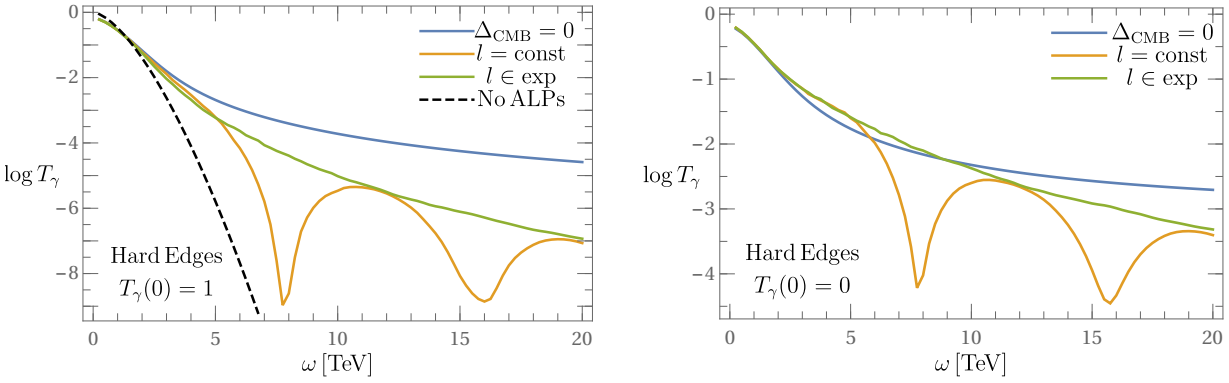

Figure 3.4: Numerical results for the mean photon transfer function for 1000 realizations of magnetic fields with hard edges for a pure photon initial state (left) and a pure ALP initial state (right). The distance to the source is assumed to be 1 Gpc and redshift is neglected. Blue lines show the results that are obtained when Δ_{CMB} is set to zero and for constant domain sizes. Orange and green lines contain the refraction on the CMB but assume different probability distributions for the domain lengths of the magnetic field: the orange curve assumes constant $l_{\mathrm{c}} = 10\,\mathrm{Mpc}$, and for the green curve l_{c} is drawn from an exponential distribution with $\langle l_{\mathrm{c}} \rangle = 5\,\mathrm{Mpc}$. The black dotted line indicates photon absorption without ALPs.

Eq. (3.26) goes through zero and $\langle P_{a\gamma} \rangle$ vanishes. The next zero of the sine is then encountered at $\omega \approx 16\,\mathrm{TeV}$.

For the conversion probability using an exponential distribution with $\langle l_{\mathrm{c}} \rangle = 5\,\mathrm{Mpc}$, we do not see a suppression. In contrast to the constant domain length we assumed above, a resonant suppression may be obtained in one domain but will in general not be obtained in the domains that follow. This is why the averaged transition probability with l_{c} being weighted by an exponential distribution does not show any suppression at $\omega = 8$ or $16\,\mathrm{TeV}$.

For $\omega \to 0$ we see that the conversion probabilities of both distributions coincide as we have enforced by choosing $\langle l_{\mathrm{c}} \rangle = 5\,\mathrm{Mpc}$ for the exponential distribution and $l_{\mathrm{c}} = 10\,\mathrm{Mpc}$ for the constant domain length.

Besides the coherence length, we will also relax the assumption about a constant absolute value of the magnetic field, which introduces relations between different components of the magnetic field, i.e., B_x and B_y are not independent. We choose a Gaussian distribution for all magnetic field directions with zero mean and variance $(2/3)\,\mathrm{nG}^2$, which yields an expectation value for the absolute value of the magnetic field similar to the upper limit of $1\,\mathrm{nG}$.

3.5.1 Numerical results for hard edges

Using the evolution equation (3.29) we compute numerically the mean photon transfer function T_γ with and without refraction on the CMB for a source with a distance $d = 1\,\mathrm{Gpc}$ from us (see Fig. 3.4). We use two different probability distributions for the domain sizes, i.e., a constant length $l_{\mathrm{c}} = 10\,\mathrm{Mpc}$ and domain sizes drawn from an exponential distribution with $\langle l_{\mathrm{c}} \rangle = 5\,\mathrm{Mpc}$. The components of the magnetic field B_x and B_y are drawn from a Gaussian distribution with zero mean and variance $(2/3)\,\mathrm{nG}^2$. The two different figures correspond to extreme initial con-

ditions: on the left we assume that a pure photon state is created in the source and on the right a pure ALP state is assumed. Each curve is an interpolation of a grid of mean transfer functions obtained with different photon energies. The mean has been evaluated by generating 1000 different magnetic field configurations. The configurations are identical within each curve of Fig. 3.4.

Special care has to be taken when we draw the domain lengths from an exponential distribution because we have to fulfill the boundary condition $\sum_n l_n = d$. This is done by resizing the last domain of every configuration to this condition. We have checked numerically that this cutting procedure does not change the statistical distribution of this last domain significantly. Nevertheless, we reshuffle the order of the domains for every configuration to further minimize the effect of this boundary condition.

In Fig. 3.4 we show in blue the result that is obtained with $\Delta_{\mathrm{CMB}} = 0$ and a constant domain size $l_{\mathrm{c}} = 10\,\mathrm{Mpc}$. This line should be compared with the black dashed line that indicates pure photon absorption, i.e., the fraction of photons that survives traversing the extragalactic space without ALP-photon oscillations. We see that for an initial state consisting of photons only (left) and for photon energies $\omega \gtrsim 4\,\mathrm{TeV}$ a possible photon signal is enhanced by many orders of magnitude. The reason for this enhancement is that some photons convert into ALPs while propagating (see "ALP production" in Fig. 3.2 left). After some time all the initial photons are either absorbed or have oscillated into ALPs which contain all the energy density. The ALPs propagate unimpeded by the EBL but some of their energy leaks back into the photonic sector, which gives the large photon population indicated by the blue line ("Propagation" in Fig. 3.2 left).

This picture is confirmed by the right-hand sides of Figs. 3.4 and 3.2. The ALPs dominate the number density from the start and transport their energy safely from the source to our detector. The initial loss of energy we observed on the left-hand side of Fig. 3.4 is prevented from the start. The expected number of photons is enhanced by two orders of magnitude.

Note that for $\Delta_{\mathrm{CMB}} = 0$ we have checked that the exact structure of the magnetic field probability distribution is of minor importance as long as we normalize $\langle P_{a\gamma} \rangle$ to be equal for low energies $\omega \approx 0$. For example, if we compare the results with a constant domain lengths $l_{\mathrm{c}} = 10\,\mathrm{Mpc}$ with those results that are obtained with domains drawn from an exponential distribution with $\langle l_{\mathrm{c}} \rangle = 5\,\mathrm{Mpc}$, we find for small energies consistent results on the 3% level as expected from 1000 different magnetic field configurations. For large energies, the transfer functions start to depend on the distribution because corrections of higher order in $\Gamma_\gamma l_{\mathrm{c}}$ become important. At $\omega = 20\,\mathrm{TeV}$ this amounts to deviations of approximately 25%.

While the probability distribution only has a minor effect when $\Delta_{\mathrm{CMB}} = 0$, it becomes of paramount importance when the CMB refraction is included. This is shown by the orange and green curves in Fig. 3.4. The orange curve is the result that is obtained with a constant domain size. It has an oscillatory feature which can be understood when looking at Fig. 3.3, i.e., we see the expected suppression of the mean ALP and photon transfer functions because the average conversion probability approaches zero. Similarly, we do not see any suppression for the curve with an exponential distribution for the domain size because the conversion probability is smooth.

3.6 Generalization: soft edges

In the preceding section we have studied magnetic fields with hard edges. We have seen that $\langle P_{a\gamma}\rangle$ plays an extraordinary role in explaining the behavior of the transfer functions. Realistic magnetic fields should not have hard edges, i.e., discontinuous magnetic field distributions but there will be some degree of continuous transition from one domain to the next ("soft edges"). We expect hard edges to be a poor approximation as soon as $l_{\rm osc} < l_{\rm c}$ such that the oscillations start to probe the magnetic field structure. In this limit the ALP-photon system should be able to adapt to the changing magnetic field adiabatically. We will now replace these hard edges by continuous soft edges.

Recently, the impact of soft edges was noticed as well in Ref. [179]. They observe that different functional dependencies of the magnetic fields lead to different photon transfer functions even without the CMB refraction. Their result is however due to not normalizing the magnetic field distribution. They compare in the maximal mixing regime magnetic field distributions with different $\langle \mathbf{B}^2 l_{\rm c}^2\rangle$, i.e., different conversion probabilities $P_{a\gamma}$. We will show that a correct normalization leads to results independent of the functional form of the magnetic fields in the maximal mixing regime; as expected from non-adiabatic propagation.

3.6.1 Magnetic field construction procedure

Our goal is to compare the hard edges approximation with a magnetic field that is smooth. In order to do this, we need a procedure to replace hard edges by soft edges, i.e., for a given magnetic field configuration with hard edges we want to find a smooth function that interpolates the structure. Depending on the interpolation function, we introduce additional degrees of freedom that we have to fix.

Extragalactic magnetic fields that have a coherent structure extending over several megaparsec may have been formed by quasar outflows, which means that magnetic fields are transported out of the center of galaxies by magnetized winds [52]. The structure of such magnetic fields is not known and we have to adopt additional assumptions. It seem reasonable that the inner part of a domain contains a magnetic field with approximately constant magnitude. Further outside, the magnetic field decreases or interacts with outflows from other quasars forming a continuous profile. The fractional volume of the constant inner part compared to the volume of each domain is unknown. This filling factor may vary from 1, which corresponds to a constant magnetic field in each domain with discontinuous transition, to 0, which indicates no constant magnetic field in the inner part of each domain.

For a given filling factor and magnetic field structure, we use the following procedure to construct continuous magnetic fields. In the center of each domain we place a constant subdomain with a size that is given by the filling factor. We want the boundaries between each subdomain and the outer magnetic field structure to be reasonably smooth, which we enforce by setting the first and second derivatives at the boundary to zero. This provides us with six conditions for each interpolation between two subdomains. We choose a fifth order polynomial between each subdomain. For example plots see Fig. 3.5.

This procedure does not fix the overall normalization of the magnetic field. In Ref. [179],

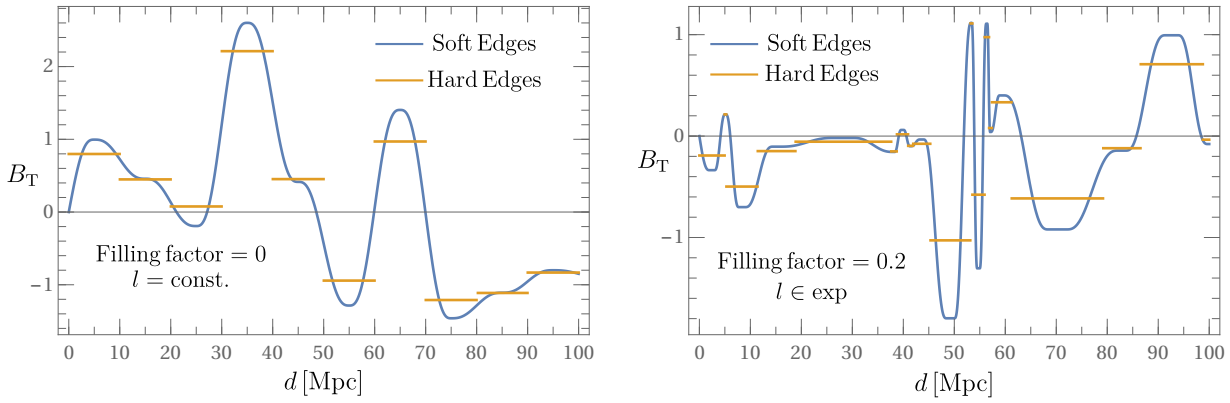

Figure 3.5: Examples for continuous magnetic fields that were obtained from the procedure described in the main text. On the left-hand side we show the interpolation of a magnetic field with constant domain size $l_\mathrm{c} = 10\,\mathrm{Mpc}$. The filling factor is zero. On the right-hand side, we assume a probability distribution for the domain size with $\langle l_\mathrm{c} \rangle = 5\,\mathrm{Mpc}$. The filling factor is 0.2.

the maximal values of the magnetic fields of the domain structure and the interpolation functions were set equal, which lead to different conversion probabilities in each domain even for the non-adiabatic $\Delta_\mathrm{CMB} = 0$ scenario. We proceed in a different way and set the conversion probabilities in the non-adiabatic limit, $\omega \to 0$, independent from the magnetic field structure. For a continuous magnetic field, the conversion probability is

$$P_{a\gamma} \propto \left| \int_0^{l_\mathrm{c}} \mathrm{d}z\, \mathbf{B}_\mathrm{T}(z) \right|^2 , \tag{3.43}$$

for a domain with length l_c. If this integral is equal in each domain for a constant magnetic field and for the interpolating field, we obtain identical results for $P_{a\gamma}$ in the $\omega \to 0$ limit. We will use this condition to fix the normalization in every domain.

3.6.2 Analytical estimates in the quasi-adiabatic limit

A state evolves adiabatically if an eigenstate of the Hamiltonian remains an eigenstate during propagation. Adiabaticity is obtained when the background varies so slowly that it cannot induce a transition from one state into another, i.e., transitions may be neglected once the first derivative of the background is small compared to the energy difference of two states.

If we apply this picture to ALP-photon oscillations, we expect a photon propagation eigenstate to stay a propagation eigenstate if the background magnetic field varies slowly enough. Especially, for the continuous magnetic fields we constructed above, adiabaticity may be expected once $l_\mathrm{c}/l_\mathrm{osc} > 1$. However, this picture breaks down when we consider absorption. To understand this, let us consider an initial photon state with no magnetic background field, i.e., interaction and propagation eigenstates coincide. If no magnetic field develops during propagation, the photon propagation will be completely adiabatic and a detector will observe a photon state at a distance d, albeit with exponentially reduced intensity due to absorption.

If the photon encounters a magnetic field during propagation, the magnetic field has to ramp up to a non-zero value. The derivatives of the magnetic field structure will generate a small population of ALPs: we obtain a tiny deviation the propagation eigenstate. This deviation may usually be neglected if the first derivative of the magnetic field is small enough. Neglecting the small ALP population is however problematic if absorption is sufficiently strong. The intensity of photons decreases exponentially, and if the distance to the detector is large enough, there will be a smaller number of photons than of ALPs no matter how slowly the magnetic field increased and decreased. The ALPs that were generated by quasi-adiabatic changes of the background will dominate the propagation after a certain distance from the source (see Fig. 3.2).

With this picture in mind, we derive now an expression for the predicted photon and ALP population if the background varies extremely slowly. For this discussion, we assume for now that the azimuthal angle of the magnetic field is zero ($\phi = 0$) so that we only have to consider one photon polarization. The system then reduces to a 2×2 matrix equation. We will also assume that the magnetic field is zero at the beginning and in the end of the propagation.

The Hamiltonian is a complex symmetric matrix so that the eigenbasis contains two orthogonal complex propagation eigenvectors: a photon-like eigenvector p_γ and an ALP-like eigenvector p_a. The photon-like propagation eigenvector is a photon interaction eigenstate in the absence of a magnetic field. It contains an admixture of ALP interaction eigenstates when a magnetic field is present; the difference between propagation and interaction eigenstates is however usually small for the magnetic fields and energy ranges we consider. Conversely, the propagation eigenstates p_a is a pure ALP interaction eigenstate $B_\mathrm{T} = 0$ and contains a photonic part for $B_\mathrm{T} \neq 0$.

In the strictly adiabatic case, p_γ is never converted into p_a and vice versa. The initial conditions and the magnetic field at the position of the detector is enough to completely predict the abundance of photons and ALPs.

To next order, we allow small changes in the magnetic field that translate into small conversions of p_γ to p_a. The standard conversion formula reads (see p. 329–331 of Ref. [197])

$$\partial_z \left[c_j(z) e^{-i\gamma_j(z)} \right] = c_k(z) \frac{\langle p_j(z) | \frac{\partial \mathsf{H}}{\partial z} | p_k(z) \rangle}{\omega_{jk}(z)} e^{i \int_0^z \mathrm{d}z' \, \omega_{jk}(z')} e^{i[\gamma_k(z) - \gamma_j(z)]} \,, \tag{3.44}$$

where c_k is explained through the solution of the Schrödinger equation $|\psi\rangle$,

$$|\psi(z)\rangle = \sum_{n=\gamma,a} c_n(z) e^{-i \int_0^z \mathrm{d}z' \, E_n(z')} |p_n(z)\rangle \,, \tag{3.45}$$

with the normalized eigenvector $|p_n(z)\rangle$, which also appears in Eq. (3.44), and the energy eigenvalues E_n

$$E_\gamma \approx \mathrm{Tr}\, \mathsf{H} \approx (\Delta_\parallel - \tfrac{i}{2}\Gamma_\gamma) \,, \tag{3.46a}$$

$$E_a \approx \frac{\det \mathsf{H}}{\mathrm{Tr}\, \mathsf{H}} \approx (-\Delta_\parallel - \tfrac{i}{2}\Gamma_\gamma) \left(\Delta_{a\gamma} / \Delta_\parallel \right)^2 \,, \tag{3.46b}$$

which enter Eq. (3.44) via $\omega_{jk} = E_j - E_k$. Finally, $\gamma_n = \langle p_n(z) | \dot{p}_n(z) \rangle$ is the Berry phase. Equation (3.44) is completely general [197] and for a given magnetic field configuration allows one

to exactly compute the photon and ALP densities. Unfortunately, this method is computationally demanding.

Let us assume that we start with a pure photon state with no magnetic field background. During the propagation a magnetic field will be encountered and some ALPs will be produced. Hence, we look at Eq. (3.44) with $j = a$ and $k = \gamma$. The solution of Eq. (3.44) can be simplified by using the first-order adiabatic approximation which amounts to setting $c_\gamma(z) = c_\gamma(0)$ [197]. Note that absorption is not contained in $c_\gamma(z)$ because it has been factored out into the complex energy eigenvalue E_n in Eq. (3.45). This allows us to set $c_\gamma(z) = c_\gamma(0)$ as long as $c_a(z)$ is small so that the back-reactions can be neglected, which is the case for the initial evolution of the system. Due to the exponential decay of photons, the first-order adiabatic approximation breaks down when the number in ALPs equals the number of photons. At this point the hierarchy of the ALP and photon transfer functions is inverted and the photon transfer function is dominated by the oscillation of ALPs into photons. As seen before, the ALP transfer function slowly decreases because of back-reactions into photons.

Let us now estimate the number of ALPs that are produced in the initial part of the evolution before the hierarchy between photon and ALP numbers is inverted. We write the off-diagonals of the Hamiltonian $\Delta_{a\gamma}(z)$ as a Fourier transform

$$\Delta_{a\gamma}(z) = \int_{-\infty}^{\infty} \mathrm{d}k\, f(k) e^{ikz}\,, \tag{3.47}$$

and plug this into Eq. (3.44). Neglecting the Berry phases and using $c_\gamma(z) = c_\gamma(0) = 1$, the solution of the differential equation reads

$$c_a(z) = \int_0^z \mathrm{d}z' \, \frac{\int_{-\infty}^{\infty} \mathrm{d}k\, ikf(k) e^{ikz'}}{\omega_{a\gamma}(z')} e^{i\int_0^{z'} \mathrm{d}z''\, \omega_{a\gamma}(z'')}\,. \tag{3.48}$$

For large energies, Δ_{CMB} dominates the energy difference between photons and ALPs, while the contribution from $\Delta_{a\gamma}$ may be neglected. Then:

$$\omega_{a\gamma} \approx -\Delta_{\mathrm{osc}} + i\frac{\Gamma_\gamma}{2}\,, \tag{3.49}$$

with Δ_{osc} given in Eq. (3.24). It follows that

$$\begin{aligned} c_a(z) &= -\int_{-\infty}^{\infty} \mathrm{d}k \int_0^z \mathrm{d}z' \, \frac{ikf(k)e^{ikz'}}{\Delta_{\mathrm{osc}} - i\Gamma_\gamma/2} e^{-i\Delta_{\mathrm{osc}}z' - \Gamma_\gamma z'/2} \\ &= -\int_{-\infty}^{\infty} \mathrm{d}k \, \frac{ikf(k)}{[\Delta_{\mathrm{osc}} - i\Gamma_\gamma/2][i(\Delta_{\mathrm{osc}} - k) + \Gamma_\gamma/2]} \left[1 - e^{-i(\Delta_{\mathrm{osc}} - k)z - \Gamma_\gamma z/2}\right] \\ &\approx -\int_{-\infty}^{\infty} \mathrm{d}k \, \frac{ikf(k)}{[\Delta_{\mathrm{osc}} - i\Gamma_\gamma/2][i(\Delta_{\mathrm{osc}} - k) + \Gamma_\gamma/2]}\,, \end{aligned} \tag{3.50}$$

where the last step is justified for sufficiently strong absorption and a large distance to the source.

Adiabaticity now means that $f(k)$ for high frequency modes falls off sufficiently fast such that the integral is dominated by $|k| \ll \Delta_{\mathrm{osc}}$. The solution then reads

$$|c_a(z)|^2 = \left(\frac{\partial_z \Delta_{a\gamma}(z)}{\Delta_{\mathrm{osc}}^2}\right)^2 \Bigg|_{z=0}\,, \tag{3.51}$$

which is valid until the inversion of the ALP-photon hierarchy. This result indicates that the number of ALPs that are produced initially is given by the derivative of the magnetic field structure at the initial point.

After the inversion of the ALP-photon hierarchy, the number of photons will be much smaller than the number of ALPs. This amounts to $\partial_z c_a(z) \approx 0$, i.e., back reactions can be neglected, and the ALP propagation proceeds solely through the evolution of the complex phase $e^{-i\int \mathrm{d}z' E_a(z')}$ [see Eq. (3.45)]. Since we are in the regime of small mixing angles, an ALP propagation eigenvector is almost purely an ALP interaction eigenstate such that the number of ALPs at distance d from the initial preparation of the system is

$$T_a(d) = \left(\frac{\partial_z \Delta_{a\gamma}(0)}{\Delta^2}\right)^2 e^{-\int_0^d \mathrm{d}z' \, \Gamma_\gamma \left(\frac{\Delta_{a\gamma}(z')}{\Delta_\parallel}\right)^2}, \tag{3.52}$$

where we used Eq. (3.46) for the eigenenergies. The photon transfer function can be obtained from Eq. (3.52) by noting that if the magnetic field at the detector is zero, the only photons at the detector are those generated by quasi-adiabatic production similar to the ALP production from the initial photons. The solution reads

$$T_\gamma(d) = \left(\frac{\partial_z \Delta_{a\gamma}(d)}{\Delta^2}\right)^2 \left(\frac{\partial_z \Delta_{a\gamma}(0)}{\Delta^2}\right)^2 e^{-\int_0^d \mathrm{d}z' \, \Gamma_\gamma \left(\frac{\Delta_{a\gamma}(z')}{\Delta_\parallel}\right)^2}, \tag{3.53}$$

which is proportional to the derivative of the magnetic field at distance d. If there is a residual magnetic field at the detector, this field will also generate photon interaction eigenstates because of the misalignment of ALP interaction and propagation eigenstates.

From Eq. (3.53) one can see how the MSW-intuition of adiabaticity is generalized in the presence of absorption. The photon transfer function still depends on the initial and final magnetic field configuration but this is not the only contribution: the background magnetic field during propagation is important as well because it determines the strength of the absorption of ALPs. The ALP absorption in this case has a different parametrical structure than for non-adiabatic absorption (cf. Ref. [178]).

We can extend this result to two polarizations if we assume that the initial azimuthal rotation of the magnetic field is so adiabatic that it can be neglected. If we prepare an unpolarized mixed state

$$\rho_0 = \begin{pmatrix} \frac{1}{2} & 0 & 0 \\ 0 & \frac{1}{2} & 0 \\ 0 & 0 & 0 \end{pmatrix}, \tag{3.54}$$

the ALP transfer function will be an incoherent sum of the ALPs produced from each photon polarization

$$T_a(d) = \frac{1}{2}|\langle a|\gamma_1(d)\rangle|^2 + \frac{1}{2}|\langle a|\gamma_2(d)\rangle|^2, \tag{3.55}$$

with $|\gamma_1(0)\rangle = (1,0,0)$ and $|\gamma_2(0)\rangle = (0,1,0)$, and $|a\rangle = (0,0,1)$. We see that the result is just the incoherent sum of the transfer function for each magnetic field direction, i.e., using Eq. (3.52)

$$T_a(d) = \frac{1}{2}\left[\left(\frac{\partial_z \Delta_{a\gamma,x}(0)}{\Delta^2_{\mathrm{osc}}}\right)^2 + \left(\frac{\partial_z \Delta_{a\gamma,y}(0)}{\Delta^2_{\mathrm{osc}}}\right)^2\right] e^{-\int_0^z \mathrm{d}z' \, \Gamma_\gamma \left(\frac{\Delta_{a\gamma}(z')}{\Delta_{\mathrm{osc}}}\right)^2}, \tag{3.56}$$

where $\Delta_{a\gamma,x}$ contains the magnetic field in the x-direction $\Delta_{a\gamma,y}$ contains the magnetic field in the y-direction. Note that the sum in the square parenthesis may be written as $(\partial_z \Delta_{a\gamma}(0)/\Delta^2)^2$ with the total magnetic field instead of its components. Our result in Eq. (3.56) is just half of the result in Eq. (3.52). This can be directly understood by noting that only the polarization parallel to the magnetic field contributes. With the initial condition Eq. (3.54) the number of photons with the parallel polarization is however only half of the number assumed in Eq. (3.52) and the number of ALPs is halved.

The factor of two suppression directly translates into the photon transfer function, which now reads

$$T_a(d) = \frac{1}{2\Delta_{\rm osc}^8} \left[\partial_z \Delta_{a\gamma}(0)\right]^2 \left[\partial_z \Delta_{a\gamma}(d)\right]^2 e^{-\int_0^z \mathrm{d}z' \, \Gamma_\gamma \left(\frac{\Delta_{a\gamma}(z')}{\Delta_{\rm osc}}\right)^2} , \tag{3.57}$$

Equations (3.52), (3.56), (3.57) and (3.53) hold for one magnetic field configuration. Since, we do not know this field, it is desirable to obtain the expectation value for the transfer functions in the adiabatic case. The mean can be obtained by assuming that spatially separated magnetic fields are not correlated. This allows us to take the individual expectation values for every piece in Eqs. (3.52), (3.56), (3.57) and (3.53).

$$T_a(d) \approx \frac{1}{2\Delta_{\rm osc}^4} \left\langle \left[\partial_z \Delta_{a\gamma}(0)\right]^2 \right\rangle_{\mathbf{B}} \exp\left[-\frac{\Gamma_\gamma}{\Delta_{\rm osc}^2} \left\langle \Delta_{a\gamma}^2 \right\rangle_{l,\mathbf{B}} d\right] , \tag{3.58}$$

$$T_\gamma(d) \approx \frac{1}{2\Delta_{\rm osc}^8} \left\langle \left[\partial_t \Delta_{a\gamma}(0)\right]^2 \right\rangle_{\mathbf{B}} \left\langle \left[\partial_z \Delta_{a\gamma}(d)\right]^2 \right\rangle_{\mathbf{B}} \exp\left[-\frac{\Gamma_\gamma}{\Delta_{\rm osc}^2} \left\langle \Delta_{a\gamma}^2 \right\rangle_{l,\mathbf{B}} d\right] , \tag{3.59}$$

where we pulled the expectation value inside the argument of the exponential, which is justified as long as absorption is small and the linear order in the Taylor expansion of the exponential dominates.

3.6.3 Numerical results for soft edges

Now that we have an analytical expectations for the photon and ALP transfer function, we may compare our expectations with numerical simulations. In order to compare the approximations with hard and soft edges, we generate 1000 different magnetic field structures with hard edges and interpolate these with the procedure described in Sec. 3.6.1 and with a filling factor equal to zero. We obtain a continuous magnetic field for every one of the 1000 realizations, which we may directly insert into the evolution equation (3.29).

The numerical results for the mean photon and ALP transfer functions are displayed in Fig. 3.6. Here, we plot the mean photon (left) and ALP (right) transfer function for an initial state consisting of unpolarized photons. We generated 1000 magnetic field configurations with hard edges and interpolated those with polynomials. The results for hard edges are shown in orange. The results for soft edges are shown in red. For $\omega \to 0$ the results for hard edges and soft edges are consistent with more than 0.1% accuracy. This confirms our suspicion that the transfer function do not depend on the exact structure of the magnetic field in the non-adiabatic regime, if the continuous magnetic field is normalized appropriately.

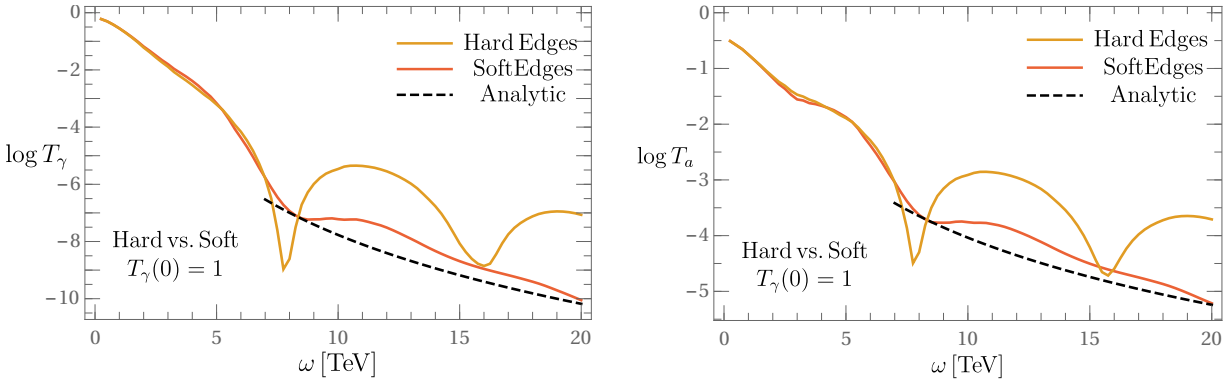

Figure 3.6: Numerical results for the mean photon transfer function (left) and mean ALP transfer function (right) for 1000 realizations of magnetic fields with $\langle l_c \rangle = 10\,\mathrm{Mpc}$ with hard edges in orange and soft edges in red. Initially, the photons are in a mixed unpolarized state. The black dashed line is the analytical prediction Eq. (3.58)*. The distance to the source is assumed to be 1 Gpc and redshift is neglected.*

The results with soft edges starts deviating significantly from the one with hard edges at around $\omega = 8\,\mathrm{TeV}$. This can be understood from the fact that the oscillation length and magnetic field coherence length become equal at approximately $8\,\mathrm{TeV}$, i.e., the ALP-photon systems starts probing the magnetic field structure considerably.

The black, dashed line in Fig. 3.6 indicates our expectation from the numerical treatment with results in Eq. (3.58). In the shown range, the analytical curve deviates from the numerical result by up to a factor 3. For much larger energies, however, we have checked that the analytical results reproduce numerical results on the 10% level for photons and on the 5% level for ALPs. We are therefore led to interpret the deviations of the black, dashed line and the red line in Fig. 3.6 as non-adiabatic contributions that are not captured in our analytical estimate.

3.7 Conclusions

Gamma rays that propagate through extragalactic space are attenuated by pair creation on the extragalactic background light. The absorption rate of gamma rays from far-away sources is altered considerably if ALPs exist. In the presence of extragalactic magnetic fields some photons oscillate into ALPs, which are absorbed much more weakly than photons, and may convert back to photons close to our galaxy. The ALPs hence shield the power of gamma rays from absorption on the EBL. Because this mechanism increases the number of gamma rays observed by Cherenkov telescopes like MAGIC, H.E.S.S., and VERITAS, it might resolve the transparency problem of the universe, i.e., that the current Cherenkov telescopes observe more energetic photons than previously expected from estimates of the EBL energy density. While the current status of this transparency problem is unclear, next generation Cherenkov telescopes like CTA might illuminate this issue further.

If we consider the ALP-photon mixing scenario, we would like to predict the spectra of individual sources. If we knew the structure of the magnetic field along the line of sight to the source,

predictions for the photon and ALP transfer functions could be obtained straightforwardly. This magnetic field is however not known, and from measurements and simulations we may only say that the extragalactic magnetic field is probably homogeneous over several megaparsec with field strengths below $1\,\mathrm{nG}$.

In order to still obtain predictions for the ALP-photon mixing scenario, previous publications often adopted a statistical approach: one may compare the mean photon transfer functions to the spectra of an ensemble of blazars if one assumes some theoretically motivated statistical properties of the extragalactic magnetic fields. The usual ansatz consisted of magnetic field domains with a constant comoving length and a constant magnetic field that changes abruptly at the border between two domains. By generating a large number of such magnetic field configurations and computing the ALP and photon transfer functions for each of these, one was able to estimate the mean photon and ALP transfer functions.

The differential equation of Mirizzi and Montanino simplifies this computationally demanding approach. It consists of a system of coupled differential equations that directly yield the mean and variance of the photon and ALP transfer functions. These equations were also derived for maximal mixing and the same approximations for the structure of the magnetic field in extragalactic space.

We have shown that the aforementioned computational methods must be reexamined once we include a recently derived contribution to the photon dispersion from CMB photons. This dispersion grows linearly with energy and becomes the largest entry of the Hamiltonian matrix for GeV–TeV photon energies. The refraction on the CMB therefore suppresses the mixing and it reduces the oscillations length of the photon-ALP system. This brings into question three of the main assumptions of previous methods: maximal mixing, constant domain sizes, and discontinuous changes of the magnetic fields at the domain borders (hard edges).

First, we have shown that the mixing angle is not maximal anymore once we include refraction on the CMB. Since maximal mixing is one of the assumptions of Mirizzi and Montanino, their differential equations cannot be used naïvely for GeV–TeV energies. We extended their formalism to non-maximal mixing in a straight-forward way: their equations may be used in the non-maximal mixing regime if the approximate conversion probability $\tilde{P}_{a\gamma} = \mathbf{B}_{\mathrm{T}}^2 l_{\mathrm{c}}^2$ is replaced by the average of the exact conversion probability per domain $\langle P_{a\gamma} \rangle$. For non-maximal mixing, $P_{a\gamma}$ is suppressed. This means that the probability for photons to oscillate into ALPs is reduced, and photons are not efficiently shielded from the EBL. Correspondingly for realistic distances to the source, the photon transfer function is orders of magnitude smaller in the non-maximal mixing regime than in the maximal mixing scenario.

We have shown that the assumption of constant domain sizes proved to be problematic in the non-maximal mixing regime. The conversion probability $P_{a\gamma}$ becomes zero in a domain where the oscillation length is equal to the domain size because the ALP-photon system undergoes one oscillation cycle and returns to its initial condition at the end of the domain. If the domain size is identical for every domain, this resonant suppression is sustained over large distances. We demonstrated that this resonance can indeed be seen in numerical simulations with a constant domain length. We discussed how this unphysical behavior can be mended by letting the domain sizes fluctuate. The resonant behavior vanished when we performed simulations with the domain lengths drawn from an exponential distribution. In the maximal mixing regime, the photon and

ALP transfer functions are not sensitive to the exact structure of the magnetic field if the field is appropriately normalized because the oscillation length is much larger than the magnetic field domain size. In this regime, we obtained consistent results for the two different probability distributions of the domain lengths. For non-maximal mixing, i.e., larger energies, the exact probability distribution becomes important because the conversion probability per domain $P_{a\gamma}$ is a nontrivial function of the domain length. Here, the average conversion probability is sensitive to higher moments of the probability distributions. These corrections become important even before $l_{\rm osc} \sim l_{\rm c}$.

The third assumption concerns hard edges, i.e., discontinuous transitions between two domains. When the oscillation length and the coherence length of the magnetic field become of similar order, we confirmed the expectation that it is important to know the functional form of the magnetic field at the transition between two domains. To show this, we interpolated with a continuous function several magnetic field configurations that were generated with a constant domain size and hard edges. For small energies, $\omega \to 0$, the oscillation length is much larger than the average domain size. As expected, the mean photon and ALP transfer functions were agnostic to the exact structure in this limit. Significant deviations from the results obtained with hard edges were obtained for $l_{\rm osc} \gtrsim l_{\rm c}$. Here, the reason is that the photon-ALP system starts probing the exact structure of the magnetic field. The evolution becomes quasi-adiabatic.

In this quasi-adiabatic limit, we performed analytical estimates for the mean photon and ALP transfer functions finding that they could be reasonably well understood from the initial and final magnetic field configurations and the mean absorption in extragalactic space. In particular for zero initial and final magnetic fields, the transfer functions are determined by the mean square of the magnetic field's derivatives.

Our findings indicate that previous results based on propagation in the extragalactic space have to be judged with a critical eye. The assumption of maximal mixing has to be discarded for GeV–TeV energies, and the corresponding results should be reexamined. Special care has to be taken if the coherence length of the magnetic field becomes of the same order as the oscillation length. In this case, one requires a realistic magnetic field configuration to make accurate predictions.

Such predictions would be helpful for current and upcoming Cherenkov telescopes. Especially the Cherenkov Telescope Array will be able to measure the spectra of distant blazars with unprecedented accuracy while at the same time being sensitive to energies up to several TeV. A significant hardening of blazar spectra would be a strong indication for the existence of axion-like particles.

Chapter 4

Pair correlations in core-collapse supernovae

Neutrinos undergo flavor oscillations because the weak-interaction and propagation eigenstates are misaligned. Similarly, helicity oscillations are induced by matter currents and electromagnetic fields that compensate for the angular momentum change. Such background media can also produce pair correlations, which are between a neutrino-antineutrino pair with opposite momentum. In this chapter, we derive the density matrix equations that unify flavor, helicity and pair correlations in one formalism. Following earlier approaches, we limit ourselves to the mean-field approximation for homogeneous yet anisotropic background media, and we explicitly show the evolution equation to first order in the neutrino mass. For Majorana neutrinos, we find contributions from lepton-number violating correlators that have been missed in previous works. We also provide a phenomenological discussion of pair correlations in comparison with helicity correlations.[1]

4.1 Introduction: the importance of neutrino transport

Neutrinos play an important role in compact astrophysical systems like core-collapse supernovae and neutron star mergers. The large densities of the order $10^4\,\mathrm{MeV}^3$ of these objects suppress the mean free path of neutrinos to lengths scales that are comparable to the dimensions of stars. All other particles are either trapped efficiently (e.g. photons, electrons) or leave unimpeded (graviton) carrying away energy. Neutrinos are therefore the most relevant vessel to transport energy and lepton number in these systems.

Indeed, our current understanding of the supernova explosion mechanism relies on neutrino energy transport to accelerate the shock wave that would otherwise be stalled by infalling matter. Computer simulations of exploding stars (see Ref. [61] for a review) confirm this picture but they also find that whether a star explodes or not depends sensitively on the approximations that are introduced into the computer code. One of these approximations is to neglect neutrino flavor oscillations.

One might argue that flavor oscillations [64, 65, 199–204] are indeed negligible because interaction and propagation eigenstates are almost aligned in dense media. In a supernova, however, neutrinos are so abundant that ν-ν-refraction contributes substantially to the evolution equations,

[1] This chapter is based on my paper "Neutrino propagation in media: Flavor, helicity, and pair correlations" [2] with A. Kartavtsev and G. Raffelt. See also the proceeding [198] for a summary.

which as a result become non-linear [66–84]. These non-linearities might significantly enhance flavor conversion. If flavor oscillations were to happen close to the shock wave, neutrino transport would be altered greatly since ν_e's are absorbed and their full energy is transmitted while the other flavors only engage in scatterings with a less efficient energy deposition. Flavor oscillations also alter the energy spectrum of neutrinos because the muon and tau neutrino flavors are typically more energetic since they decouple at hotter, more dense areas of the supernova core.

The sensitivity of supernova simulations to neutrino physics highlights the importance of fully understanding the transport equations. A significant step towards this goal was taken by Sigl and Raffelt in Ref. [26], where the authors derived kinetic equations in the density matrix formalism that accounted for flavor oscillations and collisions. The equations described the dynamics of matrices of one-particle correlators $\rho_{ij} \propto \langle a_j^\dagger a_i \rangle$ with number densities on the diagonals and flavor coherence on the off-diagonals (see Sec. 2.4). These authors discarded other possible combinations of creation/annihilations operators: helicity flips, i.e, correlators between particles with different helicity, e.g., $\langle a_{j,+}^\dagger a_{i,-} \rangle$, were neglected because they would appear to the order $[m/(2E)]^2$ in the collision term, which is of the tiny order $\sim 10^{-18}$ for typical neutrino masses m and energies E. Moreover, they argued that correlators between neutrinos and antineutrinos, $\kappa \propto \langle a^\dagger b^\dagger \rangle$, feature fast oscillations with a frequency $\sim 2E$ and would average out to zero. Recently, the interest in these two types of correlators was renewed in the community [85–90, 205, 206], and also our paper [2] contributed to this discussion.

In a detailed quantum kinetic calculation using the closed-time path formalism [85, 86], Vlasenko, Cirigliano and Fuller found that helicity flips occur already at the refractive level and are therefore only suppressed by one mass insertion, $m/(2E)$. While this value is still small, they showed that a resonant enhancement through an adiabatic branch crossing is conceivable (although a substantial amount of tuning is necessary [87]). The impact of helicity flips on supernovae might be significant but depends on the mass type, i.e., if neutrinos have Dirac or Majorana masses. When the neutrinos are of Dirac type, a helicity flip converts an active into a sterile neutrino. This sterile partner interacts even more feebly than the active neutrino such that it streams out of the supernova core unimpeded and its energy is not dumped into the shock wave. If neutrinos are of Majorana type, a helicity flip converts a neutrino into an antineutrino. Besides an altered energy transport, such conversions affect the proton-neutron ratio in the outer parts of the supernova.

Similarly to flavor oscillations, refractive helicity oscillations occur when the background medium is able to mix different helicity states. Because of angular momentum conservation, possible candidates for these background media are matter (axial-)vector currents as well as electromagnetic fields [207–212]. All of the above currents may induce flavor conversions at the same time.

Helicity flips are clear both conceptually and physically. They feature in this chapter because they help us to answer questions pertaining to the second type of correlations mentioned above: the pair correlations denoted by κ. These correlations that were discarded in Ref. [26] reappeared in the works of Volpe and collaborators [88–90]. They argued that pair correlations are an important concept in nuclear physics and that even if they oscillated fast, the average does not necessarily vanish. In order to treat these correlators on the same footing as flavor oscillations, they derived [90] the neutrino density matrix equations in the mean-field limit that included he-

licity flips and pair correlations, explicitly calculating the contributions to first order in $m/(2E)$.

The resulting equations have some perplexing characteristics. The evolution equation for the pair correlators κ contain a source term that is non-zero even if the system does not contain neutrinos, i.e., non-zero coherence is inevitable. Moreover, it is not obvious how the naïve expectation that the pair correlators oscillate with a large frequency is reflected in the kinetic equations.

Besides these technical issues, the physical interpretation of the concept of pair correlations has never been discussed in the works [88–90] and their importance for neutrino propagation in supernovae remained unclear. With these formal and phenomenological questions in mind, we study pair correlations in the mean-field density matrix formalism in this chapter. We re-derive the kinetic equations including flavor, helicity and pair correlations for neutrinos of Dirac and Majorana type. We confirm the previously derived equations for Dirac neutrinos, but find previously missed [90] additional lepton-number violating contributions in the Majorana case. In order to arrive at a physical interpretation, we extract a minimal working model of pair correlations by restricting the equations to a one-generation Weyl neutrino propagating in an anisotropic background; a system that resembles the simplest model of helicity flips (one-flavor Dirac neutrino in anisotropic media) in many regards. We show that pair correlations are equivalent to a coherence between the vacuum and a state that is filled with a neutrino-antineutrino pair with opposite momentum. Hence, non-zero pair correlations lead to spontaneous pair creation. We confirm that the oscillation frequency between these two states is given by the energy difference $2E$, as naïvely expected. On the other hand, the average value for κ is indeed non-vanishing but typically negligibly small for supernova environments. Finally, we comment on our finding that Lorentz covariance is not obtained for pair correlations; a problem that still remains open.

Note that our results have been applied recently [205] to argue that efficient flavor conversion may be triggered by the fast temporal variations inherent to pair correlations. It remains to be seen if the conversions can be sustained long enough to be of relevance [206].

This chapter is be ordered in the following way: in the next section we will motivate our approximations and show how flavor and pair correlations can be unified in a single density matrix equation. As a warm-up, we will parallel Ref. [90] in the derivation of the kinetic equations for Dirac neutrinos in Sec. 4.3, which will be followed (Sec. 4.4) by the corresponding derivation for Majorana neutrinos. Here, we will also find the lepton-number violating contributions that were absent in Ref. [90]. Section 4.5 is devoted to the massless neutrino for two reasons: first, it will elucidate the perplexing feature that the lepton-number violating correlators of the Majorana neutrino do not vanish in the zero-mass limit. Second, the Weyl neutrino is a simple toy model to understand pair correlations. The derived equations will therefore be used in the less technical sections. For completeness, we show how to include electromagnetic fields to the kinetic equations in Sec. 4.6. The physical aspects of helicity and pair correlations will be discussed in Secs. 4.7 and 4.8. There, helicity oscillations are discussed in great detail to facilitate the understanding of the physical interpretation of pair correlations. We conclude this chapter in Sec. 4.9.

4.2 Formalism

Standard Model neutrinos couple via the weak interaction only. For typical core-collapse supernovae neutrinos have a maximal energy of 200 MeV (for degenerate ν_e), which is below the mass scale of the weak gauge bosons. Their cross sections are strongly suppressed by the intermediate propagators of W- and Z-bosons, which may be integrated out. In this Fermi limit the interactions with charged leptons read

$$\mathcal{L}^{\rm cc} = \frac{\mathsf{G}_{\rm F}}{\sqrt{2}}[\bar{\ell}_\alpha \gamma^\mu (1-\gamma^5)\nu_\alpha][\bar{\nu}_\beta \gamma_\mu (1-\gamma^5)\ell_\beta]\,, \tag{4.1}$$

where $\mathsf{G}_{\rm F} = \sqrt{2} g_{\rm W}^2/(8 m_{\rm W}^2) \approx 1.17 \times 10^{-5}\,{\rm GeV}^{-2}$ [10] is the Fermi constant, which contains the weak coupling constant $g_{\rm W}$ and the W-boson mass $m_{\rm W}$. The indices α and β are flavor indices. Measurements of the width of the Z-boson resonance suggest that there are three light neutrino flavors [213]; a result which is consistent with cosmological observations of the number of light degrees of freedom [189].

To describe flavor oscillations in the density matrix formalism, Ref. [26] did not need to distinguish between Dirac and Majorana neutrinos because neutrinos and antineutrinos propagated separately. As soon as we want to describe helicity and pair correlations, the distinction becomes important: for Majorana neutrinos a helicity flip corresponds to a conversion of a particle to an antiparticle, which is not the case for a Dirac neutrino. Pair correlations, on the other hand, couple the propagation of neutrinos and antineutrinos for both Dirac and Majorana neutrinos, but additional consistency relations apply for Majorana neutrinos because of the reduced number of degrees of freedom.

As described in Sec. 2.4 for Dirac neutrinos, we may describe the evolution in terms of the following density matrices and pair correlations that take into account flavor and helicity coherence [26, 85, 90, 123, 214]. The matrices that only include either particles or antiparticles read

$$(2\pi)^3\delta^{(3)}(\mathbf{p}-\mathbf{k})\rho_{ij,sh}(t,\mathbf{p}) = \langle a^\dagger_{j,h}(t,+\mathbf{k}) a_{i,s}(t,+\mathbf{p})\rangle\,, \tag{4.2a}$$

$$(2\pi)^3\delta^{(3)}(\mathbf{p}-\mathbf{k})\bar{\rho}_{ij,sh}(t,\mathbf{p}) = \langle b^\dagger_{i,s}(t,-\mathbf{p}) b_{j,h}(t,-\mathbf{k})\rangle\,, \tag{4.2b}$$

with flavor-basis indices i, j, which we choose to represent mass eigenstates in the following while flavor eigenstates will be denoted with Greek letters α, β, and helicity indices $s, h \in \{+,-\}$. We stress that we use a convention where the density matrix for antineutrinos $\bar{\rho}_{ij,sh}(t,\mathbf{p})$ with momentum $\mathbf{p}$ actually corresponds to the occupation numbers of antineutrinos with physical momentum $-\mathbf{p}$. This convention is necessary to combine ρ and $\bar{\rho}$ in one matrix equation together with the pair correlations, which are defined as [89, 90]

$$(2\pi)^3\delta^{(3)}(\mathbf{p}-\mathbf{k})\kappa_{ij,sh}(t,\mathbf{p}) = \langle b_{j,h}(t,-\mathbf{k}) a_{i,s}(t,+\mathbf{p})\rangle\,, \tag{4.3a}$$

$$(2\pi)^3\delta^{(3)}(\mathbf{p}-\mathbf{k})\kappa^\dagger_{ij,sh}(t,\mathbf{p}) = \langle a^\dagger_{j,h}(t,+\mathbf{p}) b^\dagger_{i,s}(t,-\mathbf{k})\rangle\,, \tag{4.3b}$$

and which involve opposite-momentum modes. We argued before in Sec. 2.4 that the expectation value of two operators with different flavor in Eq. (4.2) violate energy conservation slightly. This

offset then leads to slow oscillations of the off-diagonal density matrix elements with a frequency that is proportional to the amount of energy violation. Similarly, we see that the κ-correlators violate energy conservation by a large amount. We therefore expect them to oscillate fast as we will confirm further below.

Following the earlier literature [88–90], we unify the Dirac expressions (4.2) and (4.3) in an extended density matrix

$$\mathsf{R} = \begin{pmatrix} \rho & \kappa \\ \kappa^\dagger & 1-\bar{\rho} \end{pmatrix} , \tag{4.4}$$

which obeys an equation of motion of the form [88–90]

$$i\dot{\mathsf{R}} = [\mathsf{H}, \mathsf{R}] . \tag{4.5}$$

Here, H is a matrix of oscillation frequencies that are derived from the Hamiltonian. Hence, we will call H the Hamiltonian matrix. It contains the dynamical information, e.g. the usual vacuum oscillations are contained in a submatrix $\mathsf{M}^2/2E$, where M^2 is the matrix of squared neutrino masses. Large parts of the following sections will be devoted to deriving its components. In order to obtain a matrix of oscillation frequencies, we will apply the mean-field approximation (see e.g. Ref. [32]). This means that we will replace pairs of creation and/or annihilation operators by their expectation value until we obtain a bilinear Hamiltonian. The frequencies associated with these bilinears will be the entries of the Hamiltonian matrix. Physically, this approximation corresponds to studying single-particle dynamics in a classical background. Note that this splitting is akin to the molecular chaos hypothesis that we applied to obtain the Boltzmann equation in Sec. 2.2. We will always assume that the background is homogeneous such that the Hamiltonian matrix describes forward-scattering and couples objects of equal momenta.

In order to structure the components of the Hamiltonian matrix, we decompose the Hamiltonian matrix into four matrix-valued entries [88]

$$\mathsf{H} = \begin{pmatrix} \mathsf{H}^{\nu\nu} & \mathsf{H}^{\nu\bar{\nu}} \\ \mathsf{H}^{\bar{\nu}\nu} & \mathsf{H}^{\bar{\nu}\bar{\nu}} \end{pmatrix} \quad . \tag{4.6}$$

The sub-matrices $\mathsf{H}^{\nu\nu}$, $\mathsf{H}^{\nu\bar{\nu}}$ etc. as well as ρ, κ and $\bar{\rho}$ are 6×6 matrices in helicity and flavor space. The product between such matrices in the commutator is defined in the obvious way $(A \cdot B)_{ij,sh} \equiv A_{in,sr} B_{nj,rh}$ with a summation over repeated indices. In the following we write the matrix structure in the form of 2×2 matrices in helicity space,

$$\begin{pmatrix} \boxed{--}_{ij} & \boxed{-+}_{ij} \\ \boxed{+-}_{ij} & \boxed{++}_{ij} \end{pmatrix} , \tag{4.7}$$

where each entry is itself a 3×3 matrix in flavor space.

For Majorana neutrinos, we have half as many degrees of freedom as for Dirac neutrinos. The

components of the extended density matrix R are now defined as

$$(2\pi)^3\delta^{(3)}(\mathbf{p}-\mathbf{k})\rho_{ij,sh}(\mathbf{p}) = \langle a^\dagger_{j,h}(+\mathbf{k})a_{i,s}(+\mathbf{p})\rangle\,, \tag{4.8a}$$

$$(2\pi)^3\delta^{(3)}(\mathbf{p}-\mathbf{k})\bar{\rho}_{ij,sh}(\mathbf{p}) = \langle a^\dagger_{i,s}(-\mathbf{p})a_{j,h}(-\mathbf{k})\rangle\,, \tag{4.8b}$$

$$(2\pi)^3\delta^{(3)}(\mathbf{p}-\mathbf{k})\kappa_{ij,sh}(\mathbf{p}) = \langle a_{j,h}(-\mathbf{k})a_{i,s}(+\mathbf{p})\rangle\,, \tag{4.8c}$$

$$(2\pi)^3\delta^{(3)}(\mathbf{p}-\mathbf{k})\kappa^\dagger_{ij,sh}(\mathbf{p}) = \langle a^\dagger_{j,h}(+\mathbf{p})a^\dagger_{i,s}(-\mathbf{k})\rangle\,, \tag{4.8d}$$

where all operators are taken at the same time t. In the Dirac case, $\kappa^\dagger$ did not have additional information relative to κ. In the Majorana case, we have additional redundancies

$$\bar{\rho}_{ij,sh}(t,\mathbf{p}) = \rho_{ji,hs}(t,-\mathbf{p})\,, \tag{4.9a}$$

$$\kappa_{ij,sh}(t,\mathbf{p}) = -\kappa_{ji,hs}(t,-\mathbf{p})\,, \tag{4.9b}$$

which reflect the reduction of degrees of freedom. Note that in the Majorana case, the pair correlations may violate total lepton number if the helicities are aligned.

4.3 Dirac neutrino

Our first goal is to derive for Dirac neutrinos the components of the Hamiltonian matrix H which govern the evolution equation (4.5) for the extended density matrix R including flavor, helicity, and pair correlations. Here, helicity correlations involve the sterile components of the neutrino field, which otherwise are completely decoupled. This technical section shows in some detail the necessary calculations which might be helpful for the understanding of the later computations for Majorana and Weyl neutrinos.

4.3.1 Two-point correlators and kinetic equations

The kinetic equations for the density matrices Eqs. (4.2) and (4.3) are obtained with the Heisenberg equation of motion as shown in Sec. 2.4. Here, we will employ the mean-field approximation, i.e., we decompose all terms in the Hamiltonian into a product of two creation/annihilation operators and a mean background field. Assuming spatial homogeneity, the interaction Hamiltonian may be written in the compact form

$$H_{\rm mf} = \int \mathrm{d}^3\mathbf{x}\,\bar{\nu}_i(t,\mathbf{x})\Gamma_{ij}\nu_j(t,\mathbf{x})\,, \tag{4.10}$$

where the summation over repeated indices is implied. The operators are carried by the neutrino field

$$\nu_i(t,\mathbf{x}) \equiv \sum_s \int \frac{\mathrm{d}^3\mathbf{p}}{(2\pi)^3}\, e^{i\mathbf{p}\cdot\mathbf{x}}\nu_{i,s}(t,\mathbf{p})\,, \tag{4.11}$$

$$\nu_{i,s}(t,\mathbf{p}) \equiv a_{i,s}(t,\mathbf{p})u_{i,s}(\mathbf{p}) + b^\dagger_{i,s}(t,-\mathbf{p})v_{i,s}(-\mathbf{p})\,. \tag{4.12}$$

The operators a, b satisfy the usual anticommutation relations (2.27). We decompose the kernel Γ_{ij} into Dirac matrices and a potential, which are both specific for the background medium and type of interaction. For a left-chiral interaction with a background medium, it reads

$$\Gamma_{ij} = \gamma_\mu P_L V^\mu_{ij} \,, \tag{4.13}$$

where $P_L = (1-\gamma^5)/2$ is the usual left-chiral projector. The current of background matter V^μ_{ij} will be defined in Eq. (4.34).

Note that Eq. (4.10) contains products of operators that lead to particle-antiparticle correlators, i.e., ab and $b^\dagger a^\dagger$. We want to extract the dynamics of the different operator combinations, which are given by the kernels Γ_{ij}. Motivated by these operator combinations and following [90], we define the matrices

$$\Gamma^{\nu\nu}_{ij,sh}(\mathbf{p}) \equiv \bar{u}_{i,s}(+\mathbf{p})\Gamma_{ij}u_{j,h}(+\mathbf{p}) \,, \tag{4.14a}$$
$$\Gamma^{\nu\bar{\nu}}_{ij,sh}(\mathbf{p}) \equiv \bar{u}_{i,s}(+\mathbf{p})\Gamma_{ij}v_{j,h}(-\mathbf{p}) \,, \tag{4.14b}$$
$$\Gamma^{\bar{\nu}\nu}_{ij,sh}(\mathbf{p}) \equiv \bar{v}_{i,s}(-\mathbf{p})\Gamma_{ij}u_{j,h}(+\mathbf{p}) \,, \tag{4.14c}$$
$$\Gamma^{\bar{\nu}\bar{\nu}}_{ij,sh}(\mathbf{p}) \equiv \bar{v}_{i,s}(-\mathbf{p})\Gamma_{ij}v_{j,h}(-\mathbf{p}) \,, \tag{4.14d}$$

in component form. We can now bring Eq. (4.10) to the desired form bilinear in the creation and annihilation operators

$$\begin{aligned} H_{\rm mf} = \int \frac{\mathrm{d}^3\mathbf{p}}{(2\pi)^3} \Big[& a^\dagger_{i,s}(+\mathbf{p})\Gamma^{\nu\nu}_{ij,sh}(\mathbf{p})a_{j,h}(+\mathbf{p}) \\ & + a^\dagger_{i,s}(+\mathbf{p})\Gamma^{\nu\bar{\nu}}_{ij,sh}(\mathbf{p})b^\dagger_{j,h}(-\mathbf{p}) \\ & + b_{i,s}(-\mathbf{p})\Gamma^{\bar{\nu}\nu}_{ij,sh}(\mathbf{p})a_{j,h}(+\mathbf{p}) \\ & + b_{i,s}(-\mathbf{p})\Gamma^{\bar{\nu}\bar{\nu}}_{ij,sh}(\mathbf{p})b^\dagger_{j,h}(-\mathbf{p}) \Big] \,, \end{aligned} \tag{4.15}$$

where we have omitted the time arguments to shorten the notation. Here again, summation over repeated indices is implied. From Eq. (4.15), we see that the Hamiltonian matrix is obtained by identifying $H^{\nu\nu}_{ij,sh} = \Gamma^{\nu\nu}_{ij,sh}$, $H^{\nu\bar{\nu}}_{ij,sh} = \Gamma^{\nu\bar{\nu}}_{ij,sh}$ etc.

4.3.2 Mean-field limit of the Dirac Hamiltonian

After having established the overall structure of the kinetic equations, we now turn to computing the mean-field limit of the various interactions that appear in the Hamiltonian. In this subsection, we only consider charged and neutral current neutrino interactions, whereas the analysis of the electromagnetic interactions is postponed to Sec. 4.6.

Charged-current interaction

We begin with charged-current (cc) interactions with charged leptons, which will form a classical background after applying the mean-field approximation. In the Fermi limit, the interaction Hamiltonian of the cc-current reads

$$H^{\rm cc} = \sum_{\alpha,\beta} \int \mathrm{d}^3x \, 2\sqrt{2}\mathsf{G}_{\rm F}[\bar{\ell}_\alpha\gamma^\mu P_L\nu_\alpha][\bar{\nu}_\beta\gamma_\mu P_L\ell_\beta] \,, \tag{4.16}$$

where ℓ denotes the spinors of charged leptons with lepton flavor given by $\alpha, \beta \in \{e, \mu, \tau\}$. Expression (4.16) can be rearranged such that charged leptons are grouped in one spinor product and the neutrinos in another. The corresponding Fierz transformation reads [215]

$$[\bar{\ell}_\alpha \gamma^\mu P_L \nu_\alpha][\bar{\nu}_\beta \gamma_\mu P_L \ell_\beta] = [\bar{\ell}_\alpha \gamma^\mu P_L \ell_\beta][\bar{\nu}_\beta \gamma_\mu P_L \nu_\alpha] \,, \tag{4.17}$$

and the charged current Hamiltonian density is thus:

$$\mathcal{H}^{\rm cc} = \sqrt{2}\mathsf{G}_{\rm F} \sum_{\alpha,\beta} \Big[\bar{\nu}_\alpha \gamma^\mu P_L \nu_\beta\Big] \Big[\bar{\ell}_\beta \gamma_\mu (1-\gamma^5) \ell_\alpha\Big] \,. \tag{4.18}$$

In order to obtain the neutrino mean-field Hamiltonian density, we replace the second bracket by its expectation value. In the supernova environment, the temperature is too low to support a substantial density of muons or tauons, and we use only the electron background. Then we find in the mass basis

$$\mathcal{H}^{\rm cc}_{\rm mf} = \sqrt{2}\mathsf{G}_{\rm F} \sum_{i,j} \Big[\bar{\nu}_i \gamma^\mu P_L \nu_j\Big] \Big[U^\dagger_{ie} I^\mu_{\rm cc} U_{ej}\Big] \,, \tag{4.19}$$

where U is the Pontecorvo-Maki-Nakagawa-Sakata (PMNS) matrix. We have introduced a linear combination of vector and axial-vector charged electron currents,

$$I^\mu_{\rm cc} \equiv c_V \langle \bar{e} \gamma^\mu e \rangle - c_A \langle \bar{e} \gamma^\mu \gamma^5 e \rangle \,, \tag{4.20}$$

where $c_V = c_A = 1$. Because electrons are the only background particles contributing to charged current interactions and to simplify the notation, an "e" index is implied in $I^\mu_{\rm cc}$. If the electrons are not polarized, the axial current vanishes and $I^\mu_{\rm cc} = J^\mu_e$, the "convective" electron current.

Neutral-current interaction with matter

The neutral-current (nc) interactions with matter are described in the mass basis by the Hamiltonian density

$$\mathcal{H}^{\rm nc} = \sqrt{2}\mathsf{G}_{\rm F} \sum_{i,f} \Big[\bar{\nu}_i \gamma_\mu P_L \nu_i\Big] \Big[\bar{\psi}_f \gamma^\mu (c^f_{\rm V} - c^f_{\rm A} \gamma^5) \psi_f\Big] \,, \tag{4.21}$$

where f denotes electrons, protons, and neutrons. The resulting contribution to the mean-field Hamiltonian density can be divided into three parts

$$\mathcal{H}^{\rm nc}_{\rm mf} = \sqrt{2}\mathsf{G}_{\rm F} \sum_{i} \Big[\bar{\nu}_i \gamma_\mu P_L \nu_i\Big] \Big[I^\mu_{\rm nc} + I^\mu_p + I^\mu_n\Big] \,, \tag{4.22}$$

where $I^\mu_{\rm nc}$ denotes the electron neutral current (index e implied), whereas the other contributions refer to protons and neutrons as explicitly indicated.

These currents are defined in analogy to Eq. (4.20) with the appropriate coupling constants. For electrons, they are given by $c_{\rm V} = -\frac{1}{2} + 2\sin^2\theta_{\rm W}$ (weak mixing angle $\theta_{\rm W}$) and $c_{\rm A} = -\frac{1}{2}$. For protons, $c_{\rm V} = \frac{1}{2} - 2\sin^2\theta_{\rm W}$, i.e., the same as for electrons with opposite sign, and for neutrons

$c_V = -\frac{1}{2}$. For the nucleon axial vector one often uses $c_\mathrm{A} = \pm 1.26/2$ in analogy to their charged current. However, the strange-quark contribution to the nucleon spin as well as modifications in a dense nuclear medium leave the exact values somewhat open [216, 217], and might lead to successful supernova simulations [62].

In an unpolarized and electrically neutral environment, the axial currents disappear and the electron and proton contributions to the convective neutral current cancel such that in Eq. (4.22) we have $I^\mu_\mathrm{nc} + I^\mu_p + I^\mu_n = -\frac{1}{2} J^\mu_n$, where J^μ_n is the neutron convective current. Neutrino refraction in such a medium depends only on the charged electron current and the neutral neutron current.

Neutrino-neutrino interaction

The most complicated interaction term is the neutral-current neutrino-neutrino scattering. In the mass basis, it is described by the Hamiltonian density

$$\mathcal{H}^{\nu\nu} = \frac{1}{\sqrt{2}} \mathsf{G}_\mathrm{F} \sum_{ij} \left[\bar{\nu}_i \gamma_\mu P_L \nu_i\right] \left[\bar{\nu}_j \gamma^\mu P_L \nu_j\right] . \tag{4.23}$$

To obtain the mean-field Hamiltonian bilinear in the neutrino fields, we need to replace products of two of the four neutrino fields in this expression by their expectation value.

To decompose Eq. (4.23), it is convenient to go to the two-component spinor representation of Ref. [218] (see also appendix A.3 in this thesis). In our convention

$$\gamma^0 \gamma^\mu \frac{1-\gamma^5}{2} = \begin{pmatrix} \bar{\sigma}^\mu & 0 \\ 0 & 0 \end{pmatrix} , \tag{4.24}$$

with the vector of Pauli-matrices

$$\bar{\sigma}^\mu = \begin{pmatrix} \sigma^0 \\ -\sigma^i \end{pmatrix} . \tag{4.25}$$

We see that only a 2×2 submatrix of the 4×4 Dirac matrices contribute, which allows us to write the Hamiltonian density of Eq. (4.23) in the form

$$\mathcal{H}^{\nu\nu} = \frac{\mathsf{G}_\mathrm{F}}{\sqrt{2}} \sum_{i,j} [\nu^\dagger_{i,\dot{\alpha}} \bar{\sigma}^{\mu,\dot{\alpha}\beta} \nu_{i,\beta}] [\nu^\dagger_{j,\dot{\zeta}} \bar{\sigma}^{\dot{\zeta}\xi}_\mu \nu_{j,\xi}] , \tag{4.26}$$

where $\dot{\alpha}, \beta, \dot{\zeta}, \xi \in \{1, 2\}$ and ν_α is the $(1/2, 0)$-part of the four-spinor ν (see appendix A.3). The second two-spinor does not appear in this expression due to the chiral projections.

If we take the expectation value and group all possible combinations of spinors, we obtain four different kinds of terms

$$\begin{aligned} \mathcal{H}^{\nu\nu}_\mathrm{mf} = \frac{\mathsf{G}_\mathrm{F}}{\sqrt{2}} \sum_{ij} \Big[& 2\nu^\dagger_{i,\dot{\alpha}} \bar{\sigma}^{\mu,\dot{\alpha}\beta} \nu_{i,\beta} \langle \nu^\dagger_{j,\dot{\zeta}} \bar{\sigma}^{\dot{\zeta}\xi}_\mu \nu_{j,\xi} \rangle + 2\nu^\dagger_{i,\dot{\alpha}} \bar{\sigma}^{\mu,\dot{\alpha}\beta} \langle \nu_{i,\beta} \nu^\dagger_{j,\dot{\zeta}} \rangle \bar{\sigma}^{\dot{\zeta}\xi}_\mu \nu_{j,\xi} \\ & - \nu^\alpha_i \sigma^\mu_{\alpha\dot{\beta}} \langle \nu^{\dagger,\dot{\beta}}_i \nu^\dagger_{j,\dot{\zeta}} \rangle \bar{\sigma}^{\dot{\zeta}\xi}_\mu \nu_{j,\xi} - \nu^\dagger_{i,\dot{\alpha}} \bar{\sigma}^{\mu,\dot{\alpha}\beta} \langle \nu_{i,\beta} \nu^\xi_j \rangle \sigma_{\mu,\xi\dot{\zeta}} \nu^{\dot{\zeta}}_j \Big] , \end{aligned} \tag{4.27}$$

where in the last two terms we anticommuted two neutrino fields and applied the identity (Eq. 2.30 in Ref. [218])

$$\sigma^{\mu}_{\alpha\dot{\alpha}} = \epsilon_{\alpha\beta}\epsilon_{\dot{\alpha}\dot{\beta}}\bar{\sigma}^{\mu,\dot{\beta}\beta} \,. \tag{4.28}$$

The last two terms in Eq. (4.27) are lepton-number violating and will be discarded in this Dirac treatment. They will reappear in the computation for the Majorana neutrinos.

The second term of Eq. (4.27) may be brought into a more convenient form by virtue of the Fierz identity[2]

$$\bar{\sigma}^{\mu,\dot{\alpha}\alpha}\bar{\sigma}^{\dot{\beta}\beta}_{\mu} = -\bar{\sigma}^{\mu,\dot{\alpha}\beta}\bar{\sigma}^{\dot{\beta}\alpha}_{\mu} \,. \tag{4.29}$$

Anticommuting again, the expression for the Dirac neutrinos reads

$$\begin{aligned}\mathcal{H}^{\nu\nu}_{\mathrm{mf}} =& \sqrt{2}\mathsf{G}_{\mathrm{F}} \sum_{ij} \left[\nu^{\dagger}_{i,\dot{\alpha}}\bar{\sigma}^{\mu,\dot{\alpha}\beta}\nu_{i,\beta}\langle\nu^{\dagger}_{j,\dot{\zeta}}\bar{\sigma}^{\dot{\zeta}\xi}_{\mu}\nu_{j,\xi}\rangle + \nu^{\dagger}_{i,\dot{\alpha}}\bar{\sigma}^{\mu,\dot{\alpha}\beta}\nu_{j,\beta}\langle\nu^{\dagger}_{j,\dot{\zeta}}\bar{\sigma}^{\dot{\zeta}\xi}_{\mu}\nu_{i,\xi}\rangle \right] \\ =& \sqrt{2}\mathsf{G}_{\mathrm{F}} \sum_{ij} \left[\bar{\nu}^{\dagger}_{i}\gamma^{\mu}P_L\nu_i\langle\bar{\nu}^{\dagger}_{j}\gamma_{\mu}P_L\nu_j\rangle + \bar{\nu}_{i}\gamma^{\mu}P_L\nu_j\langle\bar{\nu}_{j}\gamma_{\mu}P_L\nu_i\rangle \right] \,,\end{aligned} \tag{4.30}$$

In line with our previous notation, we denote the mean-field as

$$I^{\mu}_{ij} \equiv \langle\bar{\nu}_j\gamma^{\mu}P_L\nu_i\rangle \,. \tag{4.31}$$

For simplicity, we avoid an explicit "neutrino" and "nc" index, i.e., expressions of the type I^{μ}_{ij} always refer to the neutral neutrino current for the mass states i and j. An explicit expression in terms of the density matrices and pair correlators will be given in Eq. (4.36) below. Altogether, we obtain

$$\mathcal{H}^{\nu\nu}_{\mathrm{mf}} = \sqrt{2}\mathsf{G}_{\mathrm{F}} \sum_{ij} \left[\bar{\nu}_i\gamma_{\mu}P_L\nu_j\right] \left[I^{\mu}_{ij} + \delta_{ij}\textstyle\sum_k I^{\mu}_{kk}\right] \tag{4.32}$$

for the neutrino-neutrino mean-field Hamiltonian.

4.3.3 Components of the Hamiltonian matrix: Dirac neutrino

We may now derive the explicit form of the components of the Hamiltonian matrix. Adding up Eqs. (4.19), (4.22), and (4.32) and using the spinor contractions defined in Eq. (4.14), we find that the components of the Hamiltonian matrix H are of the form

$$\mathsf{H}^{\nu\nu}_{ij,sh} = (\gamma_{\mu}P_L)^{\nu\nu}_{ij,sh}V^{\mu}_{ij} + \delta_{sh}\delta_{ij}E_i \,, \tag{4.33a}$$

$$\mathsf{H}^{\nu\bar{\nu}}_{ij,sh} = (\gamma_{\mu}P_L)^{\nu\bar{\nu}}_{ij,sh}V^{\mu}_{ij} \,, \tag{4.33b}$$

$$\mathsf{H}^{\bar{\nu}\nu}_{ij,sh} = (\gamma_{\mu}P_L)^{\bar{\nu}\nu}_{ij,sh}V^{\mu}_{ij} \,, \tag{4.33c}$$

$$\mathsf{H}^{\bar{\nu}\bar{\nu}}_{ij,sh} = (\gamma_{\mu}P_L)^{\bar{\nu}\bar{\nu}}_{ij,sh}V^{\mu}_{ij} - \delta_{sh}\delta_{ij}E_i \,, \tag{4.33d}$$

[2]The identity can be found in Eq. B.1.31 in Ref. [218]. Note, however, that there is a typo and the σ-matrices on the right-hand side have to be replaced by $\bar{\sigma}$ as follows for example from Eq. B.1.34 of Ref. [218].

where $E_i = (\mathbf{p}^2 + m_i^2)^{\frac{1}{2}}$ is the neutrino energy, and we have identified $\mathsf{H}^{\nu\nu} = \Gamma^{\nu\nu}$, $\mathsf{H}^{\nu\bar{\nu}} = \Gamma^{\nu\bar{\nu}}$, etc.[3]. The currents V_i^μ is given by

$$V_{ij}^\mu = \sqrt{2}\mathsf{G}_\mathrm{F}\Big[U_{ie}^\dagger I_{\mathrm{cc}}^\mu U_{ej} + \delta_{ij}(I_{\mathrm{nc}}^\mu + I_p^\mu + I_n^\mu) + I_{ij}^\mu + \delta_{ij}\textstyle\sum_k I_{kk}^\mu\Big]\,, \tag{4.34}$$

and we have used the compact notation

$$(\gamma_\mu P_L)_{ij,sh}^{\nu\nu} \equiv \bar{u}_{i,s}(+\mathbf{p})\gamma_\mu P_L u_{j,h}(+\mathbf{p})\,, \tag{4.35a}$$
$$(\gamma_\mu P_L)_{ij,sh}^{\nu\bar{\nu}} \equiv \bar{u}_{i,s}(+\mathbf{p})\gamma_\mu P_L v_{j,h}(-\mathbf{p})\,, \tag{4.35b}$$
$$(\gamma_\mu P_L)_{ij,sh}^{\bar{\nu}\nu} \equiv \bar{v}_{i,s}(-\mathbf{p})\gamma_\mu P_L u_{j,h}(+\mathbf{p})\,, \tag{4.35c}$$
$$(\gamma_\mu P_L)_{ij,sh}^{\bar{\nu}\bar{\nu}} \equiv \bar{v}_{i,s}(-\mathbf{p})\gamma_\mu P_L v_{j,h}(-\mathbf{p})\,. \tag{4.35d}$$

Later we will use similar expressions for contractions with other Dirac structures. The neutrino mean-field current itself contains spinor contractions of the type of Eq. (4.35) and can be expressed in terms of the density matrices and pair correlations as

$$\begin{aligned} I_{ij}^\mu = \sum_{s,h}\int \frac{\mathrm{d}^3\mathbf{p}}{(2\pi)^3}\Big[&(\gamma^\mu P_L)_{ji,hs}^{\nu\nu}\rho_{ij,sh} + (\gamma^\mu P_L)_{ji,hs}^{\bar{\nu}\bar{\nu}}(\delta_{ij}\delta_{sh} - \bar{\rho}_{ij,sh}) \\ &+(\gamma^\mu P_L)_{ji,hs}^{\bar{\nu}\nu}\kappa_{ij,sh} + (\gamma^\mu P_L)_{ji,hs}^{\nu\bar{\nu}}\kappa_{ij,sh}^\dagger\Big]\,. \end{aligned} \tag{4.36}$$

Note that in this case there is no implied summation over i and j. The second term on the right-hand side contains a divergent vacuum contribution that must be renormalized.

In order to evaluate the spinor contractions explicitly to lowest order in neutrino masses, we introduce

$$n^\mu = \begin{pmatrix}1\\ \hat{\mathbf{p}}\end{pmatrix}\,, \quad \bar{n}^\mu = \begin{pmatrix}1\\ -\hat{\mathbf{p}}\end{pmatrix}\,, \quad \epsilon^\mu = \begin{pmatrix}0\\ \hat{\boldsymbol{\epsilon}}\end{pmatrix}\,, \tag{4.37}$$

where $\hat{\mathbf{p}}$ is a unit vector in the momentum direction and the complex polarization vectors $\hat{\boldsymbol{\epsilon}}$ and $\hat{\boldsymbol{\epsilon}}^*$ span the plane orthogonal to $\mathbf{p}$ (see Appendix A.3 for more details). We also use ϕ to denote the polar angle of $\mathbf{p}$ in spherical coordinates. To lowest order in m_i, the spinor contractions are found to be (see Appendix A.3)

$$(\gamma_\mu P_L)_{ij,sh}^{\nu\nu} \approx \begin{pmatrix} n_\mu & -e^{+i\phi}\frac{m_j}{2p}\epsilon_\mu^* \\ -e^{-i\phi}\frac{m_i}{2p}\epsilon_\mu & 0\end{pmatrix}\,, \tag{4.38a}$$

$$(\gamma_\mu P_L)_{ij,sh}^{\nu\bar{\nu}} \approx \begin{pmatrix} -e^{+i\phi}\frac{m_j}{2p}n_\mu & \epsilon_\mu^* \\ 0 & -e^{-i\phi}\frac{m_i}{2p}\bar{n}_\mu\end{pmatrix}\,, \tag{4.38b}$$

$$(\gamma_\mu P_L)_{ij,sh}^{\bar{\nu}\nu} \approx \begin{pmatrix} -e^{-i\phi}\frac{m_i}{2p}n_\mu & 0 \\ \epsilon_\mu & -e^{+i\phi}\frac{m_j}{2p}\bar{n}_\mu\end{pmatrix}\,, \tag{4.38c}$$

$$(\gamma_\mu P_L)_{ij,sh}^{\bar{\nu}\bar{\nu}} \approx \begin{pmatrix} 0 & -e^{-i\phi}\frac{m_i}{2p}\epsilon_\mu^* \\ -e^{+i\phi}\frac{m_j}{2p}\epsilon_\mu & \bar{n}_\mu\end{pmatrix}\,, \tag{4.38d}$$

[3]This distinction between Γ and H may seem rather superfluous at this point. It will be of importance for the Majorana case, however.

where in the denominator we identify $p = |\mathbf{p}|$, and we use the notation introduced in Eq. (4.7). As an example, the $\nu\nu$ term, Eq. (4.38a), reads explicitly

$$\boxed{--}^{\nu\nu}_{ij} = \begin{pmatrix} 1 & 1 & 1 \\ 1 & 1 & 1 \\ 1 & 1 & 1 \end{pmatrix} n_\mu \,, \tag{4.39a}$$

$$\boxed{-+}^{\nu\nu}_{ij} = -\frac{1}{2p} \begin{pmatrix} m_1 & m_2 & m_3 \\ m_1 & m_2 & m_3 \\ m_1 & m_2 & m_3 \end{pmatrix} e^{+i\phi} \epsilon^*_\mu \,, \tag{4.39b}$$

$$\boxed{+-}^{\nu\nu}_{ij} = -\frac{1}{2p} \begin{pmatrix} m_1 & m_1 & m_1 \\ m_2 & m_2 & m_2 \\ m_3 & m_3 & m_3 \end{pmatrix} e^{-i\phi} \epsilon_\mu \,, \tag{4.39c}$$

$$\boxed{++}^{\nu\nu}_{ij} = 0 \,. \tag{4.39d}$$

These results agree with those obtained by Serreau and Volpe [90].

4.4 Majorana neutrino

From a theoretical perspective, it is quite natural for neutrino masses to be of Majorana type because this allows them to be created via a type I seesaw mechanism that may also lead to successful Leptogenesis (see chapter 5). In this case, the total number of degrees of freedom is reduced. In the massless limit, the two helicity states of a given family can be identified with neutrino and antineutrino states. A mass term allows mixing between the helicity states and therefore violates lepton number conservation. There are no sterile degrees of freedom. We work out the modifications of the results of the previous section for the Majorana case, concentrating again on technical issues.

4.4.1 Mean-field limit of the Majorana Hamiltonian

In the Majorana case, the momentum decomposition of the neutrino field looks the same as for the Dirac case Eq. (4.11). However, because there are no independent antiparticle degrees of freedom, the field mode $\mathbf{p}$ has the simpler form

$$\nu_{i,s}(t, \mathbf{p}) = a_{i,s}(t, \mathbf{p}) u_{i,s}(\mathbf{p}) + a^\dagger_{i,s}(t, -\mathbf{p}) v_{i,s}(-\mathbf{p}) \,. \tag{4.40}$$

The creation and annihilation operators satisfy the anticommutation relations Eq. (2.27) and the bispinors are the same as in the Dirac case.

The mean-field Hamiltonian, bilinear in the neutrino creation and annihilation operators, is identically formed as the Dirac mean-field Hamiltonian Eq. (4.10). However, because of the lepton-number violating terms we discarded in Eq. (4.27), the kernel has a more general structure as we will demonstrate below,

$$\Gamma_{ij} = \gamma_\mu P_L V^\mu_{ij} + P_L V^R_{ij} + P_R V^L_{ij} \,. \tag{4.41}$$

The first piece, V_{ij}^{μ}, is defined as in Eq. (4.34). In addition, there are two scalar pieces

$$V_{ij}^{L,R} = \sqrt{2}\mathsf{G}_{\mathrm{F}} I_{ij}^{L,R}\,, \tag{4.42}$$

depending, as we will see, on the left-chiral and right-chiral neutrino mean-field scalar background

$$I_{ij}^{L,R} = \langle \bar{\nu}_j P_{L,R} \nu_i \rangle\,. \tag{4.43}$$

These scalar pieces are missing in the previous literature [90], and are one of the main result of this chapter. Their explicit form in terms of the density matrices and pair correlators will be given in Eq. (4.55).

The mean-field Hamiltonian can be written in a form similar to Eq. (4.15),

$$\begin{aligned} H_{\mathrm{mf}} = \sum_{s,h} \int \frac{\mathrm{d}^3\mathbf{p}}{(2\pi)^3} \Big[& a_{i,s}^{\dagger}(+\mathbf{p}) \Gamma_{ij,sh}^{\nu\nu}(\mathbf{p}) a_{j,h}(+\mathbf{p}) \\ & + a_{i,s}^{\dagger}(+\mathbf{p}) \Gamma_{ij,sh}^{\nu\bar{\nu}}(\mathbf{p}) a_{j,h}^{\dagger}(-\mathbf{p}) \\ & + a_{i,s}(-\mathbf{p}) \Gamma_{ij,sh}^{\bar{\nu}\nu}(\mathbf{p}) a_{j,h}(+\mathbf{p}) \\ & + a_{i,s}(-\mathbf{p}) \Gamma_{ij,sh}^{\bar{\nu}\bar{\nu}}(\mathbf{p}) a_{j,h}^{\dagger}(-\mathbf{p}) \Big]\,, \end{aligned} \tag{4.44}$$

where the matrices $\Gamma^{\nu\nu}$, $\Gamma^{\nu\bar{\nu}}$, etc. are the spinor contractions defined in Eq. (4.14). Using the Heisenberg equation of motion with the Hamiltonian Eq. (4.44) one recovers the equation of motion $i\dot{\mathsf{R}} = [\mathsf{H}, \mathsf{R}]$, where R and H have the same structure as in Eq. (4.6). The components of the effective Hamiltonian now read [90]

$$\mathsf{H}_{ij,sh}^{\nu\nu}(\mathbf{p}) = \Gamma_{ij,sh}^{\nu\nu}(\mathbf{p}) - \Gamma_{ji,hs}^{\bar{\nu}\bar{\nu}}(-\mathbf{p})\,, \tag{4.45a}$$

$$\mathsf{H}_{ij,sh}^{\nu\bar{\nu}}(\mathbf{p}) = \Gamma_{ij,sh}^{\nu\bar{\nu}}(\mathbf{p}) - \Gamma_{ji,hs}^{\nu\bar{\nu}}(-\mathbf{p})\,, \tag{4.45b}$$

$$\mathsf{H}_{ij,sh}^{\bar{\nu}\nu}(\mathbf{p}) = \Gamma_{ij,sh}^{\bar{\nu}\nu}(\mathbf{p}) - \Gamma_{ji,hs}^{\bar{\nu}\nu}(-\mathbf{p})\,, \tag{4.45c}$$

$$\mathsf{H}_{ij,sh}^{\bar{\nu}\bar{\nu}}(\mathbf{p}) = \Gamma_{ij,sh}^{\bar{\nu}\bar{\nu}}(\mathbf{p}) - \Gamma_{ji,hs}^{\nu\nu}(-\mathbf{p})\,. \tag{4.45d}$$

Not all of these components are independent. In particular

$$\mathsf{H}_{ij,sh}^{\bar{\nu}\bar{\nu}}(\mathbf{p}) = -\mathsf{H}_{ji,hs}^{\nu\nu}(-\mathbf{p})\,, \tag{4.46a}$$

$$\mathsf{H}_{ij,sh}^{\nu\bar{\nu}}(\mathbf{p}) = -\mathsf{H}_{ji,hs}^{\nu\bar{\nu}}(-\mathbf{p})\,, \tag{4.46b}$$

and together with the Hermiticity of the Hamiltonian, only two of the four sub-matrices of H are independent.

Neutrino-neutrino mean-field Hamiltonian

The Majorana neutrino interaction with matter is described by the same charged- and neutral-current Hamiltonian densities Eqs. (4.18) and (4.21) which lead to the same mean-field currents of electrons and nucleons [see Eqs. (4.19) and (4.22)].

The neutrino-neutrino interaction in the Majorana case is also described by Eq. (4.23). However, Majorana neutrinos violate lepton-number conservation, so we should not discard the previously neglected lepton-number violating combinations $\langle \nu_i \nu_j \rangle$ and $\langle \bar{\nu}_i \bar{\nu}_j \rangle$. Let us therefore take a look at the lepton-violating terms:

$$\mathcal{H}^{\nu\nu}_{\mathrm{mf},\not l} = -\frac{\mathsf{G}_\mathrm{F}}{\sqrt{2}} \sum_{ij} \left[\nu_i^\alpha \sigma^\mu_{\alpha\dot\beta} \langle \nu_i^{\dagger,\dot\beta} \nu^\dagger_{j,\dot\zeta} \rangle \bar\sigma_\mu^{\dot\zeta\xi} \nu_{j,\xi} + \nu^\dagger_{i,\dot\alpha} \bar\sigma^{\mu,\dot\alpha\beta} \langle \nu_{i,\beta} \nu_j^\xi \rangle \sigma_{\mu,\xi\dot\zeta} \nu_j^{\dot\zeta} \right] . \tag{4.47}$$

The Pauli matrices can be rewritten using the identity (Eq. B.1.32 of Ref. [218])

$$\sigma^\mu_{\alpha\dot\alpha} \bar\sigma_\mu^{\dot\beta\beta} = 2 \delta_\alpha^{\ \beta} \delta^{\dot\beta}_{\ \dot\alpha} . \tag{4.48}$$

With the resulting identity matrices and after anticommuting two spinors, we obtain

$$\mathcal{H}^{\nu\nu}_{\mathrm{mf},\not l} = \sqrt{2} \mathsf{G}_\mathrm{F} \sum_{ij} \left[\nu_i^\alpha \nu_{j,\alpha} \langle \nu^\dagger_{j,\dot\beta} \nu_i^{\dagger,\dot\beta} \rangle + \nu^\dagger_{i,\dot\alpha} \nu_j^{\dagger,\dot\alpha} \langle \nu_j^\beta \nu_{i,\beta} \rangle \right] . \tag{4.49}$$

The contractions may be rewritten in bispinor language by noting that for Majorana fields

$$\bar\nu \nu = \left(\nu^\alpha, \nu^\dagger_{\dot\alpha} \right) \begin{pmatrix} \nu_\alpha \\ \nu^{\dagger,\dot\alpha} \end{pmatrix} = \nu^\alpha \nu_\alpha + \nu^\dagger_{\dot\alpha} \nu^{\dagger,\dot\alpha} , \tag{4.50}$$

and

$$\begin{aligned} \nu^\alpha \nu_\alpha &= \bar\nu P_L \nu , \\ \nu^\dagger_{\dot\alpha} \nu^{\dagger,\dot\alpha} &= \bar\nu P_R \nu . \end{aligned} \tag{4.51}$$

Hence, the contractions are just products of two bispinors with a chirality projection. Writing the expectation values as I^L_{ij} and I^R_{ij}, we obtain for the new contribution to the mean-field Hamiltonian density

$$\mathcal{H}^{\nu\nu}_\mathrm{mf} = \sqrt{2} \mathsf{G}_\mathrm{F} \sum_{ij} \left(\left[\bar\nu_i P_R \nu_j \right] I^L_{ij} + \left[\bar\nu_i P_L \nu_j \right] I^R_{ij} \right) . \tag{4.52}$$

These new terms supplement the expression for the effective Majorana Hamiltonian obtained in the previous literature [90].

An alternative way to write the above equation is in terms of charged conjugates. Equation (4.47) reads

$$\mathcal{H}^{\nu\nu}_\mathrm{mf} = \sqrt{2} \mathsf{G}_\mathrm{F} \sum \left(\left[\bar\nu \nu^c \right] I^L + \left[\overline{\nu^c} \nu \right] I^R \right) , \tag{4.53}$$

with the definitions of appendix A.3 and

$$I^L = \langle \overline{\nu^c} \nu \rangle \quad \text{and} \quad I^R = \langle \bar\nu \nu^c \rangle . \tag{4.54}$$

But $\overline{\nu^c} \nu$ is a component of a Majorana mass term. Hence, we see again that these terms are indeed lepton-number violating.

4.4.2 Components of the Hamiltonian matrix: Majorana neutrino

The new contributions stemming from neutrino-neutrino interactions can be expressed in terms of the (anti)particle densities and pair correlators,

$$\begin{aligned} I^L_{ij} = \sum_{s,h} \int \frac{\mathrm{d}^3\mathbf{p}}{(2\pi)^3} \Big[& (P_L)^{\nu\nu}_{ji,hs}\rho_{ij,sh} + (P_L)^{\bar\nu\bar\nu}_{ji,hs}(\delta_{ij}\delta_{sh} - \bar\rho_{ij,sh}) \\ & + (P_L)^{\bar\nu\nu}_{ji,hs}\kappa_{ij,hs} + (P_L)^{\nu\bar\nu}_{ji,hs}\kappa^\dagger_{ij,sh} \Big] , \end{aligned} \tag{4.55}$$

where we have again suppressed the common arguments $(t, \mathbf{p})$. The notation for the scalar contractions $(P_L)^{\nu\nu}_{ij,sh}$ etc. is analogous to Eq. (4.35), except that now there is no γ^μ included.

To lowest order in the small neutrino masses we find, using the explicit form of the chiral spinors of Appendix A.3,

$$(P_L)^{\nu\nu}_{ij,sh} \approx \begin{pmatrix} \frac{m_i}{2p} & 0 \\ 0 & \frac{m_j}{2p} \end{pmatrix} , \tag{4.56a}$$

$$(P_L)^{\nu\bar\nu}_{ij,sh} \approx \begin{pmatrix} 0 & 0 \\ 0 & -e^{-i\phi} \end{pmatrix} , \tag{4.56b}$$

$$(P_L)^{\bar\nu\nu}_{ij,sh} \approx \begin{pmatrix} e^{-i\phi} & 0 \\ 0 & 0 \end{pmatrix} , \tag{4.56c}$$

$$(P_L)^{\bar\nu\bar\nu}_{ij,sh} \approx \begin{pmatrix} -\frac{m_j}{2p} & 0 \\ 0 & -\frac{m_i}{2p} \end{pmatrix} . \tag{4.56d}$$

The components of (P_R) can be obtained from these results using the relations $(P_R)^{\nu\nu}_{ij,sh} = [(P_L)^{\nu\nu}_{ji,hs}]^*$ and $(P_R)^{\nu\bar\nu}_{ij,sh} = [(P_L)^{\bar\nu\nu}_{ji,hs}]^*$, as well as similar relations for the remaining two components.

Using the definitions Eq. (4.45) combined with Eq. (4.38) and the corresponding definition for the scalar case, we obtain for the $\nu\nu$ component of H

$$\begin{aligned} \mathsf{H}^{\nu\nu}_{ij,sh}(\mathbf{p}) = {} & \delta_{sh}\delta_{ij}E_i + (\gamma_\mu P_L)^{\nu\nu}_{ij,sh}(\mathbf{p})V^\mu_{ij} - (\gamma_\mu P_L)^{\bar\nu\bar\nu}_{ji,hs}(-\mathbf{p})V^\mu_{ji} \\ & + (P_L)^{\nu\nu}_{ij,sh}(\mathbf{p})V^R_{ij} - (P_L)^{\bar\nu\bar\nu}_{ji,hs}(-\mathbf{p})V^R_{ji} \\ & + (P_R)^{\nu\nu}_{ij,sh}(\mathbf{p})V^L_{ij} - (P_R)^{\bar\nu\bar\nu}_{ji,hs}(-\mathbf{p})V^L_{ji} . \end{aligned} \tag{4.57}$$

The first line generalizes the Dirac result of Eq. (4.33a) to the Majorana case and has been obtained in Ref. [90]. The second and third lines stem from the the contractions Eq. (4.52) and supplement the previous results.

The $\bar\nu\bar\nu$ term follows from the identity Eq. (4.46). For the $\nu\bar\nu$ component we find

$$\begin{aligned} \mathsf{H}^{\nu\bar\nu}_{ij,sh}(\mathbf{p}) = {} & (\gamma_\mu P_L)^{\nu\bar\nu}_{ij,sh}(\mathbf{p})V^\mu_{ij} - (\gamma_\mu P_L)^{\nu\bar\nu}_{ji,hs}(-\mathbf{p})V^\mu_{ji} \\ & + (P_L)^{\nu\bar\nu}_{ij,sh}(\mathbf{p})V^R_{ij} - (P_L)^{\nu\bar\nu}_{ji,hs}(-\mathbf{p})V^R_{ji} \\ & + (P_R)^{\nu\bar\nu}_{ij,sh}(\mathbf{p})V^L_{ij} - (P_R)^{\nu\bar\nu}_{ji,hs}(-\mathbf{p})V^L_{ji} . \end{aligned} \tag{4.58}$$

The $\bar{\nu}\nu$ component follows from replacing $\nu\bar{\nu}$ with $\bar{\nu}\nu$ everywhere in this result.

Inspection of Eqs. (4.55) and (4.56) shows that the last two lines of Eq. (4.57) contain terms proportional to κ and $\kappa^\dagger$ that are linear in the neutrino masses, and additionally terms quadratic in the neutrino masses which we neglect here.

A peculiar feature of Eq. (4.58) is that its last two lines contain terms proportional to κ and $\kappa^\dagger$ that are not suppressed by the neutrino masses and therefore do not vanish when we set the masses to zero. This is somewhat surprising because we expect that Dirac and Majorana neutrinos are equivalent for $m_\nu \to 0$. Therefore, the components of H must coincide in this limit. We return to this questions in Sec. 4.5, where we study the case of massless two-component neutrinos and demonstrate that in the massless limit these additional terms, which are proportional to the lepton-number violating correlators, are not produced if they are zero initially.

On the other hand, one important finding of this section is that for a Majorana neutrino with an arbitrary small mass, lepton-number violating correlators are automatically produced and, in turn, induce the additional scalar background terms of the mean-field Hamiltonian which then affect the dynamics of the density matrices. Lepton-number violating correlators cannot be avoided.

4.5 Weyl neutrino

In the previous section we have found that the additional scalar contributions to the mean-field Hamiltonian, that naturally arise for Majorana neutrinos, do not vanish in the massless limit. This is somewhat surprising because we expect no difference between Dirac and Majorana neutrinos in this case. In order to clarify this paradox, we study a single generation of massless neutrinos. The equations presented in this section will also be used later to study particle-antiparticle coherence.

4.5.1 Standard two-point correlators and kinetic equations

In the Weyl case, the momentum decomposition of the neutrino field looks the same as for the Dirac case Eq. (4.11). However, because a Weyl fermion has only two degrees of freedom the field mode $\mathbf{p}$ does not carry a spin index,

$$\nu(t,\mathbf{p}) = a(t,\mathbf{p})u_{-}(\mathbf{p}) + b^\dagger(t,-\mathbf{p})v_{+}(-\mathbf{p})\,. \tag{4.59}$$

It is automatically left-chiral because the right-chiral components of the chiral spinors $u_{-}(\mathbf{p})$ and $v_{+}(-\mathbf{p})$ vanish in the massless limit, see Appendix A.3.

If we require lepton-number conservation then the only correlators that do not vanish are

$$(2\pi)^3\delta^{(3)}(\mathbf{p}-\mathbf{k})\rho_{--}(\mathbf{p}) = \langle a^\dagger(+\mathbf{k})a(+\mathbf{p})\rangle\,, \tag{4.60a}$$

$$(2\pi)^3\delta^{(3)}(\mathbf{p}-\mathbf{k})\bar{\rho}_{++}(\mathbf{p}) = \langle b^\dagger(-\mathbf{k})b(-\mathbf{p})\rangle\,, \tag{4.60b}$$

$$(2\pi)^3\delta^{(3)}(\mathbf{p}-\mathbf{k})\kappa_{-+}(\mathbf{p}) = \langle b(-\mathbf{k})a(+\mathbf{p})\rangle\,, \tag{4.60c}$$

$$(2\pi)^3\delta^{(3)}(\mathbf{p}-\mathbf{k})\kappa^\dagger_{+-}(\mathbf{p}) = \langle a^\dagger(+\mathbf{p})b^\dagger(-\mathbf{k})\rangle\,. \tag{4.60d}$$

Note that we keep helicity indices in the definitions of the density matrices to distinguish the lepton-number conserving correlators from the lepton-number violating ones, which we introduce below in Sec. 4.5.2.

We can extract the explicit form of the kinetic equations for these correlators from Eq. (4.5),

$$i\dot{\rho}_{--} = \mathsf{H}^{\nu\nu}_{--}\rho_{--} - \rho_{--}\mathsf{H}^{\nu\nu}_{--} + \mathsf{H}^{\nu\bar{\nu}}_{-+}\kappa^{\dagger}_{+-} - \kappa_{-+}\mathsf{H}^{\bar{\nu}\nu}_{+-}\,, \tag{4.61a}$$

$$i\dot{\bar{\rho}}_{++} = \mathsf{H}^{\bar{\nu}\bar{\nu}}_{++}\bar{\rho}_{++} - \bar{\rho}_{++}\mathsf{H}^{\bar{\nu}\bar{\nu}}_{++} - \mathsf{H}^{\bar{\nu}\nu}_{+-}\kappa_{-+} + \kappa^{\dagger}_{+-}\mathsf{H}^{\nu\bar{\nu}}_{-+}\,, \tag{4.61b}$$

$$i\dot{\kappa}_{-+} = \mathsf{H}^{\nu\nu}_{--}\kappa_{-+} - \kappa_{-+}\mathsf{H}^{\bar{\nu}\bar{\nu}}_{++} - \mathsf{H}^{\nu\bar{\nu}}_{-+}\bar{\rho}_{++} - \rho_{--}\mathsf{H}^{\nu\bar{\nu}}_{-+} + \mathsf{H}^{\nu\bar{\nu}}_{-+}\,, \tag{4.61c}$$

where we omit the arguments $(t, \mathbf{p})$, which are common to all the functions, to shorten the notation. Note that for a single neutrino generation the first two terms in Eqs. (4.61a) and (4.61b) cancel each other and we have retained them only to keep the resemblance with the general form of the kinetic equations.

A peculiar feature of (4.61c) is that κ, i.e., coherence between $|00\rangle$ and $|11\rangle$ states, is automatically induced provided that the mean-field Hamiltonian matrix $\mathsf{H}_{\rm mf}$ has nonzero off-diagonals because of the last term on the right-hand side. The off-diagonals are non-zero even if all neutrino two-point functions are zero initially if the background medium contains, for instance, a transverse neutron current [cf. Eq. (4.33) with Eq. (4.34)].

The explicit form of the mean-field Hamiltonian can be obtained from Eq. (4.38) by setting the masses to zero,

$$\mathsf{H}^{\nu\nu}_{--}(\mathbf{p}) = E + V^0 - \hat{\mathbf{p}}\cdot\mathbf{V}\,, \tag{4.62a}$$

$$\mathsf{H}^{\nu\bar{\nu}}_{-+}(\mathbf{p}) = -\hat{\boldsymbol{\epsilon}}^*\cdot\mathbf{V}\,, \tag{4.62b}$$

$$\mathsf{H}^{\bar{\nu}\nu}_{+-}(\mathbf{p}) = -\hat{\boldsymbol{\epsilon}}\cdot\mathbf{V}\,, \tag{4.62c}$$

$$\mathsf{H}^{\bar{\nu}\bar{\nu}}_{++}(\mathbf{p}) = -E + V^0 + \hat{\mathbf{p}}\cdot\mathbf{V}\,, \tag{4.62d}$$

where $E = |\mathbf{p}|$. Note that the $\hat{\mathbf{p}}\cdot\mathbf{V}$ term in Eq. (4.62a) accounts for the enhancement (suppression) of the mean-field potential for the matter flowing antiparallel (parallel) to the neutrino momentum. This point has been observed in Ref. [208].

It remains to express the neutrino current I^μ in terms of the density matrices and pair correlations. For its zero component we obtain from Eq. (4.36), $I^0 = \int \mathrm{d}^3\mathbf{p}/(2\pi)^3\,\ell$, where $\ell(t,\mathbf{p}) \equiv \rho(t,\mathbf{p}) - \bar{\rho}(t,-\mathbf{p})$ has the meaning of lepton number in mode $\mathbf{p}$. For the spatial components we find

$$\mathbf{I} = \int \frac{\mathrm{d}^3\mathbf{p}}{(2\pi)^3}\,\left(\hat{\mathbf{p}}\,\ell + \hat{\boldsymbol{\epsilon}}\,\kappa + \hat{\boldsymbol{\epsilon}}^*\kappa^\dagger\right)\,, \tag{4.63}$$

which is identical to the result of Ref. [90].

4.5.2 Lepton-number violating correlators and kinetic equations

Without lepton-number violating correlators we reproduced the standard result. If we allow for $\langle\nu\nu\rangle$ and $\langle\bar{\nu}\bar{\nu}\rangle$ contractions then, similarly to the Majorana case, the mean-field Hamiltonian

receives contributions of the type (4.49). For Weyl spinors, we may again rewrite this term as

$$\mathcal{H}^{\nu\nu}_{\rm mf} = \sqrt{2}\mathsf{G}_{\rm F}\sum\Big(\Big[\bar{\nu}\nu^c\Big]I^L + \Big[\overline{\nu^c}\nu\Big]I^R\Big)\,, \tag{4.64}$$

and

$$I^L = \langle\overline{\nu^c}\nu\rangle \quad \text{and} \quad I^R = \langle\bar{\nu}\nu^c\rangle\,. \tag{4.65}$$

As has been mentioned above $\overline{\nu^c}\nu$ and $\bar{\nu}\nu^c$ have the structure of the Majorana mass term, which is known to violate lepton number. Therefore, we expect that also here the Hamiltonian (4.64) leads to lepton-number violation. However, for Weyl neutrinos the inclusion of these additional terms is somewhat artificial because, as we will show below, these correlations are not produced if they are zero initially. They are considered here to better understand the Majorana case, where they are naturally produced by the lepton-number violating interactions.

The contribution of Eq. (4.64) to the mean-field Hamiltonian is given by

$$\begin{aligned} H_{\rm mf} \supset \int \frac{{\rm d}^3\mathbf{p}}{(2\pi)^3}\Big[&a^\dagger(+\mathbf{p})\Gamma^{\nu\bar{\nu}}_{--}(\mathbf{p})a^\dagger(-\mathbf{p}) + b(-\mathbf{p})\Gamma^{\bar{\nu}\nu}_{++}(\mathbf{p})b(+\mathbf{p}) \\ &+b^\dagger(+\mathbf{p})\Gamma^{\nu\bar{\nu}}_{++}(\mathbf{p})b^\dagger(-\mathbf{p}) \\ &+a(-\mathbf{p})\Gamma^{\bar{\nu}\nu}_{--}(\mathbf{p})a(+\mathbf{p})\Big]\,, \end{aligned} \tag{4.66}$$

and strongly resembles the mean-field Hamiltonian of Majorana neutrinos Eq. (4.44). From the structure of Eq. (4.66) it is evident that, as expected, it leads to the violation of lepton number. We are also forced to introduce the following lepton-number violating correlators,

$$(2\pi)^3\delta^{(3)}(\mathbf{p}-\mathbf{k})\kappa_{--}(\mathbf{p}) = \langle a(-\mathbf{k})a(+\mathbf{p})\rangle\,, \tag{4.67a}$$
$$(2\pi)^3\delta^{(3)}(\mathbf{p}-\mathbf{k})\kappa_{++}(\mathbf{p}) = \langle b(-\mathbf{k})b(+\mathbf{p})\rangle\,, \tag{4.67b}$$
$$(2\pi)^3\delta^{(3)}(\mathbf{p}-\mathbf{k})\kappa^\dagger_{--}(\mathbf{p}) = \langle a^\dagger(+\mathbf{p})a^\dagger(-\mathbf{k})\rangle\,, \tag{4.67c}$$
$$(2\pi)^3\delta^{(3)}(\mathbf{p}-\mathbf{k})\kappa^\dagger_{++}(\mathbf{p}) = \langle b^\dagger(+\mathbf{p})b^\dagger(-\mathbf{k})\rangle\,, \tag{4.67d}$$

which also resemble the Majorana definitions Eq. (4.8). These correlators are dictated by the structure of the Hamiltonian Eq. (4.66) and are the only lepton-number violating correlators we consider in this section.

The lepton-number violating correlators contribute to the dynamics of the lepton number conserving ones,

$$i\dot{\rho}_{--}(\mathbf{p}) \supset +\Big(\Gamma^{\nu\bar{\nu}}_{--}(\mathbf{p}) - [\Gamma^{\nu\bar{\nu}}_{--}(-\mathbf{p})]^T\Big)\kappa^\dagger_{--}(\mathbf{p}) - \kappa_{--}(\mathbf{p})\Big(\Gamma^{\bar{\nu}\nu}_{--}(\mathbf{p}) - [\Gamma^{\bar{\nu}\nu}_{--}(\mathbf{p})]^T\Big)\,, \tag{4.68a}$$
$$i\dot{\bar{\rho}}_{++}(\mathbf{p}) \supset -\Big(\Gamma^{\bar{\nu}\nu}_{++}(\mathbf{p}) - [\Gamma^{\bar{\nu}\nu}_{++}(-\mathbf{p})]^T\Big)\kappa_{++}(\mathbf{p}) + \kappa^\dagger_{++}(\mathbf{p})\Big(\Gamma^{\nu\bar{\nu}}_{++}(\mathbf{p}) - [\Gamma^{\nu\bar{\nu}}_{++}(-\mathbf{p})]^T\Big)\,, \tag{4.68b}$$

where terms that already appeared in Eq. (4.61) have been omitted and the superscript T stands for transposition of the flavor and helicity indices. Comparing Eq. (4.68) with Eqs. (4.45b) and (4.45c) we see that we automatically recover the 'Majorana' definitions of the Hamiltonian matrix. Note that to avoid confusion with the definitions of the elements of the mean-field Hamiltonian matrix H_{sh}, which are different for Dirac and Majorana neutrinos, we write the right-hand

side of Eq. (4.68) directly in terms of the spinor contractions Γ_{sh} defined in Eq. (4.14). The dynamics of κ_{-+}, see Eq. (4.61c), does not obtain additional terms from lepton-number violating correlators. The reason is that the components of the mean-field Hamiltonian that are needed in Eq. (4.61c) to form the right spin combination with the lepton-number violating correlators (4.67) vanish for Weyl neutrinos. The kinetic equations for the lepton-number violating pair correlations read

$$\begin{aligned} i\dot{\kappa}_{--}(\mathbf{p}) = &\left[\Gamma^{\nu\nu}_{--}(\mathbf{p}) + [\Gamma^{\nu\nu}_{--}(-\mathbf{p})]^T\right]\kappa_{--}(\mathbf{p}) - \left[\Gamma^{\nu\bar{\nu}}_{--}(\mathbf{p}) - [\Gamma^{\nu\bar{\nu}}_{--}(-\mathbf{p})]^T\right]\rho_{--}(\mathbf{p}) \\ &- \left[\Gamma^{\nu\bar{\nu}}_{--}(\mathbf{p}) - [\Gamma^{\nu\bar{\nu}}_{--}(-\mathbf{p})]^T\right][\rho_{--}(-\mathbf{p})]^T + \left[\Gamma^{\nu\bar{\nu}}_{--}(\mathbf{p}) - [\Gamma^{\nu\bar{\nu}}_{--}(-\mathbf{p})]^T\right], \end{aligned} \tag{4.69a}$$

$$\begin{aligned} i\dot{\kappa}_{++}(\mathbf{p}) = &-\left[\Gamma^{\bar{\nu}\bar{\nu}}_{++}(\mathbf{p}) + [\Gamma^{\bar{\nu}\bar{\nu}}_{++}(-\mathbf{p})]^T\right]\kappa_{++}(\mathbf{p}) - \left[\Gamma^{\nu\bar{\nu}}_{++}(\mathbf{p}) - [\Gamma^{\nu\bar{\nu}}_{++}(-\mathbf{p})]^T\right]\bar{\rho}_{++}(\mathbf{p}) \\ &- \left[\Gamma^{\nu\bar{\nu}}_{++}(\mathbf{p}) - [\Gamma^{\nu\bar{\nu}}_{++}(-\mathbf{p})]^T\right][\bar{\rho}_{++}(-\mathbf{p})]^T + \left[\Gamma^{\nu\bar{\nu}}_{++}(\mathbf{p}) - [\Gamma^{\nu\bar{\nu}}_{++}(-\mathbf{p})]^T\right]. \end{aligned} \tag{4.69b}$$

Their form can be guessed from Eq. (4.61c) by replacing components of the mean-field Hamiltonian with their 'Majorana' counterparts, taking into account that $\Gamma^{\bar{\nu}\bar{\nu}}_{--} = \Gamma^{\nu\nu}_{++} = 0$, and replacing $\bar{\rho}_{--}(\mathbf{p})$ by $[\rho_{--}(-\mathbf{p})]^T$ as well as $\rho_{++}(\mathbf{p})$ by $[\bar{\rho}_{++}(-\mathbf{p})]^T$.

Using the explicit form of the chiral spinors, see appendix A.3, we obtain

$$\Gamma^{\nu\bar{\nu}}_{--}(\mathbf{p}) = +e^{+i\phi}V^L\,, \qquad \Gamma^{\nu\bar{\nu}}_{++}(\mathbf{p}) = -e^{-i\phi}V^R\,, \tag{4.70a}$$

$$\Gamma^{\bar{\nu}\nu}_{--}(\mathbf{p}) = +e^{-i\phi}V^R\,, \qquad \Gamma^{\bar{\nu}\nu}_{++}(\mathbf{p}) = -e^{+i\phi}V^L\,, \tag{4.70b}$$

where $V^{L(R)} = \sqrt{2}\mathsf{G}_{\rm F}I^{L(R)}$ are defined analogously to Eq. (4.42). Let us now recall that I^L and I^R are produced only by neutrino self-interactions and are proportional to the lepton number violating pair correlations [cf. Eqs. (4.67)],

$$I^L = \int \frac{\mathrm{d}^3\mathbf{p}}{(2\pi)^3}\, e^{-i\phi}\left[\kappa_{--} - \kappa^\dagger_{++}\right], \tag{4.71}$$

and a similar expression for I^R. Thus, if the lepton-number violating correlators are zero initially, then the components in Eqs. (4.70) are zero, and κ_{--} and κ_{++} remain zero in the course of the system's evolution. For this reason the inclusion of lepton-number violating correlators for Weyl neutrinos is rather artificial because they could only exist if they were put in by hand initially.

This observation explains why similar contributions did not vanish for Majorana neutrinos in the limit of zero neutrino masses in Sec. 4.4.2. These correlators might still evolve dynamically for vanishing Majorana mass, but only if the initial conditions allow them to deviate from zero. If they vanish at the beginning, they may only deviate from zero if there is a Majorana mass.

4.6 Electromagnetic background fields

A supernova environment is characterized not only by matter currents, but also by strong magnetic fields. Electromagnetic (EM) fields polarize both background media and the vacuum. Although neutrinos do not couple directly to the electromagnetic fields, they feel the induced polarization through quantum loops of charged particles. The coupling to a polarized background

medium has been treated in the previous sections. We now turn to the interaction with the vacuum polarization.

The effect of vacuum polarization is described by electromagnetic form factors. The most prominent examples, the magnetic and electric dipole moments, are inevitable for massive neutrinos and have to be included to obtain consistent evolution equations linear in the neutrino mass. The main effects of electromagnetic fields are spin and spin-flavor oscillations, which can be significant. We treat Dirac and Majorana neutrinos separately.

4.6.1 General vertex structure

The coupling of neutrinos to an external vector potential A^μ can be written as an effective vertex $\mathcal{H}^{\rm em} = A_\mu \bar{\nu} \Gamma^\mu \nu$, where Γ^μ contains all irreducible combinations of Lorentz vectors and pseudovectors generated by external momenta and Dirac matrices. Neglecting a hypothetical minicharge, in coordinate space the most general Hamiltonian density can be reduced to

$$\mathcal{H}^{\rm em} = \frac{1}{2} F_{\mu\nu}\, \bar{\nu}_i \Big(f_{\rm M}^{ij} \sigma^{\mu\nu} + i f_{\rm E}^{ij} \sigma^{\mu\nu}\gamma^5 \Big) \nu_j + \partial^\nu F_{\mu\nu}\, \bar{\nu}_i \Big(f_Q^{ij} \gamma^\mu + f_A^{ij} \gamma^\mu \gamma^5 \Big) \nu_j \,, \tag{4.72}$$

where the electromagnetic field strength tensor is defined as usual, $F^{\mu\nu} = \partial^\mu A^\nu - \partial^\nu A^\mu$, and $\sigma^{\mu\nu} = \frac{i}{2}[\gamma^\mu, \gamma^\nu]$. The form factors are $f_{\rm M}$ (magnetic), $f_{\rm E}$ (electric), $f_{\rm Q}$ (reduced charge [219]), and $f_{\rm A}$ (anapole). The form factors carry generation indices. Diagonal elements describe the usual electromagnetic properties of a neutrino in the mass basis, and reduce to electromagnetic *moments* in the static limit. The off-diagonal elements describe transitions between neutrinos of different masses.

Maxwell's equations tell us that $\partial_\nu F^{\mu\nu} = -J^\mu_{\rm em}$, where $J^\mu_{\rm em}$ is some charged matter background that sources electromagnetic fields. In supernovae, the sources are electrons and protons. In the Standard Model with massless neutrinos, the value for the anapole moment has to be $f_{\rm A} = -f_{\rm Q}$ to reproduce the left-chiral form of the interaction. For models with neutrino masses, the Hamiltonian matrix might obtain contributions that are not purely left-chiral, but we assume that these are always small so that we can neglect them. The charge and anapole form factors then only yield radiative corrections to the left-chiral tree level coupling in Eq. (4.18). We neglect these moments because we are not interested in corrections to leading order effects.

4.6.2 Dipole moments of Dirac neutrinos

To study the dipole moments, we first turn to the somewhat simpler case of Dirac neutrinos. Because we assume neutrinos to carry no charge, $\mu = f_{\rm M}(0)$ is defined as the magnetic moment and $\epsilon = f_{\rm E}(0)$ as the electric dipole moment [219]. In the minimal extension of the Standard

Model, the magnetic moments are found to be [220]

$$\mu_{ij} = \frac{3e\sqrt{2}\mathsf{G}_{\mathrm{F}}(m_i + m_j)}{2(4\pi)^2}\left(\delta_{ij} - \frac{m_\tau^2}{2m_W^2}\mathcal{F}_{ij}\right), \tag{4.73a}$$

$$i\epsilon_{ij} = -\frac{3e\sqrt{2}\mathsf{G}_{\mathrm{F}}}{2(4\pi)^2}(m_i - m_j)\left(\frac{m_\tau^2}{2m_W^2}\right)\mathcal{F}_{ij}\,, \tag{4.73b}$$

$$\mathcal{F}_{ij} = \sum_{\alpha=e,\mu,\tau} U_{i\alpha}^\dagger \left(\frac{m_\alpha}{m_\tau}\right)^2 U_{\alpha j}\,, \tag{4.73c}$$

where m_τ is the tau mass. The electric dipole moment does not have a diagonal component because it would violate CP [219], and the transition electric dipole moment carries a phase relative to the transition magnetic dipole moment.

Note that the appearance of the masses in Eq. (4.73) is such that the sum of magnetic and electric dipole transition moments are always proportional to the mass of the "wrong-helicity" neutrino [221]. This is in agreement with our results in Sec. 4.3.2 about spin flips from convective media, where the corresponding mass appears in the Hamiltonian matrix.

Numerically, the above expressions yield for the diagonal magnetic moments

$$\mu_{ii} \simeq 3.2 \times 10^{-19}\left(\frac{m_i}{\mathrm{eV}}\right)\mu_{\mathrm{B}}\,, \tag{4.74}$$

where μ_{B} is the Bohr magneton. The transition moments are

$$\mu_{ij} \simeq -3.9 \times 10^{-23}\mathcal{F}_{ij}\left(\frac{m_i + m_j}{\mathrm{eV}}\right)\mu_{\mathrm{B}}\,, \tag{4.75a}$$

$$\epsilon_{ij} \simeq 3.9\,i \times 10^{-23}\mathcal{F}_{ij}\left(\frac{m_i - m_j}{\mathrm{eV}}\right)\mu_{\mathrm{B}}\,. \tag{4.75b}$$

Note that the transition moments are much smaller than the diagonal moments due to GIM suppression.

4.6.3 Hamiltonian matrix for Dirac neutrinos

We treat electromagnetic effects on the same footing as background matter. To this end, we have to evaluate the components of the Hamiltonian matrix, which for Dirac neutrinos are equal to the spinor contractions in Eq. (4.14). For these contractions we need to evaluate the Lorentz structure of the vertex in Eq. (4.72).

Considering only magnetic and electric form factors, the Hamiltonian reduces to

$$\frac{1}{2}F_{\mu\nu}\bar{\nu}_i\Big(f_{\mathrm{M}}^{ij}\sigma^{\mu\nu} + if_{\mathrm{E}}^{ij}\sigma^{\mu\nu}\gamma^5\Big)\nu_j\,, \tag{4.76}$$

which depends on the electric and magnetic fields, $\mathbf{E}$ and $\mathbf{B}$, through $F^{\mu\nu}$. The Lorentz structure can be decomposed into the contractions $\left(i\gamma^0\boldsymbol{\gamma}\right)_{ij,sh}$ and $\left(\gamma^0\boldsymbol{\gamma}\gamma^5\right)_{ij,sh}$, the latter appearing

through the identity $\epsilon^{abc}\gamma^0\gamma_c\gamma^5 = \sigma^{ab}$ with spatial indices $a, b, c = 1, 2$ or 3, and the asymmetric tensor ϵ^{abc}. These contractions are three-vectors that are multiplied by the electric and magnetic fields. We calculate the resulting expressions in momentum space.

Explicitly, the coupling of the magnetic field through the magnetic form factor, superscript $\mu\mathrm{B}$, has the structures

$$\mathsf{H}^{\mu\mathrm{B}\nu\nu}_{ij,sh} = -\left(\gamma^0\boldsymbol{\gamma}\gamma^5\right)^{\nu\nu}_{ij,sh} f^{ij}_{\mathrm{M}}(q^2)\mathbf{B}\,, \qquad \mathsf{H}^{\mu\mathrm{B}\nu\bar{\nu}}_{ij,sh} = -\left(\gamma^0\boldsymbol{\gamma}\gamma^5\right)^{\nu\bar{\nu}}_{ij,sh} f^{ij}_{\mathrm{M}}(l^2)\mathbf{B}\,, \tag{4.77a}$$

$$\mathsf{H}^{\mu\mathrm{B}\bar{\nu}\nu}_{ij,sh} = -\left(\gamma^0\boldsymbol{\gamma}\gamma^5\right)^{\bar{\nu}\nu}_{ij,sh} f^{ij}_{\mathrm{M}}(l^2)\mathbf{B}\,, \qquad \mathsf{H}^{\mu\mathrm{B}\bar{\nu}\bar{\nu}}_{ij,sh} = -\left(\gamma^0\boldsymbol{\gamma}\gamma^5\right)^{\bar{\nu}\bar{\nu}}_{ij,sh} f^{ij}_{\mathrm{M}}(q^2)\mathbf{B}\,, \tag{4.77b}$$

where we identify $\mathsf{H}^{\nu\nu} = \Gamma^{\nu\nu}$, $\mathsf{H}^{\nu\bar{\nu}} = \Gamma^{\nu\bar{\nu}}$, etc., and the minus sign in the metric $g^{\mu\nu} = \mathrm{diag}(1, -1, -1, -1)$ has already been taken care of. In Eq. (4.77), the form factors still depend on the momentum transfer. For the $\nu\nu$ and $\bar{\nu}\bar{\nu}$ components, the form factors contain $q^\mu = p^\mu_{\mathrm{out}} - p^\mu_{\mathrm{in}}$, where $q^\mu \to 0$ in the forward scattering limit. These components are then proportional to the dipole moments. For the neutrino-antineutrino components of the H matrices, the argument of the form factor contains l^2 with $l^\mu = p^\mu_{\mathrm{out}} + p^\mu_{\mathrm{in}}$, the sum of neutrino and antineutrino four-momenta.

The coupling of the magnetic field to the electric form factor, superscript $\epsilon\mathrm{B}$, is

$$\mathsf{H}^{\epsilon\mathrm{B}\nu\nu}_{ij,sh} = -\left(i\gamma^0\boldsymbol{\gamma}\right)^{\nu\nu}_{ij,sh} f^{ij}_{\mathrm{E}}(q^2)\mathbf{B}\,, \qquad \mathsf{H}^{\epsilon\mathrm{B}\nu\bar{\nu}}_{ij,sh} = -\left(i\gamma^0\boldsymbol{\gamma}\right)^{\nu\bar{\nu}}_{ij,sh} f^{ij}_{\mathrm{E}}(l^2)\mathbf{B}\,, \tag{4.78a}$$

$$\mathsf{H}^{\epsilon\mathrm{B}\bar{\nu}\nu}_{ij,sh} = -\left(i\gamma^0\boldsymbol{\gamma}\right)^{\bar{\nu}\nu}_{ij,sh} f^{ij}_{\mathrm{E}}(l^2)\mathbf{B}\,, \qquad \mathsf{H}^{\epsilon\mathrm{B}\bar{\nu}\bar{\nu}}_{ij,sh} = -\left(i\gamma^0\boldsymbol{\gamma}\right)^{\bar{\nu}\bar{\nu}}_{ij,sh} f^{ij}_{\mathrm{E}}(q^2)\mathbf{B}\,. \tag{4.78b}$$

The coupling of an electric field to the magnetic form factor is

$$\mathsf{H}^{\mu\mathrm{E}\nu\nu}_{ij,sh} = \left(i\gamma^0\boldsymbol{\gamma}\right)^{\nu\nu}_{ij,sh} f^{ij}_{\mathrm{M}}(q^2)\mathbf{E}\,, \qquad \mathsf{H}^{\mu\mathrm{E}\nu\bar{\nu}}_{ij,sh} = \left(i\gamma^0\boldsymbol{\gamma}\right)^{\nu\bar{\nu}}_{ij,sh} f^{ij}_{\mathrm{M}}(l^2)\mathbf{E}\,, \tag{4.79a}$$

$$\mathsf{H}^{\mu\mathrm{E}\bar{\nu}\nu}_{ij,sh} = \left(i\gamma^0\boldsymbol{\gamma}\right)^{\bar{\nu}\nu}_{ij,sh} f^{ij}_{\mathrm{M}}(l^2)\mathbf{E}\,, \qquad \mathsf{H}^{\mu\mathrm{E}\bar{\nu}\bar{\nu}}_{ij,sh} = \left(i\gamma^0\boldsymbol{\gamma}\right)^{\bar{\nu}\bar{\nu}}_{ij,sh} f^{ij}_{\mathrm{M}}(q^2)\mathbf{E}\,, \tag{4.79b}$$

which is indicated by $\mu\mathrm{E}$, and to the electric form factor, $\epsilon\mathrm{E}$,

$$\mathsf{H}^{\epsilon\mathrm{E}\nu\nu}_{ij,sh} = -\left(\gamma^0\boldsymbol{\gamma}\gamma^5\right)^{\nu\nu}_{ij,sh} f^{ij}_{\mathrm{E}}(q^2)\mathbf{E}\,, \qquad \mathsf{H}^{\epsilon\mathrm{E}\bar{\nu}\bar{\nu}}_{ij,sh} = -\left(\gamma^0\boldsymbol{\gamma}\gamma^5\right)^{\bar{\nu}\bar{\nu}}_{ij,sh} f^{ij}_{\mathrm{E}}(q^2)\mathbf{E}\,, \tag{4.80a}$$

$$\mathsf{H}^{\epsilon\mathrm{E}\bar{\nu}\nu}_{ij,sh} = -\left(\gamma^0\boldsymbol{\gamma}\gamma^5\right)^{\bar{\nu}\nu}_{ij,sh} f^{ij}_{\mathrm{E}}(l^2)\mathbf{E}\,, \qquad \mathsf{H}^{\epsilon\mathrm{E}\nu\bar{\nu}}_{ij,sh} = -\left(\gamma^0\boldsymbol{\gamma}\gamma^5\right)^{\nu\bar{\nu}}_{ij,sh} f^{ij}_{\mathrm{E}}(l^2)\mathbf{E}\,. \tag{4.80b}$$

One can see that a magnetic field couples to both, the electric and the magnetic form factor. Also electric fields couple to both form factors. This can be understood as follows. In the neutrino rest frame, the magnetic field only couples to the magnetic dipole moment, and the electric field only couples to the electric dipole moment (if any), as suggested by the nomenclature. Lorentz covariance then demands that both electric and magnetic fields couple to the magnetic form factor in a system where the neutrino moves with non-zero velocity. A moving neutrino also exhibits spin precession in a pure electric field through its magnetic moment [222].

The Lorentz structure of Eqs. (4.77)–(4.80) can now be readily calculated. In contrast to the previous sections, we neglect all contributions proportional to the mass since the magnetic and

electric form factors are small and, in the models considered here, proportional to the neutrino mass already. The $(\gamma^0\boldsymbol{\gamma}\gamma^5)$ components are

$$\left(\gamma^0\boldsymbol{\gamma}\gamma^5\right)^{\nu\nu}_{ij,sh} \approx \begin{pmatrix} 0 & e^{+i\phi}\hat{\boldsymbol{\epsilon}}^* \\ e^{-i\phi}\hat{\boldsymbol{\epsilon}} & 0 \end{pmatrix}, \tag{4.81a}$$

$$\left(\gamma^0\boldsymbol{\gamma}\gamma^5\right)^{\nu\bar{\nu}}_{ij,sh} \approx \begin{pmatrix} -e^{+i\phi}\hat{\mathbf{p}} & 0 \\ 0 & -e^{-i\phi}\hat{\mathbf{p}} \end{pmatrix}, \tag{4.81b}$$

$$\left(\gamma^0\boldsymbol{\gamma}\gamma^5\right)^{\bar{\nu}\nu}_{ij,sh} \approx \begin{pmatrix} -e^{-i\phi}\hat{\mathbf{p}} & 0 \\ 0 & -e^{+i\phi}\hat{\mathbf{p}} \end{pmatrix}, \tag{4.81c}$$

$$\left(\gamma^0\boldsymbol{\gamma}\gamma^5\right)^{\bar{\nu}\bar{\nu}}_{ij,sh} \approx \begin{pmatrix} 0 & -e^{-i\phi}\hat{\boldsymbol{\epsilon}}^* \\ -e^{+i\phi}\hat{\boldsymbol{\epsilon}} & 0 \end{pmatrix}. \tag{4.81d}$$

The remaining Lorentz structures are of the form $\left(i\gamma^0\boldsymbol{\gamma}\right)$. They read

$$\left(i\gamma^0\boldsymbol{\gamma}\right)^{\nu\nu}_{ij,sh} \approx \begin{pmatrix} 0 & ie^{+i\phi}\hat{\boldsymbol{\epsilon}}^* \\ -ie^{-i\phi}\hat{\boldsymbol{\epsilon}} & 0 \end{pmatrix}. \tag{4.82a}$$

$$\left(i\gamma^0\boldsymbol{\gamma}\right)^{\nu\bar{\nu}}_{ij,sh} \approx \begin{pmatrix} -ie^{+i\phi}\hat{\mathbf{p}} & 0 \\ 0 & ie^{-i\phi}\hat{\mathbf{p}} \end{pmatrix}, \tag{4.82b}$$

$$\left(i\gamma^0\boldsymbol{\gamma}\right)^{\bar{\nu}\nu}_{ij,sh} \approx \begin{pmatrix} ie^{-i\phi}\hat{\mathbf{p}} & 0 \\ 0 & -ie^{+i\phi}\hat{\mathbf{p}} \end{pmatrix}, \tag{4.82c}$$

$$\left(i\gamma^0\boldsymbol{\gamma}\right)^{\bar{\nu}\bar{\nu}}_{ij,sh} \approx \begin{pmatrix} 0 & ie^{-i\phi}\hat{\boldsymbol{\epsilon}}^* \\ -ie^{+i\phi}\hat{\boldsymbol{\epsilon}} & 0 \end{pmatrix}. \tag{4.82d}$$

To this level of approximation, the $\nu\bar{\nu}$ and $\bar{\nu}\nu$ components are diagonal in helicity space, i.e., electric and magnetic fields mainly couple spin-0 neutrino-antineutrino pairs. The $\nu\nu$ and $\bar{\nu}\bar{\nu}$ components are off-diagonal in helicity space. The dominant effect of magnetic and electric fields on neutrinos and antineutrinos is spin precession.

4.6.4 Dipole moments of Majorana neutrinos

For Majorana neutrinos, electromagnetic transitions always contain two contributions, e.g.,

$$\langle \nu_{\mathbf{p}_{\rm out}} | \mathcal{H}^{\rm em} | \nu_{\mathbf{p}_{\rm in}} \rangle = A_\mu \left(\bar{u}_{\mathbf{p}_{\rm out}} \Gamma^\mu u_{\mathbf{p}_{\rm in}} - \bar{v}_{\mathbf{p}_{\rm in}} \Gamma^\mu v_{\mathbf{p}_{\rm out}} \right). \tag{4.83}$$

This difference of two amplitudes leads to the cancellation of all the diagonal moments except for the anapole moment [219]. This can also be understood by noting that the last two terms (including the minus sign) in Eq. (4.83) are charge conjugates of each other. Because the Lorentz structure of the magnetic, electric, and charge form factor are *C*-odd the combination vanishes. The Lorentz structure of the anapole moment is *C*-even and does not cancel.

Because the magnetic moment of the Majorana neutrino vanishes, it does not couple directly to a magnetic field. However, magnetic fields polarize the background medium, and this effect does lead to helicity oscillations, see Sec. 4.4.

Electromagnetic moments of neutrinos depend on the details of the mechanism that creates the neutrino mass. When neglecting the model-dependent amplitudes, one can compare the moments of Dirac and Majorana neutrinos. The main differences are that the Majorana amplitudes contain Majorana PMNS-matrices, which may contain more phases than Dirac PMNS-matrices, and that Eq. (4.83) has to be taken into account for Majorana neutrinos.

After these adjustments, the off-diagonal form factors of Majorana neutrinos can be obtained from Eq. (4.73a). They depend on the relative *CP*-phases of two neutrino species [223]. This phase can either be equal or opposite, i.e., the ratio is ± 1. For neutrinos with equal *CP*-phases, the magnetic transition moments vanish [223], while for opposite *CP*-phase the magnetic transition moments are non-zero and can be obtained from Eq. (4.73a) by substituting $\mathcal{F}_{ij}$ with $2i\,\mathrm{Im}\,\mathcal{F}_{ij}$.

For *electric* dipole moments, the role of the CP-phases is inverted. Opposite CP-phases force the electric transition moments to vanish, while for equal CP-phases the electric transition moments are non-zero and are obtained by substituting $\mathcal{F}_{ij}$ with $2\,\mathrm{Re}\,\mathcal{F}_{ij}$ [223] in Eq. (4.73b).

4.6.5 Hamiltonian matrix for Majorana neutrinos

The density matrix formalism naturally reproduces the results for the electromagnetic moments discussed in the last section. Similarly to Eq. (4.83), each component of the Hamiltonian matrix has two contributions from Γ contractions, e.g., $\mathsf{H}^{\nu\nu}_{ij,sh}(\mathbf{p}) = \Gamma^{\nu\nu}_{ij,sh}(\mathbf{p}) - \Gamma^{\bar\nu\bar\nu}_{ji,hs}(-\mathbf{p})$, see Eq. (4.45). The spinor contractions $\Gamma^{\nu\nu}$ and $\Gamma^{\bar\nu\bar\nu}$ have the same structure as for Dirac neutrinos, see Eq. (4.14). Again neglecting the model dependence, the only difference is that the Dirac PMNS-matrix have to be replaced by Majorana PMNS-matrix. For example, a magnetic field coupling to a Majorana neutrino through the magnetic form factor yields

$$\begin{aligned}\mathsf{H}^{\nu\nu}_{ij,\text{-+}} &= -\left[f^{ij}_{\mathrm{M}}(q^2) - \text{c.c.}\right] e^{+i\phi}\hat{\boldsymbol{\epsilon}}^* \cdot \mathbf{B} \\ &= -\,2i\,\mathrm{Im}[f^{ij}_{\mathrm{M}}(q^2)] e^{+i\phi}\hat{\boldsymbol{\epsilon}}^* \cdot \mathbf{B}\,,\end{aligned} \tag{4.84}$$

where we have used the Hermiticity of the form factors. In the static limit, $2i\,\mathrm{Im}[f^{ij}_{\mathrm{M}}]$ is the magnetic moment of Majorana neutrinos [220]. It is zero for equal CP-phases since $\mathcal{F}_{ij}$ becomes real. It is non-vanishing for opposite CP-phases because $\mathcal{F}_{ij}$ becomes imaginary. An analogous argument holds for the electric dipole moment.

4.7 Helicity coherence

In this section we neglect pair correlations and discuss helicity coherence effects. To separate the latter from the usual flavor coherence effects, we consider only one neutrino generation. Furthermore, for definiteness we assume that neutrinos are Dirac particles.

4.7.1 Order of magnitude estimate

Two different mean-field backgrounds cause spin oscillations and create spin coherence: matter and neutrino currents, and electromagnetic fields. However, it is not clear which of these is dominant in a supernova. In the following we perform a crude estimate.

For Dirac neutrinos without pair correlations, the kinetic equations of neutrinos and antineutrinos decouple, $i\dot{\rho} = [\mathsf{H}^{\nu\nu}, \rho]$ and $i\dot{\bar{\rho}} = [\mathsf{H}^{\bar{\nu}\bar{\nu}}, \bar{\rho}]$, and, for one family, we only have to look at a 2×2 subsystem of the full evolution equation. We start with a matter background with non-relativistic velocity β, which flows orthogonal to the neutrino's momentum. The Hamiltonian matrix reads

$$\mathsf{H}^{\nu\nu} \approx V \begin{pmatrix} 1 & \frac{m}{2p}\beta \\ \frac{m}{2p}\beta & 0 \end{pmatrix} , \tag{4.85}$$

where V is the usual matter potential. For instance for ν_μ or ν_τ it is given by $V = \mathsf{G}_\mathrm{F} n_n/\sqrt{2}$, where n_n is the neutron density. We have omitted the neutrino kinetic energy because it is diagonal in helicity space, and for a single generation trivially cancels in the commutator. In the same way we obtain the 2×2 subsystem of the Hamiltonian matrix for a neutrino in a transverse magnetic field

$$\mathsf{H}^{\nu\nu} \approx -\mu B \begin{pmatrix} 0 & 1 \\ 1 & 0 \end{pmatrix} , \tag{4.86}$$

see Sec. 4.6 for more details. Spin coherence is instigated by the off-diagonals of Eqs. (4.85) and (4.86), and to find the relative importance of the matter and magnetic contributions it is sufficient to estimate their relative size. Typical magnetic fields in a supernova are of order $10^{12}\,\mathrm{G}$ and much larger in magnetars. Using the standard value for the magnetic moment given in Eq. (4.74), and assuming a neutrino mass of $0.1\,\mathrm{eV}$, we find for the contribution of the magnetic field $\mu B \sim 10^{-16}\,\mathrm{eV}$. For a typical neutron mass density $10^{12}\ \mathrm{g/cm^3}$, which corresponds to a number density $n_n \sim 10^4\,\mathrm{MeV}^3$, the matter potential is of the order of the neutrino mass, $V \sim 0.1\,\mathrm{eV}$. Thus, for a typical momentum $p \sim 30\,\mathrm{MeV}$ we obtain $V\beta m/(2p) \sim 10^{-10}\beta\,\mathrm{eV}$. For maximal background velocities of $3000\,\mathrm{km/s}$, $\beta \sim 0.01$, the matter contribution dominates. Surprisingly, the magnetic field is only important if the background moves very slowly, if the matter density has decreased sufficiently, or if the magnetic moment is enhanced.

Turning now to the density matrix, the size of the off-diagonal elements depends on the initial conditions and history of the evolution. To obtain a rough estimate, we can assume that the system has reached equilibrium and, hence, its previous evolution is irrelevant. In equilibrium, the system is in an eigenstate of the Hamiltonian, i.e., $\mathsf{H}^{\nu\nu}$ and ρ commute. This condition alone allows us to express the off-diagonals of the density matrix in terms of the diagonals and components of the Hamiltonian matrix,

$$\rho_{\text{-+}} = \frac{\mathsf{H}^{\nu\nu}_{\text{-+}}}{\mathsf{H}^{\nu\nu}_{\text{--}} - \mathsf{H}^{\nu\nu}_{\text{++}}}(\rho_{\text{--}} - \rho_{\text{++}}) . \tag{4.87}$$

Keeping only the (dominant) matter contribution, Eq. (4.85), we find $\rho_{\text{-+}} = (\rho_{\text{--}} - \rho_{\text{++}})\, m\beta/2p \sim m\beta/2p$. For $m \sim 0.1\,\mathrm{eV}$ and a typical momentum $p \sim 30\,\mathrm{MeV}$ this results in $\rho_{\text{-+}} \sim 10^{-11}$, where we have used $\beta \sim 0.01$.

The same result can be obtained by noting that if ρ and $\mathsf{H}^{\nu\nu}$ commute, they can be simultaneously diagonalized by a rotation that mixes positive and negative helicity states. The rotation

angle is $\tan 2\vartheta = m\beta/p$. Considering e.g. the $\rho_{--} = 1$ eigenstate of the diagonalized Hamiltonian and rotating back to the basis where the Hamiltonian has the form Eq. (4.85) we find to leading order

$$\rho \sim \begin{pmatrix} 1 & \frac{m}{2p}\beta \\ \frac{m}{2p}\beta & 0 \end{pmatrix} \sim \begin{pmatrix} 1 & 10^{-11} \\ 10^{-11} & 0 \end{pmatrix} . \tag{4.88}$$

The corrections to the diagonals are not included in Eq. (4.88) because they are of the order of $\delta\rho_{--} \sim \delta\bar{\rho}_{++} \sim \rho_{-+}^2 \sim 10^{-22}$ and are therefore negligibly small.

4.7.2 Resonant enhancement

For a magnetic field, the diagonal elements of the Hamiltonian matrix, Eq. (4.86), are zero for very relativistic neutrinos. This allows for the magnetic fields to completely flip the spin of a population of neutrinos. On the other hand, the diagonals of Eq. (4.85) are in general non-zero and suppress a complete conversion. In general, the matter contribution is given by

$$\mathsf{H}^{\nu\nu} \approx \begin{pmatrix} V^0 - V_\parallel & \frac{m}{2p}V_\perp \\ \frac{m}{2p}V_\perp & 0 \end{pmatrix} , \tag{4.89}$$

see Eq. (4.57), where $V_\parallel \equiv \hat{\mathbf{p}} \cdot \mathbf{V}$ and $V_\perp \equiv \hat{\boldsymbol{\epsilon}} \cdot \mathbf{V}$ are components of the matter flux parallel and orthogonal to the neutrino momentum. Thus, if there are relativistic currents parallel to the momentum of the neutrino such that the diagonals vanish, Eq. (4.87) implies that a resonant enhancement of the spin conversion is possible. For vanishing diagonals, Eq. (4.89) can be rotated into its diagonal form with a rotation angle $\vartheta = \pi/4$. In other words, mixing of the helicity states becomes maximal, similarly to the MSW resonance mixing, and hence in equilibrium

$$\rho \sim \begin{pmatrix} 1/2 & 1/2 \\ 1/2 & 1/2 \end{pmatrix} , \tag{4.90}$$

where we have again assumed that the system is in an eigenstate of the diagonalized Hamiltonian.

Making use of Eq. (4.34), we can re-write the resonance condition, $\mathsf{H}^{\nu\nu}_{--} - \mathsf{H}^{\nu\nu}_{++} = V^0 - V_\parallel = 0$, in the form [87]

$$Y_e + \frac{4}{3}\left(Y_\nu - \frac{V_\parallel}{2n_\mathrm{B}}\right) = \frac{1}{3} , \tag{4.91}$$

where $Y_e \equiv n_e/n_\mathrm{B}$ and $Y_\nu = (n_\nu - n_{\bar{\nu}})/n_\mathrm{B}$ are the electron and neutrino asymmetry fractions respectively and n_B is the baryon number density, The resonance condition can potentially be fulfilled in or near the proto-neutron star in a core collapse supernova, or near the central region of a compact object merger, see Ref. [87] and references therein.

4.7.3 Lorentz covariance

Helicity coherence builds up only if the off-diagonal elements of the Hamiltonian matrix differ from zero. On the other hand, because the off-diagonals are proportional to the component of the matter flow orthogonal to the neutrino momentum, one can always find a frame where the off-diagonals vanish and no helicity coherence builds up. In other words, at first sight physical results seem to depend on the frame. This seeming contradiction raises the question of Lorentz-covariance of the kinetic equations.

To be specific, let us consider the following simple example. We have two identical observers moving with velocity β with respect to each other. In the frame of the first observer, the neutrino has momentum $\mathbf{p}$ along the z axis and the matter is at rest, i.e., $V_\parallel = V_\perp = 0$,

$$\mathsf{H}^{\nu\nu} \approx V \begin{pmatrix} 1 & 0 \\ 0 & 0 \end{pmatrix} . \tag{4.92}$$

Thus no helicity coherence builds up. In the frame of the second observer which moves with velocity β along the x axis the Hamiltonian is no longer diagonal,

$$\mathsf{H}^{\nu\nu} \approx \frac{V}{\gamma} \begin{pmatrix} 1 & \frac{m}{2p}\beta \\ \frac{m}{2p}\beta & 0 \end{pmatrix} , \tag{4.93}$$

and we expect helicity coherence to build up. Here γ is the usual Lorentz factor and V and p denote the potential and neutrino momentum in the frame of the first observer.

Do the Hamiltonian matrices Eqs. (4.92) and (4.93) lead to different physical results? The answer is no, but to demonstrate this point we need to take into account that a helicity state is also not Lorentz-invariant. Let the neutrino be in a state of definite helicity in the frame of the first observer, e.g. $|p\hat{\mathbf{z}}, -\rangle$, where $\hat{\mathbf{z}}$ is the unit vector along the z axis. The corresponding density matrix reads

$$\rho = \mathrm{Tr}\{|p\hat{\mathbf{z}}, -\rangle\langle p\hat{\mathbf{z}}, -|\} = \begin{pmatrix} 1 & 0 \\ 0 & 0 \end{pmatrix} . \tag{4.94}$$

The Hamiltonian matrix Eq. (4.92) and the density matrix commute and therefore the state is constant in time. A boost to the frame of the second observer transforms $|p\hat{\mathbf{z}}, -\rangle$ into a mixed helicity state with momentum $\mathbf{q}$,

$$|\psi\rangle = c_{\theta/2}|\mathbf{q}, -\rangle - s_{\theta/2}|\mathbf{q}, +\rangle , \tag{4.95}$$

where θ is a rotation angle defined through $\tan\theta = -m\beta/p$. Note that the angle vanishes in the limit of zero neutrino mass which reflects chirality conservation. The density matrix develops off-diagonal elements,

$$\rho = \mathrm{Tr}\{|\psi\rangle\langle\psi|\} = \frac{1}{2} \begin{pmatrix} 1 + c_\theta & -s_\theta \\ -s_\theta & 1 - c_\theta \end{pmatrix} . \tag{4.96}$$

The Hamiltonian matrix and the density matrix again commute. In other words, the second observer sees a mixed helicity state which, as expected, is also time independent. This result reflects Lorentz covariance of the kinetic equations, the lesson being that one has to transform the initial conditions consistently to obtain covariant results.

Let us now consider this result from a slightly different viewpoint. In each frame, we can diagonalize the effective Hamiltonian by performing a Bogolyubov transformation that mixes annihilation (creation) operators of the positive and negative helicity states, $a_s \to c_\vartheta\, a_s + s_\vartheta\, a_{-s}$. In particular Eq. (4.93) is diagonalized by a Bogolyubov transformation with the angle $\tan 2\vartheta = m\beta/p$. This transformation brings the density matrix Eq. (4.96) back to the form Eq. (4.94). In other words, there is a connection between the Lorentz and Bogolyubov transformations. In particular, if in every frame we diagonalize the Hamiltonian then the transformed density matrix remains invariant under the boosts, i.e., the information about the frame is then carried by the Bogolyubov angle which appears in the transformed Hamiltonian.

To summarize, as far as helicity coherence is concerned, both the Hamiltonian and the density matrix transform under Lorentz boosts in such a way that the kinetic equation is Lorentz covariant. We will rely on this result in the discussion of particle-antiparticle coherence whose Lorentz transformation properties are not as evident as for the helicity coherence.

4.8 Particle-antiparticle coherence

In contrast to helicity coherence, particle-antiparticle coherence arises already for a single massless neutrino generation. For a massless neutrino the only 'natural' correlators are ρ_{--}, ρ_{++} and κ_{-+}. To shorten the notation in this section we suppress the spin indices.

4.8.1 Quantum-mechanical example

To clarify the interpretation of the particle-antiparticle coherence, let us first study a simple quantum-mechanical example. We consider a system that can be in a linear combination of one of four pure states. These are i) the empty state $|00\rangle$ without particles; ii) the paired state $|11\rangle = a^\dagger(\mathbf{p})b^\dagger(-\mathbf{p})|00\rangle$, which contains a neutrino with momentum $\mathbf{p}$ and an antineutrino with momentum $-\mathbf{p}$; iii) the one neutrino state $|10\rangle$; and iv) the one antineutrino state $|01\rangle$. Note that in all these states the antineutrinos stream in the direction opposite to that of neutrinos. A general state can be expressed in terms of these four states, $|\psi\rangle = A_{00}|00\rangle + A_{11}|11\rangle + A_{10}|10\rangle + A_{01}|01\rangle$, where the coefficients A_{ij} are time-dependent and normalized to unity, $|A_{00}|^2 + |A_{11}|^2 + |A_{10}|^2 + |A_{01}|^2 = 1$.

In analogy to Eq. (4.15) we write the Hamiltonian in the form

$$H = a^\dagger(\mathbf{p})\mathsf{H}^{\nu\nu}a(\mathbf{p}) + a^\dagger(\mathbf{p})\mathsf{H}^{\nu\bar{\nu}}b^\dagger(-\mathbf{p}) + b(-\mathbf{p})\mathsf{H}^{\bar{\nu}\nu}a(\mathbf{p}) - b^\dagger(-\mathbf{p})\mathsf{H}^{\bar{\nu}\bar{\nu}}b(-\mathbf{p})\,. \tag{4.97}$$

The Schrödinger equation for the coefficients A_{ij} then splits into three independent equations,

$$i\partial_t \begin{pmatrix} A_{00} \\ A_{11} \end{pmatrix} = \begin{pmatrix} 0 & \mathsf{H}^{\bar{\nu}\nu} \\ \mathsf{H}^{\nu\bar{\nu}} & \mathsf{H}^{\nu\nu} - \mathsf{H}^{\bar{\nu}\bar{\nu}} \end{pmatrix} \begin{pmatrix} A_{00} \\ A_{11} \end{pmatrix} , \tag{4.98a}$$

$$i\partial_t A_{10} = \mathsf{H}^{\nu\nu} A_{10} , \tag{4.98b}$$

$$i\partial_t A_{01} = -\mathsf{H}^{\bar{\nu}\bar{\nu}} A_{01} . \tag{4.98c}$$

Thus the evolution of the single particle states completely decouples because a homogeneous background medium cannot mix states of different total momentum. They simply suffer the usual energy shift by the weak potential of the medium, i.e., $i\partial_t|10\rangle = (E+V)|10\rangle$ and $i\partial_t|01\rangle = (E-V)|01\rangle$. On the other hand, the $|00\rangle$ and $|11\rangle$ states have zero momenta and therefore can be mixed by a homogeneous medium through the $\mathsf{H}^{\bar{\nu}\nu}$ term of the Hamiltonian. However, the $|00\rangle$ and $|11\rangle$ states have different angular momentum. Hence, an anisotropic background medium, e.g. a transverse matter flux, is needed to absorb the angular momentum and to mix the two states. Note that in the presence of such fluxes, the true ground state of our system is not $|00\rangle$, but a suitable combination of $|00\rangle$ and $|11\rangle$ which follows from diagonalizing the matrix in Eq. (4.98a).

To make the connection to the density matrix equations, we note that the number of neutrinos and antineutrinos is given by $\rho = |A_{11}|^2 + |A_{10}|^2$ and $\bar{\rho} = |A_{11}|^2 + |A_{01}|^2$ respectively. Their time-evolution can be derived from Eq. (4.98) and takes the form expected from the density matrix equations (4.61),

$$\dot{\rho} = -2\,\mathrm{Im}\left(\mathsf{H}^{\bar{\nu}\nu}\kappa\right) , \tag{4.99a}$$

$$\dot{\bar{\rho}} = -2\,\mathrm{Im}\left(\mathsf{H}^{\bar{\nu}\nu}\kappa\right) , \tag{4.99b}$$

if we identify $\kappa = A_{00}^* A_{11}$. Equation (4.98) also leads to an evolution equation for κ

$$i\dot{\kappa} = \left(\mathsf{H}^{\nu\nu} - \mathsf{H}^{\bar{\nu}\bar{\nu}}\right)\kappa + \mathsf{H}^{\nu\bar{\nu}}\left(1-\rho-\bar{\rho}\right) , \tag{4.100}$$

which can be obtained by using the normalization of the state $|\psi\rangle$. Equation (4.100) is again consistent with Eq. (4.61) and coincides with the result of Ref. [90] in the one-flavor limit.

From these kinetic equations we infer that while ρ and $\bar{\rho}$ are not separately conserved in the presence of nonzero κ, their difference is conserved [90]. Because $\rho(t,\mathbf{p})$ describes neutrinos with momentum $\mathbf{p}$ whereas $\bar{\rho}(t,\mathbf{p})$ antineutrinos with momentum $-\mathbf{p}$, the conservation of $\rho-\bar{\rho}$ implies that κ induces the production of neutrino-antineutrino pairs with opposite momentum.

The kinetic equation for κ describes a driven harmonic oscillator with frequency $\mathsf{H}^{\nu\nu} - \mathsf{H}^{\bar{\nu}\bar{\nu}} \sim 2E$. Hence κ oscillates with a frequency that is twice the neutrino energy as expected. From the definition $\kappa = A_{00}^* A_{11}$ we see that nonzero particle-antiparticle coherence means that the system is not in an eigenstate of the unperturbed Hamiltonian, but instead in a mixture of the $|00\rangle$ and $|11\rangle$ states. Such states do not have a definite particle number. This observation clarifies the physical interpretation of particle-antiparticle coherence.

4.8.2 Order of magnitude estimate

As a next step we perform an order of magnitude estimate of κ. For a single neutrino generation the extended density matrix reduces to a 2×2 matrix of the form, see Eq. (4.4),

$$\mathsf{R} = \begin{pmatrix} \rho & \kappa \\ \kappa^\dagger & 1-\bar{\rho} \end{pmatrix} , \tag{4.101}$$

where now ρ and $\bar{\rho}$ are real numbers and κ is a complex number. We again start with an example of a matter background with non-relativistic velocity β, which flows orthogonal to the neutrino's momentum. Then, as follows from Eq. (4.62), the Hamiltonian matrix reads,

$$\mathsf{H} = E \begin{pmatrix} 1 & 0 \\ 0 & -1 \end{pmatrix} + V \begin{pmatrix} 1 & -\beta \\ -\beta & 1 \end{pmatrix} . \tag{4.102}$$

Unlike for helicity coherence, the neutrino kinetic energy E no longer cancels out in the commutator.

Similarly to the case of spin coherence we can get a crude estimate of the κ magnitude by assuming that the system has reached equilibrium and hence $\dot{\kappa} = 0$. Eq. (4.100) then gives

$$\kappa = -\frac{\mathsf{H}^{\nu\bar{\nu}}}{\mathsf{H}^{\nu\nu} - \mathsf{H}^{\bar{\nu}\bar{\nu}}}(1-\rho-\bar{\rho}) . \tag{4.103}$$

If we insert this result into Eq. (4.99) and use the Hermiticity of the Hamiltonian matrix, we see that indeed $\dot{\rho} = \dot{\bar{\rho}} = 0$.

Let us assume for a moment that the neutrino-neutrino interactions are small compared to the neutrino interaction with matter. For typical supernova parameters $V \sim 0.1\,\mathrm{eV}$ and $E \sim 30\,\mathrm{MeV}$ and we then find $V/E \sim 10^{-9}$. Thus to a good approximation $\mathsf{H}^{\nu\bar{\nu}}/(\mathsf{H}^{\nu\nu} - \mathsf{H}^{\bar{\nu}\bar{\nu}}) \sim V\beta/2E \sim 10^{-11}$, where we have used $\beta \sim 0.01$. Because typically $|1-\rho-\bar{\rho}| \sim 1$ we conclude that the 'natural' size of the particle-antiparticle coherence is $\kappa \sim 10^{-11}$.

The same result can be obtained by noting that in equilibrium R and H commute and can be simultaneously diagonalized by a Bogolyubov transformation that mixes neutrinos of momentum $\mathbf{p}$ with antineutrinos of momentum $-\mathbf{p}$. Under this transformation the creation and annihilation operators transform as

$$\begin{aligned} a(\mathbf{p}) &\to e^{-i\phi/2} c_\vartheta\, a(\mathbf{p}) + e^{i\phi/2} s_\vartheta b^\dagger(-\mathbf{p}) , \\ b^\dagger(-\mathbf{p}) &\to e^{i\phi/2} c_\vartheta\, b^\dagger(-\mathbf{p}) - e^{-i\phi/2} s_\vartheta\, a(\mathbf{p}) , \end{aligned} \tag{4.104}$$

respectively, where the rotation angle is $\tan 2\vartheta = 2|\mathsf{H}^{\nu\bar{\nu}}|/(\mathsf{H}^{\nu\nu} - \mathsf{H}^{\bar{\nu}\bar{\nu}}) \sim V\beta/E$ and the phase $\phi = \arg \mathsf{H}^{\nu\bar{\nu}}$. In the basis where the Hamiltonian is diagonal, the system is described by (anti)neutrino densities, which we denote by ϱ and $\bar{\varrho}$ respectively, and pairing correlator, which we denote by $\varkappa$. From the transformation properties of the creation/annihilation operators, we can infer the following relations

$$\rho = c_\vartheta^2 \varrho - c_\vartheta s_\vartheta \varkappa - c_\vartheta s_\vartheta \varkappa^\dagger + s_\vartheta^2 (1-\bar{\varrho}) , \tag{4.105a}$$

$$\bar{\rho} = c_\vartheta^2 \bar{\varrho} - c_\vartheta s_\vartheta \varkappa - c_\vartheta s_\vartheta \varkappa^\dagger + s_\vartheta^2 (1-\varrho) , \tag{4.105b}$$

$$\kappa = e^{i\phi} \left[c_\vartheta^2 \varkappa + c_\vartheta s_\vartheta \varrho - c_\vartheta s_\vartheta (1-\bar{\varrho}) - s_\vartheta^2 \varkappa^\dagger \right] , \tag{4.105c}$$

see Ref. [89] for a detailed discussion. Eigenstates of the diagonalized Hamiltonian are characterized by $\varkappa = 0$. Assuming, e.g., that the system is in an eigenstate of the diagonalized Hamiltonian with some ϱ and $\bar{\varrho}$, and rotating back to the basis where the Hamiltonian has the form Eq. (4.102), we find to leading order

$$\mathsf{R} \sim \begin{pmatrix} \rho & \frac{V\beta}{2E} \\ \frac{V\beta}{2E} & 1-\bar{\rho} \end{pmatrix} \sim \begin{pmatrix} \rho & 10^{-11} \\ 10^{-11} & 1-\bar{\rho} \end{pmatrix}, \tag{4.106}$$

which again leads to the tiny $\kappa \sim s_\vartheta \sim 10^{-11}$.

Pair correlations themselves are not measurable, and only their effect on the number densities can be observed. A quick inspection of Eq. (4.105) shows that in equilibrium the difference between e.g. ρ and ϱ is of the order of $s_\vartheta^2 \sim \kappa^2$. In other words, the induced corrections to ρ and $\bar{\rho}$ are quadratic in κ.

This can also be understood from Eq. (4.100). If the system has not yet reached equilibrium, then κ oscillates around its stationary value Eq. (4.103), provided that the components of the Hamiltonian matrix only vary slowly with time compared to $\mathsf{H}^{\nu\nu} - \mathsf{H}^{\bar{\nu}\bar{\nu}}$. This assumptions allows us to approximate the evolution of κ as a driven harmonic oscillator with an amplitude that depends on the initial conditions. Assuming that pairing correlations are not created during neutrino production, the amplitude is of the order of the equilibrium value, Eq. (4.103). We then find again that the mean number density created by pairing correlations is $\sim \kappa^2$. Therefore, the inclusion of the particle-antiparticle coherence leads to a negligibly small perturbation of the number densities $\delta\rho \sim \delta\bar{\rho} \sim \kappa^2 \sim 10^{-22}$.

Including neutrino-neutrino interactions

Until now we have neglected neutrino-neutrino interactions in our order of magnitude estimate. However, in a supernova the neutrino density is very large and the neutrino background may play an important role. These additional interactions complicate the estimate of κ because $\mathsf{H}^{\nu\bar{\nu}}$ in Eq. (4.103) itself depends on κ once we include neutrino-neutrino interactions,

$$\mathsf{H}^{\nu\bar{\nu}} = -V\beta - 2\sqrt{2}\mathsf{G}_\mathrm{F}\,\hat{\boldsymbol{\epsilon}}^* \cdot \int \frac{\mathrm{d}^3\mathbf{q}}{(2\pi)^3} \left[\hat{\mathbf{q}}\ell + \hat{\boldsymbol{\epsilon}}\kappa + \hat{\boldsymbol{\epsilon}}^*\kappa^\dagger\right], \tag{4.107}$$

see Eqs. (4.62) and (4.63). Furthermore, the stationary value for κ of one momentum mode $\mathbf{p}$ depends on the pair correlations of all other momentum modes $\mathbf{q}$. Note also that the phase space integral in Eq. (4.107) is unbounded. Pairing correlations with a momentum typical for the supernova environment couple to pairing correlations of arbitrary high momentum. This coupling pushes us beyond the limitations of the Fermi approximation, and in principle a fully renormalizable theory has to be studied to make sense of these high momentum modes. To stay within the realm of applicability of the effective theory, we use a phenomenological cutoff $|\mathbf{q}| = M_W$ in the phase space integrals.

To estimate the contribution of the κ terms to the integral in Eq. (4.107), we take into account that pair correlators of different momentum modes oscillate incoherently such that we can replace κ by its approximate mean value in every mode, $\kappa \approx -\mathsf{H}^{\nu\bar{\nu}}/2E$, where we use that $V \ll E$ and

assume $\rho + \bar{\rho} \ll 1$ in Eq. (4.103). To proceed we recall that $\mathsf{H}^{\nu\bar{\nu}} = -\hat{\boldsymbol{\epsilon}}^* \cdot \mathbf{V}$, see Eq. (4.62), where $\mathbf{V}$ is the total potential that includes matter and neutrino contributions. Note further that $\mathbf{V}$ is momentum-independent. With these substitutions, the integrals involving κ in Eq. (4.107) read

$$\mathrm{Re}\int \frac{\mathrm{d}^3\mathbf{q}}{(2\pi)^3}\,\hat{\boldsymbol{\epsilon}}\kappa \sim \mathrm{Re}\int \frac{\mathrm{d}^3\mathbf{q}}{(2\pi)^3}\,\hat{\boldsymbol{\epsilon}}\frac{\hat{\boldsymbol{\epsilon}}^*\cdot\mathbf{V}}{2E} = \frac{\sqrt{2}}{2}\frac{\mathsf{G}_\mathrm{F}M_W^2}{3\pi^2}\mathbf{V}\,, \tag{4.108}$$

where we have integrated up to the cut-off $|\mathbf{q}| = M_W$. Let us introduce the notation

$$\mathsf{H}_0^{\nu\bar{\nu}} = -V\beta - 2\sqrt{2}\mathsf{G}_\mathrm{F}\,\hat{\boldsymbol{\epsilon}}^*\cdot\int\frac{\mathrm{d}^3\mathbf{q}}{(2\pi)^3}\,\hat{\mathbf{q}}\ell\,. \tag{4.109}$$

Then using Eq. (4.108) we can write Eq. (4.107) as

$$\mathsf{H}^{\nu\bar{\nu}} \approx \mathsf{H}_0^{\nu\bar{\nu}}\left(1 - \sqrt{2}\frac{\mathsf{G}_\mathrm{F}M_W^2}{3\pi^2}\right)^{-1}. \tag{4.110}$$

In other words the κ terms in Eq. (4.107) effectively lead to a renormalization of the total potential produced by the matter and neutrino backgrounds. Numerically, the correction is small, $\sqrt{2}\mathsf{G}_\mathrm{F}M_W^2/(3\pi^2) \approx 3\times10^{-3}$, and can be neglected.

In a supernova the neutrino density is comparable to that of matter. Whereas each individual neutrino is relativistic, the bulk velocity of the neutrino background is also comparable to the matter velocity. Thus, the neutrino density contribution to Eq. (4.109) is not expected to be larger than the matter contribution. Furthermore, because the direction of the neutrino background flux is more likely to be parallel to the momenta of individual neutrinos, whereas the build up of the particle-antiparticle coherence requires a current component orthogonal to the neutrino momentum, there is an additional suppression as compared to the matter effect. All in all, the estimates of κ presented above remain essentially unaltered by the inclusion of the neutrino-neutrino interactions.

4.8.3 Resonance condition

As follows from Eq. (4.103), particle-antiparticle coherence can be resonantly enhanced if $\mathsf{H}^{\nu\nu} = \mathsf{H}^{\bar{\nu}\bar{\nu}}$. In general for a relativistic matter flow that also includes the neutrino flux, the Hamiltonian matrix reads [see Eq. (4.62)]

$$\mathsf{H} = E\begin{pmatrix}1 & 0\\ 0 & -1\end{pmatrix} + \begin{pmatrix}V^0 - V_\parallel & -V_\perp\\ -V_\perp & V^0 + V_\parallel\end{pmatrix}, \tag{4.111}$$

where, as before, $V_\parallel \equiv \hat{\mathbf{p}}\cdot\mathbf{V}$ and $V_\perp \equiv \hat{\boldsymbol{\epsilon}}\cdot\mathbf{V}$ are components of the matter flux parallel and orthogonal to the neutrino momentum. The resonance condition then translates into $E = V_\parallel$. Even assuming a relativistic matter flow, for typical supernova parameters $V_\parallel/E \sim 10^{-9}$. In other words, the resonance condition cannot be fulfilled in a supernova and there is no reason to expect κ to be larger than the estimate presented above.

Note also that for $V \sim E$ not only the Fermi approximation breaks down, but also the perturbative description is no longer applicable. In other words it is in principle not possible to hit the resonance without rendering the developed formalism meaningless.

4.8.4 Initial conditions

All physical processes in which neutrinos are created have time scales much larger than the time scale of κ oscillation. Hence, even during the production process neutrinos would adiabatically adapt to the propagation basis with respect to pair correlations. On the other hand, the time scales of flavor and helicity oscillation are much larger than those associated with production and detection. This separation of time scales is crucial for the idea that neutrinos are produced in eigenstate of interaction, i.e., in a coherent superposition of propagation eigenstates. For the same physical reason, as neutrinos stream away from the supernova, they have enough time to adiabatically adapt to the external background. Thus, κ does not oscillate but instead closely tracks its equilibrium value. This makes dynamical equations for κ essentially superfluous. As the neutrinos leave the supernova, the mean pair correlations approach zero adiabatically and decouple from the evolution of ρ and $\bar{\rho}$.

4.8.5 Lorentz covariance

In the early Universe, the rest frame of the plasma is the only natural reference frame and the question of Lorentz transformation properties of the pair correlators does not arise [224]. In a supernova environment the situation is more complicated. In particular, the comoving frame of the matter can in some cases be more convenient than the rest frame of a distant observer. Similarly to helicity coherence, the particle-antiparticle coherence builds up only if the off-diagonal components of the Hamiltonian matrix are not zero. However, because the off-diagonals are proportional to the component of the matter flow orthogonal to the neutrino momentum, their value depends on the frame. In particular, one can find a frame where the off-diagonals vanish and no particle-antiparticle coherence builds up.

Let us consider the same example as in Sec. 4.7. We have two identical observers moving with velocity β with respect to each other. In the frame of the first observer, the neutrino has momentum $\mathbf{p}$ along the z axis and the matter is at rest, i.e., $V_{\parallel} = V_{\perp} = 0$,

$$\mathsf{H} = E \begin{pmatrix} 1 & 0 \\ 0 & -1 \end{pmatrix} + V \begin{pmatrix} 1 & 0 \\ 0 & 1 \end{pmatrix} . \tag{4.112}$$

Thus no particle-antiparticle coherence builds up. In the frame of the second observer which moves with velocity β along the x axis the Hamiltonian is no longer diagonal,

$$\mathsf{H} = \gamma E \begin{pmatrix} 1 & 0 \\ 0 & -1 \end{pmatrix} + V \begin{pmatrix} 1/\gamma & -\beta \\ -\beta & 1/\gamma \end{pmatrix} , \tag{4.113}$$

and we expect helicity coherence to build up. In other words, physical results seem to depend on the frame.

As we have learned from the analysis of an analogous problem for helicity coherence, the kinetic equations are covariant only if the initial conditions also transform under the boost. Pair correlations 'couple' neutrinos of opposite momenta. The notion of opposite momenta is not Lorentz invariant and is violated by, e.g., a boost orthogonal to the neutrino momentum. This

point alone implies that the initial conditions, which include specifying κ for all momentum modes, are not Lorentz covariant.

We have argued in the previous subsection that neutrinos are produced and propagate in an eigenstate with respect to particle-antiparticle coherence. In Sec. 4.7 we have observed that if in every frame we diagonalize the Hamiltonian then the transformed density matrix remains invariant under the boosts. Here we assume that the same holds true also for particle-antiparticle coherence. As a particularly interesting example let us assume that in the frame of the first observer the system is in the vacuum state of the interacting Hamiltonian, i.e., $\rho = \bar{\rho} = \kappa = 0$,

$$\mathsf{R} = \begin{pmatrix} 0 & 0 \\ 0 & 1 \end{pmatrix} . \tag{4.114}$$

The Hamiltonian matrix Eq. (4.112) and the extended density matrix Eq. (4.114) commute and therefore the latter is constant in time. According to our assumption, after diagonalizing Eq. (4.113) by a Bogolyubov transformation, the transformed R takes the form Eq. (4.114). Transforming back to the initial basis we obtain,

$$\mathsf{R} = \frac{1}{2} \begin{pmatrix} 1 - c_\vartheta & s_\vartheta \\ s_\vartheta & 1 + c_\vartheta \end{pmatrix} , \tag{4.115}$$

where ϑ is the angle of the Bogolyubov transformation that diagonalizes Eq. (4.113), $\tan 2\vartheta = (\beta V/\gamma E)/[1 - \beta^2(V/E)]$. By construction the Hamiltonian matrix Eq. (4.113) and the extended density matrix Eq. (4.115) commute and the latter is time-independent as well.

A perplexing feature of Eq. (4.115) is that it seems to describe a state with a nonzero number of particles and antiparticles. Whereas the first observer would see neither neutrinos nor antineutrinos, the second observer that moves with respect to the first one with a *constant* velocity β seems to observe a nonzero density of neutrinos and antineutrinos. Put in other words, the empty space perceived by the first observer appears to be filled with neutrino-antineutrino pairs in the frame of the second observer. However, it is not entirely clear if the (anti)particle densities in Eq. (4.115) describe electroweak interaction eigenstates and thus would actually manifest themselves via, e.g., particle production or momentum transfer to nuclei in scattering processes.

4.8.6 Interpretation of Bogolyubov transformation

To better understand the meaning of the Bogolyubov transformation, we solve the equation of motion for a massless neutrino field coupled to a constant classical current V^μ, and demonstrate that this solution reproduces the results obtained using the Bogolyubov transformation.

In the Fermi limit $\mathcal{L} = \nu^\dagger_{\dot{\alpha}} \bar{\sigma}^{\mu,\dot{\alpha}\alpha}(i\partial_\mu - V_\mu)\nu_\alpha$. Varying the Lagrangian with respect to the neutrino field, we obtain the equation of motion, $\bar{\sigma}^{\mu,\dot{\alpha}\alpha}(i\partial_\mu - V_\mu)\nu_\alpha = 0$. Its solution can be written in a form similar to Eq. (4.59),

$$\nu(t, \mathbf{p}) = a(t, \mathbf{p})\chi_-(\hat{\mathbf{p}}_\mathbf{V}) + b^\dagger(t, -\mathbf{p})\chi_+(\hat{\mathbf{p}}_\mathbf{V}) , \tag{4.116}$$

where we emphasize the different arguments of the operators $a, b^\dagger$ and the spinors $\chi_\mp$: $\hat{\mathbf{p}}_\mathbf{V}$ is the unit vector in the direction of $\mathbf{p} - \mathbf{V}$. The creation/annihilation operators $a(t, \mathbf{p}) = a(\mathbf{p})e^{-i\omega_+ t}$

and $b^\dagger(t,-\mathbf{p}) = b^\dagger(-\mathbf{p})e^{i\omega_- t}$ satisfy the usual anticommutation relations, with the energy spectrum given by $\omega_\pm \equiv |\mathbf{p}-\mathbf{V}| \pm V^0$.

Using the orthogonal vectors $\hat{\mathbf{p}}$ and $\hat{\boldsymbol{\epsilon}}$ we can write the energy eigenvalues $\omega_\pm$ in the form $\omega_\pm = \sqrt{(E-\hat{\mathbf{p}}\cdot\mathbf{V})^2 + |\hat{\boldsymbol{\epsilon}}\cdot\mathbf{V}|^2} \pm V^0$. The spinor contractions in Eq. (4.14) now include the spinors with the new argument $\chi_\mp(\hat{\mathbf{p}}_\mathbf{V})$. By construction, the Hamiltonian becomes diagonal, i.e., $\Gamma^{\nu\bar{\nu}}$ and $\Gamma^{\bar{\nu}\nu}$ vanish, once we use the solution of the equations of motion. The diagonal elements can be expanded in terms of $\chi_\mp(\hat{\mathbf{p}})$. For example for $\Gamma^{\nu\nu}$ we obtain

$$\chi_-^\dagger(\hat{\mathbf{p}}_\mathbf{V})\bar{\sigma}^\mu\chi_-(\hat{\mathbf{p}}_\mathbf{V}) = c_1 n^\mu(\hat{\mathbf{p}}) + \mathrm{Re}[c_2\epsilon^\mu(\hat{\mathbf{p}})]\,. \tag{4.117}$$

Multiplied by V_μ, Eq. (4.117) reproduces the interaction part of the $\mathsf{H}^{\nu\nu}$ element of the diagonalized Hamiltonian matrix. The decomposition coefficients

$$c_1 \equiv \frac{E-\hat{\mathbf{p}}\cdot\mathbf{V}}{|\mathbf{p}-\mathbf{V}|} \quad \text{and} \quad c_2 \equiv -\frac{\hat{\boldsymbol{\epsilon}}^*\cdot\mathbf{V}}{|\mathbf{p}-\mathbf{V}|}\,, \tag{4.118}$$

are related to the angle of the Bogolyubov transformation by $c_1 = \cos 2\vartheta$ and $|c_2| = \sin 2\vartheta$ respectively. In other words, diagonalizing the Hamiltonian matrix by a Bogolyubov transformation in every frame is equivalent to using the equation of motion. This equivalence suggests to interpret physical particle densities as propagation eigenstates of the full Hamiltonian in line with the discussion in Sec. 4.8.4.

4.9 Summary and conclusions

Neutrino flavor conversion is an important phenomenon to correctly describe neutrino transport in supernovae. This description is complicated by the fact that the evolution equations are nonlinear because of neutrino-neutrino refraction, which may lead to efficient flavor conversion. However, flavor oscillations alone might not be enough to fully incorporate all effects relevant for neutrino propagation.

Motivated by these concerns, we have studied extended kinetic equations that treat flavor correlations on the same footing as helicity and pair correlations. We have limited ourselves to the mean-field approximation in which all the interactions of the Hamiltonian are reduced to refraction. We have classified the contributions to the mean-field Hamiltonian matrix in terms of the Lorentz structures that appear for the chiral interactions of the neutrinos. These spinor contractions are shown explicitly to first order in the neutrino mass, similar to previous studies in the literature. For Dirac neutrinos, we confirm previous results. For Majorana neutrinos, we find a small correction to the mean-field Hamiltonian which arises from lepton-number violating contractions. To analyze the behavior of these additional terms in the limit of vanishing neutrino masses, we have studied extended kinetic equations for Weyl neutrinos.

We also supplemented the kinetic equations by helicity- and flavor-changing effects due to electromagnetic background fields. Because electric and magnetic fields were studied in the same formalism as matter effects, we were able to judge their relative importance. For typical parameters of core-collapse supernovae and SM-like electromagnetic moments of neutrinos, matter currents dominate over magnetic fields.

Flavor and helicity oscillations can be complicated in detail, but they are conceptually straightforward. Their importance arises because charged-current interactions produce neutrinos in flavor eigenstates, and all interactions create almost perfect helicity states. The generated interaction eigenstate is a coherent superposition of propagation eigenstates because the energy uncertainty of the neutrino production is much larger than the energy difference of the propagation eigenstates. This coherence leads to the various flavor and helicity oscillation phenomena.

Taken at face-value, pair correlations lead to similar oscillations. In the simplest case of massless neutrinos, the pair correlations are between neutrinos and antineutrinos of opposite momentum, and the oscillations are between the empty state and the one filled with a neutrino/antineutrino pair, i.e., we obtain spontaneous pair creation.

While such fluctuations are physically conceivable, they lead to a number of puzzling questions about how we define physical particle numbers: if we include pair correlations two observers with relative velocities seem to observe inconsistent particle numbers. We have shown that this problem may be solved by defining particles as eigenstates of the in-medium Dirac equation. When we include pair correlations, there is no preferred basis as to which we could define particles. Different definitions can be related via mixing particle and antiparticle operators via Bogolyubov transformations. Invoking the Dirac equation projects the space of possible particle definitions onto physical degrees of freedom. Unfortunately, such a treatment is in general not viable since we already approximate neutrinos to be quasi-free particles by invoking the mean-field approximation or by expanding the equations of motion perturbatively, i.e., we usually define particles as solutions to the free Dirac equation which leads to the mentioned problems.

For practical considerations, it may be best to discard pair correlations altogether and to interpret particles as eigenstates of pair correlations, i.e., to remove the $H^{\nu\bar{\nu}}$ submatrix from the Hamiltonian matrix. Firstly, this treatment resembles invoking the Dirac equation, which would send the discarded terms to zero. Secondly, the terms discarded this way induce very small correlations of the order $\kappa \sim 10^{-11}$, which seem to be irrelevant compared to $\mathcal{O}(1)$ number densities in any case. Note however that this small number for κ is a crude estimate and especially the treatment of UV-modes of κ might be improved. Finally, even if pair correlations are included in the evolution equations, their numerical value will probably be very close to its equilibrium value for which the density matrices and pair correlations decouple. The reason is that in contrast to flavor and helicity oscillations, there is no separation of scales in the dynamics of pair correlations. The oscillation frequency is here given by twice the neutrino energy which is of the same order as typical neutrino production time scales. We therefore expect a neutrino to relax to the equilibrium state of pair correlations during the production process.

If one wants to continue using pair correlations in the kinetic equations, one may try to proceed in the two following ways to resolve the existing issues. First, one may attempt to abstain from the assumption of homogeneity of the pair correlations to remove the problematic back-to-back condition of the pair correlations. This would allow us to track the momentum modes for different frames consistently and may prevent inconsistent particle numbers. Alternatively, one may try to use a full non-equilibrium treatment like the closed-time path formalism to obtain a constraint equation. Similarly to invoking the in-medium Dirac equation, the constraint equation filters for the correct excitations. Solving the kinetic and the constraint equation simultaneously may lead to consistent physical solutions.

Chapter 5

Lepton asymmetry from mixing and oscillations

We study a toy model of leptogenesis in the closed-time-path formalism and compare the generated lepton asymmetry in two conceptually different formalisms, i.e., the Heisenberg- and interaction-picture Kadanoff-Baym equations, demonstrating for the first time their equivalence in the weak-washout regime. Three energy shells emerge and we identify two of these shells as resonant mixing whereas the third shell contains oscillations. In contrast to earlier works, we find that the third shell also features a destructive interference between mixing and oscillations. We compare our results to the density-matrix approach for which we confirm that the asymmetry is underestimated, in line with previous discussions. We also find that the effective Yukawa approach often used to describe resonant mixing has to be supplemented by the interference contribution in the resonant and weak-washout regimes.[1]

5.1 Introduction: kinetic equations and resonant leptogenesis

Our universe is not symmetric with respect to baryons and antibaryons [9]. The amount of antiprotons that are observed in cosmic rays is about four orders of magnitude smaller than the amount of protons [225] and consistent with purely secondary production through pair production from high energy particles [226]. Moreover, no heavy antinuclei have been observed [227], which could have pointed towards fusion of antimatter nuclei in antimatter stars. In cosmology, the baryon-asymmetry is reflected in the present baryon-to-photon ratio [10]

$$\eta = \frac{n_b}{n_\gamma} = 6.05 \pm 0.07 \times 10^{-10}\,, \tag{5.1}$$

with baryon number density n_b and photon number density n_γ. This quantity would be vanishingly small if the universe was completely symmetric with respect to baryon symmetry, since protons and antiprotons would annihilate in pairs and suppress n_b.

In order to generate this baryon asymmetry in the early universe, we require processes that violate baryon number, C and CP-symmetry, and that occur sufficiently far from equilibrium [11]. In principle, all of these ingredients can be found in the Standard Model and for a standard cosmology [12, 95, 96] but the resulting baryon asymmetry is too small to explain the observed value in Eq. (5.1).

[1] The detailed computations that are shown in this chapter have been presented before in "Lepton asymmetry from mixing and oscillations" [3] by A. Kartavtsev, P. Millington and the present author.

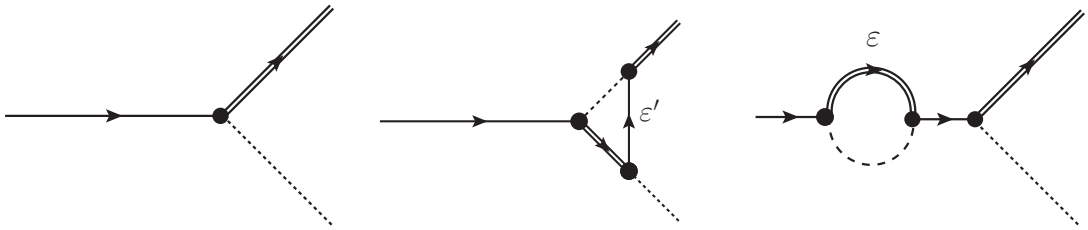

Figure 5.1: Feynman diagrams for the decay of a heavy Majorana neutrino. The tree-level diagram is shown on the left. The one-loop vertex correction is depicted in the middle. This diagram gives rise to the ε'-type CP-violations. ε-type CP-violation is shown on the right-hand side. Here, a self-energy was inserted on the external leg.

The failure to explain the baryon asymmetry has to be mended by new physics, for which several approaches exist in the literature (see [12, 96]). In this chapter, we focus on resonant leptogenesis which generates an asymmetry in the lepton number from decays of quasi-degenerate heavy Majorana neutrinos. Lepton-number conservation is broken explicitly by the Majorana masses, and complex Yukawa couplings provide CP-violation. The asymmetry is then generated in out-of-equilibrium decays and converted to a baryon asymmetry through the sphaleron processes [98, 228].

In contrast to the original leptogenesis scenario by Fukugita and Yanagida [97], resonant leptogenesis [106, 107, 229, 230] relies on resonant mixing in the decay of Majorana neutrinos. *CP*-violation in the decay of Majorana neutrinos arises at leading order through the interference of the tree level decay and the absorptive part of one-loop corrections (see Fig.5.1). In Ref. [97], only the loop at the vertex was considered to interfere (ε'-type *CP*-violation). An additional source of *CP*-violation (ε-type) arises however through the interference of the tree-level decay with the self-energy correction to the external neutrino leg (see Fig. 5.1). While for a hierarchical spectrum this mixing contribution is of the same order as ε'-type *CP*-violation [231], for quasi-degenerate Majorana neutrinos the ε-type *CP*-violation dominates over the ε'- effect [229, 230], which then may be neglected.

The asymmetry for a hierarchical mass spectrum can be readily calculated using a system of Boltzmann equations (see e.g. Refs [232–236]). The Boltzmann approach has also been used for quasi-degenerate spectra [237, 238], and resonant mixing may be treated semi-classically by defining effective Yukawa couplings [106, 107] that contain all contributions from mixing.

For quasi-degenerate mass spectra, one has to worry about the build-up of correlations between the Majorana neutrinos; an effect that is not captured by the Boltzmann formalism. In the density matrix formalism, one finds indeed that the correlations are important and that flavor oscillations of heavy neutrinos give an additional contribution to the *CP*-violation besides the mixing source [239–245]. Whereas it is widely accepted that the mixing source is important for all mass spectra of the heavy neutrinos, the relative importance of the oscillation source is still under debate, and it is one goal of this chapter to compare the oscillation to the traditional mixing in a simplified model of leptogenesis.

For this comparison we have to start from first principles of statistical mechanics and quantum field theory (see Sec. 2.5). In the Schwinger-Keldysh [91, 92] closed-time-path formalism

of non-equilibrium thermal field theory (see also Refs. [125, 246, 247]) one may obtain coupled quantum transport equations that are well-suited to describe non-equilibrium dynamics; the Kadanoff-Baym equations [93, 94] (for a review, see Ref. [128]). The closed-time-path formalism has the advantage that all quantum-mechanical effects are in principle accounted for consistently and systematically. In the literature a huge effort in deriving and solving the Kadanoff-Baym equations has been made [110, 112, 113, 130, 132, 248–266]. Nevertheless, it remains an extraordinarily difficult task to obtain tractable solutions and to extract physically meaningful observables. The quantum transport equations have to be simplified using suitable approximations, but different approaches make it often difficult to compare directly the results of different analyses or to ascertain to what extent relevant physical effects are accounted for.

In this chapter, we will be mainly concerned with the works of Garbrecht and collaborators [112, 113] and those of Dev and collaborators [108–110]. Both approaches highlight the physical relevance of the oscillation source in leptogenesis but with differing approaches. The works of Garbrecht and collaborators [112, 113] use the Heisenberg-picture Kadanoff-Baym equations to compute the asymmetry. The advantage of these equations is that they contain all information about plasma excitations and memory effects. On the downside, one has to solve a system of coupled integro-differential equations to obtain a solution: this is a difficult task both analytically and numerically. Garbrecht and collaborators [112, 113] use a quasi-particle ansatz to simplify the resulting equations, i.e., they approximate the Wightman propagators of all Majorana neutrinos to be proportional to a single delta function (density matrix approach). While this forces the Majorana neutrinos to have the same energies in the spectral function, the kinetic equation still contains mass and energy differences that may lead to flavor oscillations. This approximation will be called the single-shell approximation, where shell is to be understood as the energy for which a delta function in the spectral function becomes non-zero (on-shell). The resulting kinetic equation is a density matrix equation which contains flavor oscillations. These oscillations then contribute to the asymmetry. Nevertheless, it is a priori not clear to what extent this kinetic equation correctly reflects the full asymmetry.

Indeed, it was argued by Dev, Millington, Pilaftsis, and Teresi [110] that such an approach would discard the effect of mixing and underestimate the generated asymmetry. To show this, they use the interaction-picture description to non-equilibrium quantum field theory [118]. There, one starts by defining particles as free vacuum excitations and reconstructs non-equilibrium effects by a perturbation series or by resuming vacuum propagators into interacting (dressed) propagators. The interaction-picture treatment may be viewed as a bottom-up approach in contrast to the top-down approach of the Heisenberg picture. While in the Heisenberg approach one had to guess what the physical excitations are by imposing a single-shell approximation, the advantage of the interaction picture is that the degrees of freedom come out of the vacuum propagators.

Dev and collaborators [108–110] applied the interaction picture to a model of leptogenesis in the strong-washout regime observing that both resonant mixing and oscillations are of equal magnitude and contribute additively to the asymmetry (for a summary, see Ref. [111]). This leads to a factor of two enhancement in the final lepton asymmetry, when both sources, rather than only one, are included.

An independent cross-check of these results is difficult to obtain because of different approximations that go into competing approaches. In this chapter, we will compare non-equilibrium

field theoretic results in the Heisenberg and interaction pictures in a simplified model of leptogenesis and in the weak-washout regime. We find exact agreement between these two formulations, illustrating for the first time the self-consistency and complementarity of these two approaches. We will demonstrate that mixing and oscillations persist, and we will illustrate how the mixing and oscillation sources can be identified in the Kadanoff-Baym formalism by means of the shell structure of the resumed heavy neutrino propagators. We will show that there are *three* distinct shells. Two of these shells correspond to resonant mixing and can be associated with the quasi-particle mass shells, whereas the third, which can be identified with oscillations, lies at an intermediate energy. In addition, we identify terms lying on the oscillation shell that can be interpreted as the interference between oscillation and mixing; a phenomenon not accounted for in Refs. [108–110].

Most significantly, we find that this interference is destructive. With respect to the "benchmark" of the Boltzmann approximation, this destructive interference can be viewed as a suppression of the oscillation source. Conversely, with respect to the "benchmark" of the density matrix approximation, this destructive interference can be viewed as a suppression of the mixing source. This observation may in part account for apparent discrepancies between competing approaches. Nevertheless, in spite of this destructive interference, we find that both oscillation and mixing sources can be of equal magnitude and contribute additively to the final asymmetry in agreement with the conclusions of Refs. [108–110].

Note however that our results were obtained in the weak-washout regime, where some approximations of Refs. [108–110, 112, 113] cannot be made, and it remains to be seen how the result generalizes to the strong-washout regime.

The remainder of this chapter is organized in the following way. In Sec. 5.2 we introduce our toy model. We focus on a scalar theory which embodies all relevant features for a cosmological asymmetry generation. Some basic concepts of non-equilibrium quantum field theory are summarized in Sec. 5.3, before we move on to explicitly calculate the asymmetry in the Heisenberg picture in Sec. 5.4. Here, we identify the three different shells and interpret them as mixing, oscillations, and interference. This result is then confirmed in Sec. 5.5 using the interaction picture approach. We also make a comparison to the density matrix approach at this point. The comparison to the effective Yukawa coupling approach is performed in Sec. 5.6. Numerical studies are then shown in Sec. 5.7, where we show that both mixing and oscillations contribute and may lead to a factor of two enhancement compared to just one of these sources. The relevance of interference will be highlighted. We conclude this chapter in Sec. 5.8.

5.2 A model for leptogenesis

We are interested in resonant leptogenesis where the baryon asymmetry is generated by a pair of quasi-degenerate heavy neutrinos. However, calculations in the CTP-formalism are technically demanding and the notation clouds the physical meaning of the results. In order to minimize this notational clutter, we resort to a simple toy model, which nevertheless contains all features necessary for successful leptogenesis. This toy model contains two real scalar fields ψ_i that mimic the heavy neutrinos. Somewhat inaccurately, we will call these real scalars "heavy neutrinos"

in the following. Additionally, we introduce one complex scalar background field b that mimics charged leptons to which the heavy neutrinos decay. The Lagrangian reads

$$\begin{aligned}\mathcal{L} = &\frac{1}{2}\partial^\mu\psi_i\,\partial_\mu\psi_i - \frac{1}{2}\psi_i M_{ij}^2\psi_j + \partial^\mu b^*\,\partial_\mu b - m^2\,b^*b \\ &- \frac{\lambda}{4}(b^*b)^2 - \frac{h_i}{2}\psi_i bb - \frac{h_i^*}{2}\psi_i b^*b^* \,.\end{aligned} \tag{5.2}$$

The first line contains the kinetic and mass terms. While the kinetic terms of the heavy neutrinos are flavor-diagonal, the mass term contains a general mass matrix M_{ij} that can be non-diagonal. The second line contains the interaction of the complex scalar that keeps the background bath in equilibrium with itself as well as the terms that describe the decay of the heavy neutrinos into complex scalars with coupling strengths h_i.

Our model Lagrangian takes the Sakharov conditions [11] into account in the following way. In the absence of the decay of the heavy neutrino, the model would exhibit a $U(1)$ global symmetry that corresponds to lepton number of the complex scalars. This symmetry is explicitly broken by the decay terms. The decays also violate *C* and *CP*-invariance if the couplings h_i are not chosen in a special way (see appendix B). Finally, departure from equilibrium is realized through out-of-equilibrium decays.

5.3 Propagators and self-energies

Our aim is to study the asymmetry of the lepton number which is carried by the complex scalar field. In Sec. 5.4 we will show that this asymmetry may be expressed in terms of two-point functions of this complex scalar and calculated using Kadanoff-Baym equations (2.57). Before we dive into the computation let us summarize the key quantities that go into the derivation.

The lepton number is carried by the complex scalar field. Its propagators are therefore tied to the produced lepton asymmetry. We will need the Wightman propagators

$$S_>(x,y) = \langle b(x)b^*(y)\rangle\,, \qquad S_<(x,y) = \langle b^*(y)b(x)\rangle\,. \tag{5.3}$$

These propagators exchange their arguments under complex conjugation

$$S_>^*(x,y) = S_>(y,x)\,, \qquad S_<^*(x,y) = S_<(y,x)\,, \tag{5.4}$$

and they are in general complex valued functions. They can be decomposed into statistical and spectral propagators $S_{\mathrm{F},\rho}$

$$S_{\gtrless}(x,y) = S_{\mathrm{F}}(x,y) \mp \frac{i}{2}S_\rho(x,y)\,, \tag{5.5}$$

which in turn are defined via commutators and anticommutators of the fields $b(x), b^*(y)$,

$$S_{\mathrm{F}}(x,y) = \frac{1}{2}\langle\{b(x),b^*(y)\}\rangle\,, \qquad S_\rho(x,y) = i\langle[b(x),b^*(y)]\rangle\,. \tag{5.6}$$

In a C-symmetric configuration, these propagators are real-valued [264], which will be important later on to distinguish source and washout terms in the asymmetry. Also they possess definite transformations under complex conjugation

$$S_{\mathrm{F}}^{*}(x,y) = S_{\mathrm{F}}(y,x)\,, \qquad S_{\rho}^{*}(x,y) = -S_{\rho}(y,x)\,. \tag{5.7}$$

CP-violation is generated through interference between tree level and one-loop decay amplitudes. Hence, we also need expressions for the one-loop self-energies. They can be derived by taking the functional derivative of the 2PI effective action with respect to the complex scalars' propagators. The 2PI part of the effective action reads [254]

$$\begin{aligned} i\Gamma_2 = &-\frac{1}{4}h_i h_j^{*}\int \mathrm{d}^4x\mathrm{d}^4y\, G^{ij}(x,y)S^2(x,y) \\ &-\frac{1}{4}h_i^{*}h_j\int \mathrm{d}^4x\mathrm{d}^4y\, G^{ij}(x,y)S^2(y,x)\,, \end{aligned} \tag{5.8}$$

The effective action contains the propagator of the real scalar G^{ij} with flavor indices i,j. The real scalars' Wightman propagators are (see Sec. 2.5)

$$G_{>}^{ij}(x,y) = \langle \psi^i(x)\psi^j(y)\rangle\,, \tag{5.9}$$

$$G_{<}^{ij}(x,y) = \langle \psi^j(y)\psi^i(x)\rangle\,, \tag{5.10}$$

and the statistical (spectral) propagators of the real scalars $G_{\mathrm{F}(\rho)}^{ij}$ are defined as

$$G_{\mathrm{F}}^{ij}(x,y) = \frac{1}{2}\langle\{\psi^i(x),\psi^j(y)\}\rangle\,, \qquad G_{\rho}^{ij}(x,y) = i\langle[\psi^i(x),\psi^j(y)]\rangle\,. \tag{5.11}$$

These matrices are real-valued [264] as can again be seen from the representation of the expectation value in terms of the Hermitian density matrix. Under the exchange of the arguments and indices, the statistical propagator is symmetric, while the spectral function is antisymmetric

$$G_{\mathrm{F}}^{ij}(x,y) = G_{\mathrm{F}}^{ji}(y,x)\,, \qquad G_{\rho}^{ij}(x,y) = -G_{\rho}^{ji}(y,x)\,. \tag{5.12}$$

With these definitions, the statistical and spectral parts of the one-loop self-energies, which for the complex scalars will be denoted by Σ, are given by

$$\Sigma_{\mathrm{F}}(x,y) = -H_{ij}^{*}\left[G_{\mathrm{F}}^{ij}(x,y)S_{\mathrm{F}}(y,x) + \frac{1}{4}G_{\rho}^{ij}(x,y)S_{\rho}(y,x)\right]\,, \tag{5.13}$$

$$\Sigma_{\rho}(x,y) = -H_{ij}^{*}\left[G_{\mathrm{F}}^{ij}(x,y)S_{\rho}(y,x) - G_{\rho}^{ij}(x,y)S_{\mathrm{F}}(y,x)\right]\,, \tag{5.14}$$

where we have introduced the dyadic product $H_{ij} \equiv h_i h_j^{*}$ and summation over the indices is implied.

The self-energies of the real scalar $\Pi_{\mathrm{F},\rho}$ are obtained from the functional derivative of the 2PI effective action with respect to the real scalars' propagators [254], which now has two complex scalars running in the loop

$$\Pi_{\mathrm{F}}^{ij}(x,y) = -\,\mathrm{Re}\,H^{ij}\left[S_{\mathrm{F}}^2(y,x) - \frac{1}{4}S_{\rho}^2(y,x)\right] \equiv \mathrm{Re}\,H^{ij}\Pi_{\mathrm{F}}(y,x)\,, \tag{5.15}$$

$$\Pi_{\rho}^{ij}(x,y) = 2\,\mathrm{Re}\,H^{ij}S_{\mathrm{F}}(y,x)S_{\rho}(y,x) \equiv \mathrm{Re}\,H^{ij}\Pi_{\rho}(y,x)\,, \tag{5.16}$$

where the equivalence serves as a definition for the amputated self-energies $\Pi_{\mathrm{F},\rho}$ for which the coupling has been factored out. We have used assumed that the complex scalars' propagators are real-valued. Finally, it is convenient to also define

$$\Pi_{\gtrless} = \Pi_{\mathrm{F}} \mp \frac{i}{2}\Pi_{\rho}\,, \tag{5.17}$$

in analogy to the definition of the Wightman propagators of the scalar fields.

Explicitly, we will only need the Wigner transform of the retarded and advanced self-energies $\Pi_{R,A}(X,Q)$. They may be decomposed into a Hermitian and an skew-Hermitian matrix:

$$\Pi^{ij}_{R(A)} = \Pi^{ij}_{\mathrm{h}} \pm \frac{i}{2}\widetilde{\Pi}^{ij}_{\rho}\,. \tag{5.18}$$

For the model in Eq. (5.2) and in the $\overline{\mathrm{MS}}$ renormalization scheme, the self-energies have been calculated explicitly in Ref. [264]. Note that their convention, denoted here with a tilde, for the time-component Wigner transform of the spectral functions includes another factor of i: $\widetilde{\Pi}_{\rho} = -i\Pi_{\rho}$. For an equilibrium system, the spectral part gives

$$\widetilde{\Pi}^{ij}_{\rho}(X,Q) \equiv -\frac{\operatorname{Re} H_{ij}}{8\pi} L_{\rho}(X,Q) = -\frac{\operatorname{Re} H_{ij}}{8\pi}\left(\theta(Q^2) + \frac{2T}{|\mathbf{Q}|}\ln\left[\frac{1-e^{-(Q_0+|\mathbf{Q}|)/(2T)}}{1-e^{-(Q_0-|\mathbf{Q}|)/(2T)}}\right]\right). \tag{5.19}$$

for $Q_0 > |\mathbf{Q}|$. The Hermitian part Π_{h} may be decomposed into a vacuum and a medium contribution

$$\Pi^{ij}_{\mathrm{h}}(X,Q) = \Pi^{ij}_{\mathrm{vac}}(Q) + \Pi^{ij}_{\mathrm{med}}(X,Q)\,. \tag{5.20}$$

The renormalized vacuum part reads [264]

$$\Pi^{ii}_{\mathrm{vac}}(Q) = \frac{H_{ii}}{16\pi^2}\ln\frac{|Q^2|}{\mu^2}\,, \tag{5.21a}$$

$$\Pi^{i\not{i}}_{\mathrm{vac}}(Q) = \frac{\operatorname{Re} H_{i\not{i}}}{16\pi^2}\ln\frac{|Q^2|}{\mu^2}\,, \tag{5.21b}$$

where μ is the renormalization scale and we have employed the notation $i, \not{i}$ to distinguish between the two flavors [110]:

$$\not{i} \equiv \begin{cases} 2\,, & \text{for} \quad i = 1 \\ 1\,, & \text{for} \quad i = 2\,. \end{cases} \tag{5.22}$$

The medium contribution is

$$\Pi^{ij}_{\mathrm{med}}(X,Q) = -\operatorname{Re} H_{ij}\frac{T}{8\pi^2|\mathbf{Q}|}\int_0^{\infty}\mathrm{d}z\, n_{\mathrm{eq}}(z)\ln\left|\frac{(2z+|\mathbf{Q}|/T)^2 - Q_0^2/T^2}{(2z-|\mathbf{Q}|/T)^2 - Q_0^2/T^2}\right|\,, \tag{5.23}$$

which holds for a *C*-symmetric medium.

5.4 Shell structure in the Heisenberg picture

In general, the calculation of the asymmetry is challenging and analytical insights are hard to achieve. For the model presented in Eq. (5.2), an analytical solution of the Kadanoff-Baym equations in the Heisenberg picture has been obtained in Ref. [264]. Using this solution, which will be motivated below, we show that mixing and oscillations between flavors provide two distinct sources of the asymmetry, in agreement with arguments presented in Refs. [108–110]. Whereas the standard mixing contributions [105, 107] are associated with the mass shells ω_i ($i = 1, 2$) of the corresponding quasi-particles, the oscillation contribution is associated with a shell at $\bar{\omega} = (\omega_1 + \omega_2)/2$, which we refer to as the *oscillation shell*.

5.4.1 Asymmetry

The asymmetry can be derived from the Noether current of the complex scalar,

$$\begin{aligned} j^\mu &= i\left[b^*(x)\left(\frac{\partial}{\partial x_\mu}b(x)\right) - b(x)\left(\frac{\partial}{\partial x_\mu}b^*(x)\right)\right] \\ &= i\lim_{y\to x}\left[\left(\frac{\partial}{\partial x_\mu}b^*(y)b(x)\right) - \left(\frac{\partial}{\partial y_\mu}b(x)b^*(y)\right)\right], \end{aligned} \tag{5.24}$$

which would be conserved in the absence of the CP-violating interactions. This current can be expressed in terms of propagators by taking the expectation value

$$J^\mu(x) = \langle j^\mu(x)\rangle = i\lim_{y\to x}\left[\frac{\partial}{\partial x_\mu}S_<(x,y) - \frac{\partial}{\partial y_\mu}S_>(x,y)\right]. \tag{5.25}$$

With the decomposition into statistical and spectral parts [Eq. (5.5)], the Noether current in Eq. (5.25) reads

$$J^\mu(x) = i\lim_{y\to x}\left(\frac{\partial}{\partial x_\mu} - \frac{\partial}{\partial y_\mu}\right)S_{\rm F}(x,y) - \lim_{y\to x}\left(\frac{\partial}{\partial x_\mu} + \frac{\partial}{\partial y_\mu}\right)S_\rho(x,y)\,. \tag{5.26}$$

The contribution from the spectral function vanishes as can be seen as follows: S_ρ is defined via the commutator [see Eq. (5.6)], and only the equal-time commutator with a time-derivative does not vanish trivially, but gives

$$[b(\mathbf{x}), \dot{b}^*(\mathbf{y})] = [\dot{b}(\mathbf{x}), b^*(\mathbf{y})] = i\delta^{(3)}(\mathbf{x}-\mathbf{y})\,. \tag{5.27}$$

Since the commutator is antisymmetric, the contributions from the derivative with respect to x^0 and y^0 cancel. We are left with

$$J^\mu(x) = i\lim_{y\to x}\left(\frac{\partial}{\partial x_\mu} - \frac{\partial}{\partial y_\mu}\right)S_{\rm F}(x,y)\,. \tag{5.28}$$

Taking the divergence of this current, we obtain

$$\partial_\mu J^\mu(x) = i \lim_{y\to x} \left(\frac{\partial}{\partial x_\mu} + \frac{\partial}{\partial y_\mu}\right)\left(\frac{\partial}{\partial x_\mu} - \frac{\partial}{\partial y_\mu}\right) S_{\rm F}(x,y) = i \lim_{y\to x} \left(\Box_x - \Box_y\right) S_{\rm F}(x,y)\,. \quad (5.29)$$

The right-hand side can be evaluated using the Kadanoff-Baym equations for the complex scalar, which have been derived in Ref. [253] for Gaussian initial conditions. They read

$$\left(\Box_x + m^2\right) S_{\rm F}(x,y) = \int_{t_0}^{y^0} {\rm d}^4 z\, \Sigma_{\rm F}(x,z) S_\rho(z,y) - \int_{t_0}^{x^0} {\rm d}^4 z\, \Sigma_\rho(x,z) S_{\rm F}(z,y)\,, \quad (5.30)$$

$$\left(\Box_x + m^2\right) S_\rho(x,y) = \int_{x^0}^{y^0} {\rm d}^4 z\, \Sigma_\rho(x,z) S_\rho(z,y)\,, \quad (5.31)$$

where t_0 is the initial time. The equations depend on the propagators of the real scalars through the self-energies $\Sigma_{{\rm F}(\rho)}$. These propagators also contain the deviation from equilibrium.

Using the symmetry properties of the statistical and spectral propagators [Eq. (5.7)], we may derive equations that are similar to Eq. (5.30) but with the derivative acting on the second argument of the propagator. Inserting these Kadanoff-Baym equations into Eq. (5.29) , the four-divergence of the lepton-number current is

$$\partial_\mu J^\mu(x) = 2\,{\rm Im} \int_{t_0}^{x^0} {\rm d}^4 z \left[\Sigma_\rho(x,z) S_{\rm F}(z,x) - \Sigma_{\rm F}(x,z) S_\rho(z,x)\right]\,. \quad (5.32)$$

In the absence of CP-violation or in equilibrium, this current would vanish.

We would like to find the expectation value for the lepton-number density, which is given by

$$\eta(t) = \frac{1}{V} \int {\rm d}^3\mathbf{x}\, \langle j^0 \rangle\,, \quad (5.33)$$

where V is the volume of space, which will cancel later on. Integrating Eq. (5.32) over the coordinate space and normalizing by the three-volume V, we obtain in the frame where the medium is homogeneous

$$\dot\eta(x^0) = \frac{2}{V}\,{\rm Im} \int_{t_0}^{x^0} {\rm d}^4 z \int {\rm d}^3\mathbf{x} \left[\Sigma_\rho(x,z) S_{\rm F}(z,x) - \Sigma_{\rm F}(x,z) S_\rho(z,x)\right]\,. \quad (5.34)$$

This equation can be manipulated and interpreted more easily if we substitute the propagators by their Wigner transforms

$$S_{\rm F}(t',t'',\mathbf{x},\mathbf{z}) = \int \frac{{\rm d}^3\mathbf{Q}}{(2\pi)^3}\, e^{i\mathbf{Q}(\mathbf{x}-\mathbf{z})} S_{\rm F}(t',t'',\mathbf{Q})\,. \quad (5.35)$$

The lepton charge density [Eq. (5.34)] then simplifies to

$$\dot\eta(x^0) = 2\,{\rm Im} \int_{t_0}^{x^0} {\rm d}z^0 \int \frac{{\rm d}^3\mathbf{Q}}{(2\pi)^3} \left[\Sigma_\rho(x^0,z^0,\mathbf{Q}) S_{\rm F}(z^0,x^0,\mathbf{Q}) - \Sigma_{\rm F}(x^0,z^0,\mathbf{Q}) S_\rho(z^0,x^0,\mathbf{Q})\right]\,, \quad (5.36)$$

where the volume has canceled with a spatial integration over the central coordinate.

The asymmetry can be further decomposed by identifying the source and washout terms. While source terms generate an asymmetry even in a *C*-symmetric configuration, the washout terms only contribute if the bath of complex scalars is not *C*-symmetric. Since in a *C*-symmetric configuration, the propagators of the complex scalars are real-valued, the washout terms are defined to be proportional to the imaginary part of $S_{\mathrm{F},\rho}$. Hence [264],

$$\dot{\eta}(x^0) \equiv S(x^0) - W(x^0)\,, \tag{5.37}$$

with the source term $S(x)$ and the washout term $W(x)$, which read

$$S(x) \equiv 2\int_{t_0}^{x^0} \mathrm{d}z^0 \frac{\mathrm{d}^3\mathbf{Q}}{(2\pi)^3}\left[\mathrm{Im}\,\Sigma_\rho(x^0,z^0)\,\mathrm{Re}\,S_\mathrm{F}(z^0,x^0) - \mathrm{Im}\,\Sigma_\mathrm{F}(x^0,z^0)\,\mathrm{Re}\,S_\rho(z^0,x^0)\right]\,, \tag{5.38}$$

$$W(x) \equiv -2\int_{t_0}^{x^0} \mathrm{d}z^0 \frac{\mathrm{d}^3\mathbf{Q}}{(2\pi)^3}\left[\mathrm{Re}\,\Sigma_\rho(x^0,z^0)\,\mathrm{Im}\,S_\mathrm{F}(z^0,x^0) - \mathrm{Re}\,\Sigma_\mathrm{F}(x^0,z^0)\,\mathrm{Im}\,S_\rho(z^0,x^0)\right]\,. \tag{5.39}$$

Here and in the following we omit the common dependence on $\mathbf{Q}$.

In phenomenological analyses, the washout terms are important since they asymptotically lead the system back to its equilibrium state. In this work, however, we concentrate on the source term and neglect the back-reactions in order to obtain analytical insights.

Integrating Eq. (5.37) over time x^0, we obtain the produced asymmetry

$$\begin{aligned}\eta(t) = \int_{t_0}^{t}\mathrm{d}x^0\int_{t_0}^{t}\mathrm{d}z^0\frac{\mathrm{d}^3\mathbf{Q}}{(2\pi)^3}\Big\{&\mathrm{Im}\left[\Sigma_\rho(x^0,z^0)\right]S_\mathrm{F}(z^0,x^0)\\ &-\mathrm{Im}\left[\Sigma_\mathrm{F}(x^0,z^0)\right]S_\rho(z^0,x^0)\Big\}\,.\end{aligned} \tag{5.40}$$

Here we assumed that the initial asymmetry $\eta(t_0) = 0$, and we used the identity

$$\int_{t_0}^{t}\mathrm{d}t'\int_{t_0}^{t'}\mathrm{d}t''\left[f(t',t'') + f(t'',t')\right] = \int_{t_0}^{t}\mathrm{d}t'\int_{t_0}^{t}\mathrm{d}t''\,f(t',t'')\,, \tag{5.41}$$

which can be derived from noting that the limits on the t''-integral can be extended by inserting a Heaviside step function

$$\int_{t_0}^{t}\mathrm{d}t'\int_{t_0}^{t'}\mathrm{d}t''\,f(t',t'') = \int_{t_0}^{t}\mathrm{d}t'\int_{t_0}^{t}\mathrm{d}t''\,\theta(t'-t'')f(t',t'')\,. \tag{5.42}$$

This trick will be used regularly in the following since it allows us to extend the bounds of integration to infinity.

For the *C*-symmetric medium we consider here, the self-energies Σ contain only real-valued propagators, and the only imaginary quantities are the off-diagonals of H_{ij}. Using the relations

between the Wightman functions and the statistical and spectral functions [Secs. 2.5 and 5.3], the produced asymmetry reduces to

$$\begin{aligned}\eta(t) = -2\,\mathrm{Im}\,H_{12} \int_{-\infty}^{t} \mathrm{d}x^0 \int_{-\infty}^{t} \mathrm{d}y^0 \int \frac{\mathrm{d}^3\mathbf{Q}}{(2\pi)^3} \\ \times\, i\left[G^{12}_{<}(x^0,y^0)\Pi_{>}(y^0,x^0) - G^{12}_{>}(x^0,y^0)\Pi_{<}(y^0,x^0)\right],\end{aligned} \tag{5.43}$$

where following Refs. [261, 264], we assumed that the system begins its evolution at $t_0 = -\infty$ with both the complex and the real scalars in an equilibrium state. This expression obtained with the Noether current is entirely equivalent to the one obtained via the definition of the number densities used in the interaction-picture approach to the Kadanoff-Baym formalism, developed in Ref. [118].

5.4.2 Analytical solution of the Kadanoff-Baym equations

The Wightman propagators in Eq. (5.43) are solutions to the Kadanoff-Baym equations for the mixing fields ψ_i. In equilibrium, no asymmetry will be produced. Since we do not consider expansion of the universe in this chapter, we emulate departure from equilibrium with an external source at $t = 0$. This source takes the real scalars out of equilibrium, thereby fulfilling the third Sakharov condition. An asymmetry between the number densities of b and b^* is then produced.

Let us first look at equilibrium to obtain some insights for the non-equilibrium case. In the absence of external sources, the transport equations read [254]

$$[\Box_x \mathbb{1} + \mathsf{M}^2]^{ik} G^{kj}_{\gtrless}(x,y) = \int_{-\infty}^{y^0} \mathrm{d}^4 z\, \Pi^{ik}_{\gtrless}(x,z) G^{kj}_{\rho}(z,y) - \int_{-\infty}^{x^0} \mathrm{d}^4 z\, \Pi^{ik}_{\rho}(x,z) G^{kj}_{\gtrless}(z,y)\,, \tag{5.44}$$

where M is the mass matrix of the renormalized Lagrangian. Using the definitions of the retarded and advanced propagators and self-energies (2.56), we can rewrite Eq. (5.44) in a form more convenient for the analysis that follows:

$$[\Box_x \mathbb{1} + \mathsf{M}^2]^{ik} G^{kj}_{\gtrless}(x,y) = -\int \mathrm{d}z^4 \left[\Pi^{ik}_{\mathrm{R}}(x,z) G^{kj}_{\gtrless}(z,y) + \Pi^{ik}_{\gtrless}(x,z) G^{kj}_{\mathrm{A}}(z,y)\right], \tag{5.45}$$

Here, we have used Heaviside step functions to extend the z^0-domain of integration to infinity. The Kadanoff-Baym equations for the retarded and advanced propagators can be derived from Eq. (5.44):

$$[\Box_x \mathbb{1} + \mathsf{M}^2]^{ik} G^{kj}_{\mathrm{R(A)}}(x,y) = \delta(x-y)\delta^{ij} - \int \mathrm{d}^4 z\, \Pi^{ik}_{\mathrm{R(A)}}(x,z) G^{kj}_{\mathrm{R(A)}}(z,y)\,. \tag{5.46}$$

At the one-loop level to which we limit ourselves here, the self-energies of the real scalar fields only contains propagators of the complex scalars [see Eqs. (5.15)]. Since they are assumed to be in equilibrium, they are translationally invariant. This invariance implies that Eq. (5.46) admits a

translationally-invariant solution, which can be seen by writing the right-hand side of Eq. (5.46) in terms of Fourier transforms. Using Eq. (5.46), one can readily check that

$$G^{ij}_{\gtrless,\mathrm{eq}}(x,y) \equiv -\int \mathrm{d}^4u\mathrm{d}^4v\, G^{im}_{\mathrm{R}}(x,u)\Pi^{mn}_{\gtrless}(u,v)G^{nj}_{\mathrm{A}}(v,y) \tag{5.47}$$

is a solution to Eq. (5.45). Since the self-energies as well as the retarded and advanced propagators on the right-hand side of Eq. (5.47) are translationally invariant, the left-hand side of Eq. (5.47) is also translationally invariant. In other words, Eq. (5.47) is an equilibrium solution for the Wightman propagators, which is denoted by the subscript "eq".

An external source at $t = 0$ brings the system instantaneously out of equilibrium. Following refs. [261, 264], we consider an external bi-local source that perturbs both Wightman self-energies in the same way $\Pi^{ij}_{\gtrless}(x,y) \to \Pi^{ij}_{\gtrless}(x,y) - K^{ij}(x,y)$ and, thus, leaves the spectral function, the retarded propagator and the advanced propagator unperturbed. Here, we take $K^{ij}(x,y) = \delta(x^0)\delta(y^0)\mathcal{K}^{ij}(\mathbf{x}-\mathbf{y})$, which renders the renders the Kadanoff-Baym equations linear at one loop, i.e. a sum of two solutions is also a solution. Using this linearity, we obtain the following equation for the non-equilibrium part $G^{ij}_{\gtrless\delta} \equiv G^{ij}_{\gtrless} - G^{ij}_{\gtrless,\mathrm{eq}}$ of the Wightman propagators induced by the external source:

$$[\Box_x \mathbb{1} + \mathsf{M}^2]^{ik} G^{kj}_{\gtrless\delta}(x,y) = -\int \mathrm{d}^4z \left[\Pi^{ik}_{\mathrm{R}}(x,z)G^{kj}_{\delta\gtrless}(z,y) - K^{ik}(x,z)G^{kj}_{\mathrm{A}}(z,y)\right] . \tag{5.48}$$

This equation can be fulfilled [261, 264] by

$$G^{ij}_{\gtrless\delta}(x,y) = \int \mathrm{d}^4u\mathrm{d}^4v\, G^{im}_{\mathrm{R}}(x,u)K^{mn}(u,v)G^{nj}_{\mathrm{A}}(v,y)\,. \tag{5.49}$$

We are only interested in this non-equilibrium part of the resummed Wightman propagators because in the absence of expansion the equilibrium solution is static and does not contribute to the asymmetry [264]. Because of the form of the external source, the non-equilibrium parts of the positive and negative frequency Wightman propagators are equal, $G^{ij}_{>\delta} = G^{ij}_{<\delta} \equiv G^{ij}_{\delta}$, and we only have to consider one deviation G^{ij}_{δ}. At the same time, the spectral functions stays unperturbed and the out-of-equilibrium part fulfills $G^{ij}_{\rho\delta} = 0$ [264].

5.4.3 Shell structure of the non-equilibrium solution

In order to unravel the shell structure of the non-equilibrium solution in Eq. (5.49), we perform a Wigner transformation (see appendix 2.64) and also write the argument of Eq. (5.49) in Wigner space. We obtain

$$\begin{aligned} G^{ij}_{\delta}(t,Q^0) = \int_0^\infty \frac{\mathrm{d}p_0}{2\pi} \int_0^\infty \mathrm{d}p_0' \Big[& \delta\left(Q_0 - \tfrac{1}{2}(p_0+p_0')\right) e^{-i(p_0-p_0')t} G^{im}_{\mathrm{R}}(p_0)\mathcal{K}^{mn}\, G^{nj}_{\mathrm{A}}(p_0') \\ & + \delta\left(Q_0 - \tfrac{1}{2}(p_0-p_0')\right) e^{-i(p_0+p_0')t} G^{im}_{\mathrm{R}}(p_0)\mathcal{K}^{mn}\, G^{nj}_{\mathrm{A}}(-p_0') \\ & + \delta\left(Q_0 - \tfrac{1}{2}(-p_0+p_0')\right) e^{i(p_0+p_0')t} G^{im}_{\mathrm{R}}(-p_0)\mathcal{K}^{mn}\, G^{nj}_{\mathrm{A}}(p_0') \\ & + \delta\left(Q_0 + \tfrac{1}{2}(p_0+p_0')\right) e^{i(p_0-p_0')t} G^{im}_{\mathrm{R}}(-p_0)\mathcal{K}^{mn}\, G^{nj}_{\mathrm{A}}(-p_0') \Big] , \end{aligned} \tag{5.50}$$

which contains the four shells. Note that in this expression p_0 and p_0' are positive. We see that the contributions in the second and third lines oscillate fast reminiscent of the κ-correlators in Chapter 4. We will discard these terms in the following and concentrate on the $Q_0 > 0$ contribution only:

$$G_\delta^{ij}(t, Q^0 > 0) \approx \int_0^\infty \frac{\mathrm{d}p_0}{2\pi} \int_0^\infty \mathrm{d}p_0' \, \delta\left(Q_0 - \tfrac{1}{2}(p_0 + p_0')\right) \, e^{-i(p_0 - p_0')t} G_{\mathrm{R}}^{im}(p_0) \, \mathcal{K}^{mn} G_{\mathrm{A}}^{nj}(p_0') \,. \quad (5.51)$$

The advantage of the Wigner space representation of the retarded and advanced propagators is their simple explicit structure. They can be inferred from Eq. (5.46) using the translational-invariance of the self-energies:

$$G_{\mathrm{R(A)}}^{ij}(Q_0) = -\frac{\mathrm{adj} D_{\mathrm{R(A)}}^{ij}(Q_0)}{\det D_{\mathrm{R(A)}}(Q_0)} \,, \quad (5.52)$$

where

$$D_{R(A)}^{ij}(Q^0) \equiv Q^2 \delta^{ij} - [\mathsf{M}^2]^{ij} - \Pi_{R(A)}^{ij}(Q_0) \,, \quad (5.53)$$

and $\mathrm{adj} D_{\mathrm{R(A)}}^{ij}$ denotes the adjugate matrix:

$$\mathrm{adj} D_{\mathrm{R}} = \begin{pmatrix} (Q^0)^2 - \mathbf{Q}^2 - M_2^2 - \Pi_{\mathrm{R}}^{22} & \Pi_{\mathrm{R}}^{12} \\ \Pi_{\mathrm{R}}^{21} & (Q^0)^2 - \mathbf{Q}^2 - M_1^2 - \Pi_{\mathrm{R}}^{11} \end{pmatrix} \,, \quad (5.54)$$

which is written in the mass basis. This basis will also be used in the rest of this chapter.

The propagator in Eq. (5.52) has four poles that are given by the zeros of $\det D_{\mathrm{R(A)}}(Q_0)$. The imaginary parts of the retarded (advanced) self-energies are odd under $Q^0 \to -Q^0$, i.e., $\mathrm{Im}\, \Pi_{\mathrm{R(A)}}(Q^0) = -\mathrm{Im}\, \Pi_{\mathrm{R(A)}}(-Q^0)$, such that all poles of $G_{\mathrm{R(A)}}^{ij}(Q^0)$ lie below (above) the real axis at $Q^0 = \Omega_i$ and $Q^0 = -\Omega_i^*$. We write these points as

$$\Omega_i = \omega_i - \frac{i}{2}\Gamma_i \,, \quad (5.55)$$

with the in-medium frequency ω_i and width Γ_i. Having not needed to employ the gradient expansion (Sec. 2.5), the shifts of the poles in the real and imaginary directions of the non-equilibrium propagators have been taken into account (see Refs. [131, 224]).

In the vicinity of the poles with $\mathrm{Re}\, Q^0 > 0$, we can approximate the determinant as [3, 264]

$$\det D_{\mathrm{R}}(q_0) \approx (Q_0^2 - \Omega_1^2)(Q_0^2 - \Omega_2^2) \,. \quad (5.56)$$

Using the residue theorem to evaluate the integrals in Eq. (5.51) approximately, we arrive at the advertised three-shell structure

$$\begin{aligned} G_\delta^{ij}(t, Q^0 > 0) \;\approx\; & \frac{1}{|\Delta\Omega^2|^2} \Bigg[\sum_{i=1}^{2} (2\pi)\delta(Q^0 - \omega_i) e^{-\Gamma_i t} \frac{\mathrm{adj} D_{\mathrm{R}}^{im}(\omega_i)}{2\omega_i} \mathcal{K}^{mn} \frac{\mathrm{adj} D_{\mathrm{A}}^{nj}(\omega_i)}{2\omega_i} \\ & - \; (2\pi)\delta(Q^0 - \bar{\omega}) e^{-i(\omega_1 - \omega_2)t} e^{-\bar{\Gamma} t} \frac{\mathrm{adj} D_{\mathrm{R}}^{im}(\omega_1)}{2\omega_1} \mathcal{K}^{mn} \frac{\mathrm{adj} D_{\mathrm{A}}^{nj}(\omega_2)}{2\omega_2} \\ & - \; (2\pi)\delta(Q^0 - \bar{\omega}) e^{-i(\omega_2 - \omega_1)t} e^{-\bar{\Gamma} t} \frac{\mathrm{adj} D_{\mathrm{R}}^{im}(\omega_2)}{2\omega_2} \mathcal{K}^{mn} \frac{\mathrm{adj} D_{\mathrm{A}}^{nj}(\omega_1)}{2\omega_1} \Bigg] \,, \end{aligned} \quad (5.57)$$

where we have defined the average in-medium decay width and the frequency difference squared

$$\bar{\Gamma} = \frac{1}{2}(\Gamma_1 + \Gamma_2)\,, \tag{5.58}$$

$$\Delta\Omega^2 \equiv \Omega_2^2 - \Omega_1^2\,. \tag{5.59}$$

In Eq. (5.57), the three distinct shells are identified by the frequencies $Q_0 = \omega_i$ $(i = 1, 2)$ and $Q_0 = \bar{\omega} \equiv \frac{1}{2}(\omega_1 + \omega_2)$. The shells with frequencies $Q_0 = \omega_i$ lie at the two poles of the retarded propagator, which can be associated with quasi-particle degrees of freedom. As such, these terms correspond to the contribution from *mixing*. On the other hand, the intermediate shell with frequency $Q_0 = \bar{\omega}$ corresponds to the contribution from *oscillations* and, as we will see, the *interference* between mixing and oscillations. This three-shell structure matches that obtained in Ref. [224], which makes use of a gradient expansion of the KB equations. The authors also find an additional fourth shell with frequency $Q_0 = \omega_1 - \omega_2$ corresponding to the second and third lines that we neglected in Eq. (5.51).

In order to gain a better understanding of the shell structure, we will now expand Eq. (5.57) to first order in the self-energies. As observed in Eq. (5.43), the produced asymmetry only depends on the off-diagonal components of the non-equilibrium part of the propagator. These components read

$$\begin{aligned} G_\delta^{i\not{i}}(t, Q_0 > 0) \approx\; & (2\pi)\delta(q_0 - \omega_i)\,\frac{1}{2\omega_i}\,e^{-\Gamma_i t}\delta n^{ii}(0)\,\Pi_{\rm A}^{i\not{i}}(\omega_i)R_{i\not{i}} \\ -\;\; & (2\pi)\delta(q_0 - \omega_{\not{i}})\,\frac{1}{2\omega_{\not{i}}}\,e^{-\Gamma_{\not{i}} t}\delta n^{\not{i}\not{i}}(0)\,\Pi_{\rm R}^{i\not{i}}(\omega_{\not{i}})R_{i\not{i}} \\ +\;\; & (2\pi)\delta(q_0 - \bar{\omega})\,\frac{1}{(2\omega_i)^{\frac{1}{2}}(2\omega_{\not{i}})^{\frac{1}{2}}}\,e^{-i(\omega_i - \omega_{\not{i}})t}e^{-\bar{\Gamma}t}\Big[\delta n^{i\not{i}}(0)\,\Delta M_{i\not{i}}^2 \\ -\;\; & \delta n^{ii}(0)\Pi_{\rm A}^{i\not{i}}(\omega_{\not{i}}) + \delta n^{\not{i}\not{i}}(0)\Pi_{\rm R}^{i\not{i}}(\omega_i)\Big]R_{i\not{i}}\,. \end{aligned} \tag{5.60}$$

In Eq. (5.60), $\Delta M_{i\not{i}}^2 \equiv M_i^2 - M_{\not{i}}^2$ is the mass splitting.

In addition, we have introduced the following notation for the initial deviation of "particle number densities" from equilibrium:

$$\delta n^{ij}(0) \equiv \frac{\mathcal{K}^{ij}}{(2\omega_i)^{\frac{1}{2}}(2\omega_j)^{\frac{1}{2}}}\,. \tag{5.61}$$

This definition anticipates the definition of the number densities in the interaction picture further below [see Sec. 5.5]. Finally,

$$R_{i\not{i}} \equiv \frac{\Delta M_{i\not{i}}^2}{(\Delta M_{i\not{i}}^2)^2 + (\omega_i\Gamma_i - \omega_{\not{i}}\Gamma_{\not{i}})^2} \tag{5.62}$$

is a regulator, which makes the asymmetry vanish in the degenerate limit. However, special care has to be taken in the doubly-degenerate limit where $M_2 \to M_1$ and $\Gamma_2 \to \Gamma_1$ [108, 261]

The first and second lines of Eq. (5.60) live on the mass shells and are proportional to the off-diagonals of the self-energies. Therefore they describe the standard *mixing* contributions to the asymmetry [105, 107]. On the other hand, the contribution from the third line lies on a third shell. Its contribution to the asymmetry is proportional to the initial coherence $\delta n^{i\not{i}}$ between the two different flavors and the difference of the square of the masses. These features are reminiscent of neutrino flavor conversion, and it will contribute to the generation of asymmetry through oscillations [108–110]. However, off-diagonal number densities will also be created dynamically; a feature that will become apparent once we introduce physical number densities in the interaction picture approach below [see Sec. 5.5]. The fourth line mixes characteristics from mixing and oscillations. These contributions lie on the oscillation shell while at the same time being proportional to the self-energy of the "wrong" shell compared to the mixing contribution. They have a structure similar to those of the i-th and $\not{i}$-th mass shell terms but with opposite signs. Therefore, there is a partial cancellation of these contributions, an effect that becomes important when approaching the resonant regime.

5.4.4 Mixing and oscillation sources of CP asymmetry

It remains for us to study how each term of Eq. (5.60) contributes to the asymmetry. This can be done by substituting Eq. (5.60) into Eq. (5.43). As identified earlier, our choice of the source $\mathcal{K}$ render the non-equilibrium part of the Wightman functions equal $G^{ij}_{>\delta} = G^{ij}_{<\delta} = G^{ij}_{\delta}$. The expression for the produced asymmetry then simplifies to

$$\eta(t) = -2\ \mathrm{Im}\, H_{12} \int_0^t \mathrm{d}x^0 \int_0^t \mathrm{d}y^0 \int \frac{\mathrm{d}^3\mathbf{Q}}{(2\pi)^3}\, G^{12}_{\delta}(x^0, y^0)\Pi_{\rho}(y^0, x^0)\,, \tag{5.63}$$

where we have taken into account that the system is brought out of equilibrium at $t_i = 0$ in the lower limits of the time integration. Next, we trade x^0 and y^0 for the central and relative coordinates $X^0 \equiv \frac{1}{2}(x^0 + y^0)$ and $r^0 \equiv x^0 - y^0$, write $G^{12}_{\delta}(x^0, y^0)$ and $\Pi_{\rho}(y^0, x^0)$ in terms of their Wigner transform and use the Markovian approximation

$$\int_{-2X^0}^{2X^0} \mathrm{d}r^0\ \sin\left(r^0 Q_0\right)\cos\left(r^0 P_0\right) = 0\,, \quad \int_{-2X^0}^{2X^0} \mathrm{d}r^0\ \sin(r^0 Q_0)\sin(r^0 P_0) \approx \pi\,\delta(Q_0 - P_0)\,, \tag{5.64}$$

to integrate out the relative time coordinate. The X^0 integral runs from 0 to the time of observations t. Taking the derivative with respect to this time of observation, we obtain

$$\frac{\mathrm{d}\eta}{\mathrm{d}t} = 4\,\mathrm{Im}\, H_{12} \int \frac{\mathrm{d}^4 Q}{(2\pi)^4}\,\theta(Q^0)\,\mathrm{Im}\left[G^{12}_{\delta}(t, Q_0, \mathbf{Q})\right]\widetilde{\Pi}_{\rho}(Q_0, \mathbf{Q})\,, \tag{5.65}$$

where $\widetilde{\Pi}_{\rho} = L_{\rho}/(8\pi)$ and we have restored the common momentum $\mathbf{Q}$. Substituting the expression for G^{12}_{δ} from Eq. (5.60) and the self-energies from Eq. (5.19) into Eq. (5.65), we obtain the

following expression for the time-derivative of the asymmetry:

$$\begin{aligned}\frac{\mathrm{d}\eta}{\mathrm{d}t} \approx\, & 2\sum_i \int \frac{\mathrm{d}^3\mathbf{Q}}{(2\pi)^3}\,\frac{M_i}{\omega_i} e^{-\Gamma_i t}\,\delta n^{ii}(0,\mathbf{Q})\Gamma_i^{\mathrm{med}}(\omega_i,\mathbf{Q})\epsilon_i^{\mathrm{med}}(\omega_i,\mathbf{Q}) \\ & +\; 2\,\mathrm{Im}\,H_{12}\,\mathrm{Im}\int \frac{\mathrm{d}^3\mathbf{Q}}{(2\pi)^3}\,\frac{1}{(\omega_1\omega_2)^{\frac{1}{2}}}\, e^{-i(\omega_1-\omega_2)t} e^{-\bar{\Gamma}t}\,\widetilde{\Pi}_\rho(\bar{\omega},\mathbf{Q})\Big[\delta n^{12}(0,\mathbf{Q})\,\Delta M_{12}^2 \\ & -\delta n^{11}(0,\mathbf{Q})\Pi_{\mathrm{A}}^{12}(\omega_2,\mathbf{Q}) + \delta n^{22}(0,\mathbf{Q})\Pi_{\mathrm{R}}^{12}(\omega_1,\mathbf{Q})\Big] R_{12}\,. \end{aligned} \tag{5.66}$$

Here, we introduced the in-medium decay probability $\Gamma_i^{\mathrm{med}}(\omega_i,\mathbf{Q}) = \Gamma_i\, L_\rho(\omega_i,\mathbf{Q})$ and in-medium asymmetry

$$\epsilon_i^{\mathrm{med}} = \mathrm{Im}\left(\frac{H_{i\not{\imath}}}{H_{i\not{\imath}}^*}\right)\frac{(M_i^2-M_{\not{\imath}}^2)M_{\not{\imath}}\Gamma_{\not{\imath}}}{(M_i^2-M_{\not{\imath}}^2)^2+(\omega_i\Gamma_i-\omega_{\not{\imath}}\Gamma_{\not{\imath}})^2} L_\rho(\omega_i,\mathbf{Q})\,, \tag{5.67}$$

which are the standard expressions for the mixing contribution [105, 107] augmented by medium corrections through the function L_ρ [253, 254].

As before, the first line of Eq. (5.66) originates from terms of Eq. (5.60) on the quasi-particle mass shells and describes the mixing source of the lepton asymmetry. The second and third lines stem from the oscillation-shell of Eq. (5.60) and contain the oscillation source and the interference between mixing and oscillations. We will now show that this simple structure can be equally obtained in the interaction picture.

5.5 Shell structure in the interaction picture

The interaction picture takes a different approach to non-equilibrium field theory. The central object is the tree-level propagator in vacuum, for which we know the fundamental field excitations. The interaction-picture description introduced in Ref. [118, 126] enables one to work in a perturbative fashion by retaining finite time effects [267, 268] without encountering so-called pinch singularities [114–117] previously thought to spoil such approaches to non-equilibrium field theory. The origin of these singularities can be understood in terms of the Fermi golden rule: for systems in which time-translational invariance is broken, the relevant expansion parameter is the product of the coupling, h, and the time t over which the interactions have been permitted to take place. Thus, for $t > 1/h$, the perturbation series will not converge. To evade these problems, we will resum the perturbation series to directly promote the tree-level propagator to the full (dressed) propagator. We therefore begin with the tree-level Wightman propagators in the next section to build up an expression for the full propagator.

5.5.1 Tree-level Wightman propagator

The tree-level Wightman propagator is given by the expectation value of two fields. This expectation value is most easily evaluated in momentum space, where we know how creation and

annihilation operators act on states. Taking the Fourier transform of the field ψ_{I} [see Eq. (2.20)], we obtain

$$\begin{aligned}\psi_{\mathrm{I}}(p;\tilde{t}_i) &= \int \mathrm{d}^4x e^{ip\cdot x}\psi_{\mathrm{I}}(x;\tilde{t}_i) \\ &=(2\pi)\delta(p^2-M^2)\left[\theta(p_0)a_{\mathrm{I},\mathbf{p}}(\tilde{t}_i;\tilde{t}_i)e^{ip_0\tilde{t}_i}+\theta(-p_0)a^\dagger_{\mathrm{I},-\mathbf{p}}(\tilde{t}_i;\tilde{t}_i)e^{-ip_0\tilde{t}_i}\right].\end{aligned} \tag{5.68}$$

Note that in the interaction picture fields and states are time dependent, and even Fourier transforms depend on the initial time surface. As shown in Ref. [118], we need for consistent calculations in the interaction picture to distinguish between microscopic times, which will be denoted with a tilde, and macroscopic times. In particular, we introduce the initial time $\tilde{t}_i$, where the boundary conditions is fixed and which will be set to zero in accordance with our treatment in the Heisenberg picture, and the final time of our CPT contour $\tilde{t}_f$ which is related to the macroscopic time of observation t via $t=\tilde{t}_f-\tilde{t}_i$. This final time enters because the density matrix in the interaction picture is time dependent and develops a phase when we evaluate it at $\tilde{t}_f$. In the end of our calculations, the dependence on microscopic times will drop out, and the physical limit will be obtained for $\tilde{t}_f = t = X^0$. In particular, the expectation values at the time of observation t read

$$\begin{aligned}\langle a^\dagger_{\mathrm{I},\mathbf{p}'}(\tilde{t}_f;\tilde{t}_i)a_{\mathrm{I},\mathbf{p}}(\tilde{t}_f;\tilde{t}_i)\rangle_t &= 2\sqrt{E(\mathbf{p})E(\mathbf{p}')}f(t,\mathbf{p},\mathbf{p}') \\ \langle a_{\mathrm{I},\mathbf{p}'}(\tilde{t}_f;\tilde{t}_i)a_{\mathrm{I},\mathbf{p}}(\tilde{t}_f;\tilde{t}_i)\rangle_t &= 2\sqrt{E(\mathbf{p})E(\mathbf{p}')}g(t,\mathbf{p},\mathbf{p}').\end{aligned} \tag{5.69}$$

Our lack of knowledge about the state $\rho(t)$ is encoded in the statistical distribution functions f and g. The Wigner transform of $f(t,\mathbf{p},\mathbf{p}')$ can be interpreted as the usual number density. The function g is non-zero when $\rho(t)$ allows for particle number and energy violation. This term is oscillating fast and will be neglected in the following [see Chapter 4].

Using these relations, we obtain an expression for the tree-level Wightman propagator $G^{0,ij}_<$,

$$\begin{aligned}G^{0,ij}_<(p,p',\tilde{t}_f;\tilde{t}_i) &= 2\pi\left[2\,\mathrm{sign}(p_0)p_0\right]^{\frac{1}{2}}\delta(p^2-M_i^2)\,e^{i(p_0-p_0')\tilde{t}_f} \\ &\quad\times\left[\theta(p_0)\theta(p_0')\,n^{ij}(t,\mathbf{p})+\theta(-p_0)\theta(-p_0')\Big(\delta^{ij}+n^{ij*}(t,-\mathbf{p})\Big)\right] \\ &\quad\times 2\pi\left[2\mathrm{sign}(p_0')p_0'\right]^{\frac{1}{2}}\delta(p'^2-M_j^2)(2\pi)^3\delta^{(3)}(\mathbf{p}-\mathbf{p}'),\end{aligned} \tag{5.70}$$

where in the following the superscript 0 denotes tree-level quantities. We differ from the corresponding equation in Ref. [118] by assuming homogeneity, which allows us to write Eq. (5.70) in terms of the number densities $n^{ij}(t,\mathbf{p})=f(t,\mathbf{p},\mathbf{p}')\delta^{(3)}(\mathbf{p}-\mathbf{p}')$ that only depend on one momentum. We also assume isotropy such that the momentum dependence of the number densities reduces to $n^{ij}(t,|\mathbf{p}|)$ and $n^{ij}(t,-\mathbf{p})=n^{ij}(t,\mathbf{p})$.

Note that, in Eq. (5.70) the phase of the exponential seems to have the wrong sign compared to Eq. (5.68). The reason is that the density matrix is evaluated at $\tilde{t}_f$ and the interaction picture operators have to be evolved from $\tilde{t}_i$ until the final time $\tilde{t}_f$. This phase is actually crucial to cancel the phase of a Wigner transform that will be carried out later on (see also Ref. [118]).

5.5.2 *Dressed Wightman propagator*

The free propagator is related to the dressed propagator through the Schwinger-Dyson equation (2.48). With the explicit representation of the free propagator in Eq. (5.70), we can try to find an approximate expression for the dressed propagator. While the Schwinger-Dyson equation in vacuum can be expanded perturbatively, inside a medium finite time effects lead to products of Dirac delta functions with identical arguments, which are not well defined. As we will see now, this problem only arises because of a truncation of the perturbation series.

Inverting the Schwinger-Dyson equation (2.48) by multiplying with the tree-level propagator from the left and with the full propagator from the right, we obtain the Feynman-Dyson series (see Ref.[118] for details)

$$\begin{aligned} G^{ij}_<(p,p',\tilde{t}_f;\tilde{t}_i) = G^{0,ij}_<(p,p',\tilde{t}_f;\tilde{t}_i) \\ - \int \frac{\mathrm{d}^4u}{(2\pi)^4}\frac{\mathrm{d}^4v}{(2\pi)^4}\Big[G^{0,ik}_\mathrm{R}(p,u)\Pi^{kl}_<(u,v,\tilde{t}_f;\tilde{t}_i)G^{lj}_\mathrm{A}(v,p') \\ + G^{0,ik}_\mathrm{R}(p,u)\Pi^{kl}_\mathrm{R}(u,v,\tilde{t}_f;\tilde{t}_i)G^{lj}_<(p,p',\tilde{t}_f;\tilde{t}_i) \\ + G^{0,ik}_<(p,p',\tilde{t}_f;\tilde{t}_i)\Pi^{kl}_\mathrm{A}(u,v,\tilde{t}_f;\tilde{t}_i)G^{lj}_\mathrm{A}(v,p')\Big]\,. \end{aligned} \tag{5.71}$$

Similarly to Sec. 5.4, we restrict ourselves to one-loop self-energies of the real scalar, which are translation invariant when the complex scalar is in thermal equilibrium. To this order, the retarded and advanced propagators become translation invariant as well. This invariance allows us to factor out the corresponding four-momentum conservation

$$G^{ij}_{\mathrm{R(A)}}(p,p',\tilde{t}_f;\tilde{t}_i) = G^{ij}_{\mathrm{R(A)}}(p,t)(2\pi)^4\delta^{(4)}(p-p')\,, \tag{5.72}$$

and similarly for the self-energies

$$\Pi^{ij}(p,p',\tilde{t}_f;\tilde{t}_i) = \Pi^{ij}(p,t)(2\pi)^4\delta^{(4)}(p-p')\,. \tag{5.73}$$

Note that the replacement in Eq. (5.73) is very non-trivial, since the self-energies contain interactions that can spoil the perturbation series when the time integral is extended to infinity, or equivalently when energy conservation is restored (see Ref. [118]). We will not rely on an expansion of the perturbation series but fully resum it. Equation (5.73) is then a good approximation.

With these approximations, the integrals over the intermediate momenta u, v can be performed, and the Feynman-Dyson series (5.71) of the Wightman propagator reduces to

$$\begin{aligned} G^{ij}_<(p,p',\tilde{t}_f;\tilde{t}_i) = G^{0,ij}_<(p,p',\tilde{t}_f;\tilde{t}_i) - G^{0,ik}_\mathrm{R}(p)\Pi^{kl}_<(p)(2\pi)^4\delta^4(p-p')G^{lj}_\mathrm{A}(p') \\ - G^{0,ik}_\mathrm{R}(p)\Pi^{kl}_\mathrm{R}(p)\,G^{lj}_<(p,p',\tilde{t}_f;\tilde{t}_i) - G^{0,ik}_<(p,p',\tilde{t}_f;\tilde{t}_i)\Pi^{kl}_\mathrm{A}(p')G^{lj}_\mathrm{A}(p')\,. \end{aligned} \tag{5.74}$$

The corresponding equations for the retarded and advanced propagators read

$$G^{ij}_{\mathrm{R(A)}}(p) = G^{0,ij}_{\mathrm{R(A)}}(p) - G^{0,ik}_{\mathrm{R(A)}}(p)\Pi^{kl}_{\mathrm{R(A)}}(p)G^{lj}_{R(A)}(p)\,. \tag{5.75}$$

Equation (5.75) only depends on propagators of the same type. Solving this equation iteratively [110], a representation for the resummed retarded and advanced propagators can be obtained by the series

$$G^{ij}_{\mathrm{R(A)}} = \sum_{n=0}^{\infty} \left[(-G^0_{\mathrm{R(A)}}\Pi_{\mathrm{R(A)}})^n G^0_{\mathrm{R(A)}}\right]^{ij} . \tag{5.76}$$

This solution allows us to find in an analogous way [110] an expression for the dressed Wightman propagator. In terms of the tree-level Wightman propagator and the dressed retarded and advanced propagators, we obtain

$$G^{ij}_{<}(p,p',\tilde{t}_f;\tilde{t}_i) = F^{ik}_{\mathrm{R}}(p) G^{0,\,kl}_{<}(p,p',\tilde{t}) F^{lj}_{\mathrm{A}}(p') - G^{ik}_{\mathrm{R}}(p)\,\Pi^{kl}_{<}(p)(2\pi)^4\delta^4(p-p')G^{lj}_{\mathrm{A}}(p')\,, \tag{5.77}$$

where we have defined

$$F^{ij}_{\mathrm{R}} \equiv \sum_{n=0}^{\infty}\left[\Big(-G^0_{\mathrm{R}}\Pi_{\mathrm{R}}\Big)^n\right]^{ij} = -\,G^{ik}_{\mathrm{R}}\,D^{0,\,kj}_{\mathrm{R}} = \delta^{ij} - G^{ik}_{\mathrm{R}}\,\Pi^{kj}_{\mathrm{R}}\,, \tag{5.78a}$$

$$F^{ij}_{\mathrm{A}} \equiv \sum_{n=0}^{\infty}\left[\Big(-\Pi_{\mathrm{A}}G^0_{A}\Big)^n\right]^{ij} = -\,D^{0,\,ik}_{\mathrm{A}}\,G^{kj}_{\mathrm{A}} = \delta^{ij} - \Pi^{ik}_{\mathrm{A}}\,G^{kj}_{\mathrm{A}}\,. \tag{5.78b}$$

The second term on the right-hand side of Eq. (5.77) is an equilibrium piece [cf. (5.47)]. We are, however, interested in the out-of-equilibrium decays that are contained in the first part. In the interaction picture, we have the advantage that we can directly formulate departure from equilibrium in terms of number densities defined via the free propagator (5.70). Writing these number densities $n^{ij}(t,\mathbf{p}) = n^{ij}_{\mathrm{eq}}(t,\mathbf{p}) + \delta n^{ij}(t,\mathbf{p})$ in terms of their equilibrium and out-of-equilibrium pieces, the non-equilibrium part G_δ of Eq. (5.77) for positive energies p_0, p_0' becomes

$$\begin{aligned} G^{ij}_{\delta}(p,p',\tilde{t}_f;\tilde{t}_i)\Big|_{p_0,p_0'>0} &= F^{ik}_{\mathrm{R}}(p)\,2\pi\,(2p_0)^{\frac{1}{2}}\theta(p_0)\delta(p^2-M_k^2)e^{i(p_0-p_0')\tilde{t}_f}\delta n^{kl}(t,\mathbf{p}) \\ &\quad\times(2\pi)^3\delta^{(3)}(\mathbf{p}-\mathbf{p}')\,2\pi\,(2p_0')^{\frac{1}{2}}\theta(p_0)\delta(p'^2-M_l^2)F^{lj}_{\mathrm{A}}(p')\,. \end{aligned} \tag{5.79}$$

5.5.3 Wrong poles of the dressed Wightman propagator

The dressed Wightman propagator in Eq. (5.79) contains Dirac delta functions that seem to give the dominant contribution. The resulting energy modes would then be interpreted as on-shell particles with mass M_i. Unfortunately, on first sight $F_{R,A}$ contain tree-level propagators that diverge on these tree-level poles reminiscent of pinch singularities. We will now show explicitly that these apparent poles do not contribute and the Wigner transform of the dressed Wightman propagator is a well-defined distribution.

After the Wigner transform and in terms of the central and relative momenta (Q_0, q_0), the non-equilibrium part of the dressed Wightman propagator reads

$$\begin{aligned} G^{ij}_{\delta}(Q_0>0,X,\tilde{t}_f;\tilde{t}_i) = \int \mathrm{d}q_0\, e^{-iq_0(X^0-\tilde{t}_f)} F^{ik}_{\mathrm{R}}\,(Q_0+q_0/2)\,2\pi(2E_k)^{\frac{1}{2}}\delta_+\left[(Q_0+q_0/2)^2-E_k^2\right] \\ \times\,\delta n^{kl}(t,\mathbf{Q})2\pi(2E_l)^{\frac{1}{2}}\delta_+\left[(Q_0-q_0/2)^2-E_l^2\right]F^{lj}_{A}(Q_0-q_0/2)\,, \end{aligned} \tag{5.80}$$

where we introduced $\delta_+(p^2 - M_i^2) \equiv \theta(p_0)\delta(p^2 - M_i^2)$, the trivial $\mathbf{Q}$ integral has been performed and the energies are set on shell $E_i^2 = \mathbf{p}^2 + M_i^2$.

We will now proceed by evaluating the q_0 integral as if the only poles were given by the Dirac delta functions. Performing the integration, we obtain

$$G_\delta^{ij}(Q_0 > 0, X, \tilde{t}_f; \tilde{t}_i) = e^{-i\Delta E_{kl}(X_0 - \tilde{t}_f)}(2\pi)\delta(Q_0 - E_{kl})F_{\mathrm{R}}^{ik}(E_k)\frac{\delta n^{kl}(t, \mathbf{Q})}{(2E_k)^{\frac{1}{2}}(2E_l)^{\frac{1}{2}}}F_A^{lj}(E_l)\,, \tag{5.81}$$

where $E_{kl} \equiv (E_k + E_l)/2$. During this integration, we did not encounter pinch singularities despite of the two Dirac deltas in Eq. (5.80). However, we still have to make sure to not have introduced any singularities in $F_{\mathrm{R(A)}}$.

The terms in Eq. (5.78) can be simplified by writing the full retarded propagator in terms of its adjunct [see Eq. (5.52)]

$$F_{\mathrm{R}}^{ik}(E_k) = \delta^{ik} - G_{\mathrm{R}}^{im}(E_k)\,\Pi_{\mathrm{R}}^{mk}(E_k) = \delta^{ik} - \frac{\Delta M_{\not{l}k}^2\delta^{im} + [\mathrm{adj}\,\Pi_{\mathrm{R}}(E_k)]^{im}}{\det D_{\mathrm{R}}(E_k)}\,\Pi_{\mathrm{R}}^{mk}(E_k)\,. \tag{5.82}$$

The determinant in the denominator can be decomposed into

$$\det D_{\mathrm{R}}(E_k) = \Delta M_{\not{k}k}^2\,\Pi_{\mathrm{R}}^{kk}(E_k) + \det\Pi_{\mathrm{R}}(E_k)\,, \tag{5.83}$$

which allows us to write Eq. (5.82) as

$$F_{\mathrm{R}}^{ik}(E_k) = \delta^{ij} - \frac{\Delta M_{\not{l}k}^2\,\Pi_{\mathrm{R}}^{ik}(E_k) + \delta^{ik}\det\Pi_{\mathrm{R}}(E_k)}{\Delta M_{\not{k}k}^2\,\Pi_{\mathrm{R}}^{kk}(E_k) + \det\Pi_{\mathrm{R}}(E_k)}\,, \tag{5.84}$$

by invoking the definition of the adjugate for the self-energies:

$$[\mathrm{adj}\,\Pi_{\mathrm{R}}(E_k)]^{im}\,\Pi_{\mathrm{R}}^{mk}(E_k) = \delta^{ik}\det\Pi_{\mathrm{R}}(E_k)\,. \tag{5.85}$$

It follows that $i = k$ and that $F_{\mathrm{R}}^{ik}(E_k)$ as well as $F_{\mathrm{A}}^{kj}(E_k)$ are identically zero.

By virtue of this calculation, it appears to be the case that the non-equilibrium part of the dressed Wightman propagator is identically zero. This observation clearly yields the wrong result. Moreover, it is in stark contrast to our initial expectation that the poles of the Dirac deltas should actually lead to ill-defined terms and exhibit singularities. It is only by resumming the whole series in Eq. (5.78) that we are safe to evaluate $F_{\mathrm{R(A)}}$ at the on-shell energies. However, at the pole of the delta function, the resummation actually breaks down because we multiply by zero in the form of D_R^0. $F_{R,(A)}$ is therefore meromorphic at the on-shell poles and its product with the Dirac distribution is not defined. We will now show that a careful treatment leads to a resummation of the poles and a shift of the on-shell poles in the complex plane, i.e., the quasi-particle obtains a finite width [131] that can be integrated approximately using the residue theorem. In this way, we will obtain meaningful quantities.

5.5.4 Correct pole structure

The tree-level retarded (advanced) propagator has the form

$$G^{0,ij}_{R(A)}(p) = -\frac{\delta^{ij}}{p^2 - M_i^2 \pm i\,\mathrm{sign}(p_0)\epsilon} = -\mathcal{P}\,\frac{\delta^{ij}}{p^2 - M_i^2} \pm i\pi\delta^{ij}\mathrm{sign}(p_0)\delta(p^2 - M_i^2)\,, \quad (5.86)$$

where we have used the identity

$$\frac{1}{x \pm i\epsilon} = \mathcal{P}\frac{1}{x} \mp i\pi\delta(x)\,, \quad (5.87)$$

in which $\mathcal{P}$ denotes the Cauchy principal value, which is defined to yield zero, when its argument encounters a pole. The identity follows from the limit representations

$$\delta(x) = \lim_{\epsilon\to 0^+} \frac{1}{\pi}\,\frac{\epsilon}{x^2 + \epsilon^2}\,, \qquad \mathcal{P}\,\frac{1}{x} = \lim_{\epsilon\to 0^+} \frac{x}{x^2 + \epsilon^2}\,, \quad (5.88)$$

from which partial fractioning leads to Eq. (5.87). As expected, this representation of the propagator extracts the poles that at finite order of resummation lead to the dreaded pinch singularities that would render this approach useless.

In order to understand how to resum the series of tree-level propagators, we first take a look at the single-flavor case. If we insert the product $\mathrm{sign}(p_0)\,\mathrm{sign}(p_0')$, which is unity in the present calculation, we can write the first half of Eq. (5.77) as

$$\begin{aligned} I_{\mathrm{R}} &\equiv \sum_{n=0}^{\infty} \Big(- G^0_{\mathrm{R}} \cdot \Pi_{\mathrm{R}}\Big)^n (2\pi)\mathrm{sign}(p_0)\delta(p^2 - M^2) \\ &= \sum_{n=0}^{\infty} \left(\frac{\Pi_{\mathrm{R}}}{p^2 - M^2 + i\,\mathrm{sign}(p_0)\epsilon}\right)^n (2\pi)\mathrm{sign}(p_0)\delta(p^2 - M^2)\,. \end{aligned} \quad (5.89)$$

We proceed by writing the Dirac delta in a representation that is consistent with complex integration contours:

$$2\pi\,\mathrm{sign}(p_0)\delta(p^2 - M^2) = \frac{i}{p^2 - M^2 + i\,\mathrm{sign}(p_0)\epsilon} - \frac{i}{p^2 - M^2 - i\,\mathrm{sign}(p_0)\epsilon}\,, \quad (5.90)$$

where the ϵ has the effect of forcing us to choose the right pole. We then decompose this expression in two parts that differ by the sign in front of the ϵ in Eq. (5.90)

$$I_{\mathrm{R}} \equiv I^+_{\mathrm{R}} - I^-_{\mathrm{R}}\,, \quad (5.91)$$

where

$$I^{\pm}_R = i\sum_{n=0}^{\infty} \left(\frac{\Pi_{\mathrm{R}}}{p^2 - M^2 + i\,\mathrm{sign}(p_0)\epsilon}\right)^n \frac{1}{p^2 - M^2 \pm i\,\mathrm{sign}(p_0)\epsilon}\,. \quad (5.92)$$

By employing the distributional identity (see pp. 48–50 of Ref. [269])

$$\left(\frac{1}{x \pm i\epsilon}\right)^n = \mathcal{P}\frac{1}{x^n} \mp \frac{(-1)^{n-1}}{(n-1)!} i\pi\partial^{n-1}[\delta(x)]\,, \quad (5.93)$$

where $\partial^n[\delta(x)]$ is the n-th derivative of the Dirac delta function, we are able to separate the principal values and the Dirac delta functions:

$$I_{\mathrm{R}}^{+} = i\sum_{n=0}^{\infty}\mathcal{P}\left(\frac{1}{p^2-M^2}\right)^{n+1}(\Pi_{\mathrm{R}})^n + \sum_{n=0}^{\infty}\frac{(-\Pi_{\mathrm{R}})^n}{n!}\pi\,\mathrm{sign}(p_0)\partial^n\left[\delta(p^2-M^2)\right]. \tag{5.94}$$

We may also show directly that

$$\mathcal{P}\frac{1}{x^n} = \frac{(-1)^{n-1}}{(n-1)!}\partial^{n-1}\left[\mathcal{P}\,\frac{1}{x}\right], \tag{5.95}$$

where $\partial^n[\mathcal{P}(x)]$ is the n-th derivative of the Cauchy principal value. We obtain

$$I_{\mathrm{R}}^{+} = i\sum_{n=0}^{\infty}\frac{(-\Pi_{\mathrm{R}})^n}{n!}\partial^n\left[\mathcal{P}\frac{1}{p^2-M^2}\right] + \sum_{n=0}^{\infty}\frac{(-\Pi_{\mathrm{R}})^n}{n!}\pi\,\mathrm{sign}(p_0)\partial^n\left[\delta(p^2-M^2)\right]. \tag{5.96}$$

Hence, the infinite sums contain increasing orders of derivatives suppressed by a factorial of n. We may interpret this sum as the Taylor series representation of the translation operator with the shift being Π_{R}. Indeed, if we insert the tree-level propagator from Eq. (5.86), we obtain the resummed retarded propagator:

$$I_{\mathrm{R}}^{+} = i\sum_{n=0}^{\infty}\frac{(-\Pi_{\mathrm{R}})^n}{n!}\frac{\partial^n}{\partial(p^2)^n}\left[-G_{\mathrm{R}}^{0}(p)\right] = -iG_{\mathrm{R}}(p)\,. \tag{5.97}$$

We now turn to I_{R}^{-}. Here, we have

$$I_{\mathrm{R}}^{-} = i\sum_{n=0}^{\infty}\left(\frac{\Pi_{\mathrm{R}}}{p^2-M^2+i\,\mathrm{sign}(p_0)\epsilon}\right)^n\frac{1}{p^2-M^2-i\,\mathrm{sign}(p_0)\epsilon}\,, \tag{5.98}$$

where the difference to Eq. (5.96) lies in the sign in front of ϵ in the last factor. This term contains at finite order of summation the pinch singularities, i.e., the product of poles at $p^2 = M^2 + i\,\mathrm{sign}(p_0)\epsilon$ and $p^2 = M^2 - i\,\mathrm{sign}(p_0)\epsilon$. Moreover, these singularities cannot be resummed straight-forwardly. Note however that the ϵ prescription becomes irrelevant, when we perform the summation over n:

$$\sum_{n=0}^{\infty}\left(\frac{\Pi_{\mathrm{R}}}{p^2-M^2+i\,\mathrm{sign}(p_0)\epsilon}\right)^n = \sum_{n=0}^{\infty}\left(\frac{\Pi_{\mathrm{R}}}{p^2-M^2-i\,\mathrm{sign}(p_0)\epsilon}\right)^n = \frac{p^2-M^2}{p^2-M^2-\Pi_{\mathrm{R}}}\,. \tag{5.99}$$

We may resum this expression as well which yields

$$\begin{aligned} I_{\mathrm{R}}^{-} &= i\sum_{n=0}^{\infty}\left(\frac{\Pi_{\mathrm{R}}}{p^2-M^2-i\,\mathrm{sign}(p_0)\epsilon}\right)^n\frac{1}{p^2-M^2-i\,\mathrm{sign}(p_0)\epsilon} \\ &= i\sum_{n=0}^{\infty}\frac{(-\Pi_{\mathrm{R}})^n}{n!}\,\partial^n\left[\mathcal{P}\,\frac{1}{p^2-M^2}\right] - \sum_{n=0}^{\infty}\frac{(-\Pi_{\mathrm{R}})^n}{n!}\pi\,\mathrm{sign}(p_0)\,\partial^n\left[\delta(p^2-M^2)\right]. \end{aligned} \tag{5.100}$$

We see that $I_{\rm R}^-$ differs from $I_{\rm R}^+$ in Eq. (5.96) by the sign of the second term. The Principal part therefore cancels and we obtain

$$I_{\rm R} = \sum_{n=0}^{\infty} \frac{(-\Pi_{\rm R})^n}{n!} 2\pi\,\mathrm{sign}(p_0)\,\partial^n \left[\delta(p^2 - M^2)\right] . \tag{5.101}$$

Following our earlier interpretation in terms of the translation operator, Eq. (5.101) contains a Dirac delta function shifted into the complex plane, $p^2 - M^2 \to p^2 - M^2 - \Pi_{\rm R}$. Physically this corresponds to having an unstable quasi-particle. In order to make sense of this object and the description of such a particle, we have to analytically continue the delta function consistently. This problem of analytically continuing real eigenvalues of the Hamiltonian to complex eigenvalues has been considered before in, e.g., Refs. [270, 271]. In the spirit of their treatment, we first write

$$2\pi\,\mathrm{sign}(p_0)\delta(p^2 - M^2) \equiv \frac{i}{(p^2 - M^2)^+} - \frac{i}{(p^2 - M^2)^-} , \tag{5.102}$$

replacing the explicit ϵ by an explicit prescription for deforming the contour in the complex plane. The $+$ and $-$ indicate that we are to deform the contour of integration in p_0 away from the real axis such that we pass always above $(+)$ or below $(-)$ the poles at $p^2 - M^2 = 0$. When we now shift the poles into the complex plane, the contour of integration has to be deformed in the same way, and we obtain

$$I_{\rm R} = \frac{i}{(p^2 - M^2 - \Pi_{\rm R})^+} - \frac{i}{(p^2 - M^2 - \Pi_{\rm R})^-} . \tag{5.103}$$

This expression is the complex delta function [270] such that

$$I_{\rm R} = (2\pi)\delta(p^2 - M^2 - \Pi_{\rm R}) , \tag{5.104}$$

which corresponds to the contribution from the poles of $i/(p^2 - M^2 - \Pi_{\rm R})$. The imaginary part of $\Pi_{\rm R}$ is positive corresponding to an unstable particle. Since it is also odd under $p_0 \to -p_0$, all of the poles lie in the lower half of the complex plane. Following Ref. [270], we therefore write the Dirac delta as

$$(2\pi)\delta(p^2 - M^2 - \Pi_{\rm R}) = \frac{if(p_0)}{p^2 - M^2 - \Pi_{\rm R}} , \tag{5.105}$$

where $f(p_0)$ is an analytic function which forces us to close the contour of integration in the lower-half complex plane. Specifically, we require [270]: (i) $f(p_0) \approx 1$ in the vicinity of the poles, (ii) $f(p_0) \approx 0$, effectively, on the real axis far away from the poles, (iii) $f(p_0)$ regular near the real axis, and (iv) $f(p_0)$ vanishing far away in the lower-half complex plane.

Now, that we have seen how to proceed in the one-flavor case, we may proceed analogously for two flavors:

$$I_{\rm R}^i = I_{\rm R}^{ii} + I_{\rm R}^{i\not{i}} \equiv \sum_{n=0}^{\infty} \left[\Big(- G_{\rm R}^0 \cdot \Pi_{\rm R}\Big)^n\right]^{ij} 2\pi\,\mathrm{sign}(p_0)\delta(p^2 - M_j^2) , \tag{5.106}$$

where the propagators and self-energies are now matrices, and a summation over both mass shells is performed. Let us first focus on $I_{\rm R}^{ii}$. Because the tree-level propagator $G_{\rm R}^{0,ii}$ is diagonal in flavor

space, matrix elements at the ii-position can be generated in two ways. The simplest component consists of the product of an arbitrary number of $G_{\rm R}^{0,ii}\Pi_{\rm R}^{ii}$. Another possibility is the insertion of a $\Pi_{\rm R}^{i\not{i}}$ self-energy, which mixes the two flavors, followed by the self-energy $\Pi_{\rm R}^{\not{i}i}$ that leads us back to flavor i. In between these two non-diagonal self-energies, we can insert an arbitrary number of $G_{\rm R}^{0,\not{i}\not{i}}\Pi_{\rm R}^{\not{i}\not{i}}$. These components form a geometric series which we can resum. The $I_{\rm R}^{ii}$ component can, hence, be written as

$$I_{\rm R}^{ii} = \sum_{n=0}^{\infty}\left[\frac{1}{p^2 - M_i^2 + i\,\mathrm{sign}(p_0)\epsilon}\left(\Pi_{\rm R}^{ii} + \frac{\Pi_{\rm R}^{i\not{i}}\Pi_{\rm R}^{\not{i}i}}{p^2 - M_{\not{i}}^2 - \Pi_R^{\not{i}\not{i}}}\right)\right]^n 2\pi\,\mathrm{sign}(p_0)\delta(p^2 - M_i^2)\,. \tag{5.107}$$

The potential pinch singularities in Eq. (5.107) are resummed in the same way as for the single-flavor case, yielding

$$\begin{aligned} I_{\rm R}^{ii} &= \sum_{n=0}^{\infty}\frac{1}{n!}\left(-\Pi_{\rm R}^{ii} - \frac{\Pi_{\rm R}^{i\not{i}}\Pi_{\rm R}^{\not{i}i}}{p^2 - M_{\not{i}}^2 - \Pi_R^{\not{i}\not{i}}}\right)^n 2\pi\,\mathrm{sign}(p_0)\,\partial^n\left[\delta^{(n)}(p^2 - M_i^2)\right] \\ &= (2\pi)\delta(-[G_{\rm R}^{-1}]^{ii})\,, \end{aligned} \tag{5.108}$$

where δ is understood to be the complex delta function, giving the contribution from the poles of

$$i\left[p^2 - M_i^2 - \Pi_{\rm R}^{ii} - \frac{\Pi_{\rm R}^{i\not{i}}\Pi_{\rm R}^{\not{i}i}}{p^2 - M_{\not{i}}^2 - \Pi_{\rm R}^{\not{i}\not{i}}}\right]^{-1}. \tag{5.109}$$

This is equal to the contribution from the poles of

$$i[\mathrm{adj}\,D_{\rm R}]^{ii}/\det D_{\rm R}\,, \tag{5.110}$$

which occur at $\det D_{\rm R} = 0$. Hence, we have

$$I_{\rm R}^{ii} = 2\pi[\mathrm{adj}\,D_{\rm R}]^{ii}\delta(\det D_{\rm R})\,. \tag{5.111}$$

We now continue with the series $I_{\rm R}^{i\not{i}}$. We proceed similarly to before, and note that we need an insertion of $G_R^{0,ii}\Pi_{\rm R}^{i\not{i}}$, to which we can attach on both sides the one-flavor series used before in $I_{\rm R}^{ii}$. We are then able to write

$$\begin{aligned} I_{\rm R}^{i\not{i}} &= \frac{\Pi_{\rm R}^{i\not{i}}}{p^2 - M_i^2 - \Pi_{\rm R}^{ii}} \\ &\quad\times\sum_{n=0}^{\infty}\left[\frac{1}{p^2 - M_{\not{i}}^2 + i\,\mathrm{sign}(p_0)\epsilon}\left(\Pi_{\rm R}^{\not{i}\not{i}} + \frac{\Pi_{\rm R}^{\not{i}i}\Pi_{\rm R}^{i\not{i}}}{p^2 - M_i^2 - \Pi_R^{ii}}\right)\right]^n 2\pi\,\mathrm{sign}(p_0)\delta(p^2 - M_{\not{i}}^2) \\ &= \frac{\Pi_{\rm R}^{i\not{i}}}{p^2 - M_i^2 - \Pi_{\rm R}^{ii}}\sum_{n=0}^{\infty}\frac{1}{n!}\left(-\Pi_{\rm R}^{\not{i}\not{i}} - \frac{\Pi_{\rm R}^{\not{i}i}\Pi_{\rm R}^{i\not{i}}}{p^2 - M_i^2 - \Pi_R^{ii}}\right)^n 2\pi\,\mathrm{sign}(p_0)\,\partial^n\left[\delta^{(n)}(p^2 - M_{\not{i}}^2)\right] \\ &= \frac{\Pi_{\rm R}^{i\not{i}}}{p^2 - M_i^2 - \Pi_{\rm R}^{ii}}(2\pi)\delta(-[G_{\rm R}^{-1}]^{\not{i}\not{i}})\,. \end{aligned} \tag{5.112}$$

Equation (5.112) corresponds to the contribution from the poles of

$$-G_{\rm R}^{i\not{\imath}} = \frac{\Pi_{\rm R}^{i\not{\imath}}}{(p^2 - M_i^2 - \Pi_{\rm R}^{ii})(p^2 - M_{\not{\imath}}^2 - \Pi_{\rm R}^{\not{\imath}\not{\imath}}) - \Pi_{\rm R}^{i\not{\imath}}\Pi_{\rm R}^{\not{\imath}i}} = [\mathrm{adj}\, D_{\rm R}]^{i\not{\imath}}/\det D_{\rm R}\,, \tag{5.113}$$

which again occur at $\det D_{\rm R} = 0$. Hence, we have

$$I_{\rm R}^{i\not{\imath}} = 2\pi[\mathrm{adj}\, D_{\rm R}]^{i\not{\imath}}\delta(\det D_{\rm R})\,. \tag{5.114}$$

Continuing similarly for the remaining components and the corresponding advanced series ($I_A = I_{\rm R}^*$), we obtain the complete expression for the non-equilibrium part of the resummed propagator:

$$\begin{aligned} G_\delta^{ij}(p,p',\tilde{t};\tilde{t}_i)\Big|_{p_0,p_0'>0} &= 2\pi\,(2p_0)^{\frac{1}{2}}\,[\mathrm{adj}\, D_{\rm R}(p)]^{ik}\delta[\det D_{\rm R}(p)] \\ &\times \delta n^{kl}(t,\mathbf{p})(2\pi)^3\delta^3(\mathbf{p}-\mathbf{p}')e^{i(p_0-p_0')\tilde{t}_f} \\ &\times 2\pi\left(2p_0'\right)^{\frac{1}{2}}\,[\mathrm{adj}\, D_{\rm A}(p')]^{lj}\delta[\det D_{\rm A}(p')]\,. \end{aligned} \tag{5.115}$$

In order to compare this result directly with the Heisenberg picture, we make use of the pole approximation in Eq. (5.56). For $p_0 > 0$, the complex delta function $\delta(\det D_{\rm R})$ corresponds to the contribution from the poles at $p_0 = \Omega_i$. Following the prescription in Eq. (5.105), we can express these two occurring poles as

$$(2\pi)\delta\Big(\det D_{\rm R}(p)\Big) \;\approx\; \frac{i}{\Delta\Omega^2}\left[\frac{1}{2\Omega_1}\,\frac{f_1(p_0)}{p_0-\Omega_1} - \frac{1}{2\Omega_2}\,\frac{f_2(p_0)}{p_0-\Omega_2}\right], \tag{5.116}$$

where the relative sign between the poles at Ω_1 and Ω_2 arises from the partial fractioning of $1/(p_0^2-\Omega_1^2)(p_0^2-\Omega_2^2)$, and where the $f_i(p_0)$ satisfy the properties highlighted above.

The pole approach in Eq. (5.56) differs from the Yukawa resummation technique [107] applied in Ref. [110]. However, the approximations in Ref. [110] are only valid in the strong-washout regime, where off-diagonal number densities are generated dynamically and are therefore of higher order in the coupling constants. In the weak-washout regime that is considered in this work, we cannot guarantee the suppression of these off-diagonals.

As in the calculation in the Heisenberg picture 5.4, we now perform a Wigner transform of Eq. (5.115). The physical limit is obtained at equal times, $x^0 = y^0 = \tilde{t}_f = X^0$ such that the exponential in Eq. (5.115) is canceled by the exponential of the Wigner transform, and we obtain the shell structure:

$$G_\delta^{ij}(t,Q_0>0) = (2\pi)\delta(Q_0-\Omega_{ab})\,[\mathrm{adj}\, D_{\rm R}(\Omega_a)]^{ik}\,\frac{g_{ab}\delta n^{kl}(t,\mathbf{Q})}{(2\Omega_a)^{\frac{1}{2}}(2\Omega_b^*)^{\frac{1}{2}}|\Delta\Omega^2|^2}[\mathrm{adj}\, D_{\rm A}(\Omega_b^*)]^{lj}\,, \tag{5.117}$$

where the sum over $a, b = 1, 2$ has been left implicit, $\Omega_{ab} \equiv (\Omega_a + \Omega_b^*)/2$, and g_{ab} is the metric defined in Sec. 2.5. Finally, performing the summations over a and b, we find

$$\begin{aligned} G_\delta^{ij}(t, Q_0 > 0) = {} & (2\pi)\delta(Q_0 - \omega_1)\,[\mathrm{adj}\, D_\mathrm{R}(\Omega_1)]^{ik}\,\frac{\delta n^{kl}(t,\mathbf{Q})}{|2\Omega_1||\Delta\Omega^2|^2}\,[\mathrm{adj}\, D_\mathrm{A}(\Omega_1^*)]^{lj} \\ & + (2\pi)\delta(Q_0 - \omega_2)\,[\mathrm{adj}\, D_\mathrm{R}(\Omega_2)]^{ik}\,\frac{\delta n^{kl}(t,\mathbf{Q})}{|2\Omega_2||\Delta\Omega^2|^2}\,[\mathrm{adj}\, D_\mathrm{A}(\Omega_2^*)]^{lj} \\ & - (2\pi)\delta(Q_0 - \bar\Omega)\,[\mathrm{adj}\, D_\mathrm{R}(\Omega_1)]^{ik}\,\frac{\delta n^{kl}(t,\mathbf{Q})}{(2\Omega_1)^{\frac12}(2\Omega_2^*)^{\frac12}|\Delta\Omega^2|^2}\,[\mathrm{adj}\, D_\mathrm{A}(\Omega_2^*)]^{lj} \\ & - (2\pi)\delta(Q_0 - \bar\Omega^*)\,[\mathrm{adj}\, D_\mathrm{R}(\Omega_2)]^{ik}\,\frac{\delta n^{kl}(t,\mathbf{Q})}{(2\Omega_1^*)^{\frac12}(2\Omega_2)^{\frac12}|\Delta\Omega^2|^2}\,[\mathrm{adj}\, D_\mathrm{A}(\Omega_1^*)]^{lj}\,, \end{aligned} \tag{5.118}$$

where $\bar\Omega = \big(\Omega_1 + \Omega_2^*\big)/2$.

Like in Sec. 5.4, we now expand the interaction-picture result in Eq. (5.118) above to first order in $\Pi_{\mathrm{R(A)}}$. This gives the following result for the off-diagonal components:

$$\begin{aligned} G_\delta^{i\not{i}}(t, Q_0 > 0) \;\approx\; & (2\pi)\delta(Q_0 - \omega_i)\,\frac{1}{2\omega_i}\delta n^{ii}(t)\,\Pi_\mathrm{A}^{i\not{i}}(\omega_i)\,R_{i\not{i}} \\ & - (2\pi)\delta(Q_0 - \omega_{\not{i}})\,\frac{1}{2\omega_{\not{i}}}\delta n^{\not{i}\not{i}}(t)\,\Pi_\mathrm{R}^{i\not{i}}(\omega_{\not{i}})\,R_{i\not{i}} \\ & + (2\pi)\delta(Q_0 - \bar\omega)\,\frac{1}{(2\omega_i)^{\frac12}(2\omega_{\not{i}})^{\frac12}}\Big[\delta n^{i\not{i}}(t)\,\Delta M^2_{i\not{i}} \\ & \quad - \delta n^{ii}(t)\,\Pi_\mathrm{A}^{i\not{i}}(\omega_{\not{i}}) + \delta n^{\not{i}\not{i}}(t)\,\Pi_\mathrm{R}^{i\not{i}}(\omega_i)\Big]R_{i\not{i}}\,. \end{aligned} \tag{5.119}$$

We are now in a position to find an explicit expression for the asymmetry. Inserting Eq. (5.119) into time-derivative of the asymmetry, we obtain

$$\begin{aligned} \frac{\mathrm{d}\eta}{\mathrm{d}t} \approx {} & 2\sum_i \int \frac{\mathrm{d}^3\mathbf{Q}}{(2\pi)^3}\,\frac{M_i}{\omega_i}\,\delta n^{ii}(t,\mathbf{Q})\,\Gamma_i^\mathrm{med}(\omega_i,\mathbf{Q})\,\epsilon_i^\mathrm{med}(\omega_i,\mathbf{Q}) \\ & + 2\,\mathrm{Im}\,H_{12}\,\mathrm{Im}\int \frac{\mathrm{d}^3\mathbf{Q}}{(2\pi)^3}\,\frac{\widetilde\Pi_\rho(\bar\omega,\mathbf{Q})}{(\omega_1\omega_2)^{\frac12}}\Big[\delta n^{12}(t,\mathbf{Q})\,\Delta M^2_{12} \\ & \quad - \delta n^{11}(t,\mathbf{Q})\Pi_\mathrm{A}^{12}(\omega_2,\mathbf{Q}) + \delta n^{22}(t,\mathbf{Q})\Pi_\mathrm{R}^{12}(\omega_1,\mathbf{Q})\Big]R_{12}\,. \end{aligned} \tag{5.120}$$

This closely resembles the final result for the asymmetry in Eq. (5.66) in the Heisenberg picture. Especially, mixing, oscillations and interference can be uniquely identified. The oscillation contributions lies on the middle shell and is proportional to the time-dependent coherence δn^{12}, while the interference is proportional to the time-dependent number densities. This time dependence is the key difference to Eq. (5.66), which was written in terms of the initial conditions at $t = 0$. We would like to stress that the interpretation of n^{ij} or equivalently $\mathcal{K}^{ij}$ in Eq. (5.66) is not immediately clear. In the interaction picture, however, δn^{ij} can be directly interpreted as the number density of free particles, which count excitations with energy E_i.

To convince ourselves that our interpretation of $\mathcal{K}$ is correct, and that also the phases of the result in Eq. (5.66) can be obtained, we have to solve for the time-dependence of the number densities $n^{ij}(t)$ in the interaction picture and write it in term of the initial conditions. This calculation will be done in Sec. 5.5.5.

Before fully establishing the equivalence of the two approaches, we would like to comment on the role of the interference in Eq. (5.120). We expand all but the regulator R_{12} and the Dirac delta functions in Eq. (5.119) around $\Delta\omega_{i\ell} = \omega_i - \omega_\ell = 0$ in $\Delta M^2_{i\ell}$. At zeroth order, we find the pure oscillation contribution

$$G^{i\ell}_\delta(t, Q_0 > 0) \supset (2\pi)\delta(Q_0 - \bar{\omega})\frac{1}{2\bar{\omega}}\delta n^{i\ell}(t)\Delta M^2_{i\ell}R_{i\ell}\,. \tag{5.121}$$

The mixing contributions have canceled which confirms the destructive nature of the interference. This interference guarantees that the asymmetry vanishes in the degenerate regime $\Delta M^2_{i\ell} \to 0$, as it should.

In Eq. (5.121), mixing is absent and only oscillations persist. As shown in Ref. [110], on-shell (Kadanoff-Baym) ansaetze like those applied in Sec. 5.5.3 would replicate only oscillations and no mixing in accordance with this result. One could therefore be tempted to argue that these on-shell ansaetze are sufficient in the quasi-degenerate regime and that including terms from mixing *and* oscillations like in Refs. [108–110] would lead to double-counting in the asymmetry. However, this is not the case, as we can observe by continuing to the next order in the expansion. It reads

$$\begin{aligned} G^{i\ell}_\delta(t, Q_0) \approx\; & (2\pi)\delta(Q_0 - \bar{\omega})\frac{1}{2\bar{\omega}}\delta n^{i\ell}(t)\Delta M^2_{i\ell}R_{i\ell} \\ & - (2\pi)\delta(Q_0 - \bar{\omega})\frac{1}{2\bar{\omega}}\left[\delta n^{ii}(t)\frac{\Pi^{i\ell}_{\mathrm{A}}(\bar{\omega})}{4\bar{\omega}^2} + \delta n^{\ell\ell}(t)\frac{\Pi^{i\ell}_{\mathrm{R}}(\bar{\omega})}{4\bar{\omega}^2}\right]\Delta M^2_{i\ell}R_{i\ell}\,, \end{aligned} \tag{5.122}$$

where the mixing terms are present but are now suppressed by an additional factor of $\Delta M^2_{i\ell}$. Here, we have neglected terms proportional to the derivative of the self-energy $\Pi^{i\ell\prime}(\bar{\omega})$, which contribute sub-dominantly to the asymmetry under the assumption that the self-energies are slowly varying functions of Q_0 for $Q_0 \sim \bar{\omega}$. The same assumption underlies the pole approximations in Eqs. (5.56), which have been verified numerically [264] to yield decent approximations.

The asymmetry now takes the form

$$\begin{aligned} \frac{\mathrm{d}\eta}{\mathrm{d}t} \approx\; & 2\sum_i \int \frac{\mathrm{d}^3\mathbf{Q}}{(2\pi)^3}\,\frac{M_i}{\bar{\omega}}\delta n^{ii}(t, \mathbf{Q})\Gamma^{\mathrm{med}}_i(\bar{\omega}, \mathbf{Q})\tilde{\epsilon}^{\mathrm{med}}_i(\bar{\omega}, \mathbf{Q}) \\ & +\; 2\,\mathrm{Im}\,H_{12}\int \frac{\mathrm{d}^3\mathbf{Q}}{(2\pi)^3}\,\frac{\widetilde{\Pi}_\rho(\bar{\omega}, \mathbf{Q})}{\bar{\omega}}\;\mathrm{Im}\,\delta n^{12}(t, \mathbf{Q})\,\Delta M^2_{12}R_{12}\,, \end{aligned} \tag{5.123}$$

where the usual *CP*-violating parameter $\epsilon^{\mathrm{med}}_i(\bar{\omega}, \mathbf{Q})$ has been modified:

$$\tilde{\epsilon}^{\mathrm{med}}_i(\bar{\omega}, \mathbf{Q}) = \frac{\Delta M^2_{\ell i}}{\bar{\omega}^2}\epsilon^{\mathrm{med}}_i(\bar{\omega}, \mathbf{Q})\,. \tag{5.124}$$

We see that to first order in $\Delta M_{ji}^2/\bar{\omega}^2$ both mixing and oscillation contributions persist in the single-shell approximation in agreement with the results of Refs. [108–110]. In contrast to Eq. (5.120), the two shells now contribute with opposite sign, and the mixing contribution is suppressed for similar mass eigenvalues and initial conditions of the two flavors. Nevertheless, the pre-factors of the oscillation and the mixing contributions possess exactly the same parametric dependence on the Yukawa couplings and mass splittings: $\sim \Delta M_{12}^2 R_{12}$, which is of order unity in the weakly-resonant regime $\Gamma_i \ll \Delta M \ll \bar{M}$. The relation between the mixing and oscillations therefore depends on the configuration of the initial conditions as well.

5.5.5 *Explicit time dependence of the number densities*

We now return to Eq. (5.119) with the aim of finding the explicit solution for the deviations from equilibrium $\delta n^{ij}(t)$. We will make use of the shell-structure derived before for the Wightman propagators. Note that a similar result could also be obtained in the single-shell or density matrix approximation [see appendix C].

The dressed number densities are related to the negative frequency Wightman propagator through [see Sec. 2.5.3]

$$n_{\rm dr}^{ij}(t) = \int \frac{{\rm d}Q^0}{\pi}\, Q^0 G_<^{ij}\,. \tag{5.125}$$

Using the Kadanoff-Baym equation for the Wightman propagator and taking only the non-equilibrium part, the transport equation for $\delta n_{\rm dr}(t)$ in the interaction picture reads [110]

$$\begin{aligned}\frac{{\rm d}\delta n_{\rm dr}^{ij}(t)}{{\rm d}t} = &\int \frac{{\rm d}p_0}{2\pi}\int \frac{{\rm d}p_0'}{2\pi}\, e^{-i(p_0-p_0')\tilde{t}_f}\theta(p_0)\theta(p_0') \\ &\times \left(-i\Big[\mathsf{M}^2+\Pi_{\rm h}, G_\delta\Big]_\star^{ij} - \tfrac{1}{2}\Big\{\Pi_<, G_\delta\Big\}_\star^{ij} + \tfrac{1}{2}\Big\{\Pi_>, G_\delta\Big\}_\star^{ij}\right).\end{aligned} \tag{5.126}$$

where the commutators and anti-commutators appearing in Eq. (5.126) are defined as

$$[A,B]_\star \equiv \int {\rm d}k\Big(A(p,k)\cdot B(k,p') - B(p,k)\cdot A(k,p')\Big)\,, \tag{5.127a}$$

$$\{A,B\}_\star \equiv \int {\rm d}k\Big(A(p,k)\cdot B(k,p') + B(p,k)\cdot A(k,p')\Big)\,. \tag{5.127b}$$

In Eq. (5.126), the first term on the right-hand side corresponds to oscillations due to mismatches of the thermal mass squared $\mathsf{M}^2+\Pi_{\rm h}$. The other terms correspond to production and annihilation through scattering.

From this transport equation, we would like to find the time-evolution of the free number densities that go into Eq. (5.120). These number densities can be obtained, if we only retain the leading order terms in the couplings h_i. For the diagonal elements of $\delta n^{ij}(t)$, it suffices to substitute G_δ by its tree-level G_δ^0 expression (5.80) with $F_{\rm R(A)}=1$, since the off-diagonals of the Wightman propagator are of higher order in the self-energies. We obtain for the diagonal elements

$$\frac{{\rm d}\delta n^{ii}}{{\rm d}t} = -\Gamma_i \delta n^{ii}\,, \tag{5.128}$$

with solution

$$\delta n^{ii}(t) = e^{-\Gamma_i t}\delta n^{ii}(0)\,. \tag{5.129}$$

For the off-diagonals $\delta n^{i\not{\imath}}(t)$, the tree-level propagator G^0_δ suffices for terms that are already proportional to self-energies. These terms are

$$\begin{aligned}\frac{\mathrm{d}\delta n^{i\not{\imath}}(t)}{\mathrm{d}t} \supset \int \frac{\mathrm{d}p_0}{2\pi} \int \frac{\mathrm{d}p_0'}{2\pi}\, e^{-i(p_0-p_0')\tilde{t}}\theta(p_0)\theta(p_0') \\ \times \left(-i\Big[\Pi_\mathrm{h}, G^0_\delta\Big]^{i\not{\imath}}_\star - \tfrac{1}{2}\Big\{\Pi_<, G^0_\delta\Big\}^{i\not{\imath}}_\star + \tfrac{1}{2}\Big\{\Pi_>, G^0_\delta\Big\}^{i\not{\imath}}_\star\right)\,.\end{aligned} \tag{5.130}$$

On the other hand, the difference of the two mass eigenvalues plays a role when off-diagonal elements of the dressed propagator G_δ are taken into account:

$$\frac{\mathrm{d}\delta n^{i\not{\imath}}(t)}{\mathrm{d}t} \supset -i \int \frac{\mathrm{d}p_0}{2\pi} \int \frac{\mathrm{d}p_0'}{2\pi}\, e^{-i(p_0-p_0')\tilde{t}}\theta(p_0)\theta(p_0') \Big[\mathsf{M}^2, G_\delta\Big]^{i\not{\imath}}_\star\,, \tag{5.131}$$

The time-evolution of the off-diagonal free number densities is now

$$\frac{\mathrm{d}\delta n^{i\not{\imath}}}{\mathrm{d}t} = -i(\omega_i-\omega_{\not{\imath}})\delta n^{i\not{\imath}} - \bar{\Gamma}\delta n^{i\not{\imath}} - \frac{i}{2\bar{\omega}}\Big(\Pi^{i\not{\imath}}_\mathrm{R}(\omega_i)\delta n^{\not{\imath}\not{\imath}} - \Pi^{i\not{\imath}}_\mathrm{A}(\omega_{\not{\imath}})\delta n^{ii}\Big)\,, \tag{5.132}$$

in which we have used the approximation $\omega_i\omega_{\not{\imath}} \approx \bar{\omega}^2$.

Note that the origin of the order $\Pi_{\mathrm{R(A)}}$ terms in Eq. (5.132) is non-trivial. Would we retain only the terms from the diagonal elements of the tree-level propagator G^0_δ in Eq. (5.130), we would obtain

$$\frac{\mathrm{d}\delta n^{i\not{\imath}}}{\mathrm{d}t} \supset -\frac{i}{2\bar{\omega}}\delta n^{\not{\imath}\not{\imath}}\,\Pi^{i\not{\imath}}_\mathrm{R}(\omega_{\not{\imath}}) + \frac{i}{2\bar{\omega}}\delta n^{ii}\,\Pi^{i\not{\imath}}_A(\omega_i)\,. \tag{5.133}$$

When compared to Eq. (5.132), we see that the arguments of the self-energies are permuted. On the other hand, the off-diagonal element of the dressed propagator G_δ used in the commutator in Eq. (5.131) yields the following terms

$$\frac{\mathrm{d}\delta n^{i\not{\imath}}}{\mathrm{d}t} \supset -\frac{i}{2\bar{\omega}}\delta n^{ii}\left[\Pi^{i\not{\imath}}_\mathrm{A}(\omega_i) - \Pi^{i\not{\imath}}_\mathrm{A}(\omega_{\not{\imath}})\right] + \frac{i}{2\bar{\omega}}\delta n^{\not{\imath}\not{\imath}}\left[\Pi^{i\not{\imath}}_\mathrm{R}(\omega_{\not{\imath}}) - \Pi^{i\not{\imath}}_\mathrm{R}(\omega_i)\right]\,, \tag{5.134}$$

which correspond to mixing and interference of the two mixing shells. When combined with Eq. (5.133) the argument of the self-energies is swapped to yield the expression in Eq. (5.132).

The leading-order solutions to the off-diagonal equations in Eq. (5.132) have the form

$$\delta n^{i\not{\imath}}(t) = e^{-i(\omega_i-\omega_{\not{\imath}})t}e^{-\bar{\Gamma}t}\delta n^{i\not{\imath}}_0(0) + \frac{\Pi^{i\not{\imath}}_\mathrm{A}(\omega_{\not{\imath}})}{\Delta M^2_{i\not{\imath}}}\,e^{-\Gamma_i t}\delta n^{ii}(0) - \frac{\Pi^{i\not{\imath}}_\mathrm{R}(\omega_i)}{\Delta M^2_{i\not{\imath}}}\,e^{-\Gamma_{\not{\imath}} t}\delta n^{\not{\imath}\not{\imath}}(0)\,, \tag{5.135}$$

where $\delta n^{i\not{\imath}}_0$ is the initial condition when back-reactions from the diagonal number densities are neglected. If we define the full initial condition for the off-diagonals $\delta n^{i\not{\imath}}(0)$

$$\delta n^{i\not{\imath}}(0) = \delta n^{i\not{\imath}}_0(0) + \frac{\Pi^{i\not{\imath}}_\mathrm{A}(\omega_{\not{\imath}})}{\Delta M^2_{i\not{\imath}}}\delta n^{ii}(0) - \frac{\Pi^{i\not{\imath}}_\mathrm{R}(\omega_i)}{\Delta M^2_{i\not{\imath}}}\delta n^{\not{\imath}\not{\imath}}(0)\,. \tag{5.136}$$

and substitute $\delta n_0^{ij}(0)$ in Eq. (5.135), we obtain the final form of the solution

$$\begin{aligned}\delta n^{i\not{i}}(t) = {} & e^{-i(\omega_i-\omega_{\not{i}})t}e^{-\bar{\Gamma}t}\delta n^{i\not{i}}(0) \\ & + \frac{\Pi_{\mathrm{A}}^{i\not{i}}(\omega_{\not{i}})}{\Delta M_{i\not{i}}^2}\left(e^{-\Gamma_i t} - e^{-i(\omega_i-\omega_{\not{i}})t}e^{-\bar{\Gamma}t}\right)\delta n^{ii}(0) \\ & - \frac{\Pi_{\mathrm{R}}^{i\not{i}}(\omega_i)}{\Delta M_{i\not{i}}^2}\left(e^{-\Gamma_{\not{i}} t} - e^{-i(\omega_i-\omega_{\not{i}})t}e^{-\bar{\Gamma}t}\right)\delta n^{\not{i}\not{i}}(0)\,. \end{aligned} \tag{5.137}$$

Substituting Eq. (5.137) into Eq. (5.119) for the off-diagonal components of G_δ, we obtain *precisely* the asymmetry in the Heisenberg picture Eq. (5.60). This is one of the main result of this chapter. The agreement of the results in the Heisenberg and interaction approaches shows that both approaches are a viable way to obtain the correct asymmetry. This is not immediately obvious because of the usual problems of a perturbative expansion in non-equilibrium systems, and one has to carefully undo the damage that is done by starting from free particles in order to obtain the correct result. Nevertheless, both approaches have their advantages and this result shows that they might complement each other.

5.6 Comparison with the effective Yukawa approach

Having established the equivalence of the results in the Heisenberg and interaction pictures, we will now compare these results with the effective Yukawa approach [106, 107], which has also been applied in Ref. [108–110] to account for the mixing contribution. The effect of oscillations on the other hand is accounted for by flavor coherences, i.e., non-vanishing off-diagonal elements of the number density. We will show that this method does not correctly treat the interference contribution and therefore becomes inaccurate in the quasi-degenerate regime.

Let us start by briefly reviewing the derivation of these effective Yukawa couplings for the present toy model, following Ref. [254]. The real scalars are unstable, and hence they cannot be written as non-zero asymptotic in or out states of S-matrix elements. Unitarity then requires us to define these particles via scattering of the stable particles b and b^* with intermediate real scalars [272].

The amplitude of the s-channel two-body scattering process $bb \to b^*b^*$ can be expressed as [107]

$$\mathcal{M}_{bb\to b^*b^*} = \sum_{i,j}\Gamma_i^A G^{ij}(s)\Gamma_j^B\,, \tag{5.138}$$

where Γ_i^A and Γ_j^B represent the vertices $\psi_i bb$ and $\psi_j b^*b^*$, including the wave functions of the initial and final complex scalars, and G^{ij} are the (time-ordered) Feynman propagators. In analogy to scattering theory, all these expressions are functions of the center of mass energy $\sqrt{s}$. The two poles in the determinant of the inverse propagator in terms of s are

$$s_i \simeq M_i^2 - iM_i\Gamma_i\,, \tag{5.139}$$

where $\Gamma_i = H_{ii}/(16\pi M_i)$ is the tree-level decay width of ψ_i. Expanding G^{ij} around the poles and using the symmetry of the time-ordered self-energies $\Pi_{\mathrm{T}}^{i\not{i}} = \Pi_{\mathrm{T}}^{\not{i}i}$, we rewrite Eq. (5.138) in analogy to Ref. [107]

$$\mathcal{M}_{bb\to b^*b^*} \simeq \sum_i V_i^A(s) \frac{1}{s - s_i} V_i^B(s)\,, \tag{5.140}$$

where the non-trivial parts of the propagator are being absorbed into the vertices:

$$V_i^{A(B)}(s) \equiv \Gamma_i^{A(B)} - \frac{[G^{-1}]^{i\not{i}}(s)}{[G^{-1}]^{\not{i}\not{i}}(s)} \Gamma_{\not{i}}^{A(B)} = \Gamma_i^{A(B)} + \frac{\Pi_{\mathrm{T}}^{i\not{i}}(s)}{s - M_{\not{i}}^2 - \Pi_{\mathrm{T}}^{\not{i}\not{i}}(s)} \Gamma_{\not{i}}^{A(B)}\,. \tag{5.141}$$

Equation (5.141) can be used to define effective one-loop Yukawa couplings $\tilde{h}_i^{(c)}$. Taking into account that the couplings in the vertices $\psi_i bb$ and $\psi_i b^* b^*$ differ by complex conjugation, we obtain

$$\tilde{h}_i \equiv h_i + \frac{\Pi_{\mathrm{T}}^{i\not{i}}(s)}{s - M_{\not{i}}^2 - \Pi_{\mathrm{T}}^{\not{i}\not{i}}(s)} h_{\not{i}}\,, \tag{5.142a}$$

$$\tilde{h}_i^{c*} \equiv h_i^* + \frac{\Pi_{\mathrm{T}}^{i\not{i}}(s)}{s - M_{\not{i}}^2 - \Pi_{\mathrm{T}}^{\not{i}\not{i}}(s)} h_{\not{i}}^*\,. \tag{5.142b}$$

Note that these two couplings are not complex conjugates of each other due to the imaginary part of the self-energies. The subscript i indicates that these couplings are to be evaluated on the mass shell of the i-th quasi-particle [107]. In vacuum and for positive energies, the time-ordered self-energies equal the retarded self-energies shown in Eq. (5.21). Using the tree-level relation $H_{ii} = 16\pi M_i \Gamma_i$, we obtain

$$\Pi_{\mathrm{T}}^{i\not{i}}(M_i^2) = -i \frac{\mathrm{Re}\, H^{i\not{i}}}{16\pi}\,, \tag{5.143a}$$

$$\Pi_{\mathrm{T}}^{\not{i}\not{i}}(M_i^2) = M^{\not{i}}\Gamma^{\not{i}} \left[\frac{1}{\pi} \ln\left(\frac{M_i^2}{\mu^2}\right) - i\right]\,. \tag{5.143b}$$

Note that if we choose $\mu = M_i$, the real part of Eq. (5.143b) vanishes, and it only grows logarithmically if we evaluate it on the second mass shell. For simplicity, we keep only the imaginary part of Eq. (5.143b), i.e. use $\Pi_{\mathrm{T}}^{\not{i}\not{i}}(M_i^2) \approx -iM^{\not{i}}\Gamma^{\not{i}}$. In this way we arrive at the effective Yukawa couplings

$$\tilde{h}_i^{(c)} = h_i \left[1 - (+) i\, \frac{H_{\not{i}\not{i}}}{32\pi} \left(1 + \frac{H_{i\not{i}}^*}{H_{i\not{i}}}\right) \frac{1}{\Delta M_{i\not{i}}^2 + (-) i M_{\not{i}} \Gamma_{\not{i}}}\right]. \tag{5.144}$$

The vacuum self-energy contribution to the asymmetry in terms of decay widths takes the form

$$\epsilon_i^{\mathrm{vac}} \equiv \frac{\Gamma_{\psi_i \to bb} - \Gamma_{\psi_i \to b^* b^*}}{\Gamma_{\psi_i \to bb} + \Gamma_{\psi_i \to b^* b^*}}\,, \tag{5.145}$$

which can be evaluated directly within this method to give

$$\epsilon_i^{\rm vac} = {\rm Im}\left(\frac{H_{i\not{i}}}{H^*_{i\not{i}}}\right)\frac{(M_i^2 - M_{\not{i}}^2)M_{\not{i}}\Gamma_{\not{i}}}{(M_i^2 - M_{\not{i}}^2)^2 + (M_{\not{i}}\Gamma_{\not{i}})^2}\,, \tag{5.146}$$

which has been derived before in medium in Eq. (5.67).

Following Ref. [110], the time derivative of the asymmetry can be written in terms of the effective Yukawa couplings as

$$\frac{{\rm d}\eta}{{\rm d}t} \approx \int \frac{{\rm d}^4Q}{(2\pi)^4}\,\theta(Q_0)\left[\tilde{h}_i\tilde{h}_j^* G_\delta^{0,\,ij}(t,Q) - \tilde{h}_i^{c*}\tilde{h}_j^c G_\delta^{0,\,ij}(t,Q)\right]\widetilde{\Pi}_\rho(Q)\,, \tag{5.147}$$

where $G_\delta^{0,\,ij}(t,Q)$ is the tree-level Green's function. In the single-shell density matrix approximation, this propagator reads

$$G_\delta^{0,\,ij}(t,Q_0>0) = (2\pi)\delta(Q_0-\bar{\omega})\frac{1}{2\bar{\omega}}\delta n^{ij}(t,\mathbf{Q})\,. \tag{5.148}$$

The time derivative of the asymmetry in this effective Yukawa approach is then found to be

$$\begin{aligned}\frac{{\rm d}\eta}{{\rm d}t} \approx\; & 2\sum_i \int \frac{{\rm d}^3\mathbf{Q}}{(2\pi)^3}\frac{M_i}{\bar{\omega}}\delta n^{ii}(t,\mathbf{Q})\Gamma_i(\bar{\omega},\mathbf{Q})\epsilon_i^{\rm vac}(\bar{\omega},\mathbf{Q}) \\ & +\; 2\,{\rm Im}\,H_{12}\int\frac{{\rm d}^3\mathbf{Q}}{(2\pi)^3}\frac{\widetilde{\Pi}_\rho(\bar{\omega},\mathbf{Q})}{\bar{\omega}}\,{\rm Im}\,\delta n^{12}(t,\mathbf{Q})\,.\end{aligned} \tag{5.149}$$

The oscillation contribution in this approach resembles the expressions derived in Eqs. (5.66) and (5.120) but lacks a factor $\Delta M_{12}^2 R_{12}$, which is of order unity in the weakly-resonant regime. Similarly, the mixing contribution in the effective Yukawa approach equals the pure mixing terms in Eqs. (5.66) and (5.120) but fails to correct the produced asymmetry for the interference between mixing and oscillations. Hence, the approach of Refs. [108–110], although accounting for both mixing and oscillations, seems not to yield the correct result when the degenerate-mass limit is approached. However, as we mentioned before, one has to be careful in comparing these results because Refs. [108–110] used approximations that are only valid in the strong-washout regime (see appendix A.1 of Ref. [110]). For future work it would be interesting to study the interference effects in the strong-washout regime as well.

5.7 Phenomenological implications

We now proceed to evaluate the asymmetry numerically. We keep track of the different contributions from the shells in order to compare their relative size. This will also allow us to study the accuracy of different approximation schemes, namely the Boltzmann and the density matrix approaches.

We evaluate the asymmetry directly without an expansion in self-energies. By substituting the non-equilibrium Wightman propagator in Eq. (5.57) into Eq. (5.65), the total asymmetry takes the form

$$\begin{aligned}\eta = 4\,\mathrm{Im}\,H_{12}\int_0^\infty \mathrm{d}t\int\frac{\mathrm{d}^3\mathbf{Q}}{(2\pi)^3}\,\frac{g_{ab}}{|\Delta\Omega^2|^2}\,\widetilde{\Pi}_\rho\left[(\omega_a+\omega_b)/2,\mathbf{Q}\right] \\ \times\,\mathrm{Im}\left[\frac{[\mathrm{adj}D_\mathrm{R}(\omega_a,\mathbf{Q})]^{1m}}{2\Omega_a}\mathcal{K}^{mn}(\mathbf{Q})\,\frac{[\mathrm{adj}D_\mathrm{A}(\omega_b,\mathbf{Q})]^{n2}}{2\Omega_b^*}e^{-i(\Omega_a-\Omega_b^*)t}\right],\end{aligned} \tag{5.150}$$

where we have restored the common momentum $\mathbf{Q}$ and performed the integral over Q_0. The contributions from mixing, oscillations and inference are then separated by their shells and by making use of Eq. (5.137). Although this separation was derived for $\Pi_{\mathrm{R(A)}}/(\Delta M^2) \ll 1$, we will also attempt to apply this separation for smaller mass differences and obtain good results.

For our numerical examples below, we have to choose values for the free parameters and the initial conditions. Following Ref. [264], we choose the temperature T and the mass of the lighter scalar M_1 to equal the $\overline{\mathrm{MS}}$ renormalization scale, $T=\mu$ and $M_1=\mu$. The second mass parameter M_2 can be expressed in terms of the degeneracy parameter

$$R \equiv \frac{M_2^2-M_1^2}{M_1\Gamma_1+M_2\Gamma_2}\,. \tag{5.151}$$

This definition is motivated in Ref. [261], where it is shown that $R=1$ corresponds to a maximal enhancement of the asymmetry. We will vary this parameter to study how the total asymmetry and its various contributions behave.

Besides the masses, we also have to choose the coupling constants. The mixing contributions are proportional to $\mathrm{Im}\,H_{12}\,\mathrm{Re}\,H_{12}$ such that they vanish if the Lagrangian is *C*-symmetric (5.2). For the oscillation contribution we only observe a proportionality to $\mathrm{Im}\,H_{12}$, but we will show below that the dependency on $\mathrm{Re}\,H_{12}$ is hidden in C-symmetric initial conditions. For non-trivial dynamics we see that a relative phase between h_1 and h_2 has to be chosen such that $\mathrm{Re}\,H_{12}\neq 0$ and $\mathrm{Im}\,H_{12}\neq 0$. We will show numerical results for the following combinations of couplings

$$\begin{aligned}&\text{Set 1}: \quad h_1 = 0.5\mu, \quad h_2 = 0.8\,e^{i\frac{2}{3}}\mu\,,\\ &\text{Set 2}: \quad h_1 = 1.0\mu, \quad h_2 = 1.6\,e^{i\frac{2}{3}}\mu\,.\end{aligned} \tag{5.152}$$

We will also choose $\mu=1$ in arbitrary units. The eigenfrequencies and the decay widths are found numerically with a three-point fit to the determinant of the retarded and advanced propagators [264].

With the parameters fixed, we have to specify the initial conditions, represented by the source term $\mathcal{K}^{mn}$. Since we are working here in the weak-washout regime, the total asymmetry will be sensitive to the initial asymmetry. If we want to make sure that the asymmetry is only generated dynamically, we have to find suitable initial conditions. In the Heisenberg picture, these conditions corresponds to choosing the correct $G_\delta^{ij}(0,0)$ (see appendix B.2.1). For non-degenerate spectra and for real scalars that transform equally under *C*-transformations, we are free to specify any initial condition, and $\mathcal{K}^{12}=0$ is a suitable choice. For *C*-transformations that act like

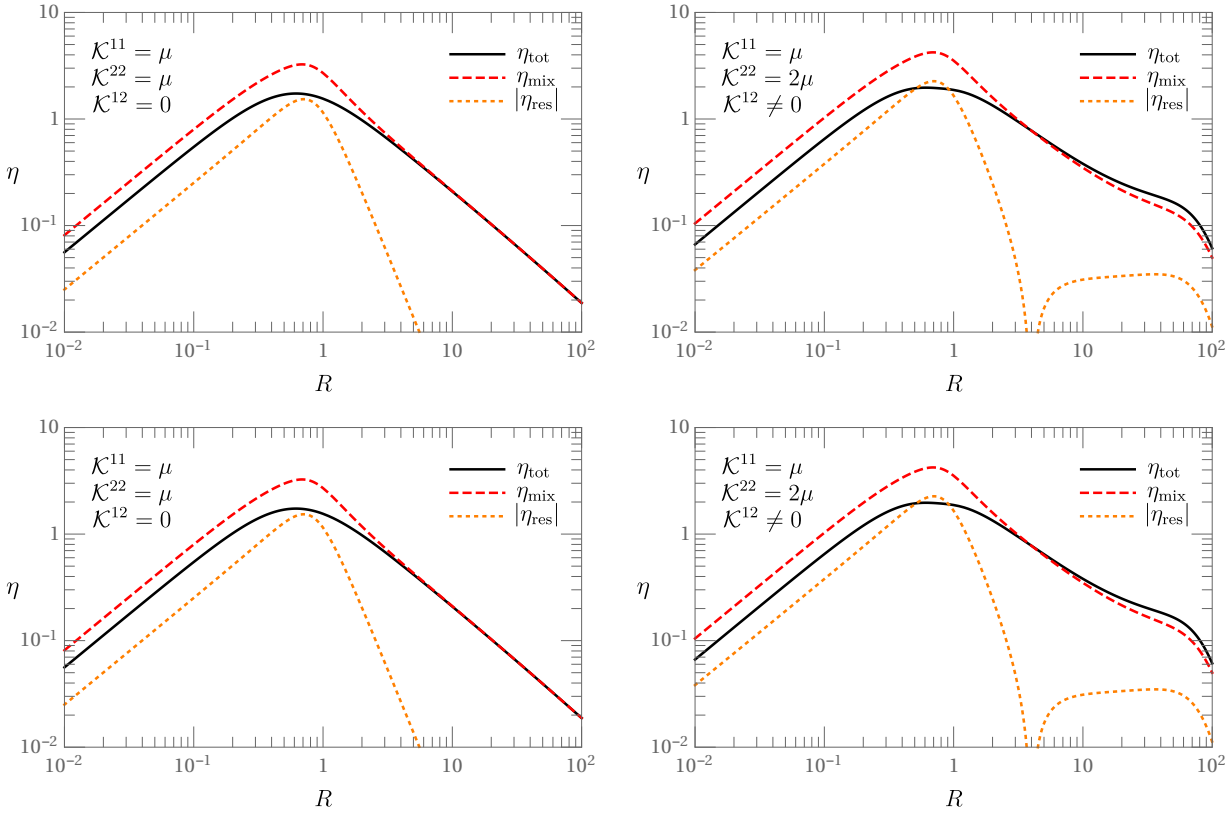

Figure 5.2: Numerical evaluation of Eq. (5.150) *as functions of the degeneracy parameter R interpreted in terms of the Boltzmann "benchmark" ($\eta_{\rm mix}$) plus corrections ($|\eta_{\rm res}|$), which contain both oscillations and interference. In between the panels we choose different C-conserving initial conditions indicated in the upper left corner of each panel. The Yukawa couplings are $h_1 = 0.5\,\mu$ and $h_2 = 0.8\,\exp(2i/3)\mu$.*

reflections, we have to be more careful to fulfill Eq. (B.12) such that in general $\mathcal{K}^{12} \neq 0$. We will show numerical results for both variants of initial values for $\mathcal{K}^{12}$.

In Fig. 5.2 we plot the total asymmetry in black. The red dashed line gives the pure mixing contribution and the orange dotted line is the combination of oscillation and interference terms. This picture corresponds to one of two ways of interpreting the sources of the asymmetry: Here, we have plotted the benchmark that the Boltzmann equation approximates the asymmetry whereas the oscillation source and the interference are viewed as corrections. In agreement with expectations, this scheme works well for hierarchical mass spectra, $R > 3$, and the chosen parameters. It is also rather accurate for small $R < 1$. For $R = 1$ we see an overestimate in the asymmetry by roughly a factor of 2.

This scenario should be compared with Fig.5.3, where we show the same asymmetry (black line) interpreted in terms of the density-matrix benchmark, i.e., the oscillation source (light-blue dashed) contributes the most to the asymmetry, and the mixing and interference constitute corrections (orange, dotted). In this case, we see that the density matrix approximation agrees well with the total asymmetry when the number densities of the two flavors are of similar magnitudes

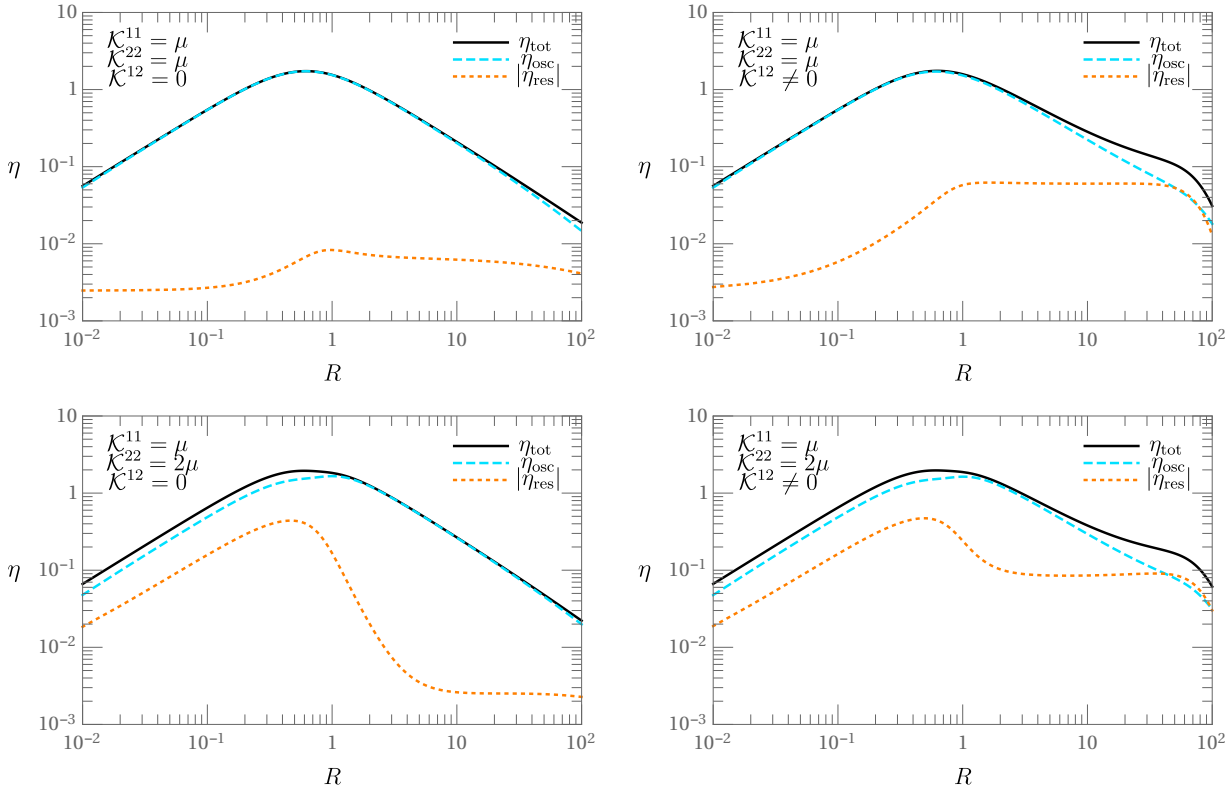

Figure 5.3: Numerical evaluation of Eq. (5.150) *as functions of the degeneracy parameter R interpreted in terms of the density matrix "benchmark" ($\eta_{\rm osc}$) plus corrections ($|\eta_{\rm res}|$), which contain both mixing and interference. In between the panels we choose different C-conserving initial conditions indicated in the upper left corner of each panel. The Yukawa couplings are $h_1 = 0.5\,\mu$ and $h_2 = 0.8\,\exp(2i/3)\mu$.*

and there is no off-diagonal source (upper left panel of Fig. 5.3). When the off-diagonal source is non-zero (upper right panel), we still see a very good agreement between the total asymmetry and the oscillations source until $R \sim 10$. At this point the correction from mixing and interference becomes of the same magnitude. On the other hand, when the number densities of the two flavors are not similar because of $\mathcal{K}^{11} \neq \mathcal{K}^{22}$ (lower left panels of Fig. 5.3), we see that the density matrix approximation underestimates the total asymmetry for smaller R. This observation can be understood from the analytic results given in Eqs. (5.123) and (5.124) for the effective *CP*-violating parameter. Specifically, with the density matrix approximation as the benchmark, the interference terms can be seen as a modification to the mixing source. This modification introduces a relative sign between the contribution to the asymmetry from the two flavors. Hence, when the deviations from equilibrium of the two flavors are similar, the mixing contribution is strongly suppressed. On the other hand, when this is not the case, the cancellation is no longer exact and both the oscillation and mixing sources contribute additively to the asymmetry, leading to an underestimate of the asymmetry in the density-matrix approach.

The interference was not included in the analysis of Refs. [108–110]. Nevertheless, we see that including only oscillations or mixing could underestimate the asymmetry by a factor of 2 in

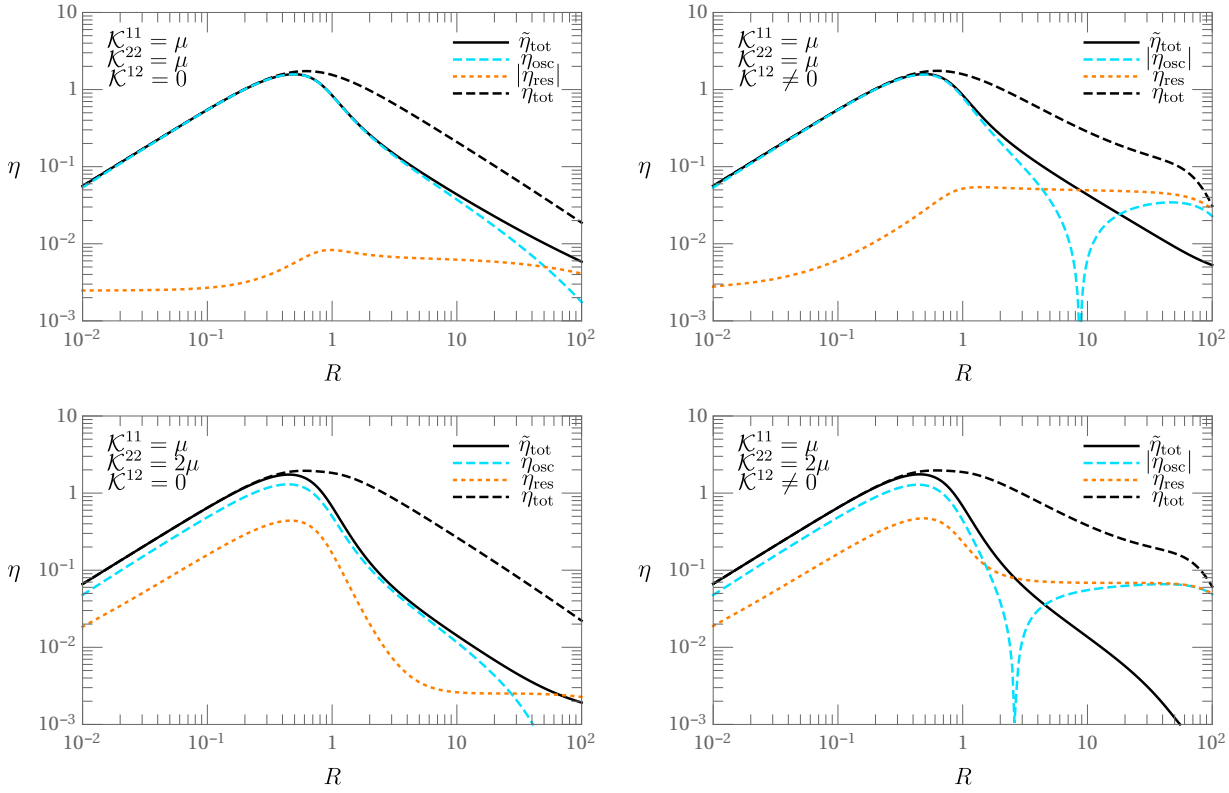

Figure 5.4: Numerical evaluation of Eq. (5.150) *for the single-shell approximation as functions of the degeneracy parameter R. The asymmetry in the single-shell approximation $\tilde{\eta}$ is given by a black line, and its components are depicted in dashed blue (oscillation source) and dotted orange (mixing plus interference). The asymmetry that would have been obtained if all three shells were distinguished is shown with a dashed black line. In between the panels we choose different C-conserving initial conditions indicated in the upper left corner of each panel. The Yukawa couplings are $h_1 = 0.5\,\mu$ and $h_2 = 0.8\,\mu\exp(2i/3)$.*

accordance with their claim. It remains to be seen to which extent the interference terms modify the final asymmetry for more realistic, phenomenological models in the strong-washout regime and for an expanding background.

To wrap up this section, we compare in Fig. 5.4 the total asymmetry including all three shells with the asymmetry calculated in the single-shell approximation $\omega_1 = \omega_2 = \omega$ (see appendix C)

$$G_{\gtrless} \propto \delta(Q^2 - \bar{M}^2)\,, \tag{5.153}$$

which was employed in Refs. [112, 113, 132]. We see that this approximation agrees well for $R < 1$ with the result that takes into account all three shells separately. For hierarchical mass spectra, however, the results differ by orders of magnitude since this approach discards the mixing contribution [110]. The oscillation contribution even vanishes completely and changes its sign if $\mathcal{K}^{12} \neq 0$. The reason is that for quasi-degenerate spectra the oscillations are mainly sourced by the diagonal number densities [see Eqs. (5.137)]. However, these contributions fall of fast enough to allow the off-diagonal number densities sourced by $\mathcal{K}^{12}$ to take over for hierarchical spectra.

5.8 Concluding remarks

Baryogenesis via leptogenesis is an attractive scenario to explain the baryon asymmetry of the universe. Lepton asymmetry is generated by out-of-equilibrium decays of heavy Majorana neutrinos that violate lepton number and CP-symmetry. This asymmetry is later transferred to the baryonic sector via sphaleron processes.

Traditionally, the asymmetry has been calculated using Boltzmann equations. This formalism accounts for the CP-violation that is generated by the mixing source, i.e., the asymmetry that it created due to interference of tree-level and one-loop decay amplitudes. For quasi-degenerate spectra one has to worry about another source to the asymmetry. Correlations between different heavy-neutrino flavors build up and lead to flavor-violating oscillations. The density matrix formalism is capable of tracking these correlations and yields the asymmetry generated from these oscillations.

It was argued by Dev, Millington, Pilaftsis, and Teresi that the mixing and oscillation sources both contribute additively to the asymmetry. For their analysis they used the interaction-picture representation of non-equilibrium field theory in the strong-washout regime. Moreover, they showed that the density matrix formalism discards the mixing source by giving all heavy Majorana neutrinos approximately the same energy. A density matrix ansatz might therefore underestimate the total asymmetry by a factor two. This result has to be compared to recent works of Garbrecht and collaborators who use a density matrix approach to compute the asymmetry. However, their results are obtained in the Heisenberg representation of non-equilibrium field theory. A direct comparison between the Heisenberg and interaction picture approach in non-equilibrium quantum field theory has never been performed.

Such a comparison has been presented in this chapter. Using Kadanoff-Baym equations, we derived analytically the expression for the asymmetry that is generated in the weak-washout regime for both the Heisenberg and interaction picture approaches. We obtained identical results in both pictures demonstrating their equivalence and consistency. We confirmed that mixing and oscillations provide two distinct sources to the lepton asymmetry, and identified three different shells that contribute to the asymmetry. The mixing contribution corresponds to the two quasiparticle shells with energy ω_i; the middle shell $\bar{\omega} = (\omega_1 + \omega_2)/2$ corresponds to the oscillation source and an additional interference term between mixing and oscillations.

We find that the mixing and oscillation sources can be of the same sign and magnitude, contributing additively to the final asymmetry, in agreement with the conclusions of Refs. [108–110]. Moreover, we have taken a look at the single-shell approximation where energy differences are neglected everywhere but in the commutator of the mass matrix. We have shown that this approximation may underestimate the total asymmetry significantly because it discards the mixing source, in line with the argument in Ref. [110]. However, we also find that this argument is not so clear-cut because the destructive interference terms suppresses the mixing contribution in the quasi-degenerate limit.

To illustrate these cancellations, we computed the asymmetry numerically and compared to each other different approaches (Boltzmann, density matrix, Kadanoff-Baym) for different mass spectra from degenerate through to hierarchical. From the perspective of the Boltzmann equation, the mixing source is the dominant contribution and the sum of oscillations and interference

constitutes the corrections. We find that this approximation works well for hierarchical mass spectra, whereas the corrections become sizable when the mass splitting is of the same order as the sum of the decay widths.

If one views the oscillation source as the dominant contribution, i.e., one uses a density matrix approach, the sum of mixing and interference constitutes the correction. This perspective captures the asymmetry well when the number densities of the two flavors are of similar size. On the other hand, when the number densities of the two flavors are not similar, the correction becomes sizable even for quasi-degenerate mass spectra, i.e., in the parameter range where the density matrix approach was believed to yield reliable results.

Since it is not clear to what extent our results generalize to the strong-washout regime, it would be of interest to perform an equivalent analysis for a realistic phenomenological model in the strong-washout regime and for an expanding background.

Chapter 6

Conclusions and outlook

Throughout this thesis, we have studied applications of the density matrix formalism to astrophysical and cosmological systems. The density matrix equation tracks the evolution of particle number densities taking into account correlations between particles with different discrete quantum numbers like flavor or helicity. It is able to describe particle transport in systems where different particle species mix, i.e., correlations between particles develop. These correlations lead to the typical oscillations of particles species into each other, e.g., neutrino flavor oscillations or the magnetic field-induced Faraday rotation. This makes the density matrix equations more general than the semi-classical Boltzmann equations that discards any correlations.

The dynamical object in the density matrix equation is a matrix of densities ρ with particle number densities on the diagonals and correlations between particle species on the off-diagonals. The density matrix equation obtains contributions from external forces, diffusion, and collisions, similar to the Boltzmann equation, as well as a refractive source term. In this thesis we were mainly concerned with this refractive term, which describes particle oscillations in media. Its functional form is determined by the commutator $[\mathsf{H}, \rho]$, where H denotes the Hamiltonian matrix, i.e., the matrix of oscillation frequencies. Large parts of this thesis were devoted to deriving this Hamiltonian matrix and studying its impact on particle oscillations. In particular, we have applied the density matrix formalism to three systems.

$\diamondsuit$

Axion-like particles couple to the scalar product of electric and magnetic field $\mathbf{E} \cdot \mathbf{B}$. If ALPs propagate in a background filled with a magnetic field, this coupling allows the ALPs to mix with photons. Laboratory experiments like ADMX, ALPS, CAST, and MADMAX are using this property to search for ALPs that convert into photons in small scale magnetic fields. If ALPs exist, these conversions will happen in the large scale magnetic fields of the galaxy or extragalactic space as well. Since ALPs are absorbed much more weakly than photons, ALP-photon oscillations make the universe appear less opaque: the power in high energy photons that oscillate into ALPs is protected from absorption on the extragalactic background light. If the ALPs convert back to photons close to our galaxy, the absorption rate in extragalactic space seems to be smaller or equivalently the power of the EBL seems to be weaker. This mechanism helps to explain a surprisingly low absorption rate that has been observed by Cherenkov telescopes and to alleviate the corresponding transparency problem of the universe.

Because the magnetic field along the line of sight to a source is unknown, ALP-photon mixing was simulated using assumptions about the statistical distribution and structure of the magnetic field that fills the extragalactic space. Previously, the magnetic field was considered to consist

of a grid of magnetic field domains with a constant comoving domain length and a constant magnetic field strength in each domain. The magnetic field was assumed to vary discontinuously at the borders of each domain ("hard edges"). By generating a large number of magnetic field configurations and computing the photon and ALP transfer functions for each of these, one could extract the statistical properties of the transfer functions. The same approximations were also used by Mirizzi and Montanino, who derived a simple system of differential equations that could substitute the more demanding Monte-Carlo approach in the maximal mixing regime.

In this thesis, we studied in detail the different refractive and absorptive terms that contribute to ALP-photon propagation in extragalactic magnetic fields. In contrast to previous works, we included the recently derived refraction of GeV–TeV photons on the CMB. This refraction increases linearly with energy becoming the most important entry of the Hamiltonian matrix for the GeV–TeV energy range. We have shown that this new dispersive term impacts three assumptions that have been adopted in previous works.

First, the mixing angle between ALPs and photons was assumed to be maximal for energies larger than a critical scale. This scale depends on the ALP mass but usually lies in the GeV-energy range. We showed that maximal mixing cannot be achieved for this energy range if refraction on the CMB is included. This refractive contribution grows linearly with energy and becomes the largest entry of the Hamiltonian matrix around 1 TeV. We demonstrated that the differential equation formalism of Mirizzi and Montanino can be extended in a straight-forward manner.

The energy range where the differential equation may be applied is limited because the refraction on the CMB also impacts the modeling of the extragalactic magnetic field. Previously, it was assumed that the oscillation length of the ALP-photon system is much larger than a typical domain size. Large dispersive terms are, however, concomitant with smaller oscillation lengths $l_{\rm osc}$. If this length scale becomes of similar size as the domain size $l_{\rm c}$, the two length scales interfere and lead to an unphysical suppression of ALP-photon conversions. We showed that letting the domain size of the magnetic field fluctuate removes this resonant behavior. However, when $l_{\rm osc}$ approaches $l_{\rm c}$ the exact probability distribution of the domain sizes became important.

As soon as $l_{\rm osc} \ll l_{\rm c}$, not only constant domain lengths have to be discarded, also the third assumption of previous works which pertains to discontinuous magnetic fields at the domain borders has to be reexamined. As soon as the oscillation length is much smaller than the typical domain size, the description of the ALP-photon propagation becomes fundamentally different: the oscillations are now fast with respect to changes of the magnetic field so that the ALP-photon system probes the detailed structure of the magnetic field. This brings into question the assumption of hard edges. By interpolating magnetic field configurations with hard edges using a continuous function, we have demonstrated that ALP-photon propagation enters the quasi-adiabatic regime when $l_{\rm osc} \ll l_{\rm c}$. For zero initial and final magnetic field, the photon and ALP transfer functions depend on the derivative of the magnetic field at the source and at the detector, as well as the mean absorption of ALPs in extragalactic space.

In the future it will be interesting to study photon propagation for more phenomenological models of magnetic fields. This task requires a realistic simulation of the magnetic field structure coming from, e.g., galactic outflows. Additionally, our computations did not include redshift. Magnetic fields and the CMB energy density grow strongly with redshift such that this effect has to be taken into account for phenomenological predictions of the photon transport function.

With all these ingredients it might be possible to predict how the spectra of blazars are modified when ALPs are included. Such predictions are crucial not only for current air-Cherenkov telescopes (MAGIC, VERITAS, H.E.S.S.) that are measuring blazar spectra up to TeV photons, the sensitivity to these high energies will improve tremendously with the upcoming Cherenkov Telescope Array. A precise measurement of far-away blazars might ultimately shed light on the transparency problem of the universe and its possible resolution with ALP-photon mixing.

$\diamondsuit$

In the second part of this thesis, we have looked at neutrino oscillations in compact astrophysical objects. Flavor oscillations are well described within the density matrix formalism. Recently, this formalism was extended to include correlations between different neutrino helicities and between neutrinos and antineutrinos (pair correlations). We have derived the corresponding kinetic equations confirming and extending previous results.

Helicity coherence describes helicity flips on the refractive level. These might be important for supernova physics because different helicity eigenstates of neutrinos interact with matter in qualitatively and quantitatively different ways. We estimated the numerical magnitude of such helicity flips confirming that these are usually negligible.

We also discussed pair correlations in detail. For this task, we simplified the kinetic equations to the simplest working toy model which consisted of one generation of massless neutrinos. By reformulating the corresponding kinetic equation in the Schrödinger picture, we were able to interpret pair correlations as coherence between the empty vacuum state and a neutrino/antineutrino pair with zero total momentum. Non-zero values for these correlators then lead to spontaneous pair creation with an oscillation frequency of the order twice the energy, i.e., approximately $10^{13}\,\mathrm{GHz}$ for typical neutrino energies in supernovae. The amount of pair creation was found to be small with typical correlators of the order $\kappa \sim 10^{-11}$. Together with the fast oscillations, this smallness led us to speculate that pair correlations are negligible.

Even if pair correlations are not negligible, one has to solve the conceptual problem that the neutrino/antineutrino pairs that are created from pair correlations are required to be back-to-back. This requirement is independent of the reference frame which leads to the apparent problem that two observers measure incompatible neutrino momenta and particle numbers.

To resolve this issue, it might be useful to proceed in the following ways. One possibility is to lift the requirement of homogeneity for the mean-fields thereby considering more momentum modes and their interactions. The homogeneity assumption is problematic because it is forces the neutrino pairs to be back-to-back in every frame. Lifting this requirement might help to reconcile the particle numbers seen by different observers.

A different and in our opinion more promising approach is to compute the full non-equilibrium equations for the neutrino propagation. In particular, the constraint equation contains the information on what our physical degrees of freedom actually are. The fact that particle numbers seem to depend on the frame indicate that we have not identified the correct degrees of freedom. This interpretation is favored by our finding that in the simplified model for the pair correlations different observations of particle numbers can be reconciled if we invoke the in-medium Dirac equation. Such a procedure projects vacuum neutrinos onto the physical in-medium degrees of freedom. Since the typical size of the pair correlations is tiny, the difference between the free and in-medium states is small. It is therefore likely that the added layer of complication from

solving the constraint equations does not justify the outcome, and it seems best to discard pair correlations for practical computations altogether.

♢

Finally, we touched upon density matrix equations in the chapter about resonant leptogenesis. We compared for the first time two methods to compute the asymmetry: the top-down Heisenberg picture and the bottom-up interaction picture approaches. For this comparison we used a toy model of leptogenesis with scalar "heavy neutrinos" and complex Yukawa couplings. In the weak-washout regime we obtained an analytical result for the generated asymmetry. This result was identical in both approaches demonstrating their consistency and complementarity.

This result contributes to the resolution of a seeming discrepancy between the amount of asymmetry that is produced in the interaction and Heisenberg picture approaches. Dev and collaborators identified in the interaction picture approach two different sources to the asymmetry. The conventional mixing source describes CP-violation from the interference of tree-level decay amplitudes with the one-loop corrections. Here, especially the self-energy correction to the outer leg of the decaying particle is important because of a resonant enhancement for quasi-degenerate Majorana neutrinos. The second source describes lepton-number violating oscillations due to correlations that build up during propagation. Dev and collaborators argued that a density matrix approach that is used by Garbrecht and collaborators would underestimate the asymmetry because this approach discards the mixing source.

In our analytical results we confirmed the existence of both sources. Moreover, we found a third contribution to the lepton asymmetry which we identified as destructive interference between the mixing and oscillation sources. This interference term has not been identified in previous computations and it suggests that previous results in the interaction and Heisenberg picture may not be in conflict with each other. Both the mixing and oscillation sources contribute additively to the asymmetry as suggested by Dev and collaborators, but the mixing source might be canceled in the quasi-degenerate regime where the density matrix approach used by Garbrecht and collaborators can be well applicable. Note that our result is not without caveat: we used here the weak-washout regime while most results in the literature are in the strong-washout regime where back-reactions of the plasma are important.

There are two aspects that deserve future attention. First, it is desirable to study if the three sources to the asymmetry persist in the strong-washout regime. Second, the heavy Majorana neutrinos are fermions that have a different propagator structure than scalars. A more realistic model should take the resulting Dirac structure into account.

♢

In summary, mixing between particles with different discrete quantum numbers is crucial to describe transport phenomena in astrophysical and cosmological systems. The density matrix generalization of the Boltzmann equation is a powerful tool that is able to account for correlations and corresponding oscillations. Moreover, the density matrix formalism is flexible and can be applied to many different systems and particle species as we have demonstrated. Far away from equilibrium, however, it becomes tricky to extract correct physical results and a full non-equilibrium treatment like the closed-time-path formalism is more convenient, albeit much tougher to apply in practice.

Appendix A

Conventions

A.1 Units and metric

Throughout this thesis we work in natural (Lorentz-Heaviside) units where the speed of light c, Planck's reduced constant $\hbar$, and the Boltzmann constant k_{B} all equal unity. All calculations in this thesis are performed in Minkowski space and we choose the metric $g^{\mu\nu} = \mathrm{diag}(+,-,-,-)$.

A.2 Coordinate conventions

Coordinate-space variables are denoted by the lower-case Roman characters $x, y, \ldots$; and their Fourier-conjugates by the four-momenta $p, p', \ldots$. The spatial components of these four-vectors are shown in bold-face. The central and relative coordinates are denoted by the Roman characters X and r, respectively, where

$$X^\mu = (x^\mu + y^\mu)/2 \qquad r^\mu = x^\mu - y^\mu \,. \tag{A.1}$$

Finally, the characters Q and q are reserved for the central and relative momenta

$$Q^\mu = (p^\mu + p^{\mu\prime})/2 \,, \qquad q^\mu = p^\mu - p^{\mu\prime} \,. \tag{A.2}$$

A.3 Dirac matrices and spinors

For fermionic fields we require a convention for the Dirac matrices for which we will follow the extensive work of Ref. [218]. The Dirac matrices in four dimensions are defined through their anticommutation relation

$$\{\gamma^\mu, \gamma^\nu\} = 2g^{\mu\nu}\mathbb{1} \,. \tag{A.3}$$

We will choose a chiral representation, in which γ^5 is diagonal:

$$\gamma^\mu = \begin{pmatrix} 0 & \sigma^\mu \\ \bar{\sigma}^\mu & 0 \end{pmatrix} \,, \qquad \gamma^5 = \begin{pmatrix} -1 & 0 \\ 0 & 1 \end{pmatrix} \,, \tag{A.4}$$

where every entry is a 2×2 submatrix. The vector of Pauli matrices are defined as

$$\sigma^\mu = \begin{pmatrix} 1 \\ \sigma^i \end{pmatrix} \,, \qquad \bar{\sigma}^\mu = \begin{pmatrix} 1 \\ -\sigma^i \end{pmatrix} \,. \tag{A.5}$$

With this convention we may write down our bispinor notation. A Dirac spinor has four components which may be written in the following way:

$$\psi(x) = \begin{pmatrix} \xi_\alpha(x) \\ \eta^{\dagger,\dot{\alpha}}(x) \end{pmatrix} , \tag{A.6}$$

where ξ and η are two-component spinors with the same mass. They transform differently under the Lorentz group as indicated by dotted and undotted indices, i.e., ξ_α transforms as $(1/2, 0)$ and $\eta^{\dagger,\dot{\alpha}}$ transforms as $(0, 1/2)$. Hermitian conjugation switches between the two representations

$$(\xi^\alpha)^\dagger = \xi^{\dagger,\dot{\alpha}} . \tag{A.7}$$

Indices can be raised and lowered with the 2×2 ϵ-tensor

$$\xi_\alpha = \epsilon_{\alpha\beta}\xi^\beta, \quad \xi^\alpha = \epsilon^{\alpha\beta}\xi_\beta, \quad \xi^\dagger_{\dot{\alpha}} = \epsilon_{\dot{\alpha}\dot{\beta}}\xi^{\dagger\dot{\beta}}, \quad \xi^{\dagger,\dot{\alpha}} = \epsilon^{\dot{\alpha}\dot{\beta}}\xi^\dagger_{\dot{\beta}} , \tag{A.8}$$

which is zero on the diagonals and

$$\epsilon^{12} = -\epsilon^{21} = \epsilon_{21} = -\epsilon_{12} = 1 . \tag{A.9}$$

In the two-component spinor notation the Dirac matrices read

$$\gamma^\mu = \begin{pmatrix} 0 & \sigma^\mu_{\alpha\dot{\beta}} \\ \bar{\sigma}^{\mu,\dot{\alpha}\beta} & 0 \end{pmatrix} , \qquad \gamma^5 = \begin{pmatrix} -\delta_\alpha^{\ \beta} & 0 \\ 0 & \delta^{\dot{\alpha}}_{\ \dot{\beta}} \end{pmatrix} . \tag{A.10}$$

For a Lorentz invariant Lagrangian we are only allowed to form Lorentz invariant spinor combinations. These can be obtained by contracting indices of the same type, i.e., $\xi^\alpha\xi_\alpha$ or $\eta_{\dot{\alpha}}\eta^{\dot{\alpha}}$, where the order of the indices is important. Lorentz invariant contractions are obtained by the product $\bar{\psi}\psi$, with

$$\bar{\psi}(x) = \psi^\dagger(x)\gamma^0 = \begin{pmatrix} \eta^\alpha(x) & \xi^\dagger_{\dot{\alpha}}(x) \end{pmatrix} . \tag{A.11}$$

For Majorana neutrinos the two-component spinors that enter the bispinor are not independent. Indeed, we may impose the Majorana condition $\psi^C = \psi$, i.e., the Majorana spinor is equal to its charge-conjugate. Charge conjugation is defined as

$$\psi^C(x) \equiv C\bar{\psi}^T(x) = \begin{pmatrix} \eta_\alpha(x) \\ \xi^{\dagger,\dot{\alpha}}(x) \end{pmatrix} , \tag{A.12}$$

with the charge conjugation matrix

$$C = i\gamma^0\gamma^2 . \tag{A.13}$$

With these definitions, the Majorana condition leads to $\eta_\alpha(x) = \xi_\alpha(x)$, and the Majorana bispinor yields

$$\psi_{\mathrm{M}}(x) = \begin{pmatrix} \xi_\alpha(x) \\ \xi^{\dagger,\dot{\alpha}}(x) \end{pmatrix} . \tag{A.14}$$

The two-component spinor formalism is well-suited for massless particles. Since they possess a definite chirality, we may define a left-chiral Weyl field by $P_L\psi = \psi$, and similarly for the right-chiral field. Hence, a representation reads

$$\psi_{\mathrm{W,L}}(x) = \begin{pmatrix} \xi_\alpha(x) \\ 0 \end{pmatrix}, \qquad \psi_{\mathrm{W,R}}(x) = \begin{pmatrix} 0 \\ \xi^{\dagger,\dot{\alpha}}(x) \end{pmatrix}. \tag{A.15}$$

With our conventions for the Dirac matrices, we may write down the explicit solutions to the free Dirac equation:

$$u_i(\mathbf{p}, s) = \begin{pmatrix} \mathcal{N}^i_{p,s}\, \chi_s(\hat{\mathbf{p}}) \\ \mathcal{N}^i_{p,-s}\, \chi_s(\hat{\mathbf{p}}) \end{pmatrix}, \tag{A.16a}$$

$$v_i(\mathbf{p}, s) = s \begin{pmatrix} -\mathcal{N}^i_{p,-s}\, \chi_{-s}(\hat{\mathbf{p}}) \\ \mathcal{N}^i_{p,s}\, \chi_{-s}(\hat{\mathbf{p}}) \end{pmatrix}, \tag{A.16b}$$

where $\hat{\mathbf{p}}$ is the unit vector in the direction of $\mathbf{p}$, $s = \pm$ a helicity index, and

$$\mathcal{N}^i_{p,s} = \sqrt{\frac{E_i - s|\mathbf{p}|}{2E_i}} \approx \delta_{s-} + \frac{m_i}{2|\mathbf{p}|}\delta_{s+}, \tag{A.17}$$

with $E_i = (\mathbf{p}^2 + m_i^2)^{1/2}$, the energy of a neutrino with mass m_i.

We may describe the modes of the neutrino field in spherical coordinates where the momentum components are $\hat{\mathbf{p}} = (\sin\theta\cos\phi, \sin\theta\sin\phi, \cos\theta)$. In this case the standard two-component helicity spinors are explicitly

$$\chi_+(\hat{\mathbf{p}}) = \begin{pmatrix} \cos\frac{\theta}{2} \\ e^{i\phi}\sin\frac{\theta}{2} \end{pmatrix}, \tag{A.18a}$$

$$\chi_-(\hat{\mathbf{p}}) = \begin{pmatrix} -e^{-i\phi}\sin\frac{\theta}{2} \\ \cos\frac{\theta}{2} \end{pmatrix}. \tag{A.18b}$$

They satisfy the orthogonality condition $\chi_s^\dagger(\hat{\mathbf{p}})\chi_h(\hat{\mathbf{p}}) = \delta_{sh}$.

The matrix elements of $\bar{\sigma}^\mu$ are found by direct evaluation to be

$$\chi_-^\dagger(\hat{\mathbf{p}})\bar{\sigma}^\mu\chi_-(\hat{\mathbf{p}}) = n^\mu = (1, \hat{\mathbf{p}}), \tag{A.19a}$$

$$\chi_+^\dagger(\hat{\mathbf{p}})\bar{\sigma}^\mu\chi_+(\hat{\mathbf{p}}) = \bar{n}^\mu = (1, -\hat{\mathbf{p}}), \tag{A.19b}$$

$$\chi_+^\dagger(\hat{\mathbf{p}})\bar{\sigma}^\mu\chi_-(\hat{\mathbf{p}}) = -e^{-i\phi}\epsilon^\mu = -e^{-i\phi}(0, \hat{\boldsymbol{\epsilon}}), \tag{A.19c}$$

$$\chi_-^\dagger(\hat{\mathbf{p}})\bar{\sigma}^\mu\chi_+(\hat{\mathbf{p}}) = -e^{i\phi}\epsilon^{\mu*} = -e^{i\phi}(0, \hat{\boldsymbol{\epsilon}}^*), \tag{A.19d}$$

where ϵ^μ is a polarization vector orthogonal to n^μ. The explicit components in spherical coordinates are

$$\hat{\boldsymbol{\epsilon}} = \begin{pmatrix} e^{i\phi}\cos^2\frac{\theta}{2} - e^{-i\phi}\sin^2\frac{\theta}{2} \\ -i\Big(e^{i\phi}\cos^2\frac{\theta}{2} + e^{-i\phi}\sin^2\frac{\theta}{2}\Big) \\ -\sin\theta \end{pmatrix}. \tag{A.20}$$

Note that the vectors n^μ and ϵ^μ depend on $\hat{\mathbf{p}}$, but we do not show this dependence explicitly to simplify the notation.

A.4 Double Fourier and Wigner transforms

The double Fourier transform $f(p,p')$ of a function $f(x,y)$ is defined as follows:

$$\begin{aligned} f(p,p') &\equiv \mathcal{F}_y[\mathcal{F}_x[f(x,y)](p)](-p') \equiv \mathcal{F}_x[\mathcal{F}_y[f(x,y)](-p')](p) \\ &\equiv \int_{-\infty}^{+\infty} \mathrm{d}^4x \int_{-\infty}^{+\infty} \mathrm{d}^4y\, e^{-ip\cdot x}\, e^{ip'\cdot y}\, f(x,y)\,. \end{aligned} \tag{A.21}$$

We emphasize the relative sign in the exponent of the right-most y-dependent kernel. This is chosen such that translational invariance $f(x,y) = f(x-y)$ corresponds to the conservation of four-momentum $p = p'$.

The Wigner transform $f(X,Q)$ of a function $f(x,y)$ is defined as follows:

$$f(X,Q) \equiv \mathcal{F}_R[f(x,y)](Q) \equiv \int_{-\infty}^{+\infty} \mathrm{d}^4R\, e^{iQ\cdot R}\, f(x,y)\,. \tag{A.22}$$

It may also be written in terms of an inverse transform of the double-momentum representation $f(p,p')$:

$$f(X,Q) \equiv \mathcal{F}_q^{-1}[f(p,p')](X) \equiv \int_{-\infty}^{+\infty} \frac{\mathrm{d}^4q}{(2\pi)^4} e^{-iq\cdot X}\, f(p,p')\,. \tag{A.23}$$

A.5 Propagator conventions

A.5.1 CTP propagators

The conventions for the CTP propagators differ in the literature. In the present thesis, we denote by the upper-case Roman character G the conventions of Ref. [264] which are used throughout the body of this thesis. Those denoted by the upper-case Greek character Δ follow the conventions of Refs. [110, 118], which we will show explicitly as well in order to allow for comparisons. Parenthesized names correspond to the nomenclature of Refs. [110, 118] and are placed in the text immediately following the corresponding nomenclature of Ref. [264].

The CTP propagator of the scalar neutrinos of the model in Eq. (5.2) is defined as

$$G_{\mathcal{C}}^{[0,]ij}(x,y[,\tilde{t}]) \equiv \langle \mathrm{T}_{\mathcal{C}}[\psi^i_{H[I]}(x)\psi^j_{H[I]}(y)]\rangle_{0[\tilde{t}]}\,, \tag{A.24}$$

where objects appearing in brackets ([]) correspond to the interaction-picture definitions. The operator $\mathrm{T}_{\mathcal{C}}$ denotes path ordering, i.e., time ordering on the positive time branch and anti-time ordering on the negative time branch. Also fields on the negative time branch are always considered to be later than those on the positive time branch. For times x^0 and y^0 on the time-ordered branch, $G_{\mathcal{C}}^{[0,]ij}(x,y[,\tilde{t}])$ is equal to the time-ordered (Feynman) propagator $G_{\mathrm{T}}^{[0]ij}(x,y[,\tilde{t}])$. For times x^0 and y^0 on the anti-time-ordered branch, $G_{\mathcal{C}}^{[0,]ij}(x,y[,\tilde{t}])$ is equal to the anti-time-ordered (Dyson) propagator $G_{\overline{\mathrm{T}}}^{[0,]ij}(x,y[,\tilde{t}])$. When x^0 is on the time-ordered branch and y^0 is on the anti-time-ordered branch, $G_{\mathcal{C}}^{[0,]ij}(x,y[,\tilde{t}])$ is equal to the negative-frequency Wightman propagator $G_{<}^{[0,]ij}(x,y[,\tilde{t}])$. On the other hand, when x^0 is on the anti-time-ordered branch and y^0 is on the time-ordered branch, $G_{\mathcal{C}}^{[0,]ij}(x,y[,\tilde{t}])$ is equal to the positive-frequency Wightman propagator $G_{>}^{[0,]ij}(x,y[,\tilde{t}])$.

A.5.2 (Anti-)Commutator functions

The spectral (Pauli-Jordan) function and the statistical (Hadamard) propagator are defined as follows:

$$G_{\rho}^{[0,]ij}(x,y[,\tilde{t}]) = i\,\langle[\psi^{i}_{\mathrm{H[I]}}(x),\,\psi^{j}_{\mathrm{H[I]}}(y)]\rangle_{0[t]} \;\equiv\; -\,\Delta^{[0,]ij}(x,y)\,, \tag{A.25a}$$

$$G_{\mathrm{F}}^{[0,]ij}(x,y[,\tilde{t}]) = \tfrac{1}{2}\,\langle\{\psi^{i}_{\mathrm{H[I]}}(x),\,\psi^{j}_{\mathrm{H[I]}}(y)\}\rangle_{0[t]} \;\equiv\; \tfrac{1}{2}\,i\Delta_{1}^{[0,]ij}(x,y[,\tilde{t}])\,. \tag{A.25b}$$

The subscript F, indicating the statistical propagator, should not be confused with the same subscript used in Refs. [110, 118] to indicate the time-ordered (Feynman) propagator.

Note that the expectation value is redundant in the definition of the spectral function in the interaction picture, since the commutator is a c-number. In addition, we draw attention to the fact that the Wigner transform of the spectral (Pauli-Jordan) function $G_{\rho}(X,Q)$ differs from the object $\widetilde{G}_{\rho}(X,Q)$ appearing in Ref. [273] by an overall factor of i. Specifically, we have

$$G_{\rho}^{ij}(X,Q[,\tilde{t}]) = \mathcal{F}_{R}[G_{\rho}^{ij}(x,y[,\tilde{t}])](Q) \;\equiv\; i\,\widetilde{G}_{\rho}^{ij}(X,Q[,\tilde{t}])\,. \tag{A.26}$$

A.5.3 Causal functions

The retarded and advanced propagators are defined in terms of the spectral function as follows:

$$G_{\mathrm{R}}^{ij}(x,y[,\tilde{t}]) = \theta(x^{0}-y^{0})G_{\rho}^{ij}(x,y[,\tilde{t}]) \equiv -\Delta_{\mathrm{R}}^{ij}(x,y[,\tilde{t}])\,, \tag{A.27a}$$

$$G_{\mathrm{A}}^{ij}(x,y[,\tilde{t}]) = -\,\theta(y^{0}-x^{0})G_{\rho}^{ij}(x,y[,\tilde{t}]) \equiv -\Delta_{\mathrm{A}}^{ij}(x,y[,\tilde{t}])\,, \tag{A.27b}$$

from which we may obtain the identity

$$G_{\rho}^{ij}(x,y[,\tilde{t}]) = G_{\mathrm{R}}^{ij}(x,y[,\tilde{t}]) - G_{\mathrm{A}}^{ij}(x,y[,\tilde{t}])\,. \tag{A.28}$$

In addition, the Hermitian (principal-part) propagator is defined via

$$\begin{aligned} G_{\mathrm{h}}^{ij}(x,y[,\tilde{t}]) &= \tfrac{1}{2}\left(G_{\mathrm{R}}^{ij}(x,y[,\tilde{t}]) + G_{\mathrm{A}}^{ij}(x,y[,\tilde{t}])\right) \\ &= \tfrac{1}{2}\,\mathrm{sign}(x^{0}-y^{0})\,G_{\rho}^{ij}(x,y[,\tilde{t}]) \equiv -\Delta_{\mathcal{P}}^{ij}(x,y[,\tilde{t}])\,. \end{aligned} \tag{A.29}$$

Note that the superscript 0 does not appear in the interaction-picture cases, since the above identities hold at any order in perturbation theory.

A.5.4 Wightman propagators

The absolutely-ordered Wightman propagators are defined as follows:

$$G_{>}^{[0,]ij}(x,y[,\tilde{t}]) = \langle\psi^{i}_{\mathrm{H[I]}}(x)\psi^{j}_{\mathrm{H[I]}}(y)\rangle \equiv i\Delta_{>}^{[0,]ij}(x,y[,\tilde{t}])\,, \tag{A.30a}$$

$$G_{<}^{[0,]ij}(x,y[,\tilde{t}]) = \langle\psi^{j}_{\mathrm{H[I]}}(y)\psi^{i}_{\mathrm{H[I]}}(x)\rangle \equiv i\Delta_{<}^{[0,]ij}(x,y[,\tilde{t}])\,. \tag{A.30b}$$

Statistical/Hadamard	$G_{\rm F}^{ij} \equiv \frac{1}{2} i\Delta_1^{ij}$
Spectral/Pauli-Jordan	$G_\rho^{ij} \equiv -\Delta^{ij}$
Retarded (Advanced)	$G_{\rm R(A)}^{ij} \equiv -\Delta_{\rm R(A)}^{ij}$
Wightman	$G_{\gtrless}^{ij} \equiv i\Delta_{\gtrless}^{ij}$
Hermitian (Principal-part)	$G_{\rm h}^{ij} \equiv -\Delta_{\mathcal{P}}^{ij}$
Self-energies	$\Pi_{\gtrless}^{ij} \longleftrightarrow i\Pi_{\gtrless}^{ij}$
	$\Pi_F^{ij} \longleftrightarrow \frac{1}{2} i\Pi_1^{ij}$
	$\Pi_{\rm R(A)}^{ij} \longleftrightarrow -\Pi_{\rm R(A)}^{ij}$

Table A.1: Comparison of the notations for the various two-point functions and self-energies used in Ref. [264] (left-hand side) versus Refs. [110, 118] (right-hand side).

These may also be written in terms of the spectral function and statistical propagator:

$$G_{\gtrless}^{ij}(x, y[, \tilde{t}]) = G_{\rm F}^{ij}(x, y[, \tilde{t}]) \mp \frac{i}{2} G_\rho^{ij}(x, y[, \tilde{t}]) \,, \tag{A.31}$$

yielding the identities

$$G_\rho^{ij}(x, y[, \tilde{t}]) = iG_>^{ij}(x, y[, \tilde{t}]) - iG_<^{ij}(x, y[, \tilde{t}]) \,, \tag{A.32a}$$

$$G_{\rm F}^{ij}(x, y[, \tilde{t}]) = \tfrac{1}{2} \left[G_>^{ij}(x, y[, \tilde{t}]) + G_<^{ij}(x, y[, \tilde{t}]) \right] . \tag{A.32b}$$

A.5.5 Time-ordered propagators

The time-ordered (Feynman) and anti-time-ordered (Dyson) propagators are defined as

$$G_{\rm T(\overline{T})}^{ij}(x, y[, \tilde{t}]) = \theta(x^0 - y^0) G_{>(<)}^{ij}(x, y[, \tilde{t}]) + \theta(y^0 - x^0) G_{<(>)}^{ij}(x, y[, \tilde{t}]) \,. \tag{A.33}$$

A.5.6 Self-energies

We follow the sign convention of Ref. [264] for the definition of the self-energies, such that a positive dispersive self-energy correction corresponds to a positive shift in the mass-squared. For example, we denote the inverse of the momentum-space resummed retarded (advanced) propagator by

$$D_{\rm R(A)}^{ij}(p) \equiv p^2 \delta^{ij} - [M^2]^{ij} - \Pi_{\rm R(A)}^{ij}(p) \,, \tag{A.34}$$

where we have adopted the notation $D_{\rm R(A)}^{ij}(p)$ from Ref. [110]. This inverse appears in Ref. [264] as $\Omega_{\rm R(A)}^{ij}(p)$ and in Refs. [110, 118] as $\Delta_{\rm R(A)}^{-1}(p)$.

The various self-energies satisfy identities analogous to those identified above for the two-point functions. In the case of the spectral function,

$$\Pi_\rho^{ij}(x, y[, \tilde{t}]) = i\Pi_>^{ij}(x, y[, \tilde{t}]) - i\Pi_<^{ij}(x, y[, \tilde{t}]) \,, \tag{A.35}$$

we have introduced the real-valued distribution

$$\widetilde{\Pi}_\rho(p, p'[, \tilde{t}]) \equiv -i\Pi_\rho(p, p'[, \tilde{t}]) = -i\mathcal{F}_y[\mathcal{F}_x[\Pi_\rho(x, y[, \tilde{t}])](p)](-p') \,. \tag{A.36}$$

Appendix B

C, *P*, and *T* symmetries

For successful leptogenesis we require the Lagrangian in Eq. (5.2) to transform non-trivially under charge conjugation *C*-, parity transformation P-, and time-reversal T such that the lepton asymmetry can be generated dynamically. In contrast to this dynamical component, we want the asymmetry from the initial conditions to vanish, which is not automatically guaranteed in the weak-washout regime (see Ref. [264]).

B.1 *CPT*-transformations

The usual transformations have to be generalized in the presence of flavor mixing by including transformations in flavor space [108]. The reason is that we define the symmetry operations to leave the kinetic terms of the Lagrangian invariant. During renormalization, however, counter-terms mix the real scalar field with a real symmetric matrix which has to be diagonalized by a transformation U [274]. Under this condition, for the model in Eq. (5.2), we have the following transformation properties under the generalized parity P, time-reversal T and charge-conjugation C transformations:

a) *Parity.* Under the linear transformation P, the scalar fields transform as

$$b(x^0, \mathbf{x})^P = \eta_P b(x^0, -\mathbf{x})\,, \tag{B.1a}$$
$$b^*(x^0, \mathbf{x})^P = \eta_P^* b(x^0, -\mathbf{x})\,, \tag{B.1b}$$
$$\psi_i(x^0, \mathbf{x})^P = \pm\psi_i(x^0, -\mathbf{x})\,, \tag{B.1c}$$

where the complex phase η_P satisfies $|\eta_P|^2 = 1$.

b) *Time-reversal.* Under the anti-linear transformation T, the scalar fields transform as

$$b(x^0, \mathbf{x})^T = \eta_T b(-x^0, \mathbf{x})\,, \tag{B.2a}$$
$$b^*(x^0, \mathbf{x})^T = \eta_T^* b^*(-x^0, \mathbf{x})\,, \tag{B.2b}$$
$$\psi_i(x^0, \mathbf{x})^T = \mathsf{U}_{ij}\psi_j(-x^0, \mathbf{x})\,, \tag{B.2c}$$

where the complex phase η_T satisfies $|\eta_T|^2 = 1$ and U is an orthogonal transformation in flavor space, i.e., $\mathsf{U}_{ik}\mathsf{U}_{jk} = \mathsf{U}_{ki}\mathsf{U}_{kj} = \delta_{ij}$.

c) *Charge-conjugation.* Under the linear charge conjugation C, the scalar fields transform as

$$b(x)^C = \eta_C b^*(x)\,, \tag{B.3a}$$
$$b^*(x)^C = \eta_C^* b(x)\,, \tag{B.3b}$$
$$\psi_i(x)^C = \mathsf{U}_{ij}\psi_j(x)\,, \tag{B.3c}$$

where the complex phase η_C satisfies $|\eta_C|^2 = 1$. In order for the Lagrangian to be invariant under CPT, the same orthogonal transformation U must appear in both the generalized T transformation in Eq. (B.2c) and the generalized C transformation in eq. (B.3c). This orthogonal transformation U may be either a rotation [$\det(\mathsf{U}_+) = 1$] in flavor space or a combination of a rotation and a reflection [$\det(\mathsf{U}_-) = -1$], having the general form

$$\mathsf{U}_+ = \begin{pmatrix} \cos(\alpha) & -\sin(\alpha) \\ \sin(\alpha) & \cos(\alpha) \end{pmatrix} \qquad \text{or} \qquad \mathsf{U}_- = \begin{pmatrix} \cos(\alpha) & \sin(\alpha) \\ \sin(\alpha) & -\cos(\alpha) \end{pmatrix}. \tag{B.4}$$

The Lagrangian in Eq. (5.2) is invariant under C so long as we can find a phase η_C and transformation U such that the mass matrix M^2 and Yukawa couplings h_i satisfy

$$\mathsf{U}_{mi}\mathsf{M}^2_{mn}\mathsf{U}_{nj} = \mathsf{M}^2_{ij}\,, \tag{B.5a}$$
$$\eta_C^2\, U_{ki}\, h_k \;=\; h_i^*\,. \tag{B.5b}$$

In order to analyze the constraint on the Yukawa couplings provided by Eq. (B.5b), it is convenient to introduce the dyadic product $H_{ij} \equiv h_i h_j^*$. The second condition Eq. (B.5b) may then be recast in the more convenient form

$$\mathsf{U}_{mi}H_{mn}\mathsf{U}_{nj} = H^*_{ij}\,, \tag{B.6}$$

in which the phase η_C of the complex scalar field has been eliminated.

In the mass eigenbasis and if the two mass eigenvalues of the mass matrix are different, $M_1^2 \neq M_2^2$, the angle α has to be $\alpha = 0$ or π for both U_+ and U_- to fulfill Eq. (B.5a). This implies that for rotations the two flavors must transform with equal phases under C, i.e.,

$$\psi_1(x)^C = \pm\psi_1(x)\,, \qquad \psi_2(x)^C = \pm\psi_2(x)\,, \tag{B.7}$$

and correspondingly equal phases under T. C-invariance follows from Eq. (B.5b) if $H_{12} = H_{12}^*$, i.e., $\mathrm{Im}\, H_{12} = 0$.

On the other hand, for reflections we see that the two flavors must transform with opposite phases under C:

$$\psi_1(x)^C = \pm\psi_1(x)\,, \qquad \psi_2(x)^C = \mp\psi_2(x)\,, \tag{B.8}$$

and correspondingly opposite phases under T. On the other hand, if $\mathsf{U} = \mathsf{U}_-$, C-invariance follows if $H_{12} = -H_{12}^*$, i.e., $\mathrm{Re}\, H_{12} = 0$. Hence, for a *C*-conserving Lagrangian for non-degenerate masses, either the real part or the imaginary part of H_{12} has to vanish.

B.2 Initial conditions

In order to obtain *C*-symmetric dynamics, we also need to specify the initial conditions. They are of particular importance if the scalar field transforms like a reflection because $\mathrm{Im}\, H_{12}$ is not automatically zero and the produced asymmetry from the oscillations term depends on the initial conditions.

B.2.1 Heisenberg picture

For the initial conditions in the Heisenberg picture, we have to derive the properties of the Wightman propagators under *C*-conjugation. These properties can be obtained from their definition in the form

$$G^{ij}_{>}(x,y) = \mathrm{Tr}[\mathscr{P}\,\psi^i(x)\psi^j(y)]\,, \tag{B.9a}$$
$$G^{ij}_{<}(x,y) = \mathrm{Tr}[\mathscr{P}\,\psi^j(y)\psi^i(x)]\,, \tag{B.9b}$$

where $\mathscr{P}$ is the density matrix. For a *C*-symmetric background medium, the density matrix will transform trivially under *C*-transformation. The Wightman propagators then transform under generalized C-conjugation as

$$G^{ij}_{\gtrless}(x,y) \xrightarrow{C} \left[\mathsf{U}G_{\gtrless}(x,y)\mathsf{U}^T\right]^{ij}\,. \tag{B.10}$$

For the case of flavor rotations in the mass eigenbasis, U_+ is proportional to the identity matrix and the propagators are automatically C-symmetric. This is consistent with the fact that if $\mathrm{Im}\, H_{12} = 0$ then no asymmetry can be produced irrespective of the value of the propagators at the initial time surface.

On the other hand, for the case of flavor rotations with $\alpha = 0$ or π the propagators are *C*-symmetric only if their off-diagonals vanish at the initial time surface. Inserting this requirement into Eq. (5.49) yields

$$G^{12}_{\delta}(0,0) = -\int \mathrm{d}^4u\mathrm{d}^4v\ \left[G_R(0,u)\mathcal{K}(u,v)G_A(v,0)\right]^{12} = 0\,, \tag{B.11}$$

and consequently

$$\mathcal{K}^{12} = \mathcal{K}^{21} = -\,\frac{\mathcal{K}^{11}G^{11}_R(0)\,G^{12}_A(0) + \mathcal{K}^{22}\,G^{12}_R(0)G^{22}_A(0)}{G^{11}_R(0)\,G^{22}_A(0) + G^{12}_R(0)\,G^{12}_A(0)}\,, \tag{B.12}$$

where $0 = 0^+$ for the retarded and $0 = 0^-$ for the advanced propagator, and we used that the external source has the same properties as the one-loop self-energies, i.e., $\mathcal{K}^{12} = \mathcal{K}^{21}$ [118].

The properties of the propagators imply $G^{ij}_{\mathrm{A}}(0) = G^{ji}_R(0)$, and therefore it is sufficient to consider only the retarded propagator to evaluate Eq. (B.12). Integrating the explicit form of the Wigner transform in Eq. (5.56), the retarded propagator takes the form

$$G^{ij}_{\mathrm{R}}(0) = 2\int_0^\infty \frac{\mathrm{d}Q_0}{2\pi}\ \mathrm{Re}\, G^{ij}_{\mathrm{R}}(Q_0) \approx -2\ \mathrm{Im}\,\frac{1}{\Delta\Omega^2}\sum_{k=1}^{2}\frac{(-1)^k}{2\omega_k}[\mathrm{adj}D_{\mathrm{R}}(\omega_k)]^{ij}\,, \tag{B.13}$$

where we used the residue theorem to evaluate the integral approximately. Since $[\mathrm{adj}D_{\mathrm{R}}(\omega_k)]^{ij}$ is proportional to $\Pi_{\mathrm{R}}^{12} \propto \mathrm{Re}\, H_{12}$, it follows from this expression that $G_{\mathrm{R}}^{12} \propto \mathrm{Re}\, H_{12}$. Thus, we find $\mathcal{K}^{12} = \mathcal{K}^{21} \propto \mathrm{Re}\, H_{12}$, such that, a *C*-symmetric choice of the initial conditions corresponds to choosing $\mathrm{Re}\, H_{12} = 0$. All in all, we conclude that either $\mathrm{Im}\, H_{12} = 0$ or $\mathrm{Re}\, H_{12} = 0$ is sufficient for *C*-conserving dynamics if the initial conditions are *C*-symmetric.

B.2.2 Interaction picture

In the interaction picture, we may begin by fixing the transformation properties of the free field operators under generalized discrete symmetry transformations in Fock space directly [108]. The matrix of number densities is defined by

$$n_{ij} = \langle a_j^\dagger a_i \rangle = \mathrm{Tr}(\mathscr{P} a_j^\dagger a_i)\,. \tag{B.14}$$

As follows from Eq. (B.7), under rotations $a_1 \xrightarrow{C} \pm a_1$ and $a_2 \xrightarrow{C} \pm a_2$. The additional phase cancels in Eq. (B.14) and therefore the matrix of number densities is automatically *C*-symmetric. This is in agreement with the observation that once $\mathrm{Im}\, H_{12} = 0$ no asymmetry can be generated irrespective of the choice of the initial conditions. On the other hand, for reflections $a_1 \xrightarrow{C} \pm a_1$ and $a_2 \xrightarrow{C} \mp a_2$ such that the off-diagonals of n_{ij} acquire a relative sign. The condition of *C*-invariance therefore implies that the matrix of number densities must be diagonal at the initial time surface.

Appendix C

Asymmetry in the single-shell approximation

In Secs. 5.4 and 5.5, we have paid particular attention to the shell structure of the propagators of the real scalar. We found that in the calculation of the asymmetry one has to carefully keep track of all shells. Moreover, the consistency of the results in the Heisenberg and the interaction picture was reached after finding the temporal evolution of the number densities in Sec. 5.5.5, where we resorted again to the same shell structure. In this Appendix, we will show that in contrast to the calculation of the asymmetry, this distinction of different shells is not necessary for the solution of the transport equation in the quasi-degenerate regime. This single-shell approximation is commonly referred to as the density matrix approximation, where the approximation [112, 132]

$$G_<(t,Q) = n(t,\mathbf{Q})\, 2\pi\, \delta(Q^2 - \bar{M}^2)\,, \tag{C.1}$$

is introduced, i.e., all components of the Whightman propagator are evaluated at one common shell.

Performing a Wigner-transform of the Kadanoff-Baym equations [Eq. (5.44)] and neglecting gradients of the central spatial coordinate, one arrives at the following equation for the Wigner transform of the Wightman propagators [112]:

$$2Q_0\partial_t G_< + i\left[\mathsf{M}^2_{\rm th}, G_<\right] = \tfrac{1}{2}\left\{\Pi_>, G_<\right\} - \tfrac{1}{2}\left\{\Pi_<, G_>\right\}\,, \tag{C.2}$$

where the term $\mathrm{Re}\,\Pi_{\rm R}$ [see Eq. (5.126)] has been absorbed into the thermal mass matrix $\mathsf{M}^2_{\rm th}$.

Substituting Eq. (C.1) into Eq. (C.2) and integrating over Q_0, we arrive at

$$\partial_t n + \frac{i}{2\bar{\omega}}\Big[\mathsf{M}^2, n\Big] = \frac{1}{4\bar{\omega}}\Big\{\Pi_>, n\Big\} - \frac{1}{4\bar{\omega}}\Big\{\Pi_<, \mathbb{1} + n\Big\}\,. \tag{C.3}$$

This equation holds for the total number density, which still contains contributions from equilibrium. The static equilibrium solution fulfills

$$2i\Big[\mathsf{M}^2, n_{\rm eq}\Big] = \Big\{\Pi_>, n_{\rm eq}\Big\} - \Big\{\Pi_<, \mathbb{1} + n_{\rm eq}\Big\}\,, \tag{C.4}$$

which can be solved by invoking the Kubo-Martin-Schwinger relation (see e.g. Ref. [275]), which relates the equilibrium Wightman propagators

$$G_>(p) = e^{\beta p_0} G_<(p)\,. \tag{C.5}$$

A similar relation holds for the self-energies $\Pi_< = n_{\rm BE}\widetilde{\Pi}_\rho$ [276], where $n_{\rm BE}$ is the Bose-Einstein distribution function. Taking into account that $\widetilde{\Pi}_\rho = \Pi_> - \Pi_<$, we obtain that $n_{\rm eq} = \mathbb{1} \cdot n_{\rm BE}$ and the right-hand side of Eq. (C.4) vanishes because of detailed balance. The left-hand side automatically vanishes for diagonal number densities. Hence, the equilibrium solution is the expected equally distributed Bose-Einstein distribution.

The non-equilibrium part is $\delta n = n - n_{\rm eq}$, and it obeys the kinetic equation

$$\partial_t \delta n + \frac{i}{2\bar{\omega}}\Big[\mathsf{M}^2, \delta n\Big] = \frac{1}{4\bar{\omega}}\Big\{\widetilde{\Pi}_\rho, \delta n\Big\}\,. \tag{C.6}$$

Linearizing the mass dependence $\mathsf{M}^2_{ii} \to 2\bar{\omega}\Omega$ with the matrix of energies Ω and using that the spectral self-energies may be interpreted as effective decay widths

$$\mathsf{\Gamma} \equiv -\frac{\widetilde{\Pi}_\rho}{2\bar{\omega}} = \frac{i\Pi_\rho}{2\bar{\omega}}\,, \tag{C.7}$$

equation (C.6) becomes (cf. Ref. [112])

$$\partial_t \delta n + i\Big[\Omega, \delta n\Big] = -\tfrac{1}{2}\Big\{\mathsf{\Gamma}, \delta n\Big\}\,. \tag{C.8}$$

It can readily be checked by substitution that the solution to Eq. (C.8) for time-independent energies and self-energies is [112]

$$\delta n(t) = e^{-i\left(\Omega - \frac{i}{2}\mathsf{\Gamma}\right)t}\,\delta n(0)\,e^{i\left(\Omega + \frac{i}{2}\mathsf{\Gamma}\right)t}\,. \tag{C.9}$$

For general initial conditions and to first order in $\mathsf{\Gamma}^{12}$, Eq. (C.9) yields

$$\begin{aligned}
\delta n^{i\not{i}}(t) \approx\; & \delta n^{i\not{i}}(0)\,e^{-i(\omega_i-\omega_{\not{i}})t}\,e^{-\bar{\Gamma}t} \\
& + \frac{i}{2}\frac{\mathsf{\Gamma}^{i\not{i}}}{(\omega_i-\omega_{\not{i}}) + \frac{i}{2}(\Gamma_i - \Gamma_{\not{i}})}\,\delta n^{ii}(0)\Big(e^{-\Gamma_i t} - e^{-i(\omega_i-\omega_{\not{i}})t}e^{-\bar{\Gamma}t}\Big) \\
& + \frac{i}{2}\frac{\mathsf{\Gamma}^{i\not{i}}}{(\omega_i-\omega_{\not{i}}) + \frac{i}{2}(\Gamma_{\not{i}} - \Gamma_i)}\,\delta n^{\not{i}\not{i}}(0)\Big(e^{-\Gamma_{\not{i}} t} - e^{-i(\omega_i-\omega_{\not{i}})t}e^{-\bar{\Gamma}t}\Big)\,.
\end{aligned} \tag{C.10}$$

Neglecting the decay width in the denominator and using the definition of the decay widths in Eq. (C.7), we arrive at

$$\begin{aligned}
\delta n^{i\not{i}}(t) \;\approx\; & \delta n^{i\not{i}}(0)\,e^{-i(\omega_i-\omega_{\not{i}})t}\,e^{-\bar{\Gamma}t} \\
& - \frac{i}{2}\frac{\widetilde{\Pi}^{i\not{i}}_\rho}{\Delta M^2_{i\not{i}}}\,\delta n^{ii}(0)\Big(e^{-\Gamma_i t} - e^{-i(\omega_i-\omega_{\not{i}})t}e^{-\bar{\Gamma}t}\Big) \\
& - \frac{i}{2}\frac{\widetilde{\Pi}^{i\not{i}}_\rho}{\Delta M^2_{i\not{i}}}\,\delta n^{\not{i}\not{i}}(0)\Big(e^{-\Gamma_{\not{i}} t} - e^{-i(\omega_i-\omega_{\not{i}})t}e^{-\bar{\Gamma}t}\Big)\,.
\end{aligned} \tag{C.11}$$

which is identical to Eq. (5.137) with the shells approximated by the middle shell. For an almost degenerate mass spectrum, we therefore find that one can safely use the density matrix equations to compute the number density of the real scalars.

Appendix D

Mean transfer function: an example

To illustrate Eq. (3.40), we show the calculation of the first diagonal term of the purely dispersive contribution to the matrix $\langle \mathsf{U}\,\bar{\rho}\,\mathsf{U}^\dagger\rangle_{\phi,\theta} - \bar{\rho}$ in detail. The dispersive contribution reads

$$l_\mathrm{c}\partial_z\bar{\rho} = \langle \mathsf{O}^T\mathsf{U}_\mathrm{dis}\mathsf{O}\bar{\rho}\mathsf{O}^T\mathsf{U}_\mathrm{dis}\mathsf{O}\rangle - \bar{\rho} \qquad \text{(dispersion only)} \tag{D.1}$$

where U_dis is defined in the $\phi = 0$ frame (cf. Eq. (3.23))

$$\begin{aligned}\mathsf{U}_\mathrm{dis}(l_\mathrm{c}) =& \exp\!\left(-i\mathsf{H}_\mathrm{dis}l_\mathrm{c}\right)\\ =& e^{-i\frac{(\Delta_a+\Delta_\parallel)l_\mathrm{c}}{2}}\begin{pmatrix} e^{-i(\delta-\Delta_{a\gamma}/2)l_\mathrm{c}} & 0 & 0\\ 0 & c_\varphi^2 e^{-i\frac{\Delta_\mathrm{osc}l_\mathrm{c}}{2}} + s_\varphi^2 e^{i\frac{\Delta_\mathrm{osc}l_\mathrm{c}}{2}} & is_{2\varphi}\sin\frac{\Delta_\mathrm{osc}l_\mathrm{c}}{2}\\ 0 & is_{2\varphi}\sin\frac{\Delta_\mathrm{osc}l_\mathrm{c}}{2} & c_\varphi^2 e^{i\frac{\Delta_\mathrm{osc}l_\mathrm{c}}{2}} + s_\varphi^2 e^{-i\frac{\Delta_\mathrm{osc}l_\mathrm{c}}{2}}\end{pmatrix},\end{aligned} \tag{D.2}$$

which is then rotated to a general frame by O

$$\mathsf{O} = \begin{pmatrix} c_\phi & -s_\phi & 0\\ s_\phi & c_\phi & 0\\ 0 & 0 & 1\end{pmatrix}. \tag{D.3}$$

As an example we show the first diagonal entry order according to their dependence on ϕ before the averaging is performed

$$\begin{aligned}(\mathsf{O}^T\mathsf{U}_\mathrm{dis}\mathsf{O}\bar{\rho}\mathsf{O}^T\mathsf{U}_\mathrm{dis}\mathsf{O})_{11} =& c_\phi^4\rho_{11} + 2c_\phi^2 s_\phi^2 f_1 + s_\phi^4 f_2 + c_\phi^3 s_\phi f_3 - c_\phi^2 s_\phi^2 f_4\\ &+2s_\phi^3 f_5 + 2c_\phi^2 s_\phi f_6 + c_\phi s_\phi^3 f_7 + c_\phi s_\phi^2 + 2s_\phi^2 f_9\,,\end{aligned} \tag{D.4}$$

where after averaging over ϕ only the following functions f survive:

$$\begin{aligned} f_1 &= \rho_{11}\left(\cos\left[\frac{1}{2}l_\mathrm{c}(\Delta_\mathrm{osc}+\delta_1)\right]c_\varphi^2 + \cos\left[\frac{1}{2}l_\mathrm{c}(-\Delta_\mathrm{osc}+\delta_1)\right]s_\varphi^2\right),\\ f_2 &= \rho_{11}\left(c_\varphi^4 + 2\cos[l_\mathrm{c}\Delta_\mathrm{osc}]c_\varphi^2 s_\varphi^2 + s_\varphi^4\right),\\ f_4 &= \left(-1 + 2\cos\left[\frac{1}{2}l(\Delta_\mathrm{osc}+\delta_1)\right]c_\varphi^2 - c_\varphi^4\right.\\ &\qquad \left. + 2\left(\cos\left[\frac{1}{2}l(-\Delta_\mathrm{osc}+\delta_1)\right] - \cos[l\Delta_\mathrm{osc}]c_\varphi^2\right)s_\varphi^2 - s_\varphi^4\right)\rho_{22}\,,\\ f_9 &= (1-\cos[l\Delta_\mathrm{osc}])c_\varphi^2 s_\varphi^2\rho_{33}\,, \end{aligned} \tag{D.5}$$

with $\delta_1 = \Delta_a + \Delta_\parallel - 2\Delta_\perp$. We obtain

$$\begin{aligned}
&(\mathsf{O}^T\mathsf{U}_{\rm dis}\mathsf{O}\bar{\rho}\mathsf{O}^T\mathsf{U}_{\rm dis}\mathsf{O})_{11} = \\
&\frac{3}{8}\rho_{11} + \frac{1}{4}\left(\cos\left[\frac{1}{2}l_{\rm c}(\Delta_{\rm osc}+\delta_1)\right]c_\varphi^2 + \cos\left[\frac{1}{2}l_{\rm c}(-\Delta_{\rm osc}+\delta_1)\right]s_\varphi^2\right)\rho_{11} \\
+&\frac{3}{8}\left(c_\varphi^4 + 2\cos[l_{\rm c}\Delta_{\rm osc}]c_\varphi^2 s_\varphi^2 + s_\varphi^4\right)\rho_{11} + (1-\cos[l_{\rm c}\Delta_{\rm osc}])c_\varphi^2 s_\varphi^2\rho_{33} \\
+&\rho_{22}\left\{\frac{7+c_{4\varphi}}{32} - \frac{1}{4}\cos\left[\frac{1}{2}l_{\rm c}(\Delta_{\rm osc}+\delta_1)\right]c_\varphi^2\right. \\
&\qquad\left. - \frac{1}{4}\left(\cos\left[\frac{1}{2}l_{\rm c}(-\Delta_{\rm osc}+\delta_1)\right] - \cos[l_{\rm c}\Delta_{\rm osc}]c_\varphi^2\right)s_\varphi^2\right\}.
\end{aligned} \tag{D.6}$$

The 22 component will look identical when $\rho_{11} \leftrightarrow \rho_{22}$. Adding these contributions and subtracting $\rho_{11} + \rho_{22}$, we obtain

$$\begin{aligned}
l_{\rm c}\partial_z\left(\rho_{11}+\rho_{22}\right) &= -\frac{1}{2}\left(\rho_{11}+\rho_{22}-2\rho_{33}\right)\sin\left(2\varphi\right)^2\sin\left(\frac{\Delta_{\rm osc}l_{\rm c}}{2}\right)^2 \qquad \text{(dispersion only)} \\
&= -P_{a\gamma}\left(\frac{T_\gamma}{2} - T_a\right),
\end{aligned} \tag{D.7}$$

which has to be averaged over the residual degrees of freedom of the magnetic field to give the dispersive part of Eq. (3.40).

Bibliography

[1] A. Kartavtsev, G. Raffelt, and H. Vogel, Separation of scales in photon-ALP oscillations (in preparation).

[2] A. Kartavtsev, G. Raffelt, and H. Vogel, Neutrino propagation in media: flavor, helicity, and pair correlations, *Phys. Rev. D* **91** (2015) 125020, arXiv:1504.03230.

[3] A. Kartavtsev, P. Millington, and H. Vogel, Lepton asymmetry from mixing and oscillations, *accepted by JHEP* (2016), arXiv:1601.03086.

[4] H. Vogel and J. Redondo, Dark radiation constraints on minicharged particles in models with a hidden photon, *JCAP* **1402** (2014) 029, arXiv:1311.2600.

[5] N. Vinyoles and H. Vogel, Minicharged particles from the Sun: a cutting-edge bound, *JCAP* **1603** (2016) 002, arXiv:1511.01122.

[6] V. Springel et al., Simulating the joint evolution of quasars, galaxies and their large-scale distribution, *Nature* **435** (2005) 629–636, arXiv:astro-ph/0504097.

[7] E. W. Kolb and M. S. Turner, *The early universe*, Westview Press, 1990.

[8] B. W. Lee and S. Weinberg, Cosmological lower bound on heavy neutrino masses, *Phys. Rev. Lett.* **39** (1977) 165–168.

[9] G. Steigman, Observational tests of antimatter cosmologies, *Ann. Rev. Astron. Astrophys.* **14** (1976) 339–372.

[10] K. A. Olive et al., Review of particle physics, *Chin. Phys. C* **38** (2014) 090001.

[11] A. D. Sakharov, Violation of CP invariance, C asymmetry, and baryon asymmetry of the universe, *JETP Letters* **5** (1967) 24–27.

[12] A. D. Dolgov, NonGUT baryogenesis, *Phys. Rept.* **222** (1992) 309–386.

[13] R. V. Wagoner, W. A. Fowler, and F. Hoyle, On the synthesis of elements at very high temperatures, *Astrophys. J.* **148** (1967) 3–49.

[14] R. V. Wagoner, Big bang nucleosynthesis revisited, *Astrophys. J.* **179** (1973) 343–360.

[15] R. Kippenhahn, A. Weigert, and A. Weiss, *Stellar Structure and Evolution*, Springer-Verlag, 2012.

[16] J. N. Bahcall, *Neutrino astrophysics*, Cambridge University Press, 1989.

[17] M. S. Longair, *High energy astrophysics*, Cambridge University Press, 2011.

[18] R. Schlickeiser, *Cosmic ray astrophysics*, Springer-Verlag, 2003.

[19] L. Boltzmann, *Vorlesungen über Gastheorie*, Publishing House of Johann Ambrosius Barth, 1910.

[20] E. A. Calzetta and B. B. Hu, *Nonequilibrium quantum field theory*, Cambridge University Press, 2008.

[21] E. P. Wigner, On the quantum correction for thermodynamic equilibrium, *Phys. Rev.* **40** (1932) 749–760.

[22] J. E. Moyal, Quantum mechanics as a statistical theory, *Proc. Cambridge Phil. Soc.* **45** (1949) 99–124.

[23] J. Bernstein, *Kinetic theory in the expanding universe*, Cambridge University Press, 1988.

[24] W. Israel, The relativistic Boltzmann equation, in: *General relativity*, **1**, 1972 pp. 201–241.

[25] Y. Abe et al., On stochastic approaches of nuclear dynamics, *Phys. Rept.* **275** (1996) 49–196.

[26] G. Sigl and G. Raffelt, General kinetic description of relativistic mixed neutrinos, *Nucl. Phys. B* **406** (1993) 423–451.

[27] C. Volpe, D. Väänänen, and C. Espinoza, Extended evolution equations for neutrino propagation in astrophysical and cosmological environments, *Phys. Rev. D* **87** (2013) 113010, arXiv:1302.2374.

[28] N. Bogolubov, Expansions into a series of powers of a small parameter in the theory of statistical equilibrium, *Journal of Physics* **10** (1946) 257–264 and 265.

[29] M. Born and H. Green, A general kinetic theory of liquids. I. The molecular distribution functions, in: *Proceedings of the Royal Society of London A: Mathematical, Physical and Engineering Sciences*, **188**, The Royal Society, 1946 pp. 10–18.

[30] J. G. Kirkwood, Statistical mechanics of fluid mixtures, *The Journal of Chemical Physics* **3** (1935) 300–313.

[31] J. Yvon, *La théorie statistique des fluides et l'équation d'état*, Hermann & cie, 1935.

[32] X.-G. Wen, *Quantum field theory of many-body systems*, Citeseer, 2004.

[33] G. C. Branco et al., Theory and phenomenology of two-Higgs-doublet models, *Phys. Rept.* **516** (2012) 1–102, arXiv:1106.0034.

[34] S. P. Martin, A supersymmetry primer, *Adv. Ser. Direct. High Energy Phys.* **18** (1998) 1, arXiv:hep-ph/9709356.

[35] A. Palazzo, Phenomenology of light sterile neutrinos: a brief review, *Mod. Phys. Lett. A* **28** (2013) 1330004, arXiv:1302.1102.

[36] T. Asaka and M. Shaposhnikov, The nuMSM, dark matter and baryon asymmetry of the universe, *Phys. Lett. B* **620** (2005) 17–26, arXiv:hep-ph/0505013.

[37] P. Galison and A. Manohar, Two Z's or not two Z's? *Phys. Lett. B* **136** (1984) 279–283.

[38] R. D. Peccei and H. R. Quinn, CP conservation in the presence of instantons, *Phys. Rev. Lett.* **38** (1977) 1440–1443.

[39] R. D. Peccei and H. R. Quinn, Constraints imposed by CP conservation in the presence of instantons, *Phys. Rev. D* **16** (1977) 1791–1797.

[40] S. Weinberg, A new light boson? *Phys. Rev. Lett.* **40** (1978) 223–226.

[41] F. Wilczek, Problem of strong P and T invariance in the presence of instantons, *Phys. Rev. Lett.* **40** (1978) 279–282.

[42] C. A. Baker et al., An Improved experimental limit on the electric dipole moment of the neutron, *Phys. Rev. Lett.* **97** (2006) 131801, arXiv:hep-ex/0602020.

[43] J. M. Pendlebury et al., Revised experimental upper limit on the electric dipole moment of the neutron, *Phys. Rev. D* **92** (2015) 092003, arXiv:1509.04411.

[44] M. Kuster, G. Raffelt, and B. Beltrán, *Axions: Theory, cosmology, and experimental searches*, Springer-Verlag, 2007.

[45] P. Sikivie, Experimental tests of the invisible axion, *Phys. Rev. Lett.* **51** (1983), 1415-1417 [Erratum: *Phys. Rev. Lett.* **52** (1984) 695].

[46] C. Hagmann et al., Results from a high sensitivity search for cosmic axions, *Phys. Rev. Lett.* **80** (1998) 2043–2046, arXiv:astro-ph/9801286.

[47] K. Ehret et al., Production and detection of axion-like particles in a HERA dipole magnet: Letter-of-intent for the ALPS experiment (2007), arXiv:hep-ex/0702023.

[48] R. Bähre et al., Any light particle search II —Technical Design Report, *JINST* **8** (2013) T09001, arXiv:1302.5647.

[49] S. Andriamonje et al., An improved limit on the axion-photon coupling from the CAST experiment, *JCAP* **0704** (2007) 010, arXiv:hep-ex/0702006.

[50] I. G. Irastorza et al., Towards a new generation axion helioscope, *JCAP* **1106** (2011) 013, arXiv:1103.5334.

[51] A. J. Millar et al., Layered dielectric haloscope: a new way to detect axion dark matter (in preparation).

[52] S. Furlanetto and A. Loeb, Intergalactic magnetic fields from quasar outflows, *Astrophys. J.* **556** (2001) 619, arXiv:astro-ph/0102076.

[53] R. Durrer and A. Neronov, Cosmological magnetic fields: their generation, eolution and observation, *Astron. Astrophys. Rev.* **21** (2013) 62, arXiv:1303.7121.

[54] A. G. Dias et al., The quest for an intermediate-scale accidental axion and further ALPs, *JHEP* **06** (2014) 037, arXiv:1403.5760.

[55] E. D. Carlson and W. D. Garretson, Photon to pseudoscalar conversion in the interstellar medium, *Phys. Lett. B* **336** (1994) 431–438.

[56] A. De Angelis, M. Roncadelli, and O. Mansutti, Evidence for a new light spin-zero boson from cosmological gamma-ray propagation? *Phys. Rev. D* **76** (2007) 121301, arXiv:0707.4312.

[57] A. De Angelis et al., Photon propagation and the VHE gamma-ray spectra of blazars: how transparent is really the universe? *Mon. Not. Roy. Astron. Soc.* **394** (2009) L21–L25, arXiv:0807.4246.

[58] G. Galanti et al., Advantages of axion-like particles for the description of very-high-energy blazar spectra (2015), arXiv:1503.04436.

[59] A. Dobrynina, A. Kartavtsev, and G. Raffelt, Photon-photon dispersion of TeV gamma rays and its role for photon-ALP conversion, *Phys. Rev. D* **91** (2015) 083003, arXiv:1412.4777.

[60] W. Heisenberg and H. Euler, Consequences of Dirac's theory of positrons, *Z. Phys.* **98** (1936) 714–732, arXiv:physics/0605038.

[61] A. Mirizzi et al., Supernova neutrinos: production, oscillations and detection, *Riv. Nuovo Cim.* **39** (2016) 1, arXiv:1508.00785.

[62] T. Melson et al., Neutrino-driven explosion of a 20 solar-mass star in three dimensions enabled by strange-quark contributions to neutrino-nucleon scattering, *Astrophys. J.* **808** (2015) L42, arXiv:1504.07631.

[63] G. G. Raffelt, *Stars as laboratories for fundamental physics*, Chicago University Press, 1996.

[64] S. P. Mikheev and A. Yu. Smirnov, Resonance amplification of oscillations in matter and spectroscopy of solar neutrinos, *Sov. J. Nucl. Phys.* **42** (1985), 913-917 [*Yad. Fiz.* **42** (1985) 1441].

[65] L. Wolfenstein, Neutrino oscillations in matter, *Phys. Rev. D* **17** (1978) 2369–2374.

[66] J. T. Pantaleone, Neutrino oscillations at high densities, *Phys. Lett. B* **287** (1992) 128–132.

[67] S. Samuel, Neutrino oscillations in dense neutrino gases, *Phys. Rev. D* **48** (1993) 1462–1477.

[68] J. T. Pantaleone, Neutrino flavor evolution near a supernova's core, *Phys. Lett. B* **342** (1995) 250–256, arXiv:astro-ph/9405008.

[69] R. F. Sawyer, Speed-up of neutrino transformations in a supernova environment, *Phys. Rev. D* **72** (2005) 045003, arXiv:hep-ph/0503013.

[70] H. Duan et al., Simulation of coherent non-linear neutrino flavor transformation in the supernova environment. 1. correlated neutrino trajectories, *Phys. Rev. D* **74** (2006) 105014, arXiv:astro-ph/0606616.

[71] S. Hannestad et al., Self-induced conversion in dense neutrino gases: pendulum in flavour space, *Phys. Rev. D* **74** (2006), 105010 [Erratum: *Phys. Rev. D* **76** (2007) 029901], arXiv:astro-ph/0608695.

[72] A. B. Balantekin and Y. Pehlivan, Neutrino-neutrino interactions and flavor mixing in dense matter, *J. Phys. G* **34** (2007) 47–66, arXiv:astro-ph/0607527.

[73] B. Dasgupta et al., Multiple spectral splits of supernova neutrinos, *Phys. Rev. Lett.* **103** (2009) 051105, arXiv:0904.3542.

[74] H. Duan, G. M. Fuller, and Y.-Z. Qian, Collective neutrino oscillations, *Ann. Rev. Nucl. Part. Sci.* **60** (2010) 569–594, arXiv:1001.2799.

[75] A. Friedland, Self-refraction of supernova neutrinos: mixed spectra and three-flavor instabilities, *Phys. Rev. Lett.* **104** (2010) 191102, arXiv:1001.0996.

[76] A. Banerjee, A. Dighe, and G. Raffelt, Linearized flavor-stability analysis of dense neutrino streams, *Phys. Rev. D* **84** (2011) 053013, arXiv:1107.2308.

[77] S. Galais and C. Volpe, The neutrino spectral split in core-collapse supernovae: a magnetic resonance phenomenon, *Phys. Rev. D* **84** (2011) 085005, arXiv:1103.5302.

[78] Y. Pehlivan et al., Invariants of collective neutrino oscillations, *Phys. Rev. D* **84** (2011) 065008, arXiv:1105.1182.

[79] G. G. Raffelt, N-mode coherence in collective neutrino oscillations, *Phys. Rev. D* **83** (2011) 105022, arXiv:1103.2891.

[80] J. F. Cherry et al., Neutrino scattering and flavor transformation in supernovae, *Phys. Rev. Lett.* **108** (2012) 261104, arXiv:1203.1607.

[81] A. de Gouvea and S. Shalgar, Effect of transition magnetic moments on collective supernova neutrino oscillations, *JCAP* **1210** (2012) 027, arXiv:1207.0516.

[82] G. Raffelt, S. Sarikas, and D. de Sousa Seixas, Axial symmetry breaking in self-induced flavor conversion of supernova neutrino fluxes, *Phys. Rev. Lett.* **111** (2013), 091101 [Erratum: *Phys. Rev. Lett.* **113** (2014) 239903], arXiv:1305.7140.

[83] H. Duan and S. Shalgar, Flavor instabilities in the neutrino line model, *Phys. Lett. B* **747** (2015) 139–143, arXiv:1412.7097.

[84] A. Mirizzi, G. Mangano, and N. Saviano, Self-induced flavor instabilities of a dense neutrino stream in a two-dimensional model, *Phys. Rev. D* **92** (2015) 021702, arXiv:1503.03485.

[85] A. Vlasenko, G. M. Fuller, and V. Cirigliano, Neutrino quantum kinetics, *Phys. Rev. D* **89** (2014) 105004, arXiv:1309.2628.

[86] V. Cirigliano, G. M. Fuller, and A. Vlasenko, A new spin on neutrino quantum kinetics, *Phys. Lett. B* **747** (2015) 27–35, arXiv:1406.5558.

[87] A. Vlasenko, G. M. Fuller, and V. Cirigliano, Prospects for neutrino-antineutrino transformation in astrophysical environments (2014), arXiv:1406.6724.

[88] C. Volpe, D. Väänänen, and C. Espinoza, Extended evolution equations for neutrino propagation in astrophysical and cosmological environments, *Phys. Rev.* **D87** (2013) 113010, arXiv:1302.2374.

[89] D. Väänänen and C. Volpe, Linearizing neutrino evolution equations including neutrino-antineutrino pairing correlations, *Phys. Rev. D* **88** (2013) 065003, arXiv:1306.6372.

[90] J. Serreau and C. Volpe, Neutrino-antineutrino correlations in dense anisotropic media, *Phys. Rev. D* **90** (2014) 125040, arXiv:1409.3591.

[91] J. S. Schwinger, Brownian motion of a quantum oscillator, *J. Math. Phys.* **2** (1961) 407–432.

[92] L. V. Keldysh, Diagram technique for nonequilibrium processes, *Zh. Eksp. Teor. Fiz.* **47** (1964) 1515–1527.

[93] G. Baym and L. P. Kadanoff, Conservation laws and correlation functions, *Phys. Rev.* **124** (1961) 287–299.

[94] L. P. Kadanoff and G. Baym, *Quantum statistical mechanics*, Benjamin, New York, 1962.

[95] S. Weinberg, *Cosmology*, Oxford University Press, 2008.

[96] S. Davidson, E. Nardi, and Y. Nir, Leptogenesis, *Phys. Rept.* **466** (2008) 105, arXiv:0802.2962.

[97] M. Fukugita and T. Yanagida, Baryogenesis without Grand Unification, *Phys. Lett. B* **174** (1986) 45.

[98] F. R. Klinkhamer and N. S. Manton, A saddle-point solution in the Weinberg-Salam theory, *Phys. Rev. D* **30** (10 1984) 2212–2220.

[99] P. Minkowski, $\mu \to e\gamma$ at a rate of one out of 10^9 muon decays? *Phys. Lett. B* **67** (1977) 421–428.

[100] M. Gell-Mann, P. Ramond, and R. Slansky, Complex spinors and unified theories, in: *Supergravity Workshop Stony Brook*, 1979, arXiv:1306.4669.

[101] T. Yanagida, Horizontal symmetry and masses of neutrinos, in: *Workshop on the Unified Theories and the Baryon Number in the Universe*, 1979.

[102] R. N. Mohapatra and G. Senjanovic, Neutrino mass and spontaneous parity violation, *Phys. Rev. Lett.* **44** (1980) 912.

[103] A. Pilaftsis, Heavy Majorana neutrinos and baryogenesis, *Int. J. Mod. Phys. A* **14** (1999) 1811–1858, arXiv:hep-ph/9812256.

[104] W. Buchmüller, P. Di Bari, and M. Plümacher, Leptogenesis for pedestrians, *Ann. Phys.* **315** (2005) 305–351, arXiv:hep-ph/0401240.

[105] A. Pilaftsis, Resonant CP violation induced by particle mixing in transition amplitudes, *Nucl. Phys. B* **504** (1997) 61–107, arXiv:hep-ph/9702393.

[106] A. Pilaftsis, CP violation and baryogenesis due to heavy Majorana neutrinos, *Phys. Rev. D* **56** (1997) 5431–5451, arXiv:hep-ph/9707235.

[107] A. Pilaftsis and T. E. J. Underwood, Resonant leptogenesis, *Nucl. Phys. B* **692** (2004) 303–345, arXiv:hep-ph/0309342.

[108] P. S. Bhupal Dev et al., Flavour covariant transport equations: an application to resonant leptogenesis, *Nucl. Phys. B* **886** (2014) 569–664, arXiv:1404.1003.

[109] P. S. B. Dev et al., Corrigendum to "Flavour covariant transport equations: an application to resonant leptogenesis", *Nucl. Phys. B* **897** (2015) 749–756, arXiv:1504.07640.

[110] P. S. Bhupal Dev et al., Kadanoff-Baym approach to flavour mixing and oscillations in resonant leptogenesis, *Nucl. Phys. B* **891** (2015) 128–158, arXiv:1410.6434.

[111] P. S. Bhupal Dev et al., Flavour effects in resonant leptogenesis from semi-classical and Kadanoff-Baym approaches, in: *4th Symposium on Prospects in the Physics of Discrete Symmetries 2014*, 2015, arXiv:1502.07987.

[112] B. Garbrecht and M. Herranen, Effective theory of resonant leptogenesis in the closed-time-path approach, *Nucl. Phys. B* **861** (2012) 17–52, arXiv:1112.5954.

[113] B. Garbrecht, F. Gautier, and J. Klaric, Strong washout approximation to resonant leptogenesis, *JCAP* **1409** (2014) 033, arXiv:1406.4190.

[114] H. A. Weldon, Thermalization of boson propagators in finite temperature field theory, *Phys. Rev. D* **45** (1992) 352–355.

[115] T. Altherr and D. Seibert, Problems of perturbation series in nonequilibrium quantum field theories, *Phys. Lett. B* **333** (1994) 149–152, arXiv:hep-ph/9405396.

[116] T. Altherr, Resummation of perturbation series in nonequilibrium scalar field theory, *Phys. Lett. B* **341** (1995) 325–331, arXiv:hep-ph/9407249.

[117] I. Dadic, Two mechanisms for elimination of pinch singularities in / out of equilibrium thermal field theories, *Phys. Rev. D* **59** (1999) 125012, arXiv:hep-ph/9801399.

[118] P. Millington and A. Pilaftsis, Perturbative nonequilibrium thermal field theory, *Phys. Rev. D* **88** (2013) 085009, arXiv:1211.3152.

[119] R. D. Present, *Kinetic theory of gases*, McGraw-Hill, 1958.

[120] H. Vogel and J. Redondo, Dark radiation from a hidden U(1), in: *AXION-WIMP 2014*, 2015, arXiv:1504.06222.

[121] O. Pisanti et al., PArthENoPE: Public Algorithm Evaluating the Nucleosynthesis of Primordial Elements, *Comput. Phys. Commun.* **178** (2008) 956–971, arXiv:0705.0290.

[122] M. E. Peskin and D. V. Schroeder, *An introduction to quantum field theory*, Addison-Wesley, 1995.

[123] M. A. Rudzsky, Kinetic equations for neutrino spin- and type-oscillations in a medium, *Astrophys. Space Sci.* **165** (1990) 465.

[124] K.-c. Chou et al., Equilibrium and nonequilibrium formalisms made unified, *Phys. Rept.* **118** (1985) 1.

[125] E. Calzetta and B. L. Hu, Nonequilibrium quantum fields: closed time path effective action, Wigner function and Boltzmann equation, *Phys. Rev. D* **37** (1988) 2878.

[126] P. Millington and A. Pilaftsis, Perturbative non-equilibrium thermal field theory to all orders in gradient expansion, *Phys. Lett. B* **724** (2013) 56–62, arXiv:1304.7249.

[127] J.-P. Blaizot and E. Iancu, The quark-gluon plasma: collective dynamics and hard thermal loops, *Phys. Rept.* **359** (2002) 355–528, arXiv:hep-ph/0101103.

[128] J. Berges, Introduction to nonequilibrium quantum field theory, *AIP Conf. Proc.* **739** (2004) 3–62, arXiv:hep-ph/0409233.

[129] J. M. Cornwall, R. Jackiw, and E. Tomboulis, Effective action for composite operators, *Phys. Rev. D* **10** (1974) 2428–2445.

[130] T. Prokopec, M. G. Schmidt, and S. Weinstock, Transport equations for chiral fermions to order h-bar and electroweak baryogenesis, *Ann. Phys.* **314** (2004) 208–265, arXiv:hep-ph/0312110.

[131] B. Garbrecht and M. Garny, Finite width in out-of-equilibrium propagators and kinetic theory, *Annals Phys.* **327** (2012) 914–934, arXiv:1108.3688.

[132] V. Cirigliano et al., Flavored quantum Boltzmann equations, *Phys. Rev. D* **81** (2010) 103503, arXiv:0912.3523.

[133] T. M. Kneiske and H. Dole, A lower-limit flux for the extragalactic background light, *Astron. Astrophys.* **515** (2010) A19, arXiv:1001.2132.

[134] F. Aharonian et al., A Low level of extragalactic background light as revealed by gamma-rays from blazars, *Nature* **440** (2006) 1018–1021, arXiv:astro-ph/0508073.

[135] D. Mazin and M. Raue, New limits on the density of the extragalactic background light in the optical to the far-infrared from the spectra of all known TeV blazars, *Astron. Astrophys.* **471** (2007) 439–452, arXiv:astro-ph/0701694.

[136] E. Aliu et al., Very-high-energy gamma rays from a distant quasar: how transparent is the universe? *Science* **320** (2008) 1752, arXiv:0807.2822.

[137] A. V. Belikov, L. Goodenough, and D. Hooper, No indications of axion-like particles from Fermi, *Phys. Rev. D* **83** (2011) 063005, arXiv:1007.4862.

[138] A. Abramowski et al., Measurement of the extragalactic background light imprint on the spectra of the brightest blazars observed with H.E.S.S, *Astron. Astrophys.* **550** (2013) A4, arXiv:1212.3409.

[139] M. Ackermann et al., The imprint of the extragalactic background light in the gamma-ray spectra of blazars, *Science* **338** (2012) 1190–1192, arXiv:1211.1671.

[140] M. Meyer et al., Limits on the extragalactic background light in the Fermi era, *Astronomy and Astrophysics* **542**, A59 (2012) A59, arXiv:1202.2867.

[141] J. Biteau and D. A. Williams, The extragalactic background light, the Hubble constant, and anomalies: conclusions from 20 years of TeV gamma-ray observations, *Astrophys. J.* **812** (2015) 60, arXiv:1502.04166.

[142] T. Matsumoto et al., IRTS observation of the near-infrared extragalactic background light, *Astrophys. J.* **626** (2005) 31–43, arXiv:astro-ph/0411593.

[143] F. Krennrich, E. Dwek, and A. Imran, Constraints to energy spectra of blazars based on recent EBL limits from galaxy counts, *Astrophys. J.* **689** (2008) L93, arXiv:0810.2522.

[144] F. A. Aharonian, A. N. Timokhin, and A. V. Plyasheshnikov, On the origin of highest energy gamma-rays from Mkn 501, *Astron. Astrophys.* **384** (2002) 834, arXiv:astro-ph/0108419.

[145] A. Dominguez, M. A. Sanchez-Conde, and F. Prada, Axion-like particle imprint in cosmological very-high-energy sources, *JCAP* **1111** (2011) 020, arXiv:1106.1860.

[146] J. Aleksic et al., MAGIC discovery of VHE Emission from the FSRQ PKS 1222+21, *Astrophys. J.* **730** (2011) L8, arXiv:1101.4645.

[147] G. I. Rubtsov and S. V. Troitsky, Breaks in gamma-ray spectra of distant blazars and transparency of the universe, *JETP Lett.* **100** (2014), 397-401 [*JETP Lett.* **100** (2014) 355], arXiv:1406.0239.

[148] E. Dwek and F. Krennrich, Simultaneous constraints on the spectrum of the extragalactic background light and the intrinsic TeV spectra of Mrk 421, Mrk 501, and H1426+428, *Astrophys. J.* **618** (2005) 657–674, arXiv:astro-ph/0406565.

[149] F. Tavecchio et al., On the origin of the gamma-ray emission from the flaring blazar PKS 1222+216, *Astron. Astrophys.* **534** (2011) A86, arXiv:1104.0048.

[150] D. Horns and M. Meyer, Indications for a pair-production anomaly from the propagation of VHE gamma-rays, *JCAP* **1202** (2012) 033, arXiv:1201.4711.

[151] A. Reimer, The redshift dependence of gamma-ray absorption in the environments of strong-line AGNs, *Astrophys. J.* **665** (2007) 1023–1029, arXiv:0705.1534.

[152] U. Jacob and T. Piran, Inspecting absorption in the spectra of extra-galactic gamma-ray sources for insight on Lorentz invariance violation, *Phys. Rev. D* **78** (2008) 124010, arXiv:0810.1318.

[153] W. Essey and A. Kusenko, A new interpretation of the gamma-ray observations of distant active galactic nuclei, *Astroparticle Physics* **33** (2010) 81–85.

[154] W. Essey and A. Kusenko, On weak redshift dependence of gamma-ray spectra of distant blazars, *Astrophys. J.* **751** (2012) L11, arXiv:1111.0815.

[155] A. Mirizzi, G. G. Raffelt, and P. D. Serpico, Signatures of axion-like particles in the spectra of TeV gamma-ray sources, *Phys. Rev. D* **76** (2007) 023001, arXiv:0704.3044.

[156] D. Hooper and P. D. Serpico, Detecting axion-like particles with gamma ray telescopes, *Phys. Rev. Lett.* **99** (2007) 231102, arXiv:0706.3203.

[157] K. A. Hochmuth and G. Sigl, Effects of axion-photon mixing on gamma-ray spectra from magnetized astrophysical sources, *Phys. Rev. D* **76** (2007) 123011, arXiv:0708.1144.

[158] O. Mena and S. Razzaque, Hints of an axion-like particle mixing in the GeV gamma-rayblazar data? *JCAP* **1311** (2013) 023, arXiv:1306.5865.

[159] M. Simet, D. Hooper, and P. D. Serpico, The Milky Way as a kiloparsec-scale axionscope, *Phys. Rev. D* **77** (2008) 063001, arXiv:0712.2825.

[160] M. Yoshimura, Resonant axion - photon conversion in magnetized plasma, *Phys. Rev. D* **37** (1988) 2039.

[161] N. Bassan and M. Roncadelli, Photon-axion conversion in active galactic nuclei? (2009), arXiv:0905.3752.

[162] M. A. Sanchez-Conde et al., Hints of the existence of axion-like-particles from the gamma-ray spectra of cosmological sources, *Phys. Rev. D* **79** (2009) 123511, arXiv:0905.3270.

[163] D. Horns et al., Hardening of TeV gamma spectrum of AGNs in galaxy clusters by conversions of photons into axion-like particles, *Phys. Rev. D* **86** (2012) 075024, arXiv:1207.0776.

[164] M. Meyer, D. Montanino, and J. Conrad, On detecting oscillations of gamma rays into axion-like particles in turbulent and coherent magnetic fields, *JCAP* **1409** (2014) 003, arXiv:1406.5972.

[165] D. Wouters and P. Brun, Anisotropy test of the axion-like particle Universe opacity effect: a case for the Cherenkov Telescope Array, *JCAP* **1401** (2014) 016, arXiv:1309.6752.

[166] F. Tavecchio et al., Evidence for an axion-like particle from PKS 1222+216? *Phys. Rev. D* **86** (2012) 085036, arXiv:1202.6529.

[167] M. Meyer, D. Horns, and M. Raue, First lower limits on the photon-axion-like particle coupling from very high energy gamma-ray observations, *Phys. Rev. D* **87** (2013) 035027, arXiv:1302.1208.

[168] A. Abramowski et al., Constraints on axionlike particles with H.E.S.S. from the irregularity of the PKS 2155-304 energy spectrum, *Phys. Rev. D* **88** (2013) 102003, arXiv:1311.3148.

[169] M. Actis et al., Design concepts for the Cherenkov Telescope Array CTA: an advanced facility for ground-based high-energy gamma-ray astronomy, *Exper. Astron.* **32** (2011) 193–316, arXiv:1008.3703.

[170] G. Raffelt and L. Stodolsky, Mixing of the photon with low mass particles, *Phys. Rev. D* **37** (1988) 1237.

[171] A. Neronov and I. Vovk, Evidence for strong extragalactic magnetic fields from Fermi observations of TeV blazars, *Science* **328** (2010) 73–75, arXiv:1006.3504.

[172] C. D. Dermer et al., Time delay of cascade radiation for TeV blazars and the measurement of the intergalactic magnetic field, *Astrophys. J.* **733** (2011) L21, arXiv:1011.6660.

[173] T. Kahniashvili, Y. Maravin, and A. Kosowsky, Faraday rotation limits on a primordial magnetic field from Wilkinson Microwave Anisotropy Probe five-year data, *Phys. Rev. D* **80** (2009) 023009, arXiv:0806.1876.

[174] K. Dolag et al., Constrained simulations of the magnetic field in the local universe and the propagation of UHECRs, *JCAP* **0501** (2005) 009, arXiv:astro-ph/0410419.

[175] K. Dolag et al., Lower limit on the strength and filling factor of extragalactic magnetic fields, *Astrophys. J.* **727** (2011) L4, arXiv:1009.1782.

[176] E. Mortsell, L. Bergstrom, and A. Goobar, Photon axion oscillations and type Ia supernovae, *Phys. Rev. D* **66** (2002) 047702, arXiv:astro-ph/0202153.

[177] E. Mortsell and A. Goobar, Constraining photon-axion oscillations using quasar spectra, *JCAP* **0304** (2003) 003, arXiv:astro-ph/0303081.

[178] A. Mirizzi and D. Montanino, Stochastic conversions of TeV photons into axion-like particles in extragalactic magnetic fields, *JCAP* **0912** (2009) 004, arXiv:0911.0015.

[179] C. Wang and D. Lai, Axion-photon propagation in magnetized universe, *accepted for publication in JCAP* (2015), arXiv:1511.03380.

[180] E. Armengaud et al., Conceptual design of the international axion observatory (IAXO), *JINST* **9** (2014) T05002, arXiv:1401.3233.

[181] R. Bradley et al., Microwave cavity searches for dark-matter axions, *Rev. Mod. Phys.* **75** (2003) 777–817.

[182] C. Csaki et al., Super GZK photons from photon axion mixing, *JCAP* **0305** (2003) 005, arXiv:hep-ph/0302030.

[183] A. Franceschini, G. Rodighiero, and M. Vaccari, The extragalactic optical-infrared background radiations, their time evolution and the cosmic photon-photon opacity, *Astron. Astrophys.* **487** (2008) 837, arXiv:0805.1841.

[184] J. Sitarek et al., Detection of very-high-energy gamma rays from the most distant and gravitationally lensed blazar QSO B0218+357 using the MAGIC telescope system, in: *34th International Cosmic Ray Conference*, 2015, arXiv:1508.04580.

[185] F. W. Stecker, M. A. Malkan, and S. T. Scully, Intergalactic photon spectra from the far IR to the UV Lyman limit for $0 < z < 6$ and the optical depth of the universe to high energy gamma-rays, *Astrophys. J.* **648** (2006) 774–783, arXiv:astro-ph/0510449.

[186] A. De Angelis, G. Galanti, and M. Roncadelli, Relevance of axion-like particles for very-high-energy astrophysics, *Phys. Rev. D* **84** (2011), 105030 [Erratum: *Phys. Rev. D* **87** (2013) 109903], arXiv:1106.1132.

[187] M. H. Salamon, F. W. Stecker, and O. C. De Jager, A new method for determining the Hubble constant from subTeV gamma-ray observations, *Astrophys. J.* **423** (1994) L1–L4.

[188] A. Payez et al., Revisiting the SN1987A gamma-ray limit on ultralight axion-like particles, *JCAP* **1502** (2015) 006, arXiv:1410.3747.

[189] P. Ade et al., Planck 2015 results. XIII. Cosmological parameters (2015), arXiv:1502.01589.

[190] R. Tarrach, Thermal effects on the speed of light, *Phys. Lett. B* **133** (1983) 259–261.

[191] G. Barton, Faster than c light between parallel mirrors: the Scharnhorst effect rederived, *Phys. Lett. B* **237** (1990) 559–562.

[192] J. I. Latorre, P. Pascual, and R. Tarrach, Speed of light in nontrivial vacua, *Nucl. Phys. B* **437** (1995) 60–82, arXiv:hep-th/9408016.

[193] X.-w. Kong and F. Ravndal, Quantum corrections to the QED vacuum energy, *Nucl. Phys. B* **526** (1998) 627–656, arXiv:hep-ph/9803216.

[194] M. H. Thoma, Photon-photon interaction in a photon gas, *Europhys. Lett.* **52** (2000) 498, arXiv:hep-ph/0005282.

[195] L. Ostman and E. Mortsell, Limiting the dimming of distant type Ia supernovae, *JCAP* **0502** (2005) 005, arXiv:astro-ph/0410501.

[196] D. Wouters and P. Brun, Irregularity in gamma ray source spectra as a signature of axionlike particles, *Phys. Rev. D* **86** (2012) 043005, arXiv:1205.6428.

[197] K. Gottfried and T.-M. Yan, *Quantum mechanics: fundamentals*, Springer-Verlag, 2013.

[198] A. Kartavtsev, G. Raffelt, and H. Vogel, Neutrino flavor, helicity, and pair oscillations, in: *Planck 2015*, 2015.

[199] B. Pontecorvo, Neutrino experiments and the problem of conservation of leptonic charge, *Sov. Phys. JETP* **26** (1968), 984-988 [*Zh. Eksp. Teor. Fiz.* **53** (1967) 1717].

[200] V. N. Gribov and B. Pontecorvo, Neutrino astronomy and lepton charge, *Phys. Lett. B* **28** (1969) 493.

[201] L. Wolfenstein, Neutrino oscillations and stellar collapse, *Phys. Rev. D* **20** (1979) 2634–2635.

[202] S. P. Mikheev and A. Yu. Smirnov, Neutrino oscillations in a variable density medium and neutrino bursts due to the gravitational collapse of stars, *Sov. Phys. JETP* **64** (1986), 4-7 [*Zh. Eksp. Teor. Fiz.* **91** (1986) 7], arXiv:0706.0454.

[203] T.-K. Kuo and J. T. Pantaleone, Neutrino oscillations in matter, *Rev. Mod. Phys.* **61** (1989) 937.

[204] A. S. Dighe and A. Yu. Smirnov, Identifying the neutrino mass spectrum from the neutrino burst from a supernova, *Phys. Rev. D* **62** (2000) 033007, arXiv:hep-ph/9907423.

[205] B. Dasgupta and A. Mirizzi, Temporal instability enables neutrino flavor conversions deep inside supernovae, *Phys. Rev. D* **92** (2015) 125030, arXiv:1509.03171.

[206] S. Chakraborty et al., Collective neutrino flavor conversion: recent developments, *Nucl. Phys. B* **908** (2016) 366–381, arXiv:1602.02766.

[207] A. M. Egorov, A. E. Lobanov, and A. I. Studenikin, Neutrino oscillations in electromagnetic fields, *Phys. Lett. B* **491** (2000) 137–142, arXiv:hep-ph/9910476.

[208] A. Grigoriev, A. Lobanov, and A. Studenikin, Effect of matter motion and polarization in neutrino flavor oscillations, *Phys. Lett. B* **535** (2002) 187–192, arXiv:hep-ph/0202276.

[209] A. I. Studenikin, Neutrinos in electromagnetic fields and moving media, *Phys. Atom. Nucl.* **67** (2004), 993-1002 [*Yad. Fiz.* **67** (2004) 1014].

[210] A. Cisneros, Effect of neutrino magnetic moment on solar neutrino observations, *Astrophys. Space Sci.* **10** (1971) 87–92.

[211] C.-S. Lim and W. J. Marciano, Resonant spin - flavor precession of solar and supernova neutrinos, *Phys. Rev. D* **37** (1988) 1368–1373.

[212] E. K. Akhmedov, Resonance enhancement of the neutrino spin precession in matter and the solar neutrino problem, *Sov. J. Nucl. Phys.* **48** (1988), 382-383 [*Yad. Fiz.* **48** (1988) 599].

[213] S. Schael et al., Precision electroweak measurements on the Z resonance, *Phys. Rept.* **427** (2006) 257–454, arXiv:hep-ex/0509008.

[214] A. D. Dolgov, Neutrinos in the early universe, *Sov. J. Nucl. Phys.* **33** (1981), [*Yad. Fiz.* **33** (1981) 1309] 700–706.

[215] C. Giunti and C. Kim, *Fundamentals of neutrino physics and astrophysics*, Oxford University Press, 2007.

[216] G. Raffelt and D. Seckel, A selfconsistent approach to neutral current processes in supernova cores, *Phys. Rev. D* **52** (1995) 1780–1799, arXiv:astro-ph/9312019.

[217] C. J. Horowitz, Weak magnetism for anti-neutrinos in supernovae, *Phys. Rev. D* **65** (2002) 043001, arXiv:astro-ph/0109209.

[218] H. K. Dreiner, H. E. Haber, and S. P. Martin, Two-component spinor techniques and Feynman rules for quantum field theory and supersymmetry, *Phys. Rept.* **494** (2010) 1–196, arXiv:0812.1594.

[219] C. Giunti and A. Studenikin, Neutrino electromagnetic interactions: a window to new physics, *Rev. Mod. Phys.* **87** (2015) 531, arXiv:1403.6344.

[220] R. E. Shrock, Electromagnetic properties and decays of Dirac and Majorana neutrinos in a general class of gauge theories, *Nucl. Phys. B* **206** (1982) 359–379.

[221] A. Dobrynina, A. Kartavtsev, and G. Raffelt, Helicity oscillations of Dirac and Majorana neutrinos (2016), arXiv:1605.04512.

[222] L. B. Okun, On the electric dipole moment of neutrino, *Sov. J. Nucl. Phys.* **44** (1986), [*Yad. Fiz.* **44** (1986) 847] 546.

[223] P. B. Pal and L. Wolfenstein, Radiative decays of massive neutrinos, *Phys. Rev. D* **25** (1982) 766.

[224] C. Fidler et al., Flavoured quantum Boltzmann equations from cQPA, *JHEP* **02** (2012) 065, arXiv:1108.2309.

[225] O. Adriani et al., A new measurement of the antiproton-to-proton flux ratio up to 100 GeV in the cosmic radiation, *Phys. Rev. Lett.* **102** (2009) 051101, arXiv:0810.4994.

[226] O. Adriani et al., PAMELA results on the cosmic-ray antiproton flux from 60 MeV to 180 GeV in kinetic energy, *Phys. Rev. Lett.* **105** (2010) 121101, arXiv:1007.0821.

[227] A. G. Mayorov et al., Upper limit on the antihelium flux in primary cosmic rays, *JETP Lett.* **93** (2011), 628-631 [*Zh. Eksp. Teor. Fiz.* **93** (2011) 704].

[228] G. 't Hooft, Symmetry breaking through Bell-Jackiw anomalies, *Phys. Rev. Lett.* **37** (1976) 8–11.

[229] M. Flanz, E. A. Paschos, and U. Sarkar, Baryogenesis from a lepton asymmetric universe, *Phys. Lett. B* **345** (1995), 248–252 [Erratum: *Phys. Lett. B* **382** (1996) 447], arXiv:hep-ph/9411366.

[230] L. Covi, E. Roulet, and F. Vissani, CP violating decays in leptogenesis scenarios, *Phys. Lett. B* **384** (1996) 169–174, arXiv:hep-ph/9605319.

[231] J. Liu and G. Segre, Reexamination of generation of baryon and lepton number asymmetries by heavy particle decay, *Phys. Rev. D* **48** (1993) 4609–4612, arXiv:hep-ph/9304241.

[232] O. Vives, Flavor dependence of CP asymmetries and thermal leptogenesis with strong right-handed neutrino mass hierarchy, *Phys. Rev. D* **73** (2006) 073006, arXiv:hep-ph/0512160.

[233] T. Endoh, T. Morozumi, and Z.-h. Xiong, Primordial lepton family asymmetries in seesaw model, *Prog. Theor. Phys.* **111** (2004) 123–149, arXiv:hep-ph/0308276.

[234] A. Abada et al., Flavour matters in leptogenesis, *JHEP* **09** (2006) 010, arXiv:hep-ph/0605281.

[235] S. Blanchet and P. Di Bari, Flavor effects on leptogenesis predictions, *JCAP* **0703** (2007) 018, arXiv:hep-ph/0607330.

[236] S. Pascoli, S. T. Petcov, and A. Riotto, Leptogenesis and low energy CP violation in neutrino physics, *Nucl. Phys. B* **774** (2007) 1–52, arXiv:hep-ph/0611338.

[237] J. R. Ellis, M. Raidal, and T. Yanagida, Observable consequences of partially degenerate leptogenesis, *Phys. Lett. B* **546** (2002) 228–236, arXiv:hep-ph/0206300.

[238] A. Pilaftsis and T. E. J. Underwood, Electroweak-scale resonant leptogenesis, *Phys. Rev. D* **72** (2005) 113001, arXiv:hep-ph/0506107.

[239] E. K. Akhmedov, V. Rubakov, and A. Y. Smirnov, Baryogenesis via neutrino oscillations, *Phys. Rev. Lett.* **81** (1998) 1359–1362, arXiv:hep-ph/9803255.

[240] M. Shaposhnikov, The nuMSM, leptonic asymmetries, and properties of singlet fermions, *JHEP* **0808** (2008) 008, arXiv:0804.4542.

[241] J.-S. Gagnon and M. Shaposhnikov, Baryon asymmetry of the universe without Boltzmann or Kadanoff-Baym equations, *Phys. Rev. D* **83** (2011) 065021, arXiv:1012.1126.

[242] T. Asaka, S. Eijima, and H. Ishida, Kinetic equations for baryogenesis via sterile neutrino oscillation, *JCAP* **1202** (2012) 021, arXiv:1112.5565.

[243] S. Blanchet et al., Leptogenesis with heavy neutrino flavours: from density matrix to Boltzmann equations, *JCAP* **1301** (2013) 041, arXiv:1112.4528.

[244] L. Canetti et al., Dark matter, baryogenesis and neutrino oscillations from right handed neutrinos, *Phys. Rev. D* **87** (2013) 093006, arXiv:1208.4607.

[245] B. Shuve and I. Yavin, Baryogenesis through neutrino oscillations: a unified perspective, *Phys. Rev. D* **89** (2014) 075014, arXiv:1401.2459.

[246] R. D. Jordan, Effective field equations for expectation values, *Phys. Rev. D* **33** (1986) 444–454.

[247] E. Calzetta and B. L. Hu, Closed time path functional formalism in curved space- time: application to cosmological back reaction problems, *Phys. Rev. D* **35** (1987) 495.

[248] W. Buchmüller and S. Fredenhagen, Quantum mechanics of baryogenesis, *Phys. Lett. B* **483** (2000) 217–224, arXiv:hep-ph/0004145.

[249] T. Prokopec, M. G. Schmidt, and S. Weinstock, Transport equations for chiral fermions to order h-bar and electroweak baryogenesis. II, *Ann. Phys.* **314** (2004) 267–320, arXiv:hep-ph/0406140.

[250] A. De Simone and A. Riotto, On resonant leptogenesis, *JCAP* **0708** (2007), arXiv:0705.2183.

[251] V. Cirigliano et al., Quantum resonant leptogenesis and minimal lepton flavour violation, *JCAP* **0801** (2008) 004, arXiv:0711.0778.

[252] A. Anisimov et al., Nonequilibrium dynamics of scalar fields in a thermal bath, *Annals Phys.* **324** (2009) 1234–1260, arXiv:0812.1934.

[253] M. Garny et al., Systematic approach to leptogenesis in nonequilibrium QFT: vertex contribution to the CP-violating parameter, *Phys. Rev. D* **80** (2009) 125027, arXiv:0909.1559.

[254] M. Garny et al., Systematic approach to leptogenesis in nonequilibrium QFT: self-energy contribution to the CP-violating parameter, *Phys. Rev. D* **81** (2010) 085027, arXiv:0911.4122.

[255] A. Anisimov et al., Leptogenesis from quantum interference in a thermal bath, *Phys. Rev. Lett.* **104** (2010) 121102, arXiv:1001.3856.

[256] M. Garny, A. Hohenegger, and A. Kartavtsev, Medium corrections to the CP-violating parameter in leptogenesis, *Phys. Rev. D* **81** (2010) 085028, arXiv:1002.0331.

[257] M. Beneke et al., Finite number density corrections to leptogenesis, *Nucl. Phys. B* **838** (2010) 1–27, arXiv:1002.1326.

[258] M. Beneke et al., Flavoured leptogenesis in the CTP formalism, *Nucl. Phys. B* **843** (2011) 177–212, arXiv:1007.4783.

[259] B. Garbrecht, Leptogenesis: the other cuts, *Nucl. Phys. B* **847** (2011) 350, arXiv:1011.3122.

[260] A. Anisimov et al., Quantum leptogenesis I, *Annals Phys.* **326** (2011) 1998, arXiv:1012.5821.

[261] M. Garny, A. Kartavtsev, and A. Hohenegger, Leptogenesis from first principles in the resonant regime, *Annals Phys.* **328** (2013) 26–63, arXiv:1112.6428.

[262] T. Frossard et al., Systematic approach to thermal leptogenesis, *Phys. Rev. D* **87** (2013) 085009, arXiv:1211.2140.

[263] B. Garbrecht and M. J. Ramsey-Musolf, Cuts, cancellations and the closed time path: the soft leptogenesis example, *Nucl. Phys. B* **882** (2014) 145–170, arXiv:1307.0524.

[264] A. Hohenegger and A. Kartavtsev, Leptogenesis in crossing and runaway regimes, *JHEP* **07** (2014) 130, arXiv:1404.5309.

[265] S. Iso, K. Shimada, and M. Yamanaka, Kadanoff-Baym approach to the thermal resonant leptogenesis, *JHEP* **04** (2014) 062, arXiv:1312.7680.

[266] S. Iso and K. Shimada, Coherent flavour oscillation and CP violating parameter in thermal resonant leptogenesis, *JHEP* **08** (2014) 043, arXiv:1404.4816.

[267] P. F. Bedaque, Thermalization and pinch singularities in nonequilibrium quantum field theory, *Phys. Lett. B* **344** (1995) 23–28, arXiv:hep-ph/9410415.

[268] C. Greiner and S. Leupold, Interpretation and resolution of pinch singularities in nonequilibrium quantum field theory, *Eur. Phys. J. C* **8** (1999) 517–522, arXiv:hep-ph/9804239.

[269] R. F. Hoskins and J. S. Pinto, *Theories of generalised functions: distributions, ultradistributions and other generalised functions*, Woodhead Publishing, 2005.

[270] N. Nakanishi, A theory of clothed unstable particles, *Prog. Theor. Phys.* **19** (1958) 607–621.

[271] T. Petrosky, I. Prigogine, and S. Tasaki, Quantum theory of non-integrable systems, *Physica A* **173** (1991) 175–242.

[272] M. J. G. Veltman, Unitarity and causality in a renormalizable field theory with unstable particles, *Physica* **29** (1963) 186–207.

[273] A. Hohenegger, A. Kartavtsev, and M. Lindner, Deriving Boltzmann equations from Kadanoff-Baym equations in curved space-time, *Phys. Rev. D* **78** (2008), arXiv:0807.4551.

[274] A. Hohenegger and A. Kartavtsev, Basis invariant measure of CP-violation and renormalization, *Nucl. Phys. B* **899** (2015) 476–488, arXiv:1309.1385.

[275] M. L. Bellac, *Thermal field theory*, Cambridge University Press, 2000.

[276] P. Millington, Thermal quantum field theory and perturbative non-equilibrium dynamics, PhD thesis, 2012.

Acknowledgments

First of all, I would like to thank Georg Raffelt for his outstanding support and excellent advice during all stages of my doctoral research. I dearly appreciate that every physics-related discussion left me with new ideas and every personal doubt could be discussed in an honest and trusting manner.

I am grateful to Alexander Kartavtsev for supervising my research on a day-to-day basis. I profited not only from his mathematical and idiomatic precision but also from his willingness to spend his evenings reading my crude drafts. Similarly, I am glad to have worked with Javier Redondo in the first months of my research endeavor. His continuous flow of ideas are still a source of inspiration.

Special thanks go to Peter Millington for patiently teaching me the ways of the interaction picture approach to non-equilibrium field theory, and to Núria Vinyoles for all the fun and discussions we had while studying the emission of minicharged particles from the Sun.

I am indebted to my amazing colleagues at the Max Planck Institute for creating a most fruitful and pleasant atmosphere. I would like to especially thank the current and former members of the astroparticle group, Tanja Geib, Frank Steffen, Edoardo Vitagliano, Alexander Merle, Maximilian Totzauer, Julia Stadler, Antonio Palazzo, and Sovan Chakraborty for their steady support and most interesting discussions. Even more so, I am grateful to Alexander Millar and Ignacio Izaguirre for carefully proofreading parts of my thesis. Additional thanks go to my office mates Ulrich Schubert-Mielnik and Johann Felix Graf von Soden-Fraunhofen for the laughs, discussions and (IT-)support, to Marcel Strzys and Christian Fruck for introductory lectures to the world of astrophysics, to Martin Ritter for coercing me into coffee breaks, to Jan Keitel for his useful career advice, to Cyril Pietsch, Stephan Hessenberger and Viktor Papara for the many table tennis matches, and to Thomas Hahn for tolerating my excessive use of Mathematica kernels.

Last but not least, I am very grateful for the steady support of my family and unconditional love of my wife Anne, who (amazingly) wants to venture out to the US with me.